MONASH University

Investigation of the adsorption properties and structures of porous materials for adsorptive removal of pollutants from water

Zahra Abbasi

M. Eng. (Chemical)

A thesis submitted for the degree of Doctor of Philosophy at

Monash University in 2017

Department of Chemical Engineering

Copyright notice

Abstract

Adsorption is a low cost and effective method for the removal of non-biodegradable and harmful pollutants from water which has been widely used in industry. Porous and nanoporous materials such as metal organic frameworks (MOFs) and fly ash wastes are promising adsorbents in adsorption applications. Zeolitic imidazolate frameworks (ZIFs) are a branch of MOF materials with high chemical and thermal stability. Among ZIF materials, ZIF-8 is specifically interesting due to easy synthesis, high surface area and porosity as well as large carbon content. However, there are still challenges in terms of practical application especially in water treatment. Some of the challenges can be addressed to handling and recycling and its low adsorption capacity for dyes. For addressing these challenges, the new methodologies are required to be uncomplicated, reproducible and environmentally friendly. Another porous material which was used for adsorption studies was Victorian brown coal fly ash which is locally available in the state of Victoria at low cost. Victorian brown coal fly ash could be considered as an interesting option for water treatment due to high alkalinity and magnetic property. Therefore, it is important to investigate its textural characteristics and adsorptive properties to address its suitability for adsorption applications.

This thesis study aimed to address the above-mentioned challenges by investigating the characteristics and adsorption properties of ZIF-8 and fly ash waste. First, ZIF-8 was utilized for adsorption of oils and organic compounds and it was shaped as beads to facilitate the handling and recycling of ZIF-8 particles. ZIF-8 powder was incorporated into polyethersulfone (PES) polymer sphere using a novel phase inversion method. The prepared ZIF-8/PES composite beads had exceptional low bulk density of 0.26 g/cm^3 (lower than that of ZIF-8) and very high BET surface area of 1030.6 m^2/g. ZIF-8 beads showed high adsorption capacity of

1260 mg/g for oils which was around 4.8, 6.3, 12.6, 3.3 and 4.2-7.5 times higher than the capacity of HKUST-1, HFGO@ZIF-8, zeolite, bentonite and activated carbons, respectively.

Second, effect of heat treatment on adsorption properties of ZIF-8 for the removal of dyes from water was investigated. The carbonized ZIF-8 exhibited high adsorption capacity of 186.3 mg/g almost 10 times the capacity of ZIF-8. The optimum carbonization temperature resulting in the highest adsorption capacity was 1000 ºC. The kinetics, thermodynamic and mechanisms of adsorption process as well as mechanism of carbonization were investigated thoroughly. Next, the magnetic carbonized ZIF-8 was prepared using wet impregnation method and re-carbonization to incorporate iron nanoparticles in the adsorbent matrix and enable the powder to be easily separated from water. The magnetic nanoporous carbon at 1000 ºC had the same adsorption performance of non-magnetic carbonized ZIF-8 despite losing half of its surface area.

Finally, the physicochemical characteristics, morphologies and adsorption properties of Victorian brown coal fly ash wastes were studied. These waste materials exhibited higher adsorption capacity for the removal of a basic dye as well as heavy metals in comparison with other reported fly ash materials. It was shown the adsorptive characteristics of fly ash materials could be enhanced by natural weathering. The alkaline and magnetic nature of the fly ash wastes make them potential adsorbents for neutralizing and treating the acidic mining wastewaters containing heavy metals.

It is expected that the knowledge gained through extensive exploration in this study would help further development of the porous materials for practical applications.

Declaration

This thesis contains no material which has been accepted for the award of any other degree or diploma at any university or equivalent institution and that, to the best of my knowledge and belief, this thesis contains no material previously published or written by another person, except where due reference is made in the text of the thesis.

Signature: ……

Print Name: …Zahra Abbasi….

Date: …….

Publications

Journal publications

1. **Z.Abbasi**, E. Shamsaei, X.-Y. Fang, B. Ladewig, H. Wang, Simple fabrication of ZIF-8 composite beads by phase inversion method for efficient oil sorption. *J. Colloid Interface Sci.* 2017, 493, 150-161.
2. **Z.Abbasi**, E. Shamsaei, S. Leong, B. Ladewig, H. Wang, Effect of carbonization temperature on adsorption property of ZIF-8 derived nanoporous carbon for water treatment. *Microporous Mesoporous Mater.* 2016, 236, 28-37.
3. **Z.Abbasi**, B. Ladewig, H. Wang, Investigation of adsorption properties of iron loaded ZIF-8 derived nanoporous carbons modified by re-carbonization for water treatment. *Asia Pac. J. Chem. Eng.* 2017 (Submitted).
4. **Z.Abbasi**, B. Ladewig, H. Wang, Enhanced removal of a basic dye and heavy metals from wastewater using magnetic Victorian brown coal fly ash modified by weathering. *J. Env. Sci.* 2017 (Submitted).

Oral and Poster Presentations

1. **Z. Abbasi**, B. Ladewig, H. Wang, ZIF-8 derived nanoporous carbon as a novel adsorbent for water treatment, AIChE Annual Meeting, Nov. 2016, San Francisco, US.
2. **Z. Abbasi**, B. Ladewig, H. Wang, Adsorptive removal of methylene blue and heavy metals by magnetic Yallourn fly ash, APCChE 2015 Congress incorporating Chemeca, Sep 2015, Melbourne, Australia

Other journal publications during enrolment

1. Shamsaei, E.; Lin, X.; Low, Z.-X.; **Abbasi, Z.**; Hu, Y.; Liu, J. Z.; Wang, H. Aqueous phase synthesis of ZIF-8 membrane with controllable location on an asymmetrically porous polymer substrate. *ACS Appl. Mater. Interfaces* 2016, 8, 6236-6244.

Acknowledgements

I would like to express my appreciation to the people who have given me support and encouragement throughout my PhD research journey.

I would like to express my gratitude to my supervisor, Professor Huanting Wang for his great support and guidance throughout my Ph.D. study. I would also like to thank my co-supervisor Prof. Bradley Ladewig for his guidance and help throughout my PhD.

I wish to extend my warm thanks to Prof. Karen Hapgood for her help and support during my PhD journey.

Thanks to the members in our group including Dr Soo Kwan Leong, Li Wan, Ranwen Ou, Xiaofang Chen, Yan Liang, Yaoxin Hu, Kang Liu, Dr Kha Tu, Dr. Ezzat Shamsaei, for their kind help. Appreciation also goes to my friends in the department, Dr Tahereh Hosseini and Dr Ali Bahmanpour who encouraged and supported me during my PhD journey. I also wish to express my gratitude to the staff in the Department of Chemical Engineering, especially Kim Phu, Jill Crisfield, Lilyanne Price, Harry Bouwmeester and Ross Ellingham for their help during my study.

I also wish to thank Dr. Xiya Fang for helping with the magnetic samples in MCEM center and for the training and the support during my research work.

I would like to acknowledge the Australian government and Monash University for my scholarship from 2013 to 2016.

Finally, I would like to thank my beloved parents and my dear sisters and brother for their love, care and support along the way.

Contents

List of figures

List of tables

Nomenclature

ASAP: Accelerated surface area and porosimetry

ATR: Attenuated total reflectance

BG: Brilliant Green

BOD: Biochemical oxygen demand

BPA: Bisphenol-A

CFA: Coal fly ash

CNT: Carbon-nanotube

COD: Chemical oxygen demand

CPO-27-M: Coordination polymer of Oslo

CR: Congo red

Cu-BDC: Copper 1, 4-benzenedicarboxylate

CVD: Chemical vapor deposition

CZIF: Carbonized zeolitic imidazolate frameworks

DFT: Density functional theory

ED: Ethylene diamine

EDS: Energy-dispersive X-ray spectroscopy

FMOF: Fluorous MOF

FTIR: Fourier transform infrared

HFGO: Highly fluorinated graphene oxide

HIPE: High internal phase emulsions

HKUST: Hong Kong University of Science and Technology

Hmim: 2-methylimidazole

IRMOF: Isoreticular metal organic framework

LMB: Leukomethylene blue

MB: Methylene blue

MG: Malachite green

MIL: Matériaux de l'Institut Lavoisier

MO: Methyl orange

MOF: Metal organic frameworks

NMP: 1-methyl-2-pyrrolidinone

NPC: Nanoporous carbon

PED: Protonated ethylene diamine

PES: Polyethersulfone

PNP: P-nitrophenol

PZC: Point of zero charge

RhB: Rhodamine B

SEM: Scanning electron microscopy

SIM: Substituted imidazolate-based MOF

TEM: Transmission electron microscopy

TGA: Thermogravimetric analyses

UiO: University of Oslo

UHMOF: Ultrahydrophobic fluorous metal organic framework

XRD: X-ray diffraction

XRF: X-ray fluorescence

XPS: X-ray photoelectron spectroscopy

ZIF: Zeolitic imidazolate frameworks

Chapter 1. Introduction

1.1. Background

The increase in the global population has resulted in high demand for treated water supply. Water quality is vital for human life and clean water resources have become a major worldwide environmental issue [1]. Treating water and wastewater is considered alternative solution for providing clean water sources. Today, water treatment methods are mainly based on biological process which is commonly used in all countries. However, the main concern is the non-biodegradable compounds which mostly come from industrial activities. Many of these contaminants are organics and heavy metals which threaten the human health as well as our ecosystem [2]. Consequently, other approaches need to be applied before or after the biological treatments considering the amount and concentration of the non-biodegradable contaminants as well as their toxicity for the microorganisms in biological treatment.

Adsorption is a simple, low cost and effective method for the removal of non-biodegradable and harmful molecules and this method has been used widely in industry. The essential need for adsorption processes is an adsorbent that can adsorb the pollutant molecules from polluted streams. Traditional porous materials such as activated carbons and zeolites have been used for water purification [3].

Porous and nanoporous materials are considered suitable options for water and wastewater treatment technologies. Due to their specific capabilities and characteristics such as high adsorption capacities and low cost, porous materials have potential applications in adsorptive

removal of pollutants from water and wastewater. There are several advantages for the usage of these materials compared with conventional or advanced membrane filtration due to their vast availability and low cost for adsorption process applications [4].

Among various porous synthetic adsorbents, metal organic frameworks (MOFs) have been investigated for gas separation, catalysis and adsorption. MOFs are known as porous crystalline materials which contain metal ions linked together by organic ligands [5]. Zeolitic imidazolate frameworks (ZIFs) are a branch of MOF materials with high chemical and thermal stability. Among a variety of available ZIF materials, ZIF-8 is specifically interesting because of the easy synthesis, high chemical and thermal stability and its potential application in adsorption [6].

In comparison with activated carbon and zeolites, the synthesis of MOF is less energy intensive [7]. For instance, fabrication of most metal organic frameworks is performed at relatively low temperatures and pressures and in particular without the use of structure-directing agent. This eliminates the need for further calcination which is used in the synthesis of zeolites. Moreover, MOFs have larger pore volumes, high surface area, low densities and uniform pore size distributions. They have advantages compared with other traditional porous materials like zeolites and activated carbons due to the fine tunable pore structures and adjustable chemical functionality [8]. However, there are still challenges in terms of practical application especially in water treatment purposes. Some of the challenges can be addressed with regard to the small pores resulting in low adsorption capacity for large organic molecules such as dyes. The other challenge includes the handling and recycling of these adsorbents. Therefore, evaluation of simple and effective methods for increasing the adsorption capacity and enhancing recyclability of these nanoporous materials is still required. For addressing these challenges, the new strategies are required to be easy, uncomplicated, reproducible and environmentally friendly.

One ongoing challenge about the utilization of adsorbents including MOFs is difficulty in handling, collections and recycling from polluted water streams. The use of powders in several applications including separation, catalysis and adsorption requires a step of shaping to generate materials with millimetre dimensions like beads and spheres with good mechanical resistance while retaining the initial particle porosity [9]. Moreover, the usage of MOFs as powders especially in catalysis and adsorption can be adversely affected by the powder loss and pipe clog which happens with flushing the fluids (gas or liquid) [10]. Although synthesis of MOFs has been well documented in literature, their shaping still requires development and investigation [9, 11].

Monodisperse porous spheres are extensively used in many applications such as separation, drug delivery and catalysis. Examples of these porous spheres are silica, carbon and polystyrene which are mostly in nano and micro scale. However, spheres with millimetre size have advantages of easy handling, collection and recycling. Also, there are no safety issues for millimetre sized beads in comparison with nano or micro sized spheres [12, 13].

There are several methods for shaping MOF powders for different applications. General methods for this purpose include compression or extrusion under high pressures with or without the usage of binders or additives to make pellets and tablets [10]. Bazer-Bachi et al. [9] prepared tablets of several MOFs including ZIF-8 using direct compression and investigated the impact of compression on gas adsorption and catalytic properties of MOF materials. Nevertheless, the results of the study showed these materials undergo amorphization depending on the amount of pressure applied and the nature of material. Therefore, since this method affects the crystallinity of these materials, the properties and performance of MOFs would be affected and hence this is not a suitable approach. In particular, since only very few MOFs such as NH_2-MIL-53(In) shows amorphization resistance [14, 15], the direct compression cannot be considered a general

and universal strategy. Other strategies include in situ growth of MOFs on porous substrates such as silica and aerogel using methods like seeding growth and layer by layer deposition [16, 17]. There are also other approaches with the usage of MOFs with some additives followed by special treatments such as sol-gel casting and dip-coating [18, 19]. Nevertheless, there are some challenges regarding these methods since they have limitation for some MOF systems due to low MOF loadings (less than %30) as well as poor mechanical stability.

Other methods also have been employed to prepare millimetre-sized porous spheres and beads. For example, Zhang et al. [20] produced large polymer beads by sedimentation polymerization. Nevertheless, the reaction is carried out at 60℃ and the surface area of the resulting beads is very low (20 $m^2.g^{-1}$) [20]. Therefore, the current preparation methods are complicated and need high temperatures. A suitable technique is required to prepare beads with high surface areas, robustness and great performance to tackle the mentioned challenges and the proposed strategy needs to be simple and effective. Phase inversion is a popular method for asymmetric membranes synthesis [21-23]. This is a simple and one step method which functions at room temperature and can be potentially utilized for preparing millimetre sized robust beads and spheres. This could be potentially a universal method for preparing composite beads with interesting features and characteristics such as high surface area and porosity. The beads prepared from this method could be used for many applications such as adsorption, separation, catalysis and water treatment. In particular, phase inversion method could be used for incorporating MOFs and ZIFs powders into polymer matrices to shape them.

The other challenge about using ZIF-8 for adsorption applications is its small pore size and low sorption capacity for the removal of organic dyes from water. There is also a lack of detailed and mechanistic study in literature regarding the applicability of this material for adsorptive removal of contaminants from water. Moreover, the literature lacks the modification methods

for improving the adsorption characteristics and capabilities of this material for water treatment and most studies are limited to gas adsorption and separation applications. This is probably due to the challenges associated with the stability of ZIF-8 in water especially in acidic solutions. Therefore, a detailed study is required to address the issues regarding the applicability of this material for the removal of hazardous contaminants from water.

One strategy for improving the adsorption performance of MOFs (in particular ZIF-8) is to convert them to nanoporous carbons. MOF materials can be converted to nanoporous carbons to introduce larger pore size and broader pore size distribution for the removal of contaminants from water. Nanoporous carbon (NPC) materials with high porosity and large surface areas have been utilized in many fields like adsorption and catalysis [24]. Nanoporous carbons are specifically attractive due to their high thermal and chemical stabilities. These porous materials have commonly been prepared by heat treatment followed by physical or chemical activation [25]. Despite the fact that the porous carbons synthesized this way have high surface areas, the preparation methods require several steps and impose high cost due to the usage of chemicals and activation stages.

Nanoporous carbons can be prepared from MOFs and ZIFs by direct carbonization without any need for physical or chemical activation. The interesting point about this approach is that the derived nanoporous carbons have interesting properties such as high porosity, high surface area and similar morphology to the original precursors. MOFs and ZIFs have large carbon content and are promising for the production of nanoporous carbons. Moreover, although activated carbon has been widely used for the removal of organic pollutants especially dyes from water [26-30], there are very few reports in literature addressing the adsorption of organic contaminants including dyes over nanoporous carbon derived from metal organic framework materials. Current literature lacks a detailed and mechanistic study for the adsorption of

pollutants over nanoporous carbons derived from MOF materials. There is also no report about the change in the adsorption properties of ZIF-8 during heat treatment in an inert atmosphere (carbonization). Therefore, a complete investigation about adsorptive properties and characterizations of ZIF-8 and its nanoporous carbons in addition to adsorption process parameters, kinetics and mechanisms would help to gain a deep and fundamental understanding about adsorption over MOF derived nanoporous carbons in particular ZIF-8 nanoporous carbons.

The study of the change in the textural and adsorption performance of the adsorbents under these new approaches would help us to understand and analyse the adsorptive behaviour of materials for the successful selection of porous adsorbents and modifying/processing techniques for future adsorption applications specifically in water treatment.

Although nanoporous carbons derived from MOF materials show good adsorption properties and performances, it is difficult to separate them from water. Thus, this issue limits their applications in water treatment. Incorporation of magnetic particles into these nanaoporous frameworks, can broaden the areas of their applications especially in adsorption since it makes the separation of the nanoporous carbon particles from aqueous solution much easier [31]. Different methods have been utilized for generating magnetic nanoporous carbons for introducing magnetic functionality into the porous frameworks and carbons but these methods usually include several steps, requires dangerous chemicals and high temperatures or are very time consuming and complicated [32-37]. For example, magnetic nanoparticles were synthesized using a very complex procedure [38] using sodium hydroxide and diethylene glycol solution by heating at 120 ºC under nitrogen atmosphere along with preparing a mixture of PAA, $FeCl_3$ and DEG heated to 220 ºC under nitrogen flow. The mixture of the chemicals including sodium hydroxide in a high temperature environment is very dangerous and it

requires special equipment which resists harsh basic and hot conditions. The usage of nitrogen flow in all of the synthesis steps (mixing, heating, etc.) also makes this procedure very difficult and complicated. Wet impregnation method is an efficient, safe, environmentally friendly and uncomplicated technique which can be utilized for introducing functionalities such as magnetic iron nano particles into the framework of the materials. This is a suitable method especially in terms of practical applications.

One of the important challenges regarding the practical usage of synthetic materials is their high price compared to the natural adsorbents which are generally locally available at low cost with almost moderate adsorption capacity. The lower adsorption capacity of the natural adsorbents could be compensated by much lower price which makes them interesting for the adsorption applications.

To address this issue, fly ash wastes could be selected as alternative adsorbents. Fly ash wastes are known to be abundant and free materials which have the potential application specifically in adsorptive removal of contaminants from water [39]. Therefore, investigation of the physicochemical and adsorption properties of locally available fly ash materials is a great help in terms of possibility of their usage for different applications especially for adsorption of pollutants from water. Victorian brown coal fly ashes are by products of coal combustion in power plants which could be investigated for adsorption applications. These materials are naturally alkaline and contain minerals which is beneficial for adsorption applications. There are mining activities in Australia such as metal and coal mines which produce a large amount of acidic wastewater polluted by heavy metals. The resulting acidic wastewater needs to be neutralized and treated. The acidic wastewater is generally neutralized using limestone, hydrated lime, soda ash, caustic soda, ammonia and fly ash [40]. However, the usage of

chemicals for neutralizing the acidic wastewater is very costly and therefore high lime fly ash could be a very suitable candidate for replacing chemicals such as lime and caustic soda.

Coal fly ash has received a considerable attention for a variety of applications but its practical usage has been limited to the cement industry. Such limitation is probably due to the drawbacks related to its low surface area and heterogeneous surface which could be addressed by modifications such as natural weathering to increase its surface area and porosity and convert it to a more suitable material for different applications. Therefore, selecting appropriate types of fly ash materials with suitable physicochemical properties is one of the technical challenges. The variation of the fly ash structures depends on their origins (source coal) as well as the combustion process conditions which could lead to different characteristics and performances for adsorption applications. Therefore, it is very essential to obtain deep understanding about fly ash characteristics and their adsorption properties towards specific pollutants. This requires to study the adsorption isotherms, kinetics and mechanisms to gain detailed information about the removal performance and mechanisms over fly ash materials.

Victorian brown coal fly ash with high lime content, has unique morphology and mineralogy which could be a suitable option for the purpose of neutralizing and treating acidic mining wastewaters. Even though there are many reports regarding the usage of fly ash in many applications, there is still a need to conduct research about the local available fly ashes especially in terms of their local practical applications. It is worth noting that there is no report about the usage of fly ash in industrial scale for water treatment.

1.2. Research Aims

The overall aim of this project is to investigate the adsorptive properties of a synthetic porous material named zeolitic imidazolate framework ZIF-8 and its derived nanoporous carbons as promising adsorbents in water treatment as well as fly ash waste materials (as abundant free wastes available in the state of Victoria) as an alternative option for treating and neutralizing acidic wastewaters.

There are relatively few studies in regard to the application of MOFs and ZIFs for adsorptive removal of pollutants from water. The investigation of the adsorptive characteristics of these materials is required and improvements are still needed in terms of modification and functionalization of these materials to enhance their adsorption performance as well as their handling and recycling in adsorption applications. There are still unexplored areas regarding the application of these materials including the effect of temperature on adsorption properties of ZIF-8 for uptaking positively charged large molecules such as methylene blue dye. In addition, although MOFs and ZIFs and the nanoporous carbons derived from them offer opportunities for adsorption of contaminants from water, there is a need for shaping them for easy handling and recycling for practical applications.

While fly ash materials have been extensively studied for the removal of different pollutants form water, the Victorian brown coal fly ash has not been investigated for water treatment purposes. Particularly, their physical, chemical and morphological as well as adsorption properties and characteristics have not been explored to date.

Therefore, the specific objectives of my thesis are as follows:

(1) Introducing a new method for shaping and fabricating ZIF-8 powder into spheres and beads and evaluate its performance for oil and organics sorption from water.

(2) Exploring the adsorption properties of ZIf-8 and its derived nanoporous carbons for adsorptive removal of methylene blue dye as a model dye compound from water and understanding the effect of carbonization temperature on their adsorption properties.

(3) Incorporating magnetic functionality into nanoporous carbon derived from ZIF-8 by wet impregnation method and investigate effect of heat treatment on magnetic nanoporous carbon's performance.

(4) Investigation of the textural and adsorptive properties of Victorian brown coal fly ash waste materials and their potential applications in water treatment.

1.3. Thesis structure and chapter outline

This thesis is organised into seven sections; the overview of each chapter is summarised below.

Chapter 1 (introduction) explains briefly the background for the motivation of this thesis as well as the research aims and an outline of the thesis structure.

Chapter 2 (literature review) provides information about MOFs, ZIFs, nanoporous carbons and fly ash wastes in addition to their applications specifically in adsorption and water treatment. The structure and chemistry of these materials are reviewed. The theory and fundamentals of adsorption, isotherms and kinetics will also be presented. Then the focus is refined to the fabrication methods for shaping the metal organic framework powders and associated challenges are reported in addition to the approaches addressing the problems.

Chapter 3 demonstrates a novel, simple, one step and environmentally friendly technique for preparation of ZIF-8/PES composite beads through a phase inversion method for oil spill clean-up from the surface of water. The composite beads exhibit excellent oil sorption in comparison with natural sorbents like activated carbon; however, they have the advantage of

easy handling, collection and recycling compared with ZIF-8 powder. This technique can be considered as a universal method for fabrication of any kind of powders as beads and spheres for water treatment or other adsorption purposes.

The results of experiments are presented and discussed.

This chapter has been published as a journal article: **Z.Abbasi**, E. Shamsaei, X.-Y. Fang, B. Ladewig, H. Wang, Simple Fabrication of ZIF-8 Composite Beads by Phase Inversion Method for Efficient Oil Sorption. *J. Colloid Interface Sci.* 2017, 493, 150-161.

Chapter 4 describes the effect of heat treatment on the structure and adsorption properties of ZIF-8 and explores the characteristics and adsorption behaviour of the derived nanoporous carbons. It is revealed that carbonization temperature plays an important role in increasing the adsorption capacity of ZIF-8. The adsorption isotherms and kinetic models as well as adsorption and carbonization mechanisms are also presented, analysed and discussed.

This chapter has been published as a journal article: **Z.Abbasi**, E. Shamsaei, S. Leong, B. Ladewig, H. Wang, Effect of carbonization temperature on adsorption property of ZIF-8 derived nanoporous carbon for water treatment. *Microporous Mesoporous Mater.* 2016, 236, 28-37.

Chapter 5 presents the experimental work regarding the introducing iron nanoparticles into nanoporous carbons derived from ZIF-8 to produce magnetic adsorbents. The characterization and performance of the magnetic samples as well as effect of heat treatment on adsorption of magnetic particles are provided and the mechanism of adsorption is discussed. This chapter has been submitted as a journal article: **Z.Abbasi**, B. Ladewig, H. Wang, Investigation of adsorption properties of iron loaded ZIF-8 derived nanoporous carbons modified by re-carbonization for water treatment. *Asia Pac. J. Chem. Eng.* 2017 (Submitted).

Chapter 6 presents the experimental work about investigation of structure, characteristics and adsorption properties of Victorian brown coal fly ash waste materials. It is shown that fly ash waste materials are capable of adsorptive removal of pollutants from water and could be utilized for neutralizing acidic mining wastewaters. The results of the experiments are presented and discussed in detail by providing a profound investigation about kinetics and mechanisms.

This chapter has been submitted as a journal article: **Z.Abbasi**, B. Ladewig, H. Wang, Enhanced Removal of a Basic Dye and Heavy Metals from Wastewater Using Magnetic Victorian Brown Coal Fly Ash Modified by Weathering. *J. Env. Sci.* 2017 (Submitted).

Finally, in chapter 7, the main findings and conclusions are summarised and recommendations for the future work are presented.

1.4. References

1. Bhatnagar, A. and M. Sillanpää, *Utilization of agro-industrial and municipal waste materials as potential adsorbents for water treatment—A review.* Chemical Engineering Journal, 2010. **157**(2–3): p. 277-296.
2. Crini, G., *Non-conventional low-cost adsorbents for dye removal: A review.* Bioresource Technology, 2006. **97**(9): p. 1061-1085.
3. Yagub, M.T., T.K. Sen, S. Afroze, and H.M. Ang, *Dye and its removal from aqueous solution by adsorption: A review.* Advances in Colloid and Interface Science, 2014. **209**: p. 172-184.
4. Rafatullah, M., O. Sulaiman, R. Hashim, and A. Ahmad, *Adsorption of methylene blue on low-cost adsorbents: A review.* Journal of Hazardous Materials, 2010. **177**(1–3): p. 70-80.
5. Adeyemo, A.A., I.O. Adeoye, and O.S. Bello, *Metal organic frameworks as adsorbents for dye adsorption: overview, prospects and future challenges.* Toxicological & Environmental Chemistry, 2012. **94**(10): p. 1846-1863.
6. Yao, J. and H. Wang, *Zeolitic imidazolate framework composite membranes and thin films: synthesis and applications.* Chemical Society Reviews, 2014.
7. Ng, E.-P. and S. Mintova, *Nanoporous materials with enhanced hydrophilicity and high water sorption capacity.* Microporous and Mesoporous Materials, 2008. **114**(1): p. 1-26.
8. Lee, J., O.K. Farha, J. Roberts, K.A. Scheidt, S.T. Nguyen, and J.T. Hupp, *Metal-organic framework materials as catalysts.* Chemical Society Reviews, 2009. **38**(5): p. 1450-1459.
9. Bazer-Bachi, D., L. Assié, V. Lecocq, B. Harbuzaru, and V. Falk, *Towards industrial use of metal-organic framework: Impact of shaping on the MOF properties.* Powder Technology, 2014. **255**: p. 52-59.
10. Chen, Y., X. Huang, S. Zhang, S. Li, S. Cao, X. Pei, J. Zhou, X. Feng, and B. Wang, *Shaping of Metal–Organic Frameworks: From Fluid to Shaped Bodies and Robust Foams.* Journal of the American Chemical Society, 2016. **138**(34): p. 10810-10813.
11. Tagliabue, M., C. Rizzo, R. Millini, P.D.C. Dietzel, R. Blom, and S. Zanardi, *Methane storage on CPO-27-Ni pellets.* Journal of Porous Materials, 2011. **18**(3): p. 289-296.
12. Zeng, Y., K. Wang, J. Yao, and H. Wang, *Hollow carbon beads fabricated by phase inversion method for efficient oil sorption.* Carbon, 2014. **69**: p. 25-31.
13. Gu, X., K. Zhou, Y. Li, and J. Yao, *Millimeter-sized carbon/TiO2 beads fabricated by phase inversion method for oil and dye adsorption.* RSC Advances, 2016. **6**(20): p. 16314-16318.
14. Couck, S., E. Gobechiya, C.E.A. Kirschhock, P. Serra-Crespo, J. Juan-Alcañiz, A. Martinez Joaristi, E. Stavitski, J. Gascon, F. Kapteijn, G.V. Baron, and J.F.M. Denayer, *Adsorption and Separation of Light Gases on an Amino-Functionalized Metal–Organic Framework: An Adsorption and In Situ XRD Study.* ChemSusChem, 2012. **5**(4): p. 740-750.
15. Serra-Crespo, P., E. Stavitski, F. Kapteijn, and J. Gascon, *High compressibility of a flexible metal-organic framework.* RSC Advances, 2012. **2**(12): p. 5051-5053.
16. Hu, Y., H. Lian, L. Zhou, and G. Li, *In situ solvothermal growth of metal–organic framework-5 supported on porous copper foam for noninvasive sampling of plant volatile sulfides.* Analytical chemistry, 2014. **87**(1): p. 406-412.

17. Shekhah, O., L. Fu, R. Sougrat, Y. Belmabkhout, A.J. Cairns, E.P. Giannelis, and M. Eddaoudi, *Successful implementation of the stepwise layer-by-layer growth of MOF thin films on confined surfaces: mesoporous silica foam as a first case study.* Chemical Communications, 2012. **48**(93): p. 11434-11436.
18. Ulker, Z., I. Erucar, S. Keskin, and C. Erkey, *Novel nanostructured composites of silica aerogels with a metal organic framework.* Microporous and Mesoporous Materials, 2013. **170**: p. 352-358.
19. Lin, K.-Y.A. and H.-A. Chang, *A zeolitic imidazole framework (ZIF)–sponge composite prepared via a surfactant-assisted dip-coating method.* Journal of Materials Chemistry A, 2015. **3**(40): p. 20060-20064.
20. Zhang, H. and A.I. Cooper, *Synthesis of Monodisperse Emulsion-Templated Polymer Beads by Oil-in-Water-in-Oil (O/W/O) Sedimentation Polymerization.* Chemistry of Materials, 2002. **14**(10): p. 4017-4020.
21. Strathmann, H. and K. Kock, *The formation mechanism of phase inversion membranes.* Desalination, 1977. **21**(3): p. 241-255.
22. Ren, Y., F. Lian, Y. Wen, and H.-Y. Guan, *A novel PVFM based membranes prepared via phase inversion method and its application in GPE.* Polymer, 2013. **54**(18): p. 4807-4813.
23. Mei, S., C. Xiao, and X. Hu, *Preparation of porous PVC membrane via a phase inversion method from PVC/DMAc/water/additives.* Journal of Applied Polymer Science, 2011. **120**(1): p. 557-562.
24. Liu, B., H. Shioyama, H. Jiang, X. Zhang, and Q. Xu, *Metal–organic framework (MOF) as a template for syntheses of nanoporous carbons as electrode materials for supercapacitor.* Carbon, 2010. **48**(2): p. 456-463.
25. Chaikittisilp, W., K. Ariga, and Y. Yamauchi, *A new family of carbon materials: synthesis of MOF-derived nanoporous carbons and their promising applications.* Journal of Materials Chemistry A, 2013. **1**(1): p. 14-19.
26. Pereira, M.F.R., S.F. Soares, J.J.M. Órfão, and J.L. Figueiredo, *Adsorption of dyes on activated carbons: influence of surface chemical groups.* Carbon, 2003. **41**(4): p. 811-821.
27. Gao, Y., S. Xu, Q. Yue, Y. Wu, and B. Gao, *Chemical preparation of crab shell-based activated carbon with superior adsorption performance for dye removal from wastewater.* Journal of the Taiwan Institute of Chemical Engineers, 2016. **61**: p. 327-335.
28. Amin, N.K., *Removal of direct blue-106 dye from aqueous solution using new activated carbons developed from pomegranate peel: Adsorption equilibrium and kinetics.* Journal of Hazardous Materials, 2009. **165**(1–3): p. 52-62.
29. Khaled, A., A.E. Nemr, A. El-Sikaily, and O. Abdelwahab, *Removal of Direct N Blue-106 from artificial textile dye effluent using activated carbon from orange peel: Adsorption isotherm and kinetic studies.* Journal of Hazardous Materials, 2009. **165**(1–3): p. 100-110.
30. Hoda, N., E. Bayram, and E. Ayranci, *Kinetic and equilibrium studies on the removal of acid dyes from aqueous solutions by adsorption onto activated carbon cloth.* Journal of Hazardous Materials, 2006. **137**(1): p. 344-351.
31. Baikousi, M., A.B. Bourlinos, A. Douvalis, T. Bakas, D.F. Anagnostopoulos, J.i. Tuček, K.r. Šafářová, R. Zboril, and M.A. Karakassides, *Synthesis and characterization of γ-Fe2O3/carbon hybrids and their application in removal of hexavalent chromium ions from aqueous solutions.* Langmuir, 2012. **28**(8): p. 3918-3930.

32. Lu, G., S. Li, Z. Guo, O.K. Farha, B.G. Hauser, X. Qi, Y. Wang, X. Wang, S. Han, X. Liu, J.S. DuChene, H. Zhang, Q. Zhang, X. Chen, J. Ma, S.C.J. Loo, W.D. Wei, Y. Yang, J.T. Hupp, and F. Huo, *Imparting functionality to a metal–organic framework material by controlled nanoparticle encapsulation.* Nat Chem, 2012. **4**(4): p. 310-316.
33. Fuertes, A.B. and P. Tartaj, *Monodisperse Carbon–Polymer Mesoporous Spheres with Magnetic Functionality and Adjustable Pore-Size Distribution.* Small, 2007. **3**(2): p. 275-279.
34. Lou, X.W. and L.A. Archer, *A General Route to Nonspherical Anatase TiO2 Hollow Colloids and Magnetic Multifunctional Particles.* Advanced Materials, 2008. **20**(10): p. 1853-1858.
35. Ni, S., X. Wang, G. Zhou, F. Yang, J. Wang, and D. He, *Designed synthesis of wide range microwave absorption Fe3O4–carbon sphere composite.* Journal of Alloys and Compounds, 2010. **489**(1): p. 252-256.
36. Yang, Y., Z. Guo, H. Zhang, D. Huang, J. Gu, Z. Huang, F. Kang, T.A. Hatton, and G.C. Rutledge, *Electrospun magnetic carbon composite fibers: Synthesis and electromagnetic wave absorption characteristics.* Journal of Applied Polymer Science, 2013. **127**(6): p. 4288-4295.
37. Pang, F., M. He, and J. Ge, *Controlled Synthesis of Fe3O4/ZIF-8 Nanoparticles for Magnetically Separable Nanocatalysts.* Chemistry - A European Journal, 2015. **21**(18): p. 6879-6887.
38. Ge, J., Y. Hu, M. Biasini, W.P. Beyermann, and Y. Yin, *Superparamagnetic Magnetite Colloidal Nanocrystal Clusters.* Angewandte Chemie International Edition, 2007. **46**(23): p. 4342-4345.
39. Wang, S., Y. Boyjoo, A. Choueib, and Z.H. Zhu, *Removal of dyes from aqueous solution using fly ash and red mud.* Water Research, 2005. **39**(1): p. 129-138.
40. Akcil, A. and S. Koldas, *Acid Mine Drainage (AMD): causes, treatment and case studies.* Journal of Cleaner Production, 2006. **14**(12): p. 1139-1145.

Chapter 2. Literature review

2.1. Overview

The aim of this literature review is to provide a summary of the recent research in literature about porous materials including metal organic frameworks (MOFs) in particular ZIF-8 as well as nanoporous carbons and coal fly ash wastes for the application in adsorption and water treatment. The structures and physicochemical characteristics of the porous materials are described in detail. The theories about adsorption process, isotherms, kinetics, mechanisms and the important parameters affecting the adsorption process are also reviewed. The shaping of MOF powders and the recent progress in this area will be introduced in detail. The conclusions and future perspectives are presented at the end of this chapter.

2.2. Waste water treatment technologies

The clean water demand is increasing due to the rapid growth of population and industries worldwide. Deficiency of water resources urges us for suitable and efficient technologies for wastewater treatment and reuse. A variety of contaminants such as organics (solvents, hydrocarbons, dyes, etc.) and heavy metals (cadmium, chromium, copper, etc.) discharge from industries which need to be treated before entering the water bodies. Efficient and low cost technologies are required to decontaminate the polluted waters [1, 2]. There are different methods for the removal of pollutants from water. The main broad approaches include physical,

chemical and biological methods. Any of these methods have benefits and drawbacks. The major disadvantage of physicochemical processes is related to high cost, low efficiency, interference with other wastewater constituents as well as handling of the generated waste. Biological treatment involves the biological activity for the removal of organic substances [3]. However, the biological treatment process is inefficient in the removal of dyes [4] and it does not provide satisfactory results for the treatment of industrial wastewater because many organic pollutants are toxic or resistant to biological treatment [5-8]. Therefore, it is essential to consider proper water treatment techniques.

2.2.1. Technologies for the removal of organics and dyes

Different types of organic and inorganic compounds as well as solids or soluble substances exist in wastewater streams. Therefore, there is no general strategy for the treatment and reuse of water. Regarding the removal of organic pollutants from wastewaters, biological treatment is considered the most cost effective approach. However, the presence of complicated and toxic chemicals, dyes and heavy metals may impose limitation for utilizing this treatment process since these hazardous contaminants are not biodegradable [9]. Therefore, a wide range of physico-chemical techniques such as filtration, coagulation, and flocculation, advanced oxidation methods such as Fenton's reaction, ozone and UV as well as chemical oxidation using chlorine, ozone and hydrogen peroxide are employed for the treatment of industrial wastewaters. Nevertheless, the usage of these techniques is restricted in practical applications since they are mostly expensive or technically complicated. For instance, using filtration method is not enough to target the discharge limits within the environmental standards. Also, coagulation and flocculation produces a large amount of sludge which cause handling and disposal problems. In addition, in chemical oxidation, a large amount of chemical and

hazardous substance are required. Finally, advanced oxidation imposes high investment costs [9].

Therefore, adsorption as an easy, inexpensive and effective method for the treatment of wastewaters was selected for this research project. This technique is specifically very efficient if adsorbents with suitable characteristics are employed. For this reason, the investigation of adsorbents' textural, physico-chemical and morphological properties is highly important to provide useful information for selecting appropriate adsorbents for future applications.

2.2.2. Technologies for the removal of heavy metals

Heavy metals have non-degradable nature and they exist in the wastewaters from mining activities, tannery, steel and battery industries as well as thermal power plants. They impose serious environmental problems and threats on human life and ecosystem [10]. The main techniques which are used for the removal of heavy metals form effluents are ion exchange, membrane process, precipitation and electro-catalytic technology [11]. However, most of these technologies are expensive and require complicated approaches and equipment. Therefore, there is a need for an effective, simple and inexpensive treatment method which can be developed, installed and utilized very easily everywhere. Adsorption is an economically feasible technology for the removal of hazardous toxic metals from wastewater [12]. The adsorption process has the advantages of flexible design and easy operation. Moreover, adsorption is in most cases reversible and the adsorbents can be recycled by appropriate desorption techniques [11].

2.3. Adsorption

Adsorption refers to the accumulation of a compound at the interface between two phases (liquid-solid interface or gas-solid interface). The substance that builds up at the interface is

called adsorbate and the solid on which adsorption process takes place is adsorbent [13]. The efficiency of physical adsorption is determined by adsorption capacity of the adsorbents, selectivity for specific compounds, durability and regenerability of the adsorbents [14].

Adsorption has been considered to be superior in comparison with other decontamination techniques because of its low cost, wide range of applications, simplicity of design, easy operation, insensitivity to toxic pollutants, low harmful secondary products and easy regeneration of the adsorbents [14, 15]. The removal of contaminants through adsorption depends on the ability of a porous adsorbent to selectively adsorb particular compounds. The substances containing suitable size and shape, can easily have access to the pores of the solid sorbents and therefore, can be eliminated via adsorption. Adsorption can be considered as a physical or chemical process according to the nature of interactions between adsorbates and porous adsorbents. In case of physical adsorption, the adsorbates are attached to the pores of the solid adsorbents with weak (van der Waals) forces. Therefore, physical adsorption is reversible in most cases and the adsorbent can be easily recovered by simple methods such as solvent exchange or physical treatments such as calcination. On the other hand, chemical adsorption occurs through the formation of strong chemical associations between molecules of adsorbate to adsorbent surface which is typically because of the exchange of electrons and therefore chemical adsorption is usually irreversible. In this case, regeneration is carried out with chemical treatment [14, 15]. Adsorption on most of the adsorbents is controlled by physical forces unless a chemisorption occurs. The main physical forces which control adsorption process are including van der Waals forces, hydrogen bonds, polarity, dipole-dipole π-π interaction, etc. Factors that influence the adsorption efficiency include adsorbate-adsorbent interaction, adsorbent surface area, adsorbent to adsorbate ratio, adsorbent particle size, temperature, pH and contact time [15].

A variety of porous adsorbents such as activated carbons, zeolites, waste materials (like fly ash), mesoporous materials and MOFs have been studied for adsorptive removal of hazardous substances. For efficient adsorptive removal, porosity, pore geometry and specific adsorption sites are required. Furthermore, active species such as different functional groups (acidic or basic), metal ions and metal oxides are typically incorporated into the framework of the porous adsorbents to enable them selectively adsorb harmful components through common interactions like acid-base, complexation, electrostatic interaction, and hydrogen bonding. The popular modification techniques including post synthetic modification, functionalization, ion exchange, impregnation, and loading of porous adsorbents have been extensively investigated [14]. Adsorption provides an attractive alternative especially if the adsorbent has low cost and does not require to undergo additional pretreatment before its application.

The efficiency of adsorption is typically described by adsorption equilibrium isotherms as well as kinetic models.

2.3.1. Adsorption isotherms

Adsorption is an equilibrium separation process [16]. To determine how adsorbed molecules interact with adsorbent surface, it is required to analyse the adsorption isotherms in an adsorption process. Adsorption isotherm demonstrates the amount of material which is adsorbed per unit mass of adsorbent as a function of the equilibrium concentration of the adsorbate. In adsorption experiments, a specified mass of adsorbent reaches equilibrium by certain volume of solution at specific concentration of a pollutant and the mass balance is introduced as below [17]:

$$Q_{e=} \frac{(C_0 - C_e) \times V}{m} \quad (1)$$

where C_0 and C_e are the initial and equilibrium concentration of the adsorbate in solution, V is the solution volume and *m* refers to the mass of adsorbent. Using these values the amount of Q which is the adsorption capacity is defined.

The equilibrium studies determine the adsorbent capacity. From the equilibrium studies, adsorption isotherms and their constants are determined. These constant values express the surface properties and affinity of the adsorbents. To understand, interpret and predict the extent of the adsorption in particular applications, it is required to realize the relationship between equilibrium data and theoretical or practical equations [18].

Among several adsorption isotherms which have been used for the adsorption process, Langmuir and Freundlich models are considered the most common isotherms because of simplicity and capability to describe experimental results in a broad range of concentrations [19].

2.3.1.1 Langmuir isotherm

Langmuir isotherm is commonly used for the adsorption on a homogeneous surface. This model is based on the assumption that the structure of the adsorbent is homogeneous and the adsorption sites have equal energies. It is considered that the adsorption process shows the monolayer formation of adsorbed molecules on the surface of the adsorbent.

In Langmuir adsorption equation, three main assumptions are considered. First, the adsorption energy is equal in all adsorption sites. Second, adsorption occurs on localized sites without any interaction between adsorbed molecules. Third, the maximum adsorption is achieved at a complete monolayer [20, 21].

This model is described by the following equation:

$$Q_e = \frac{Q_m K_L C_e}{1 + K_L C_e} \tag{2}$$

To determine the Langmuir model constants, two versions of linearization can be employed. One relationship can be represented by plotting $^1/_{C_e}$ versus $^1/_{Q_e}$ while the other equation is plotted using C_e versus $^{C_e}/_{Q_e}$ as shown below.

$$\frac{C_e}{Q_e} = \frac{C_e}{Q_m} + \frac{1}{K_L Q_m} \tag{3}$$

$$\frac{1}{Q_e} = \frac{1}{Q_m} + \frac{1}{K_L Q_m}\frac{1}{C_e} \tag{4}$$

where Q_m is the maximum adsorption capacity expressed as $mg\ g^{-1}$ with a complete coverage of the monolayer on the adsorbent surface. This means Q_m refers to the maximum number of moles (or the amount) of a contaminant adsorbed per mass of adsorbent when the surface sites are saturated with an adsorbate (full monolayer) and $Q_e(mg\ g^{-1})$ is the number of moles (or the amount of) adsorbate per mass of adsorbent at equilibrium.

K_L is the Langmuir constant which is related to the energy of adsorption ($l\ mg^{-1}$) and C_e is the equilibrium concentration (mgl^{-1}).

From the linear plot of $^1/_{C_e}$ versus $^1/_{Q_e}$, the Langmuir constants K_L and Q_m can be determined.

Favourable adsorption is explained by the dimensionless factor (R_L) of Langmuir model [22]:

$$R_L = \frac{1}{1 + K_L C_i} \quad (5)$$

The R_L values are classified into different groups as mentioned in Table 2-1:

Table 2-1 R_L values according to adsorption isotherms

R_L	Type of isotherm
$R_L > 1$	Unfavorable
$R_L = 1$	Linear
$0 < R_L < 1$	Favorable
$R_L = 0$	Irreversible

2.3.1.2 Freundlich isotherm

The Langmuir model involves the assumption that the energy of adsorption is the same for all adsorption sites but in reality the energy of adsorption may differ since the real surfaces are heterogeneous. Therefore, the Freundlich adsorption model is introduced to take this heterogeneity in consideration [23, 24]:

$$Q_e = K_F C_e^{1/n} \quad (6)$$

where C_e is the equilibrium concentration in solution, K_F is the equilibrium constant indicative of sorption strength and n is the degree of non-linearity. A linear form of the above equation can be obtained by taking logarithms and rearranging the relationship:

$$\log Q_e = \log K_F + \frac{1}{n} \log C_e \quad (7)$$

where $K_F(mg^{1-1/n}l^{1/n}g^{-1})$ and n are the Freundlich adsorption isotherm constants. K_F and $1/n$ values can be calculated from the intercept and slope of the linear plot of $\log C_e$ versus $\log Q_e$.

In an adsorption process, favourable adsorption can be defined through the Freundlich constants. n is an indication of deviation from linearity of the adsorption and can be applied to determine different kinds of adsorption. Generally, when n is below unity, it shows that the adsorption is a chemical process; while, the n values greater than unity demonstrate a favourable adsorption and a physical process. The n value equal to unity shows a linear adsorption [23].

2.3.2. Adsorption kinetics and mechanisms

Kinetic studies are performed to have a better understanding of adsorption mechanisms. The kinetic studies determine the rate of adsorption and kinetic models are beneficial to determine the feasible application of the adsorbent in adsorption process. A slow adsorption rate shows significant limitations and issues for the practical applications.

The adsorption mechanism includes three stages as film diffusion, pore diffusion and adhesion of the solute molecules to the adsorbent surface. Film diffusion includes the diffusion of the adsorbate molecule through the films surrounding the particle's surface. Pore diffusion involves the penetration of the molecules into the pores to the adsorption site. When the adsorbate molecule reaches the surface of the pore then adhesion occurs and the molecule attaches to the surface [25].

2.3.2.1 Pseudo-first order model

Lagergren's kinetics equation (pseudo-first order equation) [26, 27] is commonly used for kinetic studies of an adsorption system. This model presents that the rate of adsorbate uptake

by time is directly proportional to the change in equilibrium concentration and the amount of solute uptake by time as follows:

$$\frac{dQ_t}{dt} = k_1(Q_e - Q_t) \quad (8)$$

where $Q_t = 0$ at $t = 0$. The integration of the equation results in the following relationship:

$$\log(Q_e - Q_t) = \log Q_e - \frac{k_1 t}{2.303} \quad (9)$$

where $Q_t(mg\ g^{-1})$ refers to the amount of adsorbed molecules per unit mass of adsorbent at time t which is the contact time (min). k_1 is the pseudo-first order rate constant (min^{-1}) which can be calculated from the plot of $\log(Q_e - Q_t)$ versus t.

2.3.2.2 Pseudo-second order model

The pseudo second order model is expressed as the following relationship [28, 29]:

$$\frac{dQ_t}{dt} = k_2(Q_e - Q_t)^2 \quad (10)$$

The integration of the above formula and rearranging into a linear form results in the following relationship:

$$\frac{t}{Q_t} = \frac{1}{k_2 Q_e^2} + \frac{t}{Q_e} \quad (11)$$

where k_2 presents the rate constant of pseudo-second order model (g mg^{-1} min^{-1}). The values of k_2 and Q_e can be calculated by plotting t/Q_t against t.

2.3.2.3 Intra-particle diffusion model

weber and Morris [30, 31] introduced the intra-particle diffusion model to explain the adsorption processes in terms of diffusion mechanisms. The adsorption processes are typically controlled by either mass transfer rate in the liquid phase or by the mass transfer inside the particles. The effect of intra-particle diffusion resistance on adsorption is presented by the following formula:

$$Q_t = k_{id} t^{1/2} + I \quad (12)$$

where k_{id} is called intra-particle diffusion rate constant (mg g^{-1} $min^{-1/2}$). This constant can be evaluated from the slope of the linear plot of Q_t versus $t^{1/2}$. If the diffusion is controlled by intra-particle diffusion, the plot is linear and it passes through the origin. Values of I refer to the thickness of the boundary layer. The larger intercept is representative of a larger boundary layer effect.

These plots normally consist of three stages since there are resistances involved in the process. The initial portion of the curve is followed by an intermediate linear portion and a plateau. The initial section of the curve is due to external mass transfer. In this portion the resistance is due to the diffusion of the molecules through a solute film onto the adsorbent particle surface. The intermediate linear part is attributed to the intra-particle diffusion and the plateau represents the stage where the intra-particle diffusion starts to slow down because of low adsorbate concentration difference (small driving force) between the solution medium and within the pores [32, 33].

2.3.3. Parameters affecting the adsorption process

The adsorption capacity of different adsorbents depends on a number of parameters. These parameters can be explained based on the adsorbent properties such as surface area, pore

structure and functional groups in addition to the adsorbate features like molecular size, functional groups, polarity and aqueous solubility [34, 35]. It is worth noting that, the process conditions such as solution pH, temperature and ionic strength might have possible impacts on the interactions between adsorbent and adsorbates during the adsorption process as well [36, 37].

2.3.3.1 Effect of adsorbate properties

There are different factors associated with adsorbate properties which affect the adsorption process. These parameters typically influence the nature of the interaction between particular adsorbates and adsorbents which eventually impact the adsorption affinity of the adsorbents toward specific adsorbate molecules.

Based on the study by Moreno-Castilla [38] some major properties of adsorbates which affect the adsorption process includes molecular size, solubility and the nature of constituents (for aromatic compounds). The molecular size is important in terms of determining the access of the adsorbates to the pores of the adsorbents. The solubility reflects the degree of hydrophobic interactions between adsorbate and surface of adsorbent. In case of aromatic compounds, the substituents of aromatic ring, can withdraw or donate electrons. This affects the non-electrostatic interactions between adsorbate and the adsorbent surface.

2.3.3.2 Point of zero charge

The point of zero charge (pzc) is the pH at which the surface charge is zero and is generally used to quantify or define the electro kinetic properties of a surface. The value of pH is used to describe pzc only for systems in which H^+/OH^- are the potential determining ions. Due to the presence of functional groups such as OH^-, cationic dye adsorption is favoured at pH > pHpzc where the surface gets negatively charged, while anionic dye adsorption is favoured at pH <

pHpzc where the surface becomes positively charged [15]. To define the pzc, the surface charge of a sample is measured as zeta potential using a Zeta sizer. Zeta potential (ζ) is an important pH related parameter that determines the surface properties of solids in aqueous solutions. This parameter is used to explain the adsorption mechanism of an adsorbate at the solid-water interface. Zeta measurements plays a significant role in understanding the adsorption mechanism of inorganic and organic molecules at the solid/solution interface as well as determining the colloid stability [39].

2.3.3.3 Effect of electron donor or acceptor groups

Radovic *et al*. [40] reported that electrostatic interactions are very important for adsorbate-adsorbent interactions; however, π-π dispersion interactions seems to be dominant in the adsorption of aromatic solutes over the carbon compounds. They concluded that both electrostatic and dispersive interactions can affect and control the equilibrium uptakes of weak aromatic systems.

The π-π interactions come from the interactions between the π-electrons in the aromatic rings of organic compounds and the π-electrons in the adsorbents such as carbon and graphene layers. This interaction results in charge transfer, dispersive force and polar electrostatic components. By introducing substituent groups, these π-π interactions between the adsorbate and the adsorbent would change. The electron withdrawing groups enhance the π-π interactions by reducing the electron density of π-electrons which leads to reducing the repulsive electrostatic interactions between the aromatic rings [41-43].

Another study by Abdul Ghaffar and Muhammad [44] shows that for the adsorption of methylene blue over carbon nanotubes, surface area was not the only factor governing the adsorption process. According to their studies, they suggested the morphology of carbon

nanotubes, π-π electron donor-acceptor, electrostatic interaction and functional groups were also the contributing factors. Their study confirms that π-π electron-donor acceptor, hydrophobic interaction, hydrogen bonding, electrostatic and covalent interactions and van der Waals forces contribute to the adsorption of organic molecules on carbon nanotubes and might affect the adsorption process simultaneously or individually.

2.3.3.4 Effect of adsorbate molecule size

The molecule size also affects the adsorption of molecules on the surfaces. Those molecules which have suitable sizes, would be adsorbed much easier due to the better contact with the adsorbent surfaces. On the other hand, if the molecule size is large, it would be difficult for the molecule to diffuse within the pores whose size is not large enough due to the steric effects. The steric effects are produced due to a number of reasons such as: some small pores may not be accessible for large molecules; the internal part of the pores might not be accessible because of being blocked by adsorbed molecules; the adsorbate molecules cannot be compact in pores since the substituent groups have occupied the pores. For example, Hinda et al. have reported that the weak adsorption of congo red dye in comparison with other dyes like methylene blue or methyl red is attributed to the large steric hindrance because of large aromatic ensembles such as central biphenyl groups and symmetric naphtalenic groups [45]. Moreover, Valix et al. reported that there is steric hindrance related to the size of the acid dye molecules which restricts the diffusion of the molecules into the pre structure of the carbon material [46].

2.3.3.5 Effect of adsorbent hydrophobicity

The hydrophobicity of an organic molecule plays an important role and affects the adsorption of the molecules on the hydrophobic surfaces [38]. For the adsorption in aqueous environments, the molecules with higher hydrophobicity have higher affinity to be adsorbed on

the surfaces or in the pores of hydrophobic materials such as carbon or ZIF-8. Therefore, hydrophobic compounds are adsorbed much higher than the hydrophilic compounds.

2.3.3.6 Effect of solution conditions

a) Solution pH

The pH of a solution is considered as an important parameter which affects the adsorption performance. The change in the pH conditions of a solution might result in change in the chemical properties on the surface of the adsorbents as well as the forms of the adsorbate molecules. The surface chemistry of the adsorbent can change depending on the interaction of acidic or basic species with the surface groups. This interaction may lead to changes in adsorption capacity of specific adsorbents [47]. It is worth noting that the behaviour of the functional groups on the surface of the adsorbents and their interactions with water molecules may depend on the pH condition of the adsorption environment. These interactions may lead to the transformation of the active sites [48]. When the pH of a solution increases, the number of negatively charged sites increases. For the adsorption of negatively charged molecules like blue-106 dye, increase of the pH reduces the adsorption of molecule because of the electrostatic repulsion [49].

The change in pH affects the surface ionic charge of adsorbate molecules and adsorbent materials. This changes the zeta potential of the adsorbent and impacts the electrostatic interaction of adsorption process. Moreover, the pH conditions affect the solubility and dissociation of adsorbate and adsorbent in solution. The pH of solution also influences the surface charge of the adsorbents and the ionization of the adsorbate molecules [23].

b) Solution temperature

The temperature of a solution is a very important factor in an adsorption process due to the fact that temperature affects the adsorption of water as well as the hydration degree of the molecules [50]. Song et al. [51] reported that the adsorption uptake of methylene blue dye increases with temperature. This behaviour is commonly seen for the adsorption of most dyes in solution. They also reported that the adsorption of MB on bentonite was endothermic. This means that by increasing the temperature, the adsorption capacity is increased which could be attributed to the stronger bonds between adsorbate molecules and the adsorbent surface at higher temperatures. Moreover, Yunjin et al. [52] studies also showed that methylene blue adsorption on carbon nanotubes was an endothermic process. It is stated that increasing the temperature results in the reduction of the solution viscosity and therefore the diffusion rate of the adsorbate molecules in the external boundary layer and the internal pores of the adsorbents increases. Additionally, the equilibrium capacity of the adsorbents for specific adsorbates changes with the change in temperature.

The following relationships are usually used to express the effect of temperature on adsorption processes [53, 54].

$$\Delta G° = \Delta H° - \Delta S°T \tag{13}$$

$$\Delta G° = -RT\ ln\ K_C \tag{14}$$

The van't Hoff equation can be derived by combining the above relationships:

$$ln\ K_C = \frac{\Delta S°}{R} - \frac{\Delta H°}{RT} \tag{15}$$

where K_C is the equilibrium constant and is explained as the ratio of the dye equilibrium concentration on the adsorbent to the dye equilibrium concentration in solution. R is the ideal

gas constant (8.314 $Jmol^{-1}K^{-1}$) and T is the adsorption temperature in Kelvin. By plotting ln K_C against $^1/_T$ a linear line would be drawn and the values of $\Delta H°(kJ\ mol^{-1})$ and $\Delta S°$ ($J\ mol^{-1}K^{-1}$) can be calculated form the slope and intercept of van't Hoff plot.

2.3.3.7 Effect of adsorbent properties

An adsorbent material is required to have high internal volume accessible to the compounds which are going to be removed from the solvent. Surface area, in particular the internal surface area, pore size distribution and the nature of the pores highly affect the adsorption process. In addition, having good mechanical properties such as strength and resistance to destruction is of great importance for an adsorbent. Moreover, the adsorbent particles should have suitable size and form. The chemical properties of the adsorbent, including the degree of ionization at the surface, types of functional groups and the how these properties variate in contact with solution are important points in determining the adsorption capacity of a solid. Active functional groups on the adsorbent surface could result in chemical interactions which typically lead to some effects different from physical adsorption and is less reversible [55].

Different kinds of adsorbents have been used for water treatment including activated carbon, clay minerals, zeolites, metal oxides, agricultural wastes, biomass and polymeric materials [56]. In particular, clays, zeolites, silica gel, soil, river sediment, activated alumina, inorganic polymer, red mud, inorganic oxides (titanium oxide, ferric oxide, hydrous zirconium oxide, etc.) fly ash, etc. have been utilized for the removal of heavy and toxic metal ions [16, 55, 57-62]. Furthermore, natural materials (clays, zeolites, etc.), bioadsorbents (biomass), waste materials (agricultural solid wastes and industrial solid wastes such as fly ash) have been investigated for the adsorption of organic pollutants including dyes [63-69].

The main parameters which influence the adsorption process are known as pore size and pore size distributions, surface area, surface chemistry (functionality) and mineral content. The suitable pore size distribution is required for providing the adsorption sites and channels for transporting the adsorbates [3, 70]. The adsorption capacity depends on accessibility of organic molecules to the micropores and this is related to the size of the molecules. Therefore, small molecules like phenol have the ability to access micropores, natural organic compounds can access mesopores and bacteria are able to access macropores only [70].

Shaobin et al. [71] studied the effect of physicochemical properties of activated carbons for adsorption of methylene blue form wastewater. They found out that physical properties of activated carbon including surface area and pore volume had margin effect on methylene blue uptake. However, other properties such as pore size distribution and surface chemical characteristics had significant effect on dye removal from water. Another study by Walker et al. [72] for adsorption of acid dyes on different adsorbents showed that the pore size distribution of the adsorbate was a very important factor in selection of a cost-effective adsorbent.

Manuel et al. [73] studied the effect of surface chemical groups on activated carbons for dye adsorption. They reported that surface chemistry of activated carbon remarkably influences the adsorption of dyes from solution. It was found that for anionic dyes such as reactive, direct and acid dyes, the surface basicity plays an important role for dye adsorption. The main adsorption mechanism was the interaction between the oxygen-free Lewis basic sites and the free electrons of dye molecule. For the anionic dyes it was shown that oxygen containing groups which are acidic had a negative impact on the adsorption uptake of these dyes. While, for the adsorption of cationic (basic) dyes, the acid oxygen-containing surface groups (mainly carboxylic) exhibited a positive effect on adsorption. However, the thermal treatment still was the most effective factor which resulted in the best performance for dye adsorption on activated

carbon. It was shown that thermal treatment at 700℃ under H_2 flow in comparison with chemical treatments was the best approach resulting in the highest adsorption capacity of activated carbon for dye removal.

Different types of modification methods including acidic treatment, base treatment, impregnation, microwave treatment, ozone treatment and plasma treatment have been used to increase the adsorption capacity of activated carbon for a variety of pollutants. Activated carbon contains oxygen, hydrogen, sulfur and nitrogen which exist in the forms of functional groups or atoms with chemical bonds to the structure. The main functional groups responsible for adsorption of contaminants are carboxyl, carbonyl, phenols, lactones and quinones. These functional groups have significant effects on adsorption properties of activated carbon and could be obtained or modified by means of activation process, precursors, thermal treatment as well as post chemical treatments [74]. It is reported that activated carbon has much higher tendency and adsorption performance for eliminating organic compounds rather than metals and other inorganic contaminants [75].

Porous materials have interesting characteristics which make them suitable for adsorption applications. An understanding of the porous adsorbents structures and properties and their effects on adsorption performance is essential particularly for designing and selecting the suitable adsorbents for specific applications such as water treatment.

2.4. Porous materials as adsorbents

Porous materials are very interesting from both scientific and technological point of view since they can interact with atoms, ions and molecules at the surface and within the bulk of the material. Therefore, they have found many applications in ion exchange, adsorption and catalysis especially for environmental purposes. The pores of solids can be classified based on

their sizes. Pore sizes below 2 nm are called micropores. The pores between 2 nm and 50 nm are mesopores and those above 50 nm are considered as macropores. Fig. 2-1 illustrates micro, meso and macropores in porous materials.

The ability of the porous materials in specific applications depends on the distribution of the pore sizes as well as shapes and volume of the void spaces in the porous structure. Apart from the pore size, the atoms in the solids are important regarding their applications. As an example, molecular sieves including pure silica are hydrophobic and therefore they are capable of adsorbing organic compounds from water. On the other hand, molecular sieves containing aluminosilicate are hydrophilic and have the ability to adsorb water from organic solvents [76].

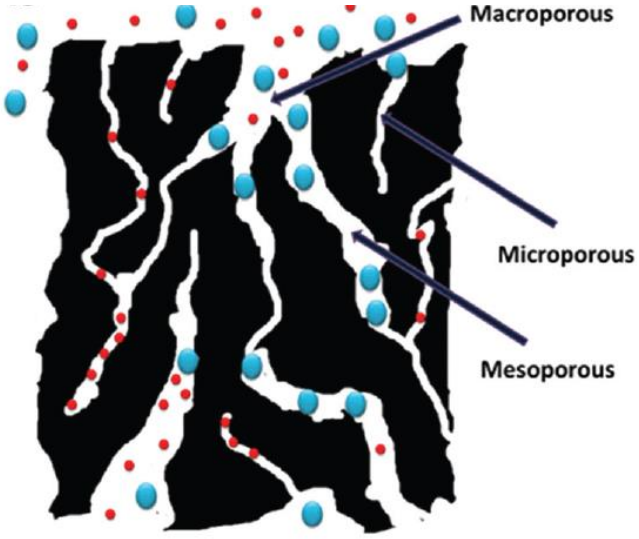

Fig. 2-1 Schematic illustration of pores [77]

Heteroatoms (atoms other than carbon) define the surface chemistry and chemical characteristics of activated carbons. In particular, oxygen is considered an important heteroatom that exists in the form of carboxylic acid groups, phenolic, hydroxyl groups and quinone carbonyl groups [78-82]. The acidic nature of activated carbons is explained by the formation

of carboxylic acid and phenolic hydroxyl groups [82]. The presence of π-electrons on the condensed polyaromatic sheets is associated with the basic characteristics of activated carbons [83, 84]. The reason for the formation of these electron rich Lewis base sites is due to the removal of oxygen from the surface of activated carbon by heat treatment in an inert atmosphere. The heat treatment results in elimination of acidic groups as well as other oxygen containing functional groups which increase the basicity of activated carbons. This happens by attracting and localizing π-electrons of condensed polyaromatic sheets [85]. The elimination of oxygen from the surface of activated carbon helps the surface to become more basic and less polar. This is very favourable for the adsorption of organic pollutants from aqueous solutions. Heat treatment in an inert environment, removes oxygen containing functionalities from activated carbon surface and leads to highly reactive sites [86]. Other studies have shown that by increasing the oxygen or acidic functional groups, the adsorption of organic compounds on activated carbon from aqueous solution decreases [87-90]. Studies have shown that water molecules can be adsorbed on oxygen containing functional groups through hydrogen bonding and then the additional water molecules cluster at these sites [80, 91-94]. The water clusters prevent the pollutant access to hydrophobic areas on activated carbon, decreases the interaction energy between contaminants and the surface of adsorbent and can block the contaminant molecules to access the micropores [87-89, 94, 95]. Therefore, adsorbents having stable hydrophobic surfaces perform much better in removal of organic pollutants from water. However, adsorbents need to be hydrophilic enough in order to get wet by water to be useful for water treatment [96].

2.4.1. Metal organic frameworks (MOFs)

Metal organic frameworks (MOFs) are emerging new functional porous materials with interesting features such as high porosity, pore functionality and open metal sites. In

comparison with inorganic microporous materials like zeolites, MOF structures have the potential for more flexible design by controlling the functionalization of the pores [97, 98]. Therefore, MOFs have attracted particular attention as nanoporous materials due to designable framework structures [99, 100]. Fig. 2-2 shows the molecular structure of MOFs.

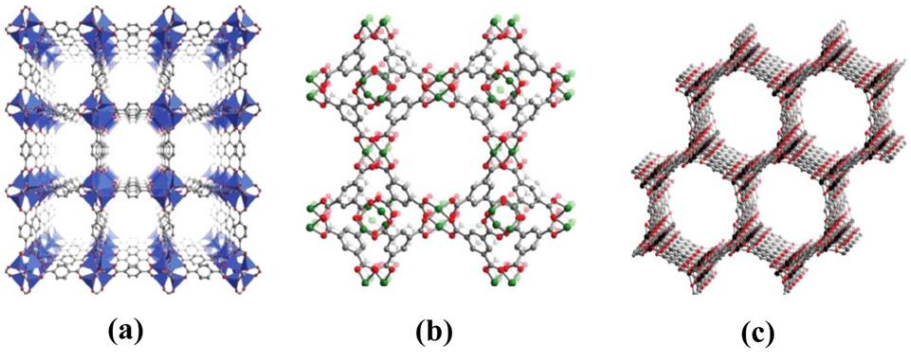

Fig. 2-2 Molecular structures of some typical MOFs. (a) MOF-5, (b) Cu-BTC and (c) CPO-27 [101]

A MOF molecular structure includes metal atoms or a cluster of metal ions in combination with an organic linker. The specific characteristics of MOFs is porosity. MOFs are similar to zeolites in terms of analogy although zeolites are known to be purely inorganic materials. In spite of the fact that MOFs and zeolites have some features in common like large internal surface areas as well as uniform pore and cavity sizes, they are different in some important aspects. For example, MOFs can be synthesized in greater variety compared with zeolites [102]. A large number of MOFs can be synthesized by a variety combinations of metal centers and organic linkers to adjust surface area as well as pore size and surface functionality (Fig. 2-3) [103].

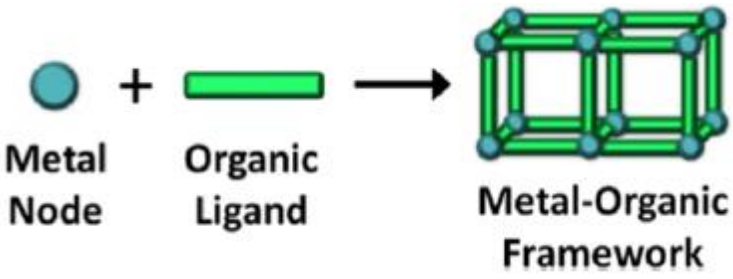

Fig. 2-3 Flexible synthesis route of MOFs composed of metal nodes and organic linkers [104]

Due to their unique characteristics and enormous porosity, MOFs have drawn much attention for many applications like adsorption in both gas and liquid [14, 98, 105, 106], separation [107-110] and catalysis [111, 112]. MOFs are generally synthesized under solvothermal or hydrothermal conditions but the recent research activities demonstrate that the synthesis of these structures is possible at room temperature in aqueous solution [113].

Many of MOF materials are unstable in water or in humid air in which they are exposed to water molecules. This is one of the major drawbacks in terms of their applications especially in industry. For example, IRMOF-1 loses its structure when exposed to water molecules. The high surface area IRMOF-1 converts to low surface area MOF-69c since water molecules can replace carboxylic groups to coordinate with zinc centers [114]. Zeolitic imidazolate framework (ZIFs) are considered to have the advantage of much higher water stability over MOFs.

2.4.2. Zeolitic imidazolate frameworks (ZIFs)

Zeolitic imidazolate frameworks (ZIFs) are a subcategory of MOFs which have permanent porosity and due to comparatively high thermal and chemical stability have the potential for development and modification [115, 116]. ZIFs are composed of metal atoms including Co, Cu, Zinc, etc. which are linked by nitrogen atoms of imidazolate linkers. ZIFs and zeolites have similar frameworks in which the T-O-T bridges with T being Si, P or Al, are substituted by M-

Im-M bridges by M being Zn, Cu or Co with the same bond angle of 145˚[117]. The structure of ZIFs and zeolites are compared in Fig. 2-4.

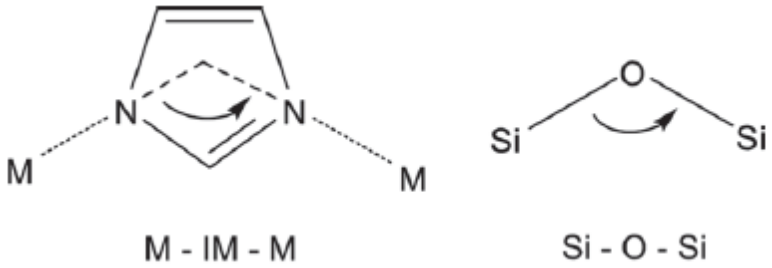

Fig. 2-4 Structures of ZIFs and zeolites [118]

Different types of ZIF structures can be made by changing the metal ions as well as imidazolate organic molecules [119]. Among the ZIF structures, ZIF-8 and ZIF-11 have shown high exceptional thermal and chemical stability [118, 120, 121]. ZIF-8 is particularly interesting owing to its exceptional thermal and chemical stability in organic solvents, aqueous alkaline solutions and water [118]. This is attributed to the fact that imidazolate linkers are more basic compared to the carboxylate linkers and this leads to stronger bonds between metal atoms and ligands. The other reason for superior stability of ZIF-8 in comparison with other ZIFs is its hydrophobicity [117].

ZIF-8 has the formula of Zn(2-methylimidazolate)$_2$ with a sodalite-related zeolite structure which consists of six membered ring pore window (0.34 nm) and much larger pore size of 1.14 nm [122]. ZIF-8 has interesting characteristics which make it important for adsorption applications. First, it has high porosity and high surface area of 1300-1600 m^2/g. The structures of ZIF-8 are shown in Fig. 2-5.

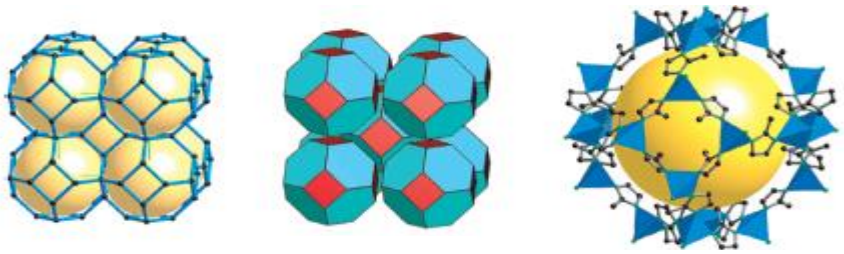

Fig. 2-5 The 3D molecular structures of ZIF-8 [118]

The chemical stability of ZIF-8 and ZIF-11 was investigated by immersing them in organic solvents (benzene and methanol) for 1-7 days at ambient temperature, 50℃ and at the boiling point of the solvents. These conditions were used to reflect the industrial chemical processes. The result of the experiments revealed that the crystal structures of ZIF-8 and ZIF-11 were not changed and they sustained their original structures. The experiment showed that both ZIF-8 and ZIF-11 maintained their structures even in water at 50℃ for 7 days. Nevertheless, ZIF-8 was the only material which was stable in boiling water and retained the original structure after 7 days while ZIF-11 structure was converted to another material after 3 days. Moreover, ZIF-8 was also stable in 0.1 and 8 M aqueous sodium hydroxide at 100℃ for up to 24 hours [118]. This proves the remarkable resistance of ZIF-8 among the metal organic framework solids. This behaviour could be explained based on two reasons. In the first place, the hydrophobic nature as well as surface structure of ZIFs repulses the water molecules. This prevents the water molecules to attack the ZnN4 units and inhibits the framework from dissolution. In the second place, the bond between imidazolate linker and Zn or Co atoms is very stable and strong. These unique features result in higher stability of ZIF-8 framework compared with the other MOF materials [118].

One major drawback about the usage of metal organic frameworks including ZIFs for adsorptive removal of some contaminants especially dyes from water is the small pore size with diameters in the micropore range. This results in the restriction of the amount of dye adsorption

in the framework [123]. Therefore, it is required to consider some solutions to overcome this obstacle. Some alternatives could be using approaches to increase the pore size and pore size distribution such as introducing pores in mesoporous range. Other alternatives could be producing some hybrid and composites with higher performance which can compensate for the small pore size of the MOF materials.

2.4.3. Nanoporous carbons derived from MOFs

Nanostructured porous carbon materials are very interesting because of their unique physical and chemical properties which makes them suitable to be used as sorbents in gas or liquid adsorption, catalyst support, electrodes and fuel cells [124-126]. Since these materials have affinity to organic contaminations, they have the potential to be used in environmental applications such as adsorptive removal of hazardous contaminants [127, 128]. These porous materials have high surface area and narrow pore size distribution as well as good thermal and chemical stability. The nanoporous carbons are produced by carbonization or chemical vapor deposition of carbon sources using the hard templates. They can also be made by carbonization of polymeric carbon gels using an organic-organic soft templating method [99]. Metal organic frameworks have been considered as alternative resources for the production of nanoporous carbons since they have diverse structures, as well as large pore volumes and high surface areas. Different kinds of MOFs including MOF-5, Al-PCP and ZIF-8 have been used to produce nanoporous carbons and demonstrated suitable properties in applications such as gas adsorption, sensing, catalysis and electrochemical capacitance [97, 99, 118, 129]. Since MOFs have large amount of carbon content, they can be converted to nanoporous carbons through direct carbonization without the need for any additional carbon source. Direct carbonization method is an easy and one-step procedure and has been utilized to convert Al-PCP to nanoporous carbon at 800℃. The study showed the obtained nanoporous carbon had very large

surface area of more than 5000 m^2/g and the large pore volume of 4.3 cm^3/g. It was concluded that the carbonization temperature was very important to reach the desired high surface area as well as large pore volume [130]. Fig. 2-6 illustrates the synthesis of nanoporous carbon derived from ZIF-8 via direct carbonization.

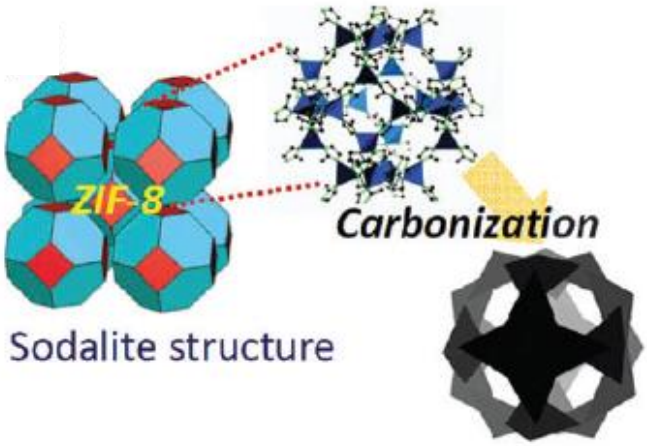

Fig. 2-6 Direct carbonization of ZIF-8 to nanoporous carbon [131]

The performance of different kinds of materials in adsorption applications extremely depends on the pore volume, pore size and pore structure. Some materials are resistant to modifications such as hydrothermal carbonization and therefore the produced carbonaceous network is non-porous exhibiting a low surface area. In particular, these materials lack micro-porosity which is an indication of high adsorption capacities. These materials need to be treated by traditional activation methods to increase the specific surface area and improve the pore volume. An example of these materials is crystalline cellulose and lignin of lignocellulosic biomass which are very resistant to hydrothermal carbonization conditions [132]. The study by Zhao et al. [133] shows that the pore volume and surface area of hydrothermally treated D-glucosamine was improved by employing traditional potassium hydroxide (KOH) activation method. These kinds of studies show that many materials which undergo heat treatment and carbonization cannot possess microporosity and high surface area after carbonization.

However, metal organic frameworks have been used for producing nanoporous carbons by one step and direct carbonization method without the need for further physical or chemical activation. The resulting nanoporous carbons had high porosity and high surface area as well as excellent performance in many applications particularly in water treatment. Moreover, most of the traditional methods used for the production of activated carbons or improvements of the pore volume and surface area of the adsorbents are multi-step and involve physical or chemical activations including surface functionalization. These multi-step methods require harsh temperatures as well as usage of harsh chemicals [134, 135].

High porosity is one of the characteristics of carbon materials. The pore structure in carbon materials needs to be controlled for different applications. Different aspects should be considered and controlled for the pore structures such as the amount and size of the pores as well as homogeneity in pore size and morphology [136]. A variety of techniques and methods have been utilized for creating pores and controlling the amount and size of the pores in carbon materials. Most of these approaches do not include activation process. Activation process has been employed for production of conventional activated carbon. Thus, since the activation method is not used for developing carbon materials, the produced carbons are called by the word “porous carbons” instead [136]. Pore structure in activated carbon and other carbon materials are controlled mainly by the precursor as well as preparation conditions including temperature, heating rate, residence time and atmosphere of carbonization process.

Direct carbonization is a very straight forward method for converting porous metal organic frameworks to nanoporous carbons by keeping the original morphology at the same time and making use of the original existed porous framework in the material matrix [137]. The important point in direct carbonization of MOFs and ZIFs is that the porous framework already exist and therefore there is no need for using a large amount of energy and harsh conditions for

creating the pores in the carbon material. The MOF material is converted to carbon and the original nano porous framework changes to a nano porous carbon framework. The pore size and pore structure also can be controlled by the carbonization temperature. This highlights the advantage of using metal organic framework as the source materials for producing nano porous carbons especially since the expensive traditional multi-step and harsh conditions are not required.

Michio [136] has reviewed different techniques for controlling the pore structures and the selection of specific carbon source materials (precursors) from the view point of porosity and the resultant carbons. Michio pointed out that the cost of the precursor would be an obstacle for industrial applications. The management of the by-products such as fluorine compounds and metal chlorides resulted from traditional activation and carbonization methods is an additional cost which should be considered. Also it is not easy to get highly porous carbon materials from any precursor. There are many precursors which do not give porous carbons in ordinary conditions and extra physical and chemical steps are required to convert them to porous carbons. For example, carbon foams can result in graphitized carbons but for creating micropores some additional steps are required [136]. However, it is very easy to get highly porous carbons from metal organic frameworks without the need for any additional complicated steps or expensive chemicals. The reason is the presence of unique and interesting exceptionally porous framework and large carbon content in MOFs and ZIFs which allows these materials to be used as efficient precursors for porous carbons. This is in particular very important in terms of costs for industrial applications.

Recently, Kim et al. [138] reported the direct carbonization of metal organic frameworks containing zinc atoms. They found out that even the non-porous MOF materials could give

highly nanoporous carbons. This is an interesting finding which shows the superior characteristics and performance of MOF materials in comparison with other compounds.

2.4.4. Fly ash waste materials

Among the porous materials, fly ash is of particular interest due to its local availability and low cost. Fly ash is a major solid waste which is produced from coal-firing power stations [139]. It is the waste product generated during the combustion of pulverized coal to generate electricity. Fly ash particles are taken away by the flue gases and is typically removed from the gas stream by utilizing electrostatic precipitators or bag filters to prevent the particles to enter the atmosphere. This waste material is made up of organic and inorganic components. There are a number of environmental risks in regard to fly ash disposal including air pollution, loss of arable land and the contamination of ground water due to the leaching of toxic and non-degradable metals and other chemicals from the ash dumps [140].

The amount of coal waste (fly ash) obtained from factories and thermal power plants, has been increasing in recent years and the disposal of large amount of fly ash has turned into a serious environmental issue.

The most important characteristics of fly ash are the calcium content that provides alkalinity in the system and increases pH to strongly alkaline values (roughly 12) and the (SiO_2+Al_2O_3+Fe_2O_3) content [59].

Fly ash has been used in many applications such as cementitious (concrete and cement) products [141, 142]. It has been utilized widely in road construction, cement production and zeolite synthesis [143, 144] and has been investigated for adsorption application in particular removal of pollutants from water [57, 59, 64, 65, 68, 145-151].

2.4.4.1 Physical and chemical properties of fly ash

The mineralogy, physical and chemical properties of coal fly ash depend on the nature and properties of the parent coal and conditions under which they are produced. The composition and properties of fly ash can also vary significantly depending on the boiler type and the gas emission control system. These properties together determine the usefulness of fly ash in different applications [152].

a) Physical properties

Coal fly ash contains very fine particles which have average diameter < 10 μm, aggregated into spherical particles of 0.01-100 μm sizes which are hallow spheres (cenospheres) filled with smaller amorphous particles or crystals (pelospheres). These cenospheres make fly ash particles easily airborne. Due to the small size of fly ash particles, fly ash has a large specific surface area which ranges from 2500 to 4000 cm^2/g reported in literature [152]. Consequently, fly ash has a high adsorption capacity. As a result, it could be used as a sorbent in air and water treatment to remove contaminants like NOx, sulphur compounds and toluene vapours from air and toxic metal ions like Cu, Pb, Cd, Ni, Zn, Cr, Hg and As, as well as inorganic anions such as fluoride and boron from waste water [152].

b) Chemical properties

The chemical characteristics of coal fly ash mainly depend on geological factors related to the coal deposits and on different operating conditions which are utilized at the power plants. Hence, fly ash from every coal-fired plant has its own chemical characteristics. The main components of fly ash are silica, alumina and iron oxides with varying amount of carbon, calcium, magnesium and sulphur [152].

2.4.4.2 Types of fly ash

Coal fly ashes (CFAs) are normally classified into two classes, i.e. class F produced from anthracite, bituminous and sub-bituminous coals containing less than 7% CaO, and class C which is obtained from lignite coal containing more liming material up to 30%. The pH of CFA is in the range of 4.5 and 13.25 depending on the sulphur (S) and CaO contents of the coal source. CFAs obtained from coals having large amount of anthracite which typically contain high amount of sulphur are acidic while those produced from lignite which are usually lower in sulphur and higher in calcium are alkaline [152].

2.4.4.3 Victorian brown coal fly ash

Every year, 50×10^9 kg of low rank brown coal is mined from the Latrobe Valley region of Victoria for the production of electricity in four main generating complexes. These include the Hazelwood (1600 MWe), Yallourn (1450 MWe), Loy Yang Power (2000 MWe) and Edison Mission Energy facilities (1000 MWe, part of the Loy Yang complex). This results in the production of over 550×10^6 kg of solid wastes per year, which is composed mostly of precipitator (fly) ash, partially burnt coal particles (char), furnace (bottom) ash, salts, sand and clay minerals. At present, the ash obtained in the power plants is mixed with water and transported to an ash disposal pond in high water-to-ash ratio slurry. Nevertheless, the ash disposal ponds have limited capacity and there are restrictions about the possibility of expanding the storage capacity or establishing new facilities [153]. The constituents that form ash in brown coal are mainly inorganic cations such as magnesium, sodium and calcium, which convert into fly ash during the combustion process [154].

a) Victorian brown coal ash mineralogy and characterization

There are physical and chemical differences between the ashes produced at Loy Yang, Hazelwood and Yallourn due to the change in coal properties between the sites and the

difference in operation. The main minerals contributing to the ash formation that have been identified in Latrobe Valley ashes include thenardite (Na_2SO_4), halite (NaCl), periclase (MgO), haematite (Fe_2O_3), magnetite (Fe_3O_4), lime (CaO), anhydrite ($CaSO_4$), alpha-quartz (α-SiO_2), alumina (Al_2O_3) and slight variations of calcium and magnesium species. Other minerals which have been determined at the Hazelwood complex in ash pond include gypsum ($CaSO_4.2H_2O$) and calcite ($CaCO_3$, formed from exposure to carbon dioxide in the atmosphere) [153]. Table 2-2 shows the analysis of some Victorian coal fly ashes.

Table 2-2 Comparison of Latrobe Valley brown coal ashes in 2000 (wt%) [153]

Species	Loy Yang	Yallourn	Hazelwood
SiO_2	60.4	1.4	6.6
Al_2O_3	13.3	2.1	1.8
Fe_2O_3	8.5	24.5	8.7
TiO_2	1.7	0.1	0.2
K_2O	1.2	0.4	0.4
MgO	2.2	18	18.8
Na_2O	2.1	11	4.5
CaO	1.0	12.3	28.4
SO_3	3.4	21.7	15.6
Cl	<0.1	<0.1	3.4

There have been some detailed reports of trace metals in Latrobe Valley ashes. However, due to the strong alkalinity of Latrobe Valley ash effluents, solubility of most metals in the leachate is limited. It is worth noting that all power stations have a moderate to strongly alkaline ash disposal system [153]. As mentioned above, the coal fly ash generated in power stations is alkaline as a result of some soluble basic oxides such as CaO and MgO. Therefore, Coal fly ash has potential to act as sinks for toxic metals due to the soluble basic oxides (CaO and MgO) content [155].

b) Weathered fly ash

Natural weathering occurs at coal power plants ash ponds through processes such as carbonation, dissolution, co-precipitation and fluid transport mechanisms which are responsible for long-term chemical, physical and geochemical changes in the ash. From mineralogical point of view, fresh ash is made up of quartz, mullite, hematite (Fe_2O_3), magnetite (Fe_3O_4) and lime while weathered and carbonated ashes are composed of additional phases such as calcite and aragonite[1] [156]. The huge amount of fly ash that is disposed cannot be separated from nature's weathering cycle since the fly ash dumps are exposed to ash disposal water, air and rainfall. The weathering of fly ash results in changes in the physical, chemical and mineralogical properties such as the formation of secondary mineral phases, decrease in the pH and electrical conductivity of the pore water in fly ash and reduction of soluble salt content. Understanding the changes in the chemical, physical, morphological properties and phase transformation of fly ash is necessary in predicting the environmental impact associated with fly ash disposal [140]. Considering the fact that wreathing of fly ash is unavoidable, reusing the weathered fly ash could be a sophisticated option to overcome the environmental issues related to these waste materials.

2.4.4.4 The usage of fly ash waste materials in water treatment

Fly ash materials have been used for the removal of inorganic and organic pollutants such as cesium, strontium, organic-basic, organic-acidic and organic reactive dyes [151, 157-160]. The acid-base properties of fly ash were found to be suitable for the removal of heavy metals such as nickel, cadmium, chromium, lead, copper, mercury and zinc from industrial wastewaters (e.g. electroplating and battery manufacture). The ionic bonding in the major

[1] calcite and aragonite are two crystal forms of calcium carbonate ($CaCO_3$)

components of fly ash (Al_2O_3 and SiO_2) causes electronegativity to attract polar molecules such as phenols. This suggests a major reuse option for fly ash, since traditional disinfection of industrial wastewaters by chlorination may produce chlorophenols if phenol is present in the water [142]. Additionally, several studies reported that significant amounts of heavy metals were removed from polluted solutions by adsorption on fly ash [161]. A lot of research work has been done for effective removal of toxic metals [59, 60, 161-167] and organic materials from aqueous solutions using fly ash [57, 59, 64, 65, 68, 145-151]. The most important characteristics of fly ash are the calcium content that provides alkalinity in the system and increases pH to strongly alkaline values (roughly 12) and the (SiO_2+Al_2O_3+Fe_2O_3) content [59]. Fly ash has been used for adsorption application in particular for water and wastewater treatment. Maria Visa et al. investigated the potential adsorption capacity of fly ash for simultaneous adsorption of dyes and heavy metals. They proved that fly ash modified with NaOH was capable of adsorbing both dyes and heavy metals [57, 168]. Moreover, many researchers have studied the adsorption of heavy metals using fly ash [59, 60, 162, 163]. Some researchers have tried to produce mesoporous fly ash by heat treatment for adsorption of heavy metals [169].

2.4.5. General adsorption mechanisms regarding MOFs

The adsorption mechanisms on metal organic frameworks is similar to the general adsorption mechanisms over the common traditional adsorbents except that MOFs have open metal sites which might act as an extra adsorption mechanism. In this section the common adsorption mechanisms are explained with specific focus on metal organic frameworks.

The adsorption process proceeds through various mechanisms including electrostatic interactions, acid-base interactions, hydrogen bonding, π-π interactions and hydrophobic interactions. It also possible that multiple interactions occur at the same time.

The overview of different adsorption mechanism for the removal of hazardous pollutants over metal organic framework is shown in Fig. 2-7.

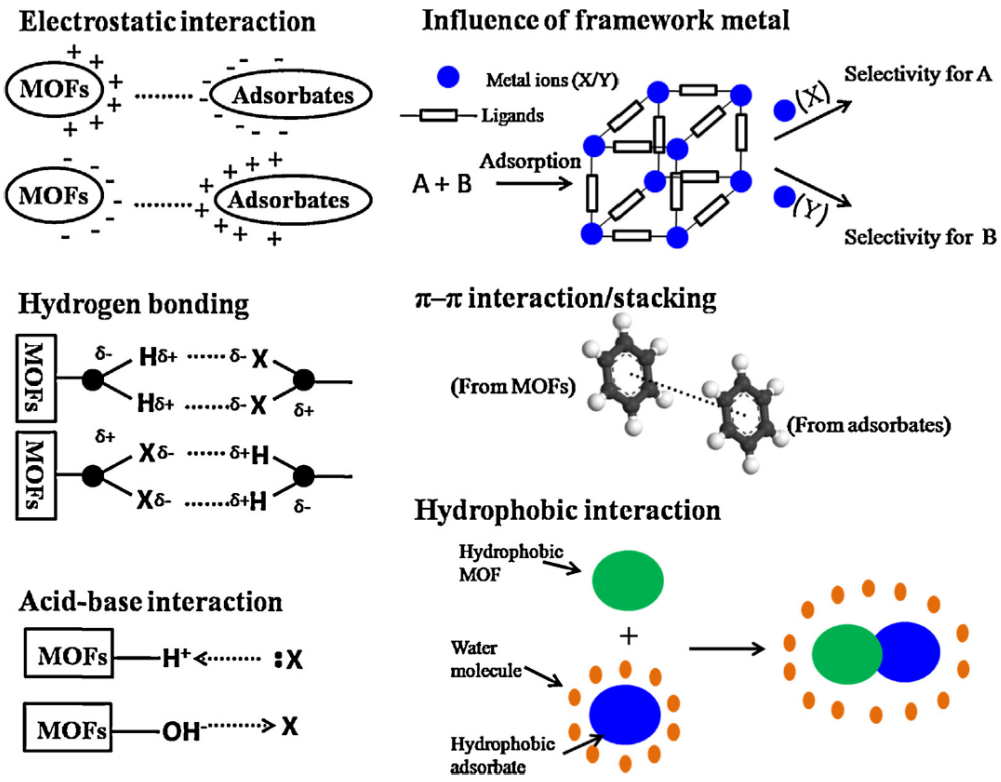

Fig. 2-7 Various adsorption mechanisms for adsorption of contaminates over MOFs [170]

2.4.5.1 Electrostatic interactions

Electrostatic interactions is the most common pathway of adsorptive removal of contaminants from water. The surface charge of an adsorbent exists at the interface when the adsorbent comes into contact with a polar environment such as water. The surface charge of the adsorbents can change with pH in water [170]. Haque and co-workers [171] studied the adsorption of methyl orange (anionic dye) over Chromium based MOFs, MIL-101-Cr and MIL-53-Cr. It was observed that MIL-101-Cr had better adsorption performance compared with MIL-53-Cr which shows the porosity and pore size distribution play a very important role in adsorption. Nevertheless, by functionalizing MIL-101-Cr through grafting by ethylene diamine

(ED) and then protonating ED (resulting in PED), higher adsorption capacity was observed despite the slight reduction of porosity and pore size after grafting. The reason for greater adsorption was due to inducing positive charge into the adsorbent material which increases the capability of adsorbent for uptaking negatively charged molecules like methyl orange. Methyl orange has a molecular structure in the sulfate form and it can interact and bond with positively charged adsorbents. The schematic of electrostatic interaction is shown in Fig. 2-8 which shows the adsorption performance sequence as MIL-101-Cr < ED-MIL-101-Cr < PED-MIL-101-Cr [171].

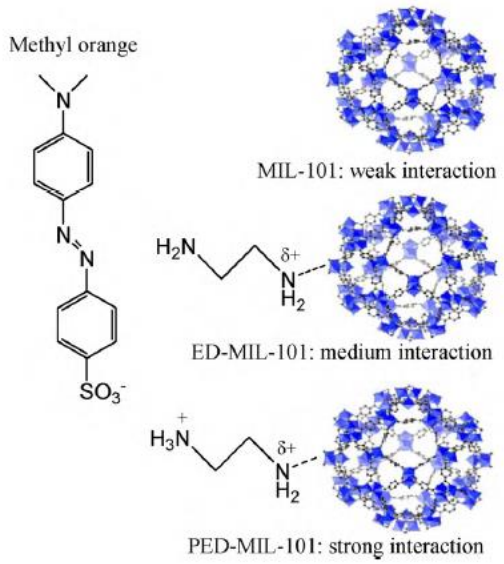

Fig. 2-8 Electrostatic interaction between methyl orange and adsorbent (MIL-101) [171]

In another study by Lin et al. [172] the adsorption of methylene blue on Cu-BTC was investigated. It was reported that pH of the solution had significant effect on the electrostatic interactions between the methylene blue molecules and adsorbent. It was shown that increasing the pH above the point of zero charge (pH at which the surface charge of the adsorbent is zero) resulted in introducing negative charges on the adsorbent. This increase in the surface negative charge, produced a favourable electrostatic interactions between negatively charged Cu-BTC and positively charged MB molecules leading to higher adsorption capacity.

2.4.5.2 Hydrogen bonding

Hydrogen bonding is another adsorption mechanism which happens in the adsorption of pollutants particularly for organic compounds on the adsorbents. The adsorption of phenol and p-nitrophenol (PNP) on different metal organic framework materials (MIL-100-Fe, Cr and NH_2-MIL-101-Al) from water has been investigated and the results showed low adsorption capacity of these MOFs for adsorption of phenol. However, NH_2-MIL-101-Al exhibited very high adsorption performance of PNP with 4.3 and 1.9 times higher than capacities of MIL-100-Fe and MIL-100-Cr, respectively [173]. This high affinity of NH_2-MIL-101-Al towards PNP was addressed to the hydrogen bonding between PNP and the amino groups in NH_2-MIL-101-Al as illustrated in Fig. 2-9.

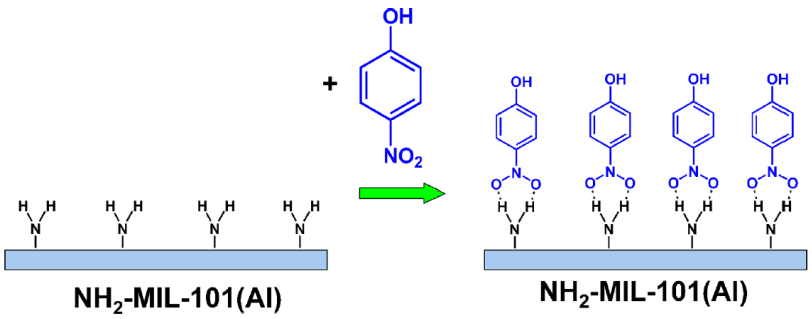

Fig. 2-9 Adsorption mechanism of PNP on NH_2-MIL-101-Al through hydrogen bonding [173]

2.4.5.3 Acid base interaction

Although acid-base interaction mechanism is not observed very often in adsorption of contaminants form water, there are some studies reporting this mechanism. For example, Khan et el. [174] studied the adsorption of phthalic acid (H_2-PA) from aqueous solution on ZIF-8 and different MOFs such as MIL-53-Cr, MIL100-Cr, NH_2-MIL-100-Cr, UiO-66 and NH_2-UiO-66. The results of the study revealed the MOF adsorbents functionalized with $–NH_2$ functional group showed higher adsorption for H_2-PA especially at low pH compared with MOFs without amino groups. It is worth noting that H_2-PA did not deprotonate at low pH. Therefore, acid-

base interactions between the basic sites (N^- functions of ZIF-8 or $-NH_2$ of amino groups in MOFs) and acidic phthalic acid molecule becomes the main parameter affecting the adsorption [170, 174] as shown in Fig. 2-10.

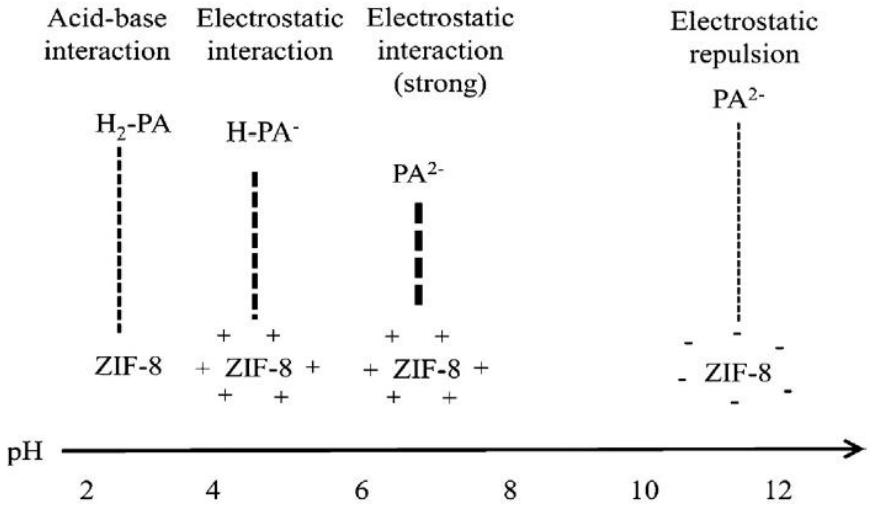

Fig. 2-10 Adsorption mechanism of phthalic acid over MOFs [174]

2.4.5.4 Effect of metal in the framework of MOFs

There are a few reports regarding the influence of metal ions in MOFs for dye adsorption from aqueous media. For instance, Tong and co-workers [175] reported the adsorption of MO and MB dyes on MIL-100-Fe and MIL-100-Cr. They observed that despite having similar surface areas and pore volumes, these two adsorbents show different behaviour for adsorption of dyes. MIL-100-Fe exhibited much higher adsorption capacity in comparison with MIL-100-Cr which was attributed to the greater bonding energy of water molecules with metal centers of MIL-100-Cr. This results in competitive adsorption of MO and water and the adsorption of water restricts the cages of MIL-100-Cr for adsorption of MO. However, for the adsorption of methylene blue, both MOF materials exhibited high adsorption due to electrostatic interactions between positively charged MB and negatively charged MOF materials.

2.4.5.5 π-π interactions

This mechanism is mostly observed for the removal of aromatic compounds from water. Qin et al. [176] reported adsorption of bisphenol-A (BPA) on MIL-101-Cr and MIL-100-Fe. It was shown MIL-101-Cr exhibited the highest adsorption capacity for BPA and it was suggested that the π-π interactions between the benzene rings of bisphenol-A and MIL-101 was the main adsorption mechanism in addition to partial hydrogen bonding. Other studies have reported this π-π interactions as the main adsorption mechanism for the adsorptive removal of malachite green using MIL-100-Fe [177] and for the adsorption of bisphenol-A on MIL-53 [178].

2.4.5.6 Hydrophobic interactions

This mechanism usually occurs for the adsorption of organic molecules from aqueous solution. Metal organic frameworks have been utilized for oil spilled clean-up as well as demusification of oil droplets. Yang et al. [179] investigated the fluoros MOF (FMOF-1) for oil spill clean-up. This MOF material is highly hydrophobic which is due to the perfluorinated inner surface. This hydrophobicity leads to hydrophobic interactions between FMOF-1 and the non-polar hydrocarbon adsorbates.

Lin et al. [180] also reported adsorption of soybean oil and demusification of oil droplets from water and the mechanism was attributed to the hydrophobic interaction as well as electrostatic interactions as it is shown in Fig. 2-11.

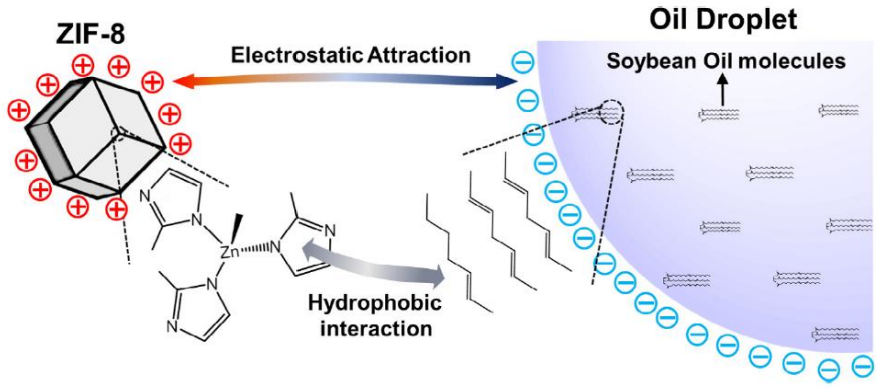

Fig. 2-11 Mechanisms of oil removal by ZIF-8 adsorbent [180]

2.4.6. Adsorptive removal of organic pollutants from water

Soluble and insoluble organic contaminants can be eliminated by adsorption technique. Adsorption has been used to remove many different organic pollutants from contaminated waters. The organic pollutants can be hydrocarbons, oils, dyes, pharmaceuticals, detergents, fertilizers, pesticides etc. Organic contaminants have general characteristics including the presence of cyclic aromatic or aliphatic rings as well as halogen substitutions which is typically chlorine [181]. Oil droplets and dyes are among the most important organic pollutants to be removed from the bodies of water. The adsorption of these organic contaminants have been in the focus of many researchers and different porous materials have been investigated for adsorptive removal of oils and dyes including activated carbons, different nanoporous carbons from a variety of sources like metal organic frameworks, MOFs and ZIFs, natural and low cost adsorbents like fly ash waste materials.

2.4.6.1 Adsorption of organic contaminants from water using MOFs

A variety of modified and unmodified MOFs have been investigated for the removal of different kinds of organic compounds from water. The important parameters affecting the adsorption over metal organic framework adsorbents are including the pore structure, open metal sites and charge interaction between the adsorbate and adsorbent [14]. MIL-100 (Fe) and

MIL-101 (Cr) were studied for the removal of naproxen and clofibric acid. The study showed these adsorbents can effectively uptake the organic contaminants from water and exhibited superior capacity compared with activated carbon [182].

In a recent work, Jinag and co-workers [122] studied the adsorption of benzotriazoles on ZIF-8 and found out the adsorption is very fast and high adsorption of capacity of the pollutant compounds was achieved. Nazmul and co-workers [174] also reported the removal of phthalic acid and diethyl phthalate from water using ZIF-8. It was revealed that ZIF-8 adsorbs phthalic acid significantly. This high adsorption uptake was attributed to electrostatic interaction between ZIF-8 (having a positively charged surface) and negatively charged phthalic acid molecules at high pH. Also it was explained that another possible reason could be addressed to the acid-base interactions between the basic sites (N^- functional groups) and OH group of the imidazolate ring of ZIF-8.

MIL-100 (Fe) was reported for the adsorption of malachite green (MG) and it was found that the open metal sites were the active species for interaction with malachite green because of the interaction between the Lewis base-$N(CH_3)_2$ in MG and Lewis acid of MIL-100(Fe). It was also proposed that the π-π interaction between the benzene rings in MG and MIL-100(Fe) is effective in the adsorption process [177]. A hierarchically mesostructured MIL-101(Cr) was synthesized by cetyltrimethylammonium bromide (CTAB) as a surfactant and it was shown that the prepared material adsorbed methylene blue dye quickly [183]. Haque et al. studied the adsorption of methylene blue and methyl orange by MOF-235. The adsorption capacities were reported as 187 and 477 mg/g for MB and MO uptake respectively [184]. Recently, Lin and Chang [185] investigated the adsorption properties of ZIF-67 for the adsorption of malachite green (MG) from water. Their study showed ZIF-67 had the ultrahigh adsorption capacity of

2430 mg/g for MG removal. They suggested the high sorption capacity was probably due to π-π interactions between MG and ZIF-67.

Hydrophobic metal organic frameworks also have been used for oil spill clean-up. Yang et al. [179] investigated the oil sorption properties of the fluorous MOF (FMOF-1 constructed from silver (1) 3,5-bis(trifluoromethyl)-1,2,4-triazolate) to remove oil spill from the surface of water. This MOF is exceptionally hydrophobic due to perfluorinated inner surface. Another study shows that soybean oil droplets can be removed from the water surface using Cu-BTC metal organic framework. The high adsorption was addressed to the interactions the soybean oil and benzene rings in Cu-BTC [186]. Another study by Lin et al. [180] reveals the oil sorption capability of ZIF-8 for demusification of oil-in-water emulsions. The results of their investigations shows that ZIF-8 is a promising adsorbent for removal of emulsified oil droplets from water.

2.4.6.2 Adsorption of organic pollutants from water by nanoporous carbons

Nanoporous carbon from different sources have been investigated for the removal of organic compounds including dyes from water. Sangjin et al. [187] developed a nanoporous carbon material using silica sol particles as templates which exhibited faster and greater adsorption of humic acid molecules compared with commercial activated carbons. Also Susan and co-workers [188] investigated the adsorption properties and porous characteristics of activated carbons and activated carbon/poly vinyl alcohol composites for the removal of cationic and anionic dyes. They reported that the interaction of dyes with porous activated carbons depends on two factors. First, the interaction is associated with the properties of dyes such as molecular size, charge sign and value as well as the symmetry of molecule. Second, it is related to the nature of the carbon surface as well as structural and textural characteristics. Nitrogen, oxygen and hydrogen atoms provide dispersion, electrostatic and hydrogen bonding

of adsorption complexes to heterogeneous surface of carbon materials [189-191]. These bonding depend on the properties of the solvent molecules [192, 193].

Ghaedi et al. [194] reported the synthesis of activated carbon loaded with silver nano particles which showed the adsorption capacity of 34.5 mg/g for the removal of methylene blue form water.

Faria et al. [195] investigated the adsorption of anionic and cationic dyes on activated carbons and reported that the adsorption of reactive and acid dyes is associated with the surface basicity of adsorbents. They revealed that the interaction between oxygen free Lewis basic sites and the free electron of dye molecules in addition to the electrostatic interactions between the protonated sites and anions play the main role in adsorption mechanism.

Activated carbon has been widely used for the removal of organic pollutants especially dyes from water [49, 73, 196-198]. For example, Hameed and Daud [199] studied the adsorption of a basic dye on activated carbon derived from agricultural waste. The activated carbon showed maximum adsorption capacity of 227.27 mg/g. In spite of the usefulness of activated carbon as an effective adsorbent for heavy metals, the high cost of activated carbon and the difficulty of its regeneration has limited its more predominant use.

However, there are very few reports in literature addressing the adsorption of organic contaminants including dyes over nanoporous carbon derived from metal organic framework materials. Torad and co-workers [127] synthesized a magnetic nanoporous carbon metal organic framework without the usage of any extra precursor by one step carbonization for the removal of methylene blue from water. In their study, the metal organic framework ZIF-67 was carbonized at 600 and 800℃ and showed high adsorption capacity of 302.1 and 502.5 mg/g for MB removal respectively. However, higher temperatures were not investigated in this work.

Xiao et al. [200] synthesized magnetic porous carbons from MIL-100(Fe) using a second precursor of furfuryl alcohol via microwave-enhanced high temperature ionothermal method. The resulting magnetic carbon exhibited adsorption capacity of 303.95 mg/g for the removal of methylene blue form aqueous solution. This synthesis method required an expensive microwave irradiation along with the usage of an extra carbon precursor. In another study by Caina and co-workers [201] a nanoporous carbon was produced from MOF-5 and the magnetic property was introduced using chemical co-precipitation of iron ions on the resulting nanoporous carbon. The resulting magnetic porous carbon showed the maximum adsorption capacity of 292.4 mg/g. Recent works have been done for carbonization of ZIF-8 at 800℃ [202] and the porous carbon showed low adsorption capacities of 59 mg/g for the adsorption of methylene blue form water. Furthermore, in this work higher temperatures were not tested. Therefore, it seems in literature, temperatures higher than 800℃ have not been tried and the effect of temperatures on adsorption capacity as well as textural properties of MOF adsorbents has not been investigated.

2.4.6.3 Adsorption of pollutants by low cost fly ash wastes

Coal fly ash has been extensively investigated for the adsorption of organic pollutants especially dyes as well as heavy metals from water [141, 158, 203, 204]. However, most of the fly ash reported in literature have low surface areas and exhibit low adsorption capacities for the removal of water contaminants. Adsorption performance of fly ash highly depends on the characteristics of the original coal and the treatment method used for the activation. Generally, raw fly ash has low adsorption capacity and modification of fly ash would enhance its adsorption capacity [141]. Moreover, elemental chemical composition of fly ash is highly variable. The variability is directly related to the source of the coal, its pre-treatment, and the operation of the plant burning the coal [205]. The majority of fly ash reported so far for the

adsorption of pollutants have low lime content which is not suitable for neutralizing acidic wastewaters. Furthermore, majority of these fly ash materials do not show any magnetic properties.

Victorian brown coal fly ash has unique physicochemical properties such as high surface area, porous framework, high lime content and magnetic properties which is quite different from other coal fly ashes and makes it an interesting adsorbent for a variety of applications such as water treatment especially neutralizing acidic mining wastewaters. There is no report in the literature regarding the characteristics and adsorption properties of Victorian brown coal fly ash in adsorptive removal of contaminants from water. Therefore, it is very essential to explore the adsorptive properties of this locally available, abundant and free waste material for further practical applications. It is worth noting that the weathering process is a low cost modification method which could be utilized for modifying the textural and adsorption properties of fly ash. The current literature lacks the investigation about the effect of weathering on physicochemical and adsorption properties of fly ash materials. Therefore, to make use of this local waste material, it is important to investigate the applicability of Victorian brown coal fly ash for water treatment purposes.

2.5. MOF shaping for adsorption applications

Shaping metal organic framework powders into macroscopic bodies is of great importance especially in regard to practical applications such as adsorption, separation and catalysis [206-208]. The resulting shaped MOFs need to have good properties such as high porosity and surface area, crystallinity and suitable performance similar to the original MOF powder [209]. Therefore, it is very important to select an appropriate shaping method which is simple and effective and at the same time preserves the MOF's unique characteristics. Some common

techniques for preparation of the shaped catalysts and adsorbents are pressing, extrusion, granulation and spray drying as well as casting and coating can also be employed for preparing the shaped MOFs in the forms of monoliths, granules, pellets and tablets [210-212]. But the challenge is that the prepared shaped MOFs need to have enough mechanical and chemical stability with the original powder's characteristics and properties.

For shaping the porous materials, a general methodology is to mix the porous powder with inorganic and organic additives, shape the powder to the required form and finally eliminating the additives by thermal treatment to obtain a mechanically strong framework [213]. Nevertheless, most of metal organic frameworks suffer from poor mechanical robustness under high pressure conditions as it is reported in Table 2-3.

Table 2-3 Mechanical strength of MOFs, zeolites and ceramics [213]

MOF	Hardness/shear stability (GPa)	Mechanical strength
ZIFs(Zn)	0.2-1.1	Weak
ZIF-8(Zn)	0.94-1.4	Weak
MOF-5(Zn)	1.16	Weak
HKUST(Cu)	1.04	Weak
UiO-67(Zr)	5.69	Medium
UiO-68(Zr)	4.18	Medium
UiO-66(Zr)	13.75	High
Zeolites	1-10	Medium to high
Ceramics	>10	High

Therefore, exposing MOF materials to pressures can often result in a collapse of their pore structures or amorphization which is significant loss of their crystallinity. Moreover, MOF materials are not thermally stable at high temperatures, therefore, they cannot be exposed to high temperatures for the removal of the additives and binders [214].

Copper (II)-benzene-1,3,5-tricarboxylate (Cu-BTC) in the form of spherical granules has been prepared by granulation shaping method. The Cu-BTC spheres were obtained with the size range of between 1 and 3 mm [215]. Also, Zr-MOF powders have been shaped into spheres with diameters of 0.5-15 mm with the usage of sucrose as a binder [216]. However, the Zr-MOF spheres showed 50% decrease in the BET surface area and pore volume which was probably due to pore blocking with the binder molecules. Therefore, with the granulation method we cannot get spheres with equal sizes or appropriate properties. In shaping MOF powders, it is very important to get spheres with equal and uniform size in terms of practical applications.

Moreover, for preparing MOF shapes with granulation process, many parameters must be controlled regarding the formulation as well as the equipment. The reason for this can be addressed to the limitation of granulation method which is due to the balance of collision stress applied to granules relative to the fracture stress of MOF materials. MOF granules take the collision stress and this results in agglomeration or breakage of spheres [213]. Thus, granulation cannot be a good option for shaping MOF materials especially for practical applications.

Spray drying is another method for producing MOF bodies for industrial products such as catalysts and adsorbents. This method can be utilized for the production of small particles in micrometre range to large particles in millimetre range. However, the millimetre-sized droplets might not be free-flowing because of the existence of large particles or powders [213]. Additives and binders are added to the feed liquid in this process which may cause problems during the process since they increase the viscosity of suspensions. Also, the interaction between the additives and MOF materials is very complicated and therefore the general design rules do not apply. The use of spray drying technology for shaping MOFs is more complex compared with other common materials [213]. Hence, this method cannot be considered as a

simple and straight forward approach since many complicated procedures and controlling parameters need to be applied.

Extrusion is another technique which has been used for shaping MOF powders. Crawford et al. [217] have utilized extrusion method to shape Cu-BTC into monoliths with millimetre sizes. The problem with this method is that the formed bodies are not uniform and not resistant to abrasion in comparison with pressed shapes. The mixture paste (mixture of MOF, additive and solvent) must have special characteristics including plasticity to enable the paste to be extruded and at the same time, exhibit cohesion to avoid creation of surface and bulk defects [213].

Pressing strategy includes compressing and pelleting the powders. The resulting pellets or tablets have high mechanical strength. For pressing MOF materials, the quality of pellets depends on the mechanical property of MOF powders. The deformation characteristics of MOF powders have a significant effect on the pressing process. It is noteworthy that the main factor which controls the properties of the resulting shaped bodies (pellets) is the response of MOF material to the pressure [218-220]. The problem with this method is that the crystalline structure of MOF changes after pressing and it gets close to an amorphous structure. Tagliabue et al. [221] investigated the adsorption performance of CPO-27(Ni) pellets without the usage of binder. Their study revealed that after pressing the sample at 1 GPa, the color of sample changes from yellow to dark brown. It was shown that the crystalline structure was lost which was due to breakdown of the MOF structure.

Bazer-Bachi et al. [222] prepared tablets of several MOFs and ZIF-8 using direct compression and investigated the impact of compression on gas adsorption and catalytic properties of MOF materials. Nevertheless, the results of the study showed these materials undergo amorphization depending on the amount of pressure applied and the nature of material.

Therefore, since this method affects the crystallinity of these materials, the properties and performances of MOFs may be affected and hence this is not a suitable approach. In particular, since only very few MOFs such as NH_2-MIL-53(In) show amorphization resistance [223, 224], the direct compression cannot be considered a general and universal strategy for shaping MOFs. Other strategies include in situ growth of MOFs on porous substrates such as silica and aerogel using methods like seeding growth and layer by layer deposition [225, 226] which requires several steps.

2.5.1. Phase inversion

Phase inversion method was first developed by Loeb and Sourirajan [227] in 1960s for the production of asymmetric reverse osmosis membranes. The formation of membrane through phase inversion method can be summarized as a three component system with usage of non-solvent, solvent and polymer. During the phase inversion process, a polymeric solution comes into contact with a non-solvent such as water. The non-solvent diffuses into the polymer while the solvent diffuses into the non-solvent bath. Since the diffusion coefficient of polymer is much lower, the movement of the polymer molecules would be restricted to short distances [228]. The exchange of the solvent and non-solvent during phase inversion results in changes in the stability of polymer solution. The polymer solution stability state changes from thermodynamically stable to a metastable or unstable. The liquid-liquid demixing occurs in solution. The solvent is replaced by non-solvent and this leads to the solidification of polymer phase which eventually results in the formation of asymmetric membrane structure [229].

Porous membranes via phase inversion method can be synthesized almost from any polymer which is soluble in a suitable solvent and can be precipitated in a non-solvent. By changing different parameters such as polymer concentration, the precipitation medium and the temperature of precipitation, porous membrane with a wide range of pore sizes in the range of

0.1 to more than 20 μm with different chemical and mechanical properties can be prepared. Nowadays, phase inversion is considered the most important technique for producing porous structures. Porous phase inversion membranes typically show a high affinity for adsorption due to their extremely large internal surface. Therefore, the porous structures prepared by phase inversion method are specifically appropriate for complete removal of pollutants such as viruses and bacteria [229].

Fig. 2-12 illustrates the schematic and mechanism of phase inversion process and the cross section structure of hollow fiber membranes produced using this method by Jianfeng et al [230]. A polymer solution is pumped through the spinneret into the water bath and the hollow fiber membrane is formed in the coagulation bath by phase inversion. The cross section SEM images illustrates how a porous framework is formed during the solvent exchange and solvent/non-solvent diffusion.

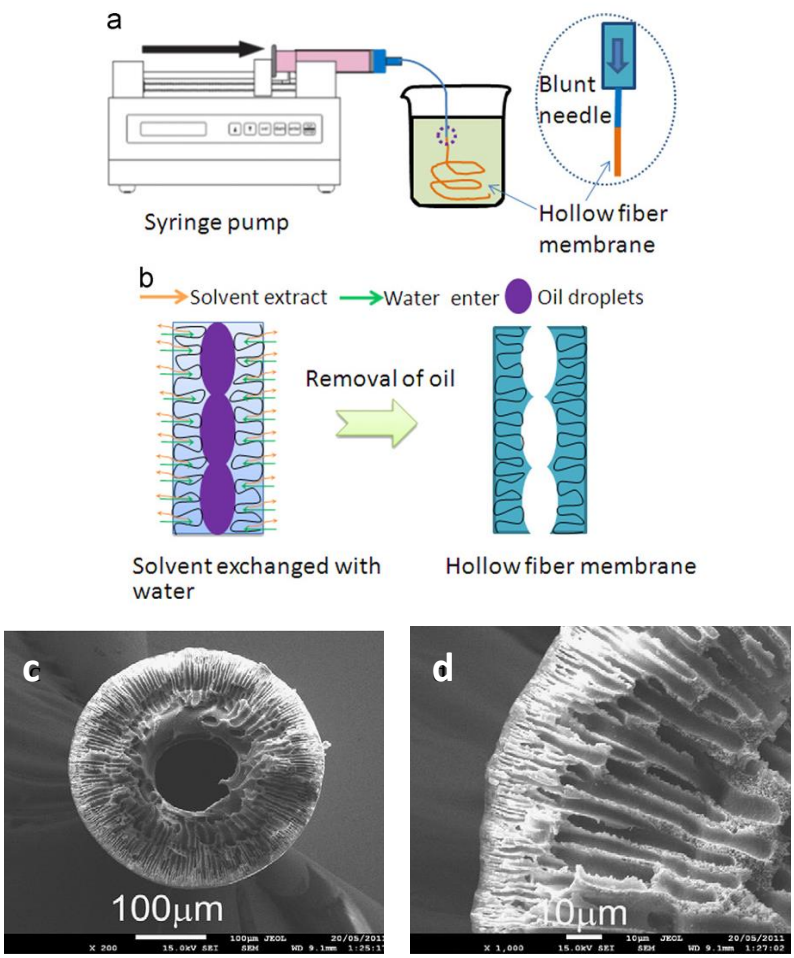

Fig. 2-12 Schematic of phase inversion process for hollow fiber membrane using a syringe tip (a), formation mechanism of hollow fiber membrane (b) and SEM images of cross section of polysulfone hollow fiber membranes (c and d) [230]

2.5.2. Formation of beads via phase inversion technique

Phase inversion method can also be employed for producing spheres and beads for many applications in particular adsorption. The mechanism and principles of beads formation using phase inversion technique is similar to that of hollow fiber membrane formation. To prepare the beads, the spinneret is placed above the non-solvent (water) bath with specified air gap which allows the polymer solution to fall into the bath with a suitable gravity. The polymer droplets resulting from the syringe, solidify as soon as they touch the non-solvent (water) and sink to the bottom of water bath. The beads/spheres prepared this way have similar structures to the hollow fiber membranes. The top of the spheres consists of a thin dense layer while the

inside shows a porous structure. The structure of membranes and spheres are affected by different parameters including choice of polymer, selection of solvent and non-solvent, gelation, crystallization behaviour of polymer, location of the demixing gap and temperature of the bath. Changing one or more of these factors can result in a various membrane/sphere structure from very open porous form to a very dense nonporous framework structure [231].

In case of preparation of spheres using this strategy, density and viscosity of polymer solution also play an important role in controlling the shape of beads. Density and viscosity of the polymer solution depends on the choice and the ratio of polymer/solvent. If the viscosity is high, the resulting beads have elongated shapes (instead of spheres) in contact with non-solvent (water) bath. Then the porosity of the spheres structure will be influenced as well which in fact results in different performance and behaviour of spheres for adsorption and separation.

Another important factor which affects the shape, structure and performance of the spheres is the air gap (distance) between the syringe tip and the surface of water. A long distance results in generation of defects resulting from gravity and elongational stresses [232]. There are some studies about the effect of air gap on the fabrication of hollow fiber membranes [233-235]. Widjojo et al. [235] reported that the number of inward-pointed macrovoids increases as the air gap distance increases and at the same time the number of outward-pointed macrovoids decreases.

The spinneret annulus gap (syringe tip size) is another factor affecting the shape, morphology and behaviour of the spheres. Widjojo and co-workers [235] pointed out that by changing the annulus gap from 0.05 to 0.25 mm, the inward-pointed macrovoids are created marginally with an increase in annulus gap. However, with larger spinneret annulus from 0.35 to 0.55 mm, both inward and outward-pointed macrovoids are created.

2.6. Conclusion and perspectives

In summary, adsorption has many advantages over other traditional water treatment methods since it provides an easy to operate, environmentally friendly and energy efficient alternative approach for the removal of hazardous contaminants from waste waters. Porous materials have interesting characteristics such as high porosity and high surface areas for many applications specifically in adsorption and water treatment. ZIFs are particularly interesting for adsorption applications because of high porosity and large carbon content. The review of the recent research shed some light on the progress achieved in the area of adsorptive removal of different contaminants from water by MOFs and ZIFs.

Nevertheless, there are still challenges regarding the application of these materials for adsorption. One challenge could be addressed to the fact that MOFs and ZIFs are generally prepared as powders which are not suitable for many practical applications including adsorption and catalysis. Therefore, shaping these materials is required for easy handling and recycling. There are many strategies for shaping MOF powders. However, there are many issues in regard to the mechanical stability of the shaped bodies obtained by these techniques including the lack of mechanical stability and loss of crystallinity. Therefore, a novel low cost and efficient method needs to be developed and investigated. The new method needs to be efficient enough to maintain the high surface area of the adsorbent while preserving its crystallinity, robustness and stability. Different strategies for shaping MOF powders were critically discussed and the suitable and novel phase inversion method was introduced.

Another challenge was discussed based on the limitation of ZIF-8 in adsorption of large molecules such as dyes in liquid medium due to the very small pores. This issue could be resolved by some modifications such as heat treatment (carbonization). The presence of unique and interesting exceptionally porous framework and large carbon content in MOFs and ZIFs

allows these materials to be used as efficient precursors for porous carbons. The pore size distribution and pore structure can be controlled by the carbonization temperature. The current literature lacks a mechanistic study about the adsorption of pollutants on nanoporous carbons derived from MOFs and ZIFs. In addition, the effect of temperature on their adsorption properties has not been explored.

Among various porous materials, fly ash wastes provide free and locally available materials which can be utilized as adsorbents for adsorptive removal of pollutants from water. Victorian brown coal fly ash has unique characteristics such as magnetic and alkaline properties as well as a porous framework featuring a unique mineralogy which makes this material very promising for neutralizing and treatment of acidic wastewaters containing heavy metals. These characteristics need to be identified and analysed for utilization in different applications.

To address the above-mentioned challenges, the new approaches need to be fast, highly reproducible and economically and environmentally viable. The study of the textural and performance change of the adsorbents under these new approaches will help us to understand and analyse the adsorptive behaviour of materials for the successful selection of porous adsorbents and modifying/processing techniques for future adsorption applications specifically in water treatment.

Therefore, the objectives of my PhD research was designed to investigate the adsorption properties of the porous materials including ZIF-8 and fly ash wastes. Firstly, an efficient phase inversion method is utilized to shape ZIF-8 powder into beads and their characteristics and oil sorption properties are investigated. Secondly, ZIF-8 undergoes direct carbonization to investigate effect of temperature on its characteristics and adsorption properties for water treatment. The kinetics and mechanisms are further investigated extensively to provide a comprehensive study in this regard to fill the current gap in literature. Next, the nanoporous

carbons are magnetized by wet impregnation for the purpose of easy handling and recycling. Effect of re-carbonization on properties of magnetic carbonized ZIF-8 is investigated as well. Finally, the textural and adsorptive properties of Victorian brown coal fly ash is explored and effect of weathering modification on characteristics and adsorption properties are identified.

2.7. References

1. Liu, X., M. Wang, S. Zhang, and B. Pan, *Application potential of carbon nanotubes in water treatment: A review.* Journal of Environmental Sciences, 2013. **25**(7): p. 1263-1280.
2. Chong, M.N., B. Jin, C.W.K. Chow, and C. Saint, *Recent developments in photocatalytic water treatment technology: A review.* Water Research, 2010. **44**(10): p. 2997-3027.
3. Tchobanoglous, G., F.L. Burton, H.D. Stensel, Metcalf, and I. Eddy, *Wastewater Engineering: Treatment and Reuse*. 2003: McGraw-Hill Education.
4. Robinson, T., G. McMullan, R. Marchant, and P. Nigam, *Remediation of dyes in textile effluent: a critical review on current treatment technologies with a proposed alternative.* Bioresource Technology, 2001. **77**(3): p. 247-255.
5. Oller, I., S. Malato, and J.A. Sánchez-Pérez, *Combination of Advanced Oxidation Processes and biological treatments for wastewater decontamination—A review.* Science of The Total Environment, 2011. **409**(20): p. 4141-4166.
6. Lapertot, M., C. Pulgarín, P. Fernández-Ibáñez, M.I. Maldonado, L. Pérez-Estrada, I. Oller, W. Gernjak, and S. Malato, *Enhancing biodegradability of priority substances (pesticides) by solar photo-Fenton.* Water Research, 2006. **40**(5): p. 1086-1094.
7. Muñoz, R. and B. Guieysse, *Algal–bacterial processes for the treatment of hazardous contaminants: A review.* Water Research, 2006. **40**(15): p. 2799-2815.
8. García, M.T., I. Ribosa, T. Guindulain, J. Sánchez-Leal, and J. Vives-Rego, *Fate and effect of monoalkyl quaternary ammonium surfactants in the aquatic environment.* Environmental Pollution, 2001. **111**(1): p. 169-175.
9. Panizza, M. and G. Cerisola, *Direct And Mediated Anodic Oxidation of Organic Pollutants.* Chemical Reviews, 2009. **109**(12): p. 6541-6569.
10. Wan Ngah, W.S. and M.A.K.M. Hanafiah, *Removal of heavy metal ions from wastewater by chemically modified plant wastes as adsorbents: A review.* Bioresource Technology, 2008. **99**(10): p. 3935-3948.
11. Fu, F. and Q. Wang, *Removal of heavy metal ions from wastewaters: A review.* Journal of Environmental Management, 2011. **92**(3): p. 407-418.
12. Allen, S.J. and P.A. Brown, *Isotherm analyses for single component and multi-component metal sorption onto lignite.* Journal of Chemical Technology & Biotechnology, 1995. **62**(1): p. 17-24.
13. Dąbrowski, A., *Adsorption — from theory to practice.* Advances in Colloid and Interface Science, 2001. **93**(1–3): p. 135-224.
14. Khan, N.A., Z. Hasan, and S.H. Jhung, *Adsorptive removal of hazardous materials using metal-organic frameworks (MOFs): A review.* Journal of Hazardous Materials, 2013. **244–245**(0): p. 444-456.
15. Yagub, M.T., T.K. Sen, S. Afroze, and H.M. Ang, *Dye and its removal from aqueous solution by adsorption: A review.* Advances in Colloid and Interface Science, 2014. **209**: p. 172-184.
16. Bhattacharyya, K.G. and S.S. Gupta, *Adsorption of a few heavy metals on natural and modified kaolinite and montmorillonite: A review.* Advances in Colloid and Interface Science, 2008. **140**(2): p. 114-131.
17. Silva, T.L., A. Ronix, O. Pezoti, L.S. Souza, P.K.T. Leandro, K.C. Bedin, K.K. Beltrame, A.L. Cazetta, and V.C. Almeida, *Mesoporous activated carbon from*

industrial laundry sewage sludge: Adsorption studies of reactive dye Remazol Brilliant Blue R. Chemical Engineering Journal, 2016. **303**: p. 467-476.
18. Lorenc-Grabowska, E. and G. Gryglewicz, *Adsorption characteristics of Congo Red on coal-based mesoporous activated carbon.* Dyes and Pigments, 2007. **74**(1): p. 34-40.
19. Altın, O., H.Ö. Özbelge, and T. Doğu, *Use of General Purpose Adsorption Isotherms for Heavy Metal–Clay Mineral Interactions.* Journal of Colloid and Interface Science, 1998. **198**(1): p. 130-140.
20. Langmuir, I., *THE ADSORPTION OF GASES ON PLANE SURFACES OF GLASS, MICA AND PLATINUM.* Journal of the American Chemical Society, 1918. **40**(9): p. 1361-1403.
21. Monte Blanco, S.P.D., F.B. Scheufele, A.N. Módenes, F.R. Espinoza-Quiñones, P. Marin, A.D. Kroumov, and C.E. Borba, *Kinetic, equilibrium and thermodynamic phenomenological modeling of reactive dye adsorption onto polymeric adsorbent.* Chemical Engineering Journal, 2017. **307**: p. 466-475.
22. Babu, B.V. and S. Gupta, *Adsorption of Cr(VI) using activated neem leaves: kinetic studies.* Adsorption, 2008. **14**(1): p. 85-92.
23. Özcan, A.S., B. Erdem, and A. Özcan, *Adsorption of Acid Blue 193 from aqueous solutions onto BTMA-bentonite.* Colloids and Surfaces A: Physicochemical and Engineering Aspects, 2005. **266**(1–3): p. 73-81.
24. Shao, Y., B. Ren, H. Jiang, B. Zhou, L. Lv, J. Ren, L. Dong, J. Li, and Z. Liu, *Dual-porosity Mn2O3 cubes for highly efficient dye adsorption.* Journal of Hazardous Materials, 2017. **333**: p. 222-231.
25. Okolo, B., C. Park, and M.A. Keane, *Interaction of Phenol and Chlorophenols with Activated Carbon and Synthetic Zeolites in Aqueous Media.* Journal of Colloid and Interface Science, 2000. **226**(2): p. 308-317.
26. Lagergren, S., *About the theory of so-called adsorption of soluble substances.* 1898.
27. Gupta, K. and O.P. Khatri, *Reduced graphene oxide as an effective adsorbent for removal of malachite green dye: Plausible adsorption pathways.* Journal of Colloid and Interface Science, 2017. **501**: p. 11-21.
28. Pei, C., G. Han, Y. Zhao, H. Zhao, B. Liu, L. Cheng, H. Yang, and S. Liu, *Superior adsorption performance for triphenylmethane dyes on 3D architectures assembled by ZnO nanosheets as thin as ~1.5nm.* Journal of Hazardous Materials, 2016. **318**: p. 732-741.
29. Zhu, Z., P. Wu, G. Liu, X. He, B. Qi, G. Zeng, W. Wang, Y. Sun, and F. Cui, *Ultrahigh adsorption capacity of anionic dyes with sharp selectivity through the cationic charged hybrid nanofibrous membranes.* Chemical Engineering Journal, 2017. **313**: p. 957-966.
30. Weber, W.J. and J.C. Morris, *Kinetics of adsorption on carbon from solution.* Journal of the Sanitary Engineering Division, 1963. **89**(2): p. 31-60.
31. Shaarani, F. and B. Hameed, *Batch adsorption of 2, 4-dichlorophenol onto activated carbon derived from agricultural waste.* Desalination, 2010. **255**(1): p. 159-164.
32. Daifullah, A.A.M., S.M. Yakout, and S.A. Elreefy, *Adsorption of fluoride in aqueous solutions using KMnO4-modified activated carbon derived from steam pyrolysis of rice straw.* Journal of Hazardous Materials, 2007. **147**(1–2): p. 633-643.
33. Fang, J., X. Huang, X. Ouyang, and X. Wang, *Study of the preparation of γ-Al2O3 nano-structured hierarchical hollow microspheres with a simple hydrothermal synthesis using methylene blue as structure directing agent and their adsorption enhancement for the dye.* Chemical Engineering Journal, 2015. **270**: p. 309-319.

34. Terzyk, A.P., *Molecular properties and intermolecular forces—factors balancing the effect of carbon surface chemistry in adsorption of organics from dilute aqueous solutions.* Journal of Colloid and Interface Science, 2004. **275**(1): p. 9-29.
35. Zhang, X., A. Li, Z. Jiang, and Q. Zhang, *Adsorption of dyes and phenol from water on resin adsorbents: Effect of adsorbate size and pore size distribution.* Journal of Hazardous Materials, 2006. **137**(2): p. 1115-1122.
36. Cañizares, P., M. Carmona, O. Baraza, A. Delgado, and M.A. Rodrigo, *Adsorption equilibrium of phenol onto chemically modified activated carbon F400.* Journal of Hazardous Materials, 2006. **131**(1–3): p. 243-248.
37. Al-Degs, Y.S., M.I. El-Barghouthi, A.H. El-Sheikh, and G.M. Walker, *Effect of solution pH, ionic strength, and temperature on adsorption behavior of reactive dyes on activated carbon.* Dyes and Pigments, 2008. **77**(1): p. 16-23.
38. Moreno-Castilla, C., *Adsorption of organic molecules from aqueous solutions on carbon materials.* Carbon, 2004. **42**(1): p. 83-94.
39. Zadaka, D., A. Radian, and Y.G. Mishael, *Applying zeta potential measurements to characterize the adsorption on montmorillonite of organic cations as monomers, micelles, or polymers.* Journal of Colloid and Interface Science, 2010. **352**(1): p. 171-177.
40. Radovic, L.R., I.F. Silva, J.I. Ume, J.A. Menéndez, C.A.L.Y. Leon, and A.W. Scaroni, *An experimental and theoretical study of the adsorption of aromatics possessing electron-withdrawing and electron-donating functional groups by chemically modified activated carbons.* Carbon, 1997. **35**(9): p. 1339-1348.
41. Wang, J.-P., Y.-Z. Chen, H.-M. Feng, S.-J. Zhang, and H.-Q. Yu, *Removal of 2,4-dichlorophenol from aqueous solution by static-air-activated carbon fibers.* Journal of Colloid and Interface Science, 2007. **313**(1): p. 80-85.
42. Wang, J.-P., H.-M. Feng, and H.-Q. Yu, *Analysis of adsorption characteristics of 2,4-dichlorophenol from aqueous solutions by activated carbon fiber.* Journal of Hazardous Materials, 2007. **144**(1–2): p. 200-207.
43. Liu, Q.-S., T. Zheng, P. Wang, J.-P. Jiang, and N. Li, *Adsorption isotherm, kinetic and mechanism studies of some substituted phenols on activated carbon fibers.* Chemical Engineering Journal, 2010. **157**(2–3): p. 348-356.
44. Ghaffar, A. and M.N. Younis, *Interaction and thermodynamics of methylene blue adsorption on oxidized multi-walled carbon nanotubes.* Green Processing and Synthesis, 2015. **4**(3): p. 209-217.
45. Lachheb, H., E. Puzenat, A. Houas, M. Ksibi, E. Elaloui, C. Guillard, and J.-M. Herrmann, *Photocatalytic degradation of various types of dyes (Alizarin S, Crocein Orange G, Methyl Red, Congo Red, Methylene Blue) in water by UV-irradiated titania.* Applied Catalysis B: Environmental, 2002. **39**(1): p. 75-90.
46. Valix, M., W.H. Cheung, and G. McKay, *Preparation of activated carbon using low temperature carbonisation and physical activation of high ash raw bagasse for acid dye adsorption.* Chemosphere, 2004. **56**(5): p. 493-501.
47. García-Araya, J.F., F.J. Beltrán, P. Álvarez, and F.J. Masa, *Activated Carbon Adsorption of Some Phenolic Compounds Present in Agroindustrial Wastewater.* Adsorption, 2003. **9**(2): p. 107-115.
48. Contescu, A., M. Vass, C. Contescu, K. Putyera, and J.A. Schwarz, *Acid buffering capacity of basic carbons revealed by their continuous pK distribution.* Carbon, 1998. **36**(3): p. 247-258.

49. Amin, N.K., *Removal of direct blue-106 dye from aqueous solution using new activated carbons developed from pomegranate peel: Adsorption equilibrium and kinetics.* Journal of Hazardous Materials, 2009. **165**(1–3): p. 52-62.
50. Dąbrowski, A., P. Podkościelny, Z. Hubicki, and M. Barczak, *Adsorption of phenolic compounds by activated carbon—a critical review.* Chemosphere, 2005. **58**(8): p. 1049-1070.
51. Hong, S., C. Wen, J. He, F. Gan, and Y.-S. Ho, *Adsorption thermodynamics of Methylene Blue onto bentonite.* Journal of Hazardous Materials, 2009. **167**(1–3): p. 630-633.
52. Yao, Y., F. Xu, M. Chen, Z. Xu, and Z. Zhu, *Adsorption behavior of methylene blue on carbon nanotubes.* Bioresource Technology, 2010. **101**(9): p. 3040-3046.
53. Saber-Samandari, S., S. Saber-Samandari, H. Joneidi-Yekta, and M. Mohseni, *Adsorption of anionic and cationic dyes from aqueous solution using gelatin-based magnetic nanocomposite beads comprising carboxylic acid functionalized carbon nanotube.* Chemical Engineering Journal, 2017. **308**: p. 1133-1144.
54. Konicki, W., M. Aleksandrzak, D. Moszyński, and E. Mijowska, *Adsorption of anionic azo-dyes from aqueous solutions onto graphene oxide: Equilibrium, kinetic and thermodynamic studies.* Journal of Colloid and Interface Science, 2017. **496**: p. 188-200.
55. Sen Gupta, S. and K.G. Bhattacharyya, *Kinetics of adsorption of metal ions on inorganic materials: A review.* Advances in Colloid and Interface Science, 2011. **162**(1–2): p. 39-58.
56. Qu, J., *Research progress of novel adsorption processes in water purification: A review.* Journal of Environmental Sciences, 2008. **20**(1): p. 1-13.
57. Visa, M., C. Bogatu, and A. Duta, *Simultaneous adsorption of dyes and heavy metals from multicomponent solutions using fly ash.* Applied Surface Science, 2010. **256**(17): p. 5486-5491.
58. Rahmani, A., H.Z. Mousavi, and M. Fazli, *Effect of nanostructure alumina on adsorption of heavy metals.* Desalination, 2010. **253**(1–3): p. 94-100.
59. Alinnor, I.J., *Adsorption of heavy metal ions from aqueous solution by fly ash.* Fuel, 2007. **86**(5–6): p. 853-857.
60. Nascimento, M., P.S.M. Soares, and V.P.d. Souza, *Adsorption of heavy metal cations using coal fly ash modified by hydrothermal method.* Fuel, 2009. **88**(9): p. 1714-1719.
61. Babel, S. and T.A. Kurniawan, *Low-cost adsorbents for heavy metals uptake from contaminated water: a review.* Journal of Hazardous Materials, 2003. **97**(1–3): p. 219-243.
62. Shyam, R., J.K. Puri, H. Kaur, R. Amutha, and A. Kapila, *Single and binary adsorption of heavy metals on fly ash samples from aqueous solution.* Journal of Molecular Liquids, 2013. **178**(0): p. 31-36.
63. Rafatullah, M., O. Sulaiman, R. Hashim, and A. Ahmad, *Adsorption of methylene blue on low-cost adsorbents: A review.* Journal of Hazardous Materials, 2010. **177**(1–3): p. 70-80.
64. Rathore, H.S., S.K. Sharma, and M. Agarwal, *Adsorption of some organic acids on fly ash impregnated with hydroxides of Al, Cd, Cu, Fe and Ni.* Environmental Pollution Series B, Chemical and Physical, 1985. **10**(4): p. 249-260.
65. Wei, L., K. Wang, Q. Zhao, C. Xie, W. Qiu, and T. Jia, *Kinetics and equilibrium of adsorption of dissolved organic matter fractions from secondary effluent by fly ash.* Journal of Environmental Sciences, 2011. **23**(7): p. 1057-1065.

66. Salleh, M.A.M., D.K. Mahmoud, W.A.W.A. Karim, and A. Idris, *Cationic and anionic dye adsorption by agricultural solid wastes: A comprehensive review.* Desalination, 2011. **280**(1–3): p. 1-13.
67. Atun, G., G. Hisarlı, A.E. Kurtoğlu, and N. Ayar, *A comparison of basic dye adsorption onto zeolitic materials synthesized from fly ash.* Journal of Hazardous Materials, 2011. **187**(1–3): p. 562-573.
68. Keleşoğlu, S., M. Kes, L. Sütçü, and H. Polat, *Adsorption of Methylene Blue from Aqueous Solution on High Lime Fly Ash: Kinetic, Equilibrium, and Thermodynamic Studies.* Journal of Dispersion Science and Technology, 2011. **33**(1): p. 15-23.
69. Andini, S., R. Cioffi, F. Colangelo, F. Montagnaro, and L. Santoro, *Adsorption of chlorophenol, chloroaniline and methylene blue on fuel oil fly ash.* Journal of Hazardous Materials, 2008. **157**(2–3): p. 599-604.
70. Dias, J.M., M.C.M. Alvim-Ferraz, M.F. Almeida, J. Rivera-Utrilla, and M. Sánchez-Polo, *Waste materials for activated carbon preparation and its use in aqueous-phase treatment: A review.* Journal of Environmental Management, 2007. **85**(4): p. 833-846.
71. Wang, S., Z.H. Zhu, A. Coomes, F. Haghseresht, and G.Q. Lu, *The physical and surface chemical characteristics of activated carbons and the adsorption of methylene blue from wastewater.* Journal of Colloid and Interface Science, 2005. **284**(2): p. 440-446.
72. Walker, G.M. and L.R. Weatherley, *Adsorption of dyes from aqueous solution — the effect of adsorbent pore size distribution and dye aggregation.* Chemical Engineering Journal, 2001. **83**(3): p. 201-206.
73. Pereira, M.F.R., S.F. Soares, J.J.M. Órfão, and J.L. Figueiredo, *Adsorption of dyes on activated carbons: influence of surface chemical groups.* Carbon, 2003. **41**(4): p. 811-821.
74. Bhatnagar, A., W. Hogland, M. Marques, and M. Sillanpää, *An overview of the modification methods of activated carbon for its water treatment applications.* Chemical Engineering Journal, 2013. **219**: p. 499-511.
75. Monser, L. and N. Adhoum, *Modified activated carbon for the removal of copper, zinc, chromium and cyanide from wastewater.* Separation and purification technology, 2002. **26**(2): p. 137-146.
76. Davis, M.E., *Ordered porous materials for emerging applications.* Nature, 2002. **417**(6891): p. 813-821.
77. Li, R., L. Zhang, and P. Wang, *Rational design of nanomaterials for water treatment.* Nanoscale, 2015. **7**(41): p. 17167-17194.
78. Boehm, H.P., E. Diehl, W. Heck, and R. Sappok, *Surface Oxides of Carbon.* Angewandte Chemie International Edition in English, 1964. **3**(10): p. 669-677.
79. Boehm, H.P., *Some aspects of the surface chemistry of carbon blacks and other carbons.* Carbon, 1994. **32**(5): p. 759-769.
80. Puri, B., *Surface complexes on carbons.* Chemistry and physics of carbon, 1970. **6**: p. 191-282.
81. Mattson, J.S. and H.B. Mark, *Activated carbon: surface chemistry and adsorption from solution*. 1971: M. Dekker.
82. Leon, C.L.Y. and L. Radovic, *Interfacial chemistry and electrochemistry of carbon surfaces.* CHEMISTRY AND PHYSICS OF CARBON, VOL 24, 1994. **24**: p. 213-310.
83. Leon y Leon, C.A., J.M. Solar, V. Calemma, and L.R. Radovic, *Evidence for the protonation of basal plane sites on carbon.* Carbon, 1992. **30**(5): p. 797-811.
84. Barton, S.S., M.J.B. Evans, E. Halliop, and J.A.F. MacDonald, *Acidic and basic sites on the surface of porous carbon.* Carbon, 1997. **35**(9): p. 1361-1366.

85. Coughlin, R.W. and F.S. Ezra, *Role of surface acidity in the adsorption of organic pollutants on the surface of carbon.* Environmental Science & Technology, 1968. **2**(4): p. 291-297.
86. Menéndez, J.A., J. Phillips, B. Xia, and L.R. Radovic, *On the Modification and Characterization of Chemical Surface Properties of Activated Carbon: In the Search of Carbons with Stable Basic Properties.* Langmuir, 1996. **12**(18): p. 4404-4410.
87. Kaneko, Y., M. Abe, and K. Ogino, *Adsorption characteristics of organic compounds dissolved in water on surface-improved activated carbon fibres.* Colloids and Surfaces, 1989. **37**: p. 211-222.
88. Franz, M., H.A. Arafat, and N.G. Pinto, *Effect of chemical surface heterogeneity on the adsorption mechanism of dissolved aromatics on activated carbon.* Carbon, 2000. **38**(13): p. 1807-1819.
89. Considine, R., R. Denoyel, P. Pendleton, R. Schumann, and S.-H. Wong, *The influence of surface chemistry on activated carbon adsorption of 2-methylisoborneol from aqueous solution.* Colloids and Surfaces A: Physicochemical and Engineering Aspects, 2001. **179**(2): p. 271-280.
90. Karanfil, T. and J.E. Kilduff, *Role of Granular Activated Carbon Surface Chemistry on the Adsorption of Organic Compounds. 1. Priority Pollutants.* Environmental Science & Technology, 1999. **33**(18): p. 3217-3224.
91. Pan, D. and M. Jaroniec, *Adsorption and Thermogravimetric Studies of Unmodified and Oxidized Active Carbons.* Langmuir, 1996. **12**(15): p. 3657-3665.
92. Müller, E.A., L.F. Rull, L.F. Vega, and K.E. Gubbins, *Adsorption of Water on Activated Carbons: A Molecular Simulation Study.* The Journal of Physical Chemistry, 1996. **100**(4): p. 1189-1196.
93. Müller, E.A. and K.E. Gubbins, *Molecular simulation study of hydrophilic and hydrophobic behavior of activated carbon surfaces.* Carbon, 1998. **36**(10): p. 1433-1438.
94. Müller, E.A., F.R. Hung, and K.E. Gubbins, *Adsorption of water vapor-methane mixtures on activated carbons.* Langmuir, 2000. **16**(12): p. 5418-5424.
95. Pendleton, P., S. Wong, R. Schumann, G. Levay, R. Denoyel, and J. Rouquero, *Properties of activated carbon controlling 2-methylisoborneol adsorption.* Carbon, 1997. **35**(8): p. 1141-1149.
96. Davis, S.W. and S.E. Powers, *Alternative sorbents for removing MTBE from gasoline-contaminated ground water.* Journal of Environmental Engineering, 2000. **126**(4): p. 354-360.
97. Li, H., M. Eddaoudi, M. O'Keeffe, and O.M. Yaghi, *Design and synthesis of an exceptionally stable and highly porous metal-organic framework.* Nature, 1999. **402**(6759): p. 276-279.
98. Ma, J., X. Guo, Y. Ying, D. Liu, and C. Zhong, *Composite ultrafiltration membrane tailored by MOF@GO with highly improved water purification performance.* Chemical Engineering Journal, 2017. **313**: p. 890-898.
99. Chaikittisilp, W., K. Ariga, and Y. Yamauchi, *A new family of carbon materials: synthesis of MOF-derived nanoporous carbons and their promising applications.* Journal of Materials Chemistry A, 2013. **1**(1): p. 14-19.
100. Rahmani, E. and M. Rahmani, *Alkylation of benzene over Fe-based metal organic frameworks (MOFs) at low temperature condition.* Microporous and Mesoporous Materials, 2017. **249**: p. 118-127.

101. Sumida, K., D.L. Rogow, J.A. Mason, T.M. McDonald, E.D. Bloch, Z.R. Herm, T.-H. Bae, and J.R. Long, *Carbon Dioxide Capture in Metal–Organic Frameworks.* Chemical Reviews, 2012. **112**(2): p. 724-781.
102. Lee, J., O.K. Farha, J. Roberts, K.A. Scheidt, S.T. Nguyen, and J.T. Hupp, *Metal-organic framework materials as catalysts.* Chemical Society Reviews, 2009. **38**(5): p. 1450-1459.
103. Han, S., Y. Huang, T. Watanabe, S. Nair, K.S. Walton, D.S. Sholl, and J. Carson Meredith, *MOF stability and gas adsorption as a function of exposure to water, humid air, SO2, and NO2.* Microporous and Mesoporous Materials, 2013. **173**(0): p. 86-91.
104. Burtch, N.C., H. Jasuja, and K.S. Walton, *Water Stability and Adsorption in Metal–Organic Frameworks.* Chemical Reviews, 2014. **114**(20): p. 10575-10612.
105. Mounfield, W.P., U. Tumuluri, Y. Jiao, M. Li, S. Dai, Z. Wu, and K.S. Walton, *Role of defects and metal coordination on adsorption of acid gases in MOFs and metal oxides: An in situ IR spectroscopic study.* Microporous and Mesoporous Materials, 2016. **227**: p. 65-75.
106. Singha, S., S.K. Maity, S. Biswas, R. Saha, and S. Kumar, *A magnesium-based bifunctional MOF: Studies on proton conductivity, gas and water adsorption.* Inorganica Chimica Acta, 2016. **453**: p. 321-329.
107. Huang, K., S. Liu, Q. Li, and W. Jin, *Preparation of novel metal-carboxylate system MOF membrane for gas separation.* Separation and Purification Technology, 2013. **119**: p. 94-101.
108. Castarlenas, S., C. Téllez, and J. Coronas, *Gas separation with mixed matrix membranes obtained from MOF UiO-66-graphite oxide hybrids.* Journal of Membrane Science, 2017. **526**: p. 205-211.
109. Huang, C., R. Sun, H. Lu, Q. Yang, J. Hu, H. Wang, and H. Liu, *A pilot trial for fast deep desulfurization on MOF-199 by simultaneous adsorption-separation via hydrocyclones.* Separation and Purification Technology, 2017. **182**: p. 110-117.
110. Chen, Y., D. Lv, J. Wu, J. Xiao, H. Xi, Q. Xia, and Z. Li, *A new MOF-505@GO composite with high selectivity for CO2/CH4 and CO2/N2 separation.* Chemical Engineering Journal, 2017. **308**: p. 1065-1072.
111. Harding, J.L., J.M. Metz, and M.M. Reynolds, *A Tunable, Stable, and Bioactive MOF Catalyst for Generating a Localized Therapeutic from Endogenous Sources.* Advanced Functional Materials, 2014. **24**(47): p. 7503-7509.
112. Wang, D. and Z. Li, *Coupling MOF-based photocatalysis with Pd catalysis over Pd@MIL-100(Fe) for efficient N-alkylation of amines with alcohols under visible light.* Journal of Catalysis, 2016. **342**: p. 151-157.
113. Yao, J., L. Li, W.H. Benjamin Wong, C. Tan, D. Dong, and H. Wang, *Formation of ZIF-8 membranes and crystals in a diluted aqueous solution.* Materials Chemistry and Physics, 2013. **139**(2–3): p. 1003-1008.
114. Wu, T., L. Shen, M. Luebbers, C. Hu, Q. Chen, Z. Ni, and R.I. Masel, *Enhancing the stability of metal-organic frameworks in humid air by incorporating water repellent functional groups.* Chemical Communications, 2010. **46**(33): p. 6120-6122.
115. Yao, J. and H. Wang, *Zeolitic imidazolate framework composite membranes and thin films: synthesis and applications.* Chemical Society Reviews, 2014.
116. James, J.B. and Y.S. Lin, *Thermal stability of ZIF-8 membranes for gas separations.* Journal of Membrane Science, 2017. **532**: p. 9-19.
117. Ge, D. and H.K. Lee, *Water stability of zeolite imidazolate framework 8 and application to porous membrane-protected micro-solid-phase extraction of polycyclic aromatic*

hydrocarbons from environmental water samples. Journal of Chromatography A, 2011. **1218**(47): p. 8490-8495.
118. Park, K.S., Z. Ni, A.P. Côté, J.Y. Choi, R. Huang, F.J. Uribe-Romo, H.K. Chae, M. O'Keeffe, and O.M. Yaghi, *Exceptional chemical and thermal stability of zeolitic imidazolate frameworks.* Proceedings of the National Academy of Sciences, 2006. **103**(27): p. 10186-10191.
119. Banerjee, R., A. Phan, B. Wang, C. Knobler, H. Furukawa, M. O'Keeffe, and O.M. Yaghi, *High-Throughput Synthesis of Zeolitic Imidazolate Frameworks and Application to CO2 Capture.* Science, 2008. **319**(5865): p. 939-943.
120. Zhang, H., D. Liu, Y. Yao, B. Zhang, and Y.S. Lin, *Stability of ZIF-8 membranes and crystalline powders in water at room temperature.* Journal of Membrane Science, 2015. **485**: p. 103-111.
121. Jiang, H., Q. Yan, R. Chen, and W. Xing, *Synthesis of Pd@ZIF-8 via an assembly method: Influence of the molar ratios of Pd/Zn2+ and 2-methylimidazole/Zn2+*. Microporous and Mesoporous Materials, 2016. **225**: p. 33-40.
122. Jiang, J.-Q., C.-X. Yang, and X.-P. Yan, *Zeolitic Imidazolate Framework-8 for Fast Adsorption and Removal of Benzotriazoles from Aqueous Solution.* ACS Applied Materials & Interfaces, 2013. **5**(19): p. 9837-9842.
123. Adeyemo, A.A., I.O. Adeoye, and O.S. Bello, *Metal organic frameworks as adsorbents for dye adsorption: overview, prospects and future challenges.* Toxicological & Environmental Chemistry, 2012. **94**(10): p. 1846-1863.
124. Jiang, H.-L., B. Liu, Y.-Q. Lan, K. Kuratani, T. Akita, H. Shioyama, F. Zong, and Q. Xu, *From Metal–Organic Framework to Nanoporous Carbon: Toward a Very High Surface Area and Hydrogen Uptake.* Journal of the American Chemical Society, 2011. **133**(31): p. 11854-11857.
125. Carlsson, J.M. and M. Scheffler, *Structural, Electronic, and Chemical Properties of Nanoporous Carbon.* Physical Review Letters, 2006. **96**(4): p. 046806.
126. Jiang, M., X. Cao, D. Zhu, Y. Duan, and J. Zhang, *Hierarchically Porous N-doped Carbon Derived from ZIF-8 Nanocomposites for Electrochemical Applications.* Electrochimica Acta, 2016. **196**: p. 699-707.
127. Torad, N.L., M. Hu, S. Ishihara, H. Sukegawa, A.A. Belik, M. Imura, K. Ariga, Y. Sakka, and Y. Yamauchi, *Direct Synthesis of MOF-Derived Nanoporous Carbon with Magnetic Co Nanoparticles toward Efficient Water Treatment.* Small, 2014. **10**(10): p. 2096-2107.
128. Angamuthu, M., G. Satishkumar, and M.V. Landau, *Precisely controlled encapsulation of Fe3O4 nanoparticles in mesoporous carbon nanodisk using iron based MOF precursor for effective dye removal.* Microporous and Mesoporous Materials, 2017. **251**: p. 58-68.
129. Comotti, A., S. Bracco, P. Sozzani, S. Horike, R. Matsuda, J. Chen, M. Takata, Y. Kubota, and S. Kitagawa, *Nanochannels of Two Distinct Cross-Sections in a Porous Al-Based Coordination Polymer.* Journal of the American Chemical Society, 2008. **130**(41): p. 13664-13672.
130. Hu, M., J. Reboul, S. Furukawa, N.L. Torad, Q. Ji, P. Srinivasu, K. Ariga, S. Kitagawa, and Y. Yamauchi, *Direct Carbonization of Al-Based Porous Coordination Polymer for Synthesis of Nanoporous Carbon.* Journal of the American Chemical Society, 2012. **134**(6): p. 2864-2867.
131. Torad, N.L., M. Hu, Y. Kamachi, K. Takai, M. Imura, M. Naito, and Y. Yamauchi, *Facile synthesis of nanoporous carbons with controlled particle sizes by direct*

carbonization of monodispersed ZIF-8 crystals. Chemical Communications, 2013. **49**(25): p. 2521-2523.
132. Unur, E., *Functional nanoporous carbons from hydrothermally treated biomass for environmental purification.* Microporous and Mesoporous Materials, 2013. **168**: p. 92-101.
133. Zhao, L., L.Z. Fan, M.Q. Zhou, H. Guan, S. Qiao, M. Antonietti, and M.M. Titirici, *Nitrogen-Containing Hydrothermal Carbons with Superior Performance in Supercapacitors.* Advanced materials, 2010. **22**(45): p. 5202-5206.
134. Sevilla, M., J.A. Macia-Agullo, and A.B. Fuertes, *Hydrothermal carbonization of biomass as a route for the sequestration of CO 2: chemical and structural properties of the carbonized products.* biomass and bioenergy, 2011. **35**(7): p. 3152-3159.
135. Gupta, V.K. and Suhas, *Application of low-cost adsorbents for dye removal – A review.* Journal of Environmental Management, 2009. **90**(8): p. 2313-2342.
136. Inagaki, M., *Pores in carbon materials-importance of their control.* New Carbon Materials, 2009. **24**(3): p. 193-232.
137. Yan, X., X. Li, Z. Yan, and S. Komarneni, *Porous carbons prepared by direct carbonization of MOFs for supercapacitors.* Applied Surface Science, 2014. **308**: p. 306-310.
138. Lim, S., K. Suh, Y. Kim, M. Yoon, H. Park, D.N. Dybtsev, and K. Kim, *Porous carbon materials with a controllable surface area synthesized from metal–organic frameworks.* Chemical communications, 2012. **48**(60): p. 7447-7449.
139. Wang, S., Q. Ma, and Z.H. Zhu, *Characteristics of coal fly ash and adsorption application.* Fuel, 2008. **87**(15–16): p. 3469-3473.
140. Eze, C.P., S.M. Nyale, R.O. Akinyeye, W.M. Gitari, S.A. Akinyemi, O.O. Fatoba, and L.F. Petrik, *Chemical, mineralogical and morphological changes in weathered coal fly ash: A case study of a brine impacted wet ash dump.* Journal of Environmental Management, 2013. **129**(0): p. 479-492.
141. Ahmaruzzaman, M., *A review on the utilization of fly ash.* Progress in Energy and Combustion Science, 2010. **36**(3): p. 327-363.
142. Iyer, R.S. and J.A. Scott, *Power station fly ash — a review of value-added utilization outside of the construction industry.* Resources, Conservation and Recycling, 2001. **31**(3): p. 217-228.
143. Nugteren, H.W., *Coal Fly Ash: From Waste to Industrial Product.* Particle & Particle Systems Characterization, 2007. **24**(1): p. 49-55.
144. Kumar, R., S. Kumar, and S.P. Mehrotra, *Towards sustainable solutions for fly ash through mechanical activation.* Resources, Conservation and Recycling, 2007. **52**(2): p. 157-179.
145. Visa, M. and A.-M. Chelaru, *Hydrothermally modified fly ash for heavy metals and dyes removal in advanced wastewater treatment.* Applied Surface Science, 2014. **303**(0): p. 14-22.
146. Hsu, T.-C., *Adsorption of an acid dye onto coal fly ash.* Fuel, 2008. **87**(13–14): p. 3040-3045.
147. Zheng, D. and P. Pi, *Adsorption Behavior of Acid Dyestuffs on the Surface of Fly Ash.* Journal of Dispersion Science and Technology, 2010. **31**(8): p. 1027-1032.
148. Lin, J.X., S.L. Zhan, M.H. Fang, X.Q. Qian, and H. Yang, *Adsorption of basic dye from aqueous solution onto fly ash.* Journal of Environmental Management, 2008. **87**(1): p. 193-200.

149. Singh, N., *Adsorption of herbicides on coal fly ash from aqueous solutions.* Journal of Hazardous Materials, 2009. **168**(1): p. 233-237.
150. Sun, D., X. Zhang, Y. Wu, and X. Liu, *Adsorption of anionic dyes from aqueous solution on fly ash.* Journal of Hazardous Materials, 2010. **181**(1–3): p. 335-342.
151. Wang, S., Y. Boyjoo, A. Choueib, and Z.H. Zhu, *Removal of dyes from aqueous solution using fly ash and red mud.* Water Research, 2005. **39**(1): p. 129-138.
152. Shaheen, S.M., P.S. Hooda, and C.D. Tsadilas, *Opportunities and challenges in the use of coal fly ash for soil improvements – A review*. Journal of Environmental Management, 2014. **145**(0): p. 249-267.
153. Mudd, G.M. and J. Kodikara, *Field studies of the leachability of aged brown coal ash.* Journal of Hazardous Materials, 2000. **76**(2–3): p. 159-192.
154. Li, C.-Z., *Preface*, in *Advances in the Science of Victorian Brown Coal*, C.-Z. Li, Editor. 2004, Elsevier Science: Amsterdam. p. v-vii.
155. Akinyemi, S.A., A. Akinlua, W.M. Gitari, and L.F. Petrik, *Mineralogy and Mobility Patterns of Chemical Species in Weathered Coal Fly Ash.* Energy Sources, Part A: Recovery, Utilization, and Environmental Effects, 2011. **33**(8): p. 768-784.
156. Muriithi, G.N., L.F. Petrik, O. Fatoba, W.M. Gitari, F.J. Doucet, J. Nel, S.M. Nyale, and P.E. Chuks, *Comparison of CO2 capture by ex-situ accelerated carbonation and in in-situ naturally weathered coal fly ash.* Journal of Environmental Management, 2013. **127**(0): p. 212-220.
157. Ahmaruzzaman, M., *Role of Fly Ash in the Removal of Organic Pollutants from Wastewater.* Energy & Fuels, 2009. **23**(3): p. 1494-1511.
158. Wang, S., Y. Boyjoo, and A. Choueib, *A comparative study of dye removal using fly ash treated by different methods.* Chemosphere, 2005. **60**(10): p. 1401-1407.
159. Banerjee, S., R. Jayaram, and M. Joshi, *Removal of nickel (II) and zinc (II) from wastewater using fly ash and impregnated fly ash.* Separation science and technology, 2003. **38**(5): p. 1015-1032.
160. An, C., S. Yang, G. Huang, S. Zhao, P. Zhang, and Y. Yao, *Removal of sulfonated humic acid from aqueous phase by modified coal fly ash waste: Equilibrium and kinetic adsorption studies.* Fuel, 2016. **165**: p. 264-271.
161. Bayat, B., *Comparative study of adsorption properties of Turkish fly ashes: I. The case of nickel(II), copper(II) and zinc(II).* Journal of Hazardous Materials, 2002. **95**(3): p. 251-273.
162. Weng, C.-H. and C.P. Huang, *Adsorption characteristics of Zn(II) from dilute aqueous solution by fly ash.* Colloids and Surfaces A: Physicochemical and Engineering Aspects, 2004. **247**(1–3): p. 137-143.
163. Hsu, T.-C., C.-C. Yu, and C.-M. Yeh, *Adsorption of Cu2+ from water using raw and modified coal fly ashes.* Fuel, 2008. **87**(7): p. 1355-1359.
164. Zhu, S., H. Hou, Y. Xue, N. Wei, Q. Sun, and X. Chen, *Modeling adsorption of copper (II) onto fly ash and bentonite complex from aqueous solutions.* Journal of Colloid and Interface Science, 2007. **315**(1): p. 8-12.
165. Sočo, E. and J. Kalembkiewicz, *Adsorption of nickel(II) and copper(II) ions from aqueous solution by coal fly ash.* Journal of Environmental Chemical Engineering, 2013. **1**(3): p. 581-588.
166. Papandreou, A.D., C.J. Stournaras, D. Panias, and I. Paspaliaris, *Adsorption of Pb(II), Zn(II) and Cr(III) on coal fly ash porous pellets.* Minerals Engineering, 2011. **24**(13): p. 1495-1501.

167. Ricou, P., I. Lécuyer, and P. Le Cloirec, *Removal of Cu2+, Zn2+ and Pb2+ by adsorption onto fly ash and fly ash/lime mixing.* Water Science and Technology, 1999. **39**(10–11): p. 239-247.
168. Visa, M., L. Isac, and A. Duta, *Fly ash adsorbents for multi-cation wastewater treatment.* Applied Surface Science, 2012. **258**(17): p. 6345-6352.
169. Wu, X.-W., H.-W. Ma, L.-T. Zhang, and F.-J. Wang, *Adsorption properties and mechanism of mesoporous adsorbents prepared with fly ash for removal of Cu(II) in aqueous solution.* Applied Surface Science, 2012. **261**(0): p. 902-907.
170. Hasan, Z. and S.H. Jhung, *Removal of hazardous organics from water using metal-organic frameworks (MOFs): plausible mechanisms for selective adsorptions.* Journal of Hazardous Materials, (0).
171. Haque, E., J.E. Lee, I.T. Jang, Y.K. Hwang, J.-S. Chang, J. Jegal, and S.H. Jhung, *Adsorptive removal of methyl orange from aqueous solution with metal-organic frameworks, porous chromium-benzenedicarboxylates.* Journal of Hazardous Materials, 2010. **181**(1–3): p. 535-542.
172. Lin, S., Z. Song, G. Che, A. Ren, P. Li, C. Liu, and J. Zhang, *Adsorption behavior of metal–organic frameworks for methylene blue from aqueous solution.* Microporous and Mesoporous Materials, 2014. **193**: p. 27-34.
173. Liu, B., F. Yang, Y. Zou, and Y. Peng, *Adsorption of Phenol and p-Nitrophenol from Aqueous Solutions on Metal–Organic Frameworks: Effect of Hydrogen Bonding.* Journal of Chemical & Engineering Data, 2014. **59**(5): p. 1476-1482.
174. Khan, N.A., B.K. Jung, Z. Hasan, and S.H. Jhung, *Adsorption and removal of phthalic acid and diethyl phthalate from water with zeolitic imidazolate and metal–organic frameworks.* Journal of Hazardous Materials, 2015. **282**: p. 194-200.
175. Tong, M., D. Liu, Q. Yang, S. Devautour-Vinot, G. Maurin, and C. Zhong, *Influence of framework metal ions on the dye capture behavior of MIL-100 (Fe, Cr) MOF type solids.* Journal of Materials Chemistry A, 2013. **1**(30): p. 8534-8537.
176. Qin, F.-X., S.-Y. Jia, Y. Liu, H.-Y. Li, and S.-H. Wu, *Adsorptive removal of bisphenol A from aqueous solution using metal-organic frameworks.* Desalination and Water Treatment, 2015. **54**(1): p. 93-102.
177. Huo, S.-H. and X.-P. Yan, *Metal-organic framework MIL-100(Fe) for the adsorption of malachite green from aqueous solution.* Journal of Materials Chemistry, 2012. **22**(15): p. 7449-7455.
178. Park, E.Y., Z. Hasan, N.A. Khan, and S.H. Jhung, *Adsorptive removal of bisphenol-a from water with a metal-organic framework, a porous chromium-benzenedicarboxylate.* Journal of nanoscience and nanotechnology, 2013. **13**(4): p. 2789-2794.
179. Yang, C., U. Kaipa, Q.Z. Mather, X. Wang, V. Nesterov, A.F. Venero, and M.A. Omary, *Fluorous Metal–Organic Frameworks with Superior Adsorption and Hydrophobic Properties toward Oil Spill Cleanup and Hydrocarbon Storage.* Journal of the American Chemical Society, 2011. **133**(45): p. 18094-18097.
180. Lin, K.-Y.A., Y.-C. Chen, and S. Phattarapattamawong, *Efficient demulsification of oil-in-water emulsions using a zeolitic imidazolate framework: Adsorptive removal of oil droplets from water.* Journal of Colloid and Interface Science, 2016. **478**: p. 97-106.
181. Ali, I., M. Asim, and T.A. Khan, *Low cost adsorbents for the removal of organic pollutants from wastewater.* Journal of Environmental Management, 2012. **113**: p. 170-183.

182. Hasan, Z., J. Jeon, and S.H. Jhung, *Adsorptive removal of naproxen and clofibric acid from water using metal-organic frameworks.* Journal of Hazardous Materials, 2012. **209–210**(0): p. 151-157.
183. Huang, X.-X., L.-G. Qiu, W. Zhang, Y.-P. Yuan, X. Jiang, A.-J. Xie, Y.-H. Shen, and J.-F. Zhu, *Hierarchically mesostructured MIL-101 metal-organic frameworks: supramolecular template-directed synthesis and accelerated adsorption kinetics for dye removal.* CrystEngComm, 2012. **14**(5): p. 1613-1617.
184. Haque, E., J.W. Jun, and S.H. Jhung, *Adsorptive removal of methyl orange and methylene blue from aqueous solution with a metal-organic framework material, iron terephthalate (MOF-235).* Journal of Hazardous Materials, 2011. **185**(1): p. 507-511.
185. Lin, K.-Y.A. and H.-A. Chang, *Ultra-high adsorption capacity of zeolitic imidazole framework-67 (ZIF-67) for removal of malachite green from water.* Chemosphere, 2015. **139**: p. 624-631.
186. Wang, H.-N., F.-H. Liu, X.-L. Wang, K.-Z. Shao, and Z.-M. Su, *Three neutral metal-organic frameworks with micro- and meso-pores for adsorption and separation of dyes.* Journal of Materials Chemistry A, 2013. **1**(42): p. 13060-13063.
187. Han, S., S. Kim, H. Lim, W. Choi, H. Park, J. Yoon, and T. Hyeon, *New nanoporous carbon materials with high adsorption capacity and rapid adsorption kinetics for removing humic acids.* Microporous and Mesoporous Materials, 2003. **58**(2): p. 131-135.
188. Sandeman, S.R., V.M. Gun'ko, O.M. Bakalinska, C.A. Howell, Y. Zheng, M.T. Kartel, G.J. Phillips, and S.V. Mikhalovsky, *Adsorption of anionic and cationic dyes by activated carbons, PVA hydrogels, and PVA/AC composite.* Journal of Colloid and Interface Science, 2011. **358**(2): p. 582-592.
189. Adamson, A.W., *Physical Chemistry of Surfaces*. 1993: John Wiley & Sons.
190. Kowalczyk, P., A.P. Terzyk, P.A. Gauden, V.M. Gun'ko, and L. Solarz, *Evaluation of the Structural and Energetic Heterogeneity of Microporous Carbons by Means of Novel Numerical Methods and Genetic Algorithms.* Journal of Colloid and Interface Science, 2002. **256**(2): p. 378-395.
191. Gregg, S.J. and K.S.W. Sing, *Adsorption, surface area, and porosity*. 1991: Academic Press.
192. Leboda, R., V.V. Turov, W. Tomaszewski, V.M. Gun'ko, and J. Skubiszewska-Zięba, *Effect of adsorption of nitroaromatic compounds on the characteristics of bound water layers in aqueous suspensions of activated carbons.* Carbon, 2002. **40**(3): p. 389-396.
193. Gun'ko, V.M., V.V. Turov, J. Skubiszewska-Ziba, R. Leboda, M.D. Tsapko, and D. Palijczuk, *Structural characteristics of a carbon adsorbent and influence of organic solvents on interfacial water.* Applied Surface Science, 2003. **214**(1–4): p. 178-189.
194. Ghaedi, M., S. Heidarpour, S. Nasiri Kokhdan, R. Sahraie, A. Daneshfar, and B. Brazesh, *Comparison of silver and palladium nanoparticles loaded on activated carbon for efficient removal of Methylene blue: Kinetic and isotherm study of removal process.* Powder Technology, 2012. **228**: p. 18-25.
195. Faria, P.C.C., J.J.M. Órfão, and M.F.R. Pereira, *Adsorption of anionic and cationic dyes on activated carbons with different surface chemistries.* Water Research, 2004. **38**(8): p. 2043-2052.
196. Gao, Y., S. Xu, Q. Yue, Y. Wu, and B. Gao, *Chemical preparation of crab shell-based activated carbon with superior adsorption performance for dye removal from wastewater.* Journal of the Taiwan Institute of Chemical Engineers, 2016. **61**: p. 327-335.

197. Khaled, A., A.E. Nemr, A. El-Sikaily, and O. Abdelwahab, *Removal of Direct N Blue-106 from artificial textile dye effluent using activated carbon from orange peel: Adsorption isotherm and kinetic studies.* Journal of Hazardous Materials, 2009. **165**(1–3): p. 100-110.
198. Hoda, N., E. Bayram, and E. Ayranci, *Kinetic and equilibrium studies on the removal of acid dyes from aqueous solutions by adsorption onto activated carbon cloth.* Journal of Hazardous Materials, 2006. **137**(1): p. 344-351.
199. Hameed, B.H. and F.B.M. Daud, *Adsorption studies of basic dye on activated carbon derived from agricultural waste: Hevea brasiliensis seed coat.* Chemical Engineering Journal, 2008. **139**(1): p. 48-55.
200. Xiao, J.-D., L.-G. Qiu, X. Jiang, Y.-J. Zhu, S. Ye, and X. Jiang, *Magnetic porous carbons with high adsorption capacity synthesized by a microwave-enhanced high temperature ionothermal method from a Fe-based metal-organic framework.* Carbon, 2013. **59**: p. 372-382.
201. Jiao, C., Y. Wang, M. Li, Q. Wu, C. Wang, and Z. Wang, *Synthesis of magnetic nanoporous carbon from metal-organic framework for the fast removal of organic dye from aqueous solution.* Journal of Magnetism and Magnetic Materials, 2016. **407**: p. 24-30.
202. Chen, B., G. Ma, D. Kong, Y. Zhu, and Y. Xia, *Atomically homogeneous dispersed ZnO/N-doped nanoporous carbon composites with enhanced CO2 uptake capacities and high efficient organic pollutants removal from water.* Carbon, 2015. **95**: p. 113-124.
203. Ricou, P., I. Lecuyer, and P. Le Cloirec, *Removal of Cu2+, Zn2+ and Pb2+ by adsorption onto fly ash and fly ash/lime mixing.* Water Science and Technology, 1999. **39**(10-11): p. 239-247.
204. Janoš, P., H. Buchtová, and M. Rýznarová, *Sorption of dyes from aqueous solutions onto fly ash.* Water research, 2003. **37**(20): p. 4938-4944.
205. El-Mogazi, D., D.J. Lisk, and L.H. Weinstein, *A review of physical, chemical, and biological properties of fly ash and effects on agricultural ecosystems.* Science of The Total Environment, 1988. **74**(0): p. 1-37.
206. Ferey, G., *Hybrid porous solids: past, present, future.* Chemical Society Reviews, 2008. **37**(1): p. 191-214.
207. Tranchemontagne, D.J., J.L. Mendoza-Cortés, M. O'Keeffe, and O.M. Yaghi, *Secondary building units, nets and bonding in the chemistry of metal–organic frameworks.* Chemical Society Reviews, 2009. **38**(5): p. 1257-1283.
208. Alaerts, L., C.E.A. Kirschhock, M. Maes, M.A. van der Veen, V. Finsy, A. Depla, J.A. Martens, G.V. Baron, P.A. Jacobs, J.F.M. Denayer, and D.E. De Vos, *Selective Adsorption and Separation of Xylene Isomers and Ethylbenzene with the Microporous Vanadium(IV) Terephthalate MIL-47.* Angewandte Chemie International Edition, 2007. **46**(23): p. 4293-4297.
209. Mueller, U., M. Schubert, F. Teich, H. Puetter, K. Schierle-Arndt, and J. Pastre, *Metal-organic frameworks-prospective industrial applications.* Journal of Materials Chemistry, 2006. **16**(7): p. 626-636.
210. Akhtar, F., L. Andersson, S. Ogunwumi, N. Hedin, and L. Bergström, *Structuring adsorbents and catalysts by processing of porous powders.* Journal of the European Ceramic Society, 2014. **34**(7): p. 1643-1666.
211. Zacher, D., O. Shekhah, C. Wöll, and R.A. Fischer, *Thin films of metal–organic frameworks.* Chemical Society Reviews, 2009. **38**(5): p. 1418-1429.

212. Schwab, M.G., I. Senkovska, M. Rose, M. Koch, J. Pahnke, G. Jonschker, and S. Kaskel, *MOF@ PolyHIPEs.* Advanced Engineering Materials, 2008. **10**(12): p. 1151-1155.
213. Lee, U., A.H. Valekar, Y.K. Hwang, and J.S. Chang, *Granulation and Shaping of Metal–Organic Frameworks.* The Chemistry of Metal Organic Frameworks: Synthesis, Characterization, and Applications: Synthesis, Characterization, and Applications, 2016: p. 551-572.
214. Yin, H., H. Kim, J. Choi, and A.C.K. Yip, *Thermal stability of ZIF-8 under oxidative and inert environments: A practical perspective on using ZIF-8 as a catalyst support.* Chemical Engineering Journal, 2015, 278,: p.293-300.
215. Cameron, I., F. Wang, C. Immanuel, and F. Stepanek, *Process systems modelling and applications in granulation: a review.* Chemical Engineering Science, 2005. **60**(14): p. 3723-3750.
216. Ren, J., N.M. Musyoka, H.W. Langmi, A. Swartbooi, B.C. North, and M. Mathe, *A more efficient way to shape metal-organic framework (MOF) powder materials for hydrogen storage applications.* international journal of hydrogen energy, 2015. **40**(13): p. 4617-4622.
217. Crawford, D., J. Casaban, R. Haydon, N. Giri, T. McNally, and S.L. James, *Synthesis by extrusion: continuous, large-scale preparation of MOFs using little or no solvent.* Chemical Science, 2015. **6**(3): p. 1645-1649.
218. Alcaniz-Monge, J., G. Trautwein, M. Pérez-Cadenas, and M. Román-Martínez, *Effects of compression on the textural properties of porous solids.* Microporous and Mesoporous Materials, 2009. **126**(3): p. 291-301.
219. Plaza, M., A. Ferreira, J. Santos, A. Ribeiro, U. Müller, N. Trukhan, J. Loureiro, and A. Rodrigues, *Propane/propylene separation by adsorption using shaped copper trimesate MOF.* Microporous and Mesoporous Materials, 2012. **157**: p. 101-111.
220. Hesse, M., U. Mueller, and O. Yaghi, *Shaped bodies containing metal-organic frameworks*. 2009, Google Patents.
221. Tagliabue, M., C. Rizzo, R. Millini, P.D. Dietzel, R. Blom, and S. Zanardi, *Methane storage on CPO-27-Ni pellets.* Journal of Porous Materials, 2011. **18**(3): p. 289-296.
222. Bazer-Bachi, D., L. Assié, V. Lecocq, B. Harbuzaru, and V. Falk, *Towards industrial use of metal-organic framework: Impact of shaping on the MOF properties.* Powder Technology, 2014. **255**: p. 52-59.
223. Couck, S., E. Gobechiya, C.E.A. Kirschhock, P. Serra-Crespo, J. Juan-Alcañiz, A. Martinez Joaristi, E. Stavitski, J. Gascon, F. Kapteijn, G.V. Baron, and J.F.M. Denayer, *Adsorption and Separation of Light Gases on an Amino-Functionalized Metal–Organic Framework: An Adsorption and In Situ XRD Study.* ChemSusChem, 2012. **5**(4): p. 740-750.
224. Serra-Crespo, P., E. Stavitski, F. Kapteijn, and J. Gascon, *High compressibility of a flexible metal-organic framework.* RSC Advances, 2012. **2**(12): p. 5051-5053.
225. Hu, Y., H. Lian, L. Zhou, and G. Li, *In situ solvothermal growth of metal–organic framework-5 supported on porous copper foam for noninvasive sampling of plant volatile sulfides.* Analytical chemistry, 2014. **87**(1): p. 406-412.
226. Shekhah, O., L. Fu, R. Sougrat, Y. Belmabkhout, A.J. Cairns, E.P. Giannelis, and M. Eddaoudi, *Successful implementation of the stepwise layer-by-layer growth of MOF thin films on confined surfaces: mesoporous silica foam as a first case study.* Chemical Communications, 2012. **48**(93): p. 11434-11436.

227. Zhenxin, Z. and T. Matsuura, *Discussions on the formation mechanism of surface pores in reverse osmosis, ultrafiltration, and microfiltration membranes prepared by phase inversion process.* Journal of Colloid and Interface Science, 1991. **147**(2): p. 307-315.
228. Wienk, I.M., R.M. Boom, M.A.M. Beerlage, A.M.W. Bulte, C.A. Smolders, and H. Strathmann, *Recent advances in the formation of phase inversion membranes made from amorphous or semi-crystalline polymers.* Journal of Membrane Science, 1996. **113**(2): p. 361-371.
229. Drioli, E. and L. Giorno, *Comprehensive membrane science and engineering*. Vol. 1. 2010: Newnes.
230. Yao, J., K. Wang, M. Ren, J. Zhe Liu, and H. Wang, *Phase inversion spinning of ultrafine hollow fiber membranes through a single orifice spinneret.* Journal of Membrane Science, 2012. **421–422**: p. 8-14.
231. Rozelle, L., J. Cadotte, R. Corneliussen, E. Erickson, K. Cobian, and C. Kopp Jr, *Phase Inversion Membranes.* 2000.
232. Li, N.N., A.G. Fane, W.W. Ho, and T. Matsuura, *Advanced membrane technology and applications*. 2011: John Wiley & Sons.
233. Chung, T.S. and X. Hu, *Effect of air-gap distance on the morphology and thermal properties of polyethersulfone hollow fibers.* Journal of applied polymer science, 1997. **66**(6): p. 1067-1077.
234. Chung, T.S., Z.L. Xu, and W. Lin, *Fundamental understanding of the effect of air-gap distance on the fabrication of hollow fiber membranes.* Journal of applied polymer science, 1999. **72**(3): p. 379-395.
235. Widjojo, N. and T.-S. Chung, *Thickness and air gap dependence of macrovoid evolution in phase-inversion asymmetric hollow fiber membranes.* Industrial & engineering chemistry research, 2006. **45**(22): p. 7618-7626.

Chapter 3. Simple fabrication of zeolitic imidazolate framework ZIF-8/polymer composite beads by phase inversion method for efficient oil sorption

3.1. Overview

In this chapter, the phase inversion technique was utilized to shape ZIF-8 powder for efficient sorption of oils and organic compounds from water. ZIF-8 with different loadings were added to polymer (PES) and effect of loading on the characteristics and performance of the beads was investigated. The composite beads exhibited very low bulk densities and high oil sorption capacities. The prepared ZIF-8/PES beads were very easy to handle and recycle which shows their advantage compared with ZIF-8 powder in adsorption applications. The outcomes of this study showed that ZIF-8 could be shaped using this technique while preserving its crystallinity and high surface area which is essential in practical applications. This study sheds light on the universal applicability of phase inversion method for preparing spheres and beads for a variety of applications especially adsorption.

This chapter has been formatted from the following published manuscript (Copyright reference number: 4071160823459, Elsevier).

Z.Abbasi, E. Shamsaei, X.-Y. Fang, B. Ladewig, H. Wang, Simple Fabrication of ZIF-8 Composite Beads by Phase Inversion Method for Efficient Oil Sorption. *J. Colloid Interface Sci.* 2017, 493, 150-161.

3.2. Introduction

Oil spillage and industrial organic pollution have become serious environmental issues around the world which pose threats to human health as well as the ecosystem [1-4]. Oil contamination can result in the increase of biochemical oxygen demand (BOD) and chemical oxygen demand (COD) causing serious environmental hazards [5]. As a result, great attention has been paid to the development of efficient and cost-effective approaches to cleaning up oil spillage, especially where it occurs in water bodies [3].

Among the various different approaches, adsorption has the advantage of being simple and cost effective with the ability of removing different types of contaminants form water [6]. Natural adsorbents such as activated carbon [7] and natural zeolites [8] have been shown to be somewhat effective in oil removal. Although these natural sorbents have the advantage of being economic, they have the limitation of low oil sorption capacity, low hydrophobicity and poor buoyancy [9]. Therefore, many efforts have been made to tackle the issue of oil spillage pollution by developing efficient adsorbents like microporous polymers [10-12], carbon-nanotube (CNT) [13], graphene [1] as well as carbon soot sponge [2], graphene aerogel [14] and macroporous carbon nanofiber film [15]. A universal and consistent drawback of these materials is their complex synthesis procedures and they usually require surface modification before oil adsorption which restricts their practical applications. For example, in the synthesis

of spongy graphene, it is required to prepare graphene oxide by oxidizing expandable graphite under 98 wt. % sulphuric acid and potassium permanganate solution at 98℃ [1] which is very dangerous. In addition, for preparation of carbon nanofiber oil sorbent, the coating of the material by polydimethylsiloxane is needed prior to application in oil adsorption [16].

Different kinds of monodisperse composite spheres have been employed in separation [17], drug delivery [18] catalysis [19] as well as adsorption [20] due to their high surface area and porous structure. However, millimetre sized spheres and beads are much easier to handle and recover compared with smaller scale (like nano scale) spheres. To date, there have been several attempts to produce beads and spheres using different techniques. For example, a templating technique involving high internal phase emulsions (HIPEs) has been developed for producing monodisperse emulsion-templated polymer beads via sedimentation polymerization. Nevertheless, this technique has a number of limitations including utilization of alkoxide precursors which are highly reactive to water and should be separated before formation of oil-in-water emulsion. Moreover, it is likely that the emulsion converts to gel before the injection process is completed [21]. In addition, this method includes several steps like immersion of polymer bead scaffolds into inorganic precursor, filtration, gelation and calcination. These steps make the process complicated and time consuming. Therefore, since the existing preparation methods are very complicated, an easy and straight forward method was established to prepare millimetre-sized beads.

Phase inversion is a common method for preparation of asymmetric membranes. This method has been utilized in our group to synthesize porous hollow fiber membrane [22], nanocomposite ultrafiltration membrane [23], hollow carbon beads for oil sorption [24], and zeolitic imidazolate framework ZIF-8 polymer spheres for gas adsorption [25].

Metal organic frame works (MOFs) are a group of porous materials composed of a metal ion or a cluster of metal ions and an organic molecule which is called a linker. MOFs have high porosity and open metal sites which makes them suitable for different applications specifically for adsorptive removal of contaminates from water [26]. Zeolitic imidazolate frameworks (ZIFs) are a category of MOF materials which exhibit satisfying chemical and thermal stability. ZIF-8 is one of the most studied ZIF materials with the formula of Zn(2-methylimidazole)$_2$ with a sodalite zeolitic structure. ZIF-8 has pore size of 1.1 nm and accessible pore window of 0.34 nm which has been investigated for a variety of applications such as adsorption, separation and catalytic applications [27-30]. Furthermore, ZIF-8 has been extensively studied for the adsorptive removal of pollutants from water [27, 31-35] since it is amongst the most stable metal organic frameworks. Recently, ZIF-8 particles in the form of powder have been utilized for adsorption of oil droplets from water [36].

Metal organic frameworks are generally prepared as powders which are not suitable for many practical applications including adsorption and catalysis. Therefore, shaping these materials is required for easy handling and recycling [37]. HKUST-1 MOF has been shaped as beads by coating onto polymer and oxide composite beads [37]. SIM-1 (an isostructural to ZIF-8) was coated on spherical alumina beads [38]. However, the methods utilized for coating MOF on the beads require high temperatures like 85℃ for 48 hours [38].

In this work we demonstrate a simple, fast and one step method at room temperature for fabricating ZIF-8 particles into polymer beads using a phase inversion method. The beads prepared by this method are very easy to handle and recover from oil-water mixture compared to ZIF-8 powder. ZIF-8/PES composite beads exhibited efficient oil sorption and they are amongst the best sorbent materials previously reported; especially in comparison with natural common sorbents like activated carbon as well as other synthesized beads.

3.3. Materials and Methods

3.3.1. Materials

Zinc nitrate hexahydrate ($Zn(NO_3)_2.6H_2O$), 2-methylimidazole (Hmim), 1-methyl-2-pyrrolidone (NMP) (99%), toluene, paraffin oil, olive oil and oil red were purchased from Sigma Aldrich. *n*-Hexane was purchased from Merck. Polyethersulfone (PES) was supplied from BASF Company. All chemicals were used as received without further purification.

3.3.2. Synthesis of ZIF-8 nanocrystals

ZIF-8 was synthesized by a synthesis method reported by Koji Kida et al. [16] in aqueous solution. 0.744 g (2.5 mmol) of $Zn(NO_3).6H_2O$ and 12.3 g (0.15 mol) of Hmim were dissolved in 10 ml and 90 ml of deionized water respectively and stirred for 24 hours. ZIF-8 nanocrystals were collected by washing with methanol and centrifuging (8000 rpm, 15 min) for three times and then dried at 60℃ overnight.

3.3.3. Preparation of polyethersulfone spheres and ZIF-8/PES composite beads by phase inversion method

Typically, 1 g of polyethersulfone was dissolved in 5.5 g NMP under magnetic stirring at room temperature overnight. The polymer solution was vertically pumped into water with an air gap (the distance between the needle tip and water surface) of about 4 cm. The flowrate of the polymer solution was set at 0.2 ml/min and the syringe tip was 18 G (inner diameter of roughly 0.84 mm). Solid polymer spheres were formed in water immediately through solvent/water exchange and kept in water overnight for further solvent/non-solvent exchange. Then formed PES spheres were dried at 80℃ overnight.

ZIF-8/PES composite beads were made by the same method except that a syringe tip with 14G (inner diameter of roughly 1.6 mm) size was used. ZIF-8/PES composite beads were prepared by ZIF-8: PES ratios of 0.5, 1, 2 and 4. The ZIF-8/polymer slurry was viscous and the resulting beads were oval in shape as with the ZIF-8: PES ratio of 4. It is worth mentioning that for higher loadings of ZIF-8, i.e. for ZIF-8: PES ratios of 2 and 4, the amount of NMP solvent increased to 8 and 10.5 g respectively. Moreover, for ZIF-8/PES-2 and ZIF-8/PES-4, the air gap had to be increased to double (8 cm) in order to be able to form the ZIF-8/PES beads in the water tank.

3.4. Characterization

Nitrogen adsorption and desorption isotherms were measured at liquid nitrogen temperature (77 K) using an accelerated surface area and porosimetry system (ASAP 2020, Micromeritics, USA) for surface area measurements. The pore size distributions of ZIF-8 powder and ZIF-8/PES composite beads were measured by nitrogen sorption using ASAP 2020. However, the pore size distribution for PES spheres was analysed by mercury porosimetry (AutoPore IV 9500 mercury porosimeter, Micromeritics, USA). The crystal structures of the samples were identified using an X-ray diffractometer (Miniflex 600, Rigaku) with Cu Kα radiation at 40 kV and 20 mA over the 2θ range of 5-40°. The morphology of the adsorbent materials was observed using a scanning electron microscope (FEI Nova NanoSEM 450 FEG SEM). The water droplet contact angle measurement was carried out at room temperature with 1 μL water droplet on the film of samples using contact angle goniometer (Dataphysics OCA15, Dataphysics, Germany). A film of the sample was made by manual pressing. An attenuated total reflectance (ATR) Fourier Transform Infrared (FTIR) (Perkin Elmer, USA) was used to collect the FTIR spectra of the samples in the range of 500-4000 cm^{-1} at an average of 32 scans with a resolution of 4 cm^{-1}.

3.5. Oil sorption experiments

For oil adsorption capacity measurement, the composite beads were immersed in several oils and organic compounds including paraffin oil, olive oil, toluene and *n*-Hexane for half an hour. Then the beads were wiped to remove the extra oil or organic compound on the surface and then weighed very quickly by a balance to minimize errors arising from solvent evaporation. The amount of adsorbed oil (the volume percentage of oil adsorbed on the composite beads) was calculated as follows:

$$Volume\ gain\ (\%) = \frac{(W_S - W_C)}{W_C} \times \frac{\rho_C}{\rho_O} \times 100\%$$

where W_s is the weight of ZIF-8 composite beads after oil adsorption and W_c is the initial weight of the beads before adsorption. ρ_c is the bulk density of ZIF-8/PES beads and ρ_o is the oil density.

The composite beads were regenerated by simple washing with ethanol to assess the recyclability of the prepared beads. The used oil-rich beads were added to ethanol and mixed for a few hours. The regenerated beads were dried at 70℃ and tested for subsequent oil sorption experiments.

3.6. Results and Discussions

3.6.1. Characterization of ZIF-8/PES composite beads

The XRD analysis on ZIF-8 beads was done to investigate the incorporation of ZIF-8 particles into the polymer (PES) framework. The X-ray diffraction patterns (Fig. 3-1) confirms the existence of ZIF-8 particles in the matrix of the polymer composite beads. All of the composite beads exhibit the diffraction patterns similar to that of pure ZIF-8 powder shown in Fig. 3-1.

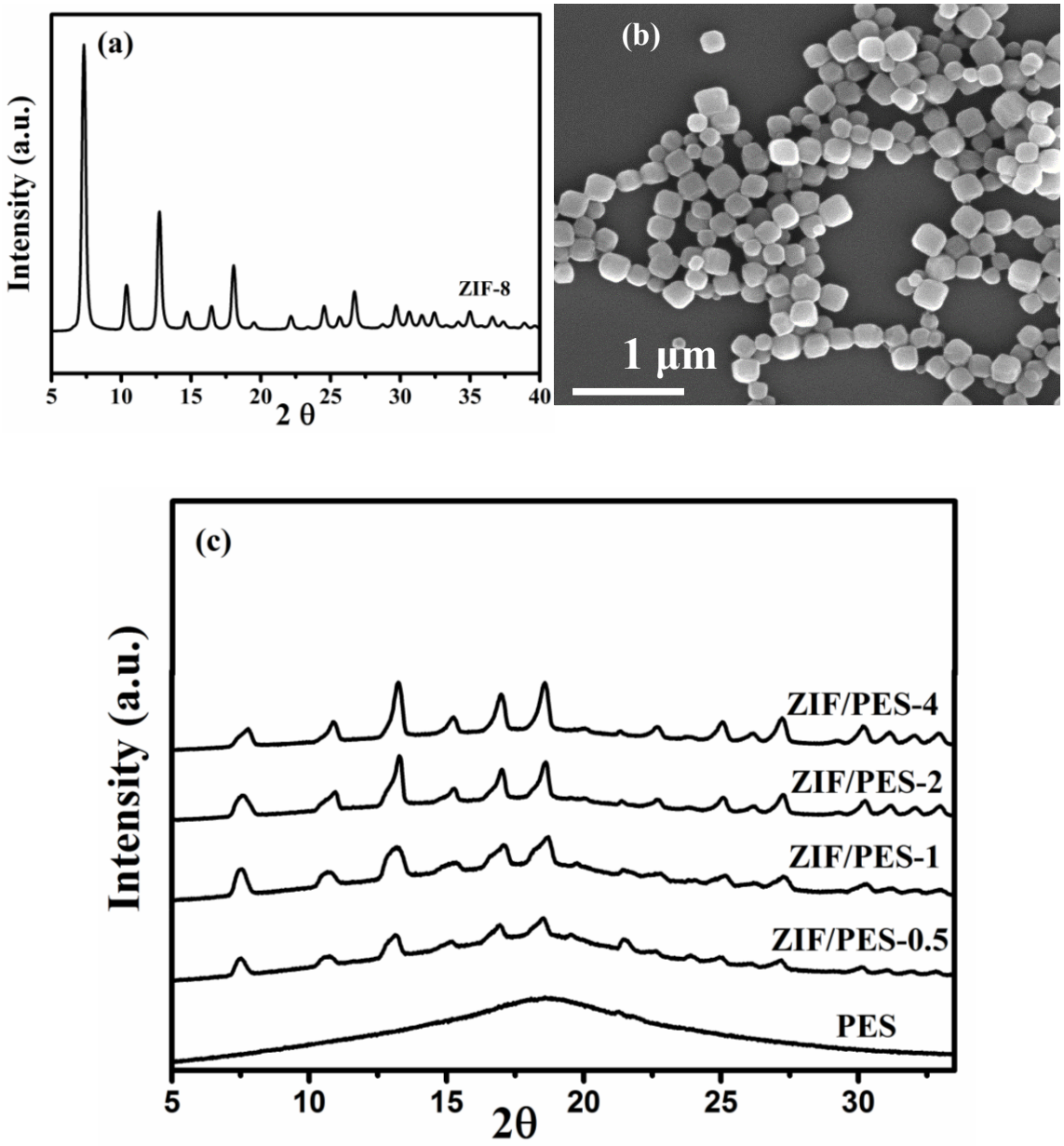

Fig. 3-1 XRD pattern (a) and SEM image (b) of ZIF-8 nanocrystals and XRD patterns of PES polymer and ZIF-8/PES composite beads with different loadings (c)

It is apparent that by increasing the ZIF-8 loading the corresponding XRD peaks intensity also increases. This also shows that ZIF-8 particles are dispersed within the beads matrices and this is consistent with SEM results.

Fig. 3-2 shows the morphology of the top surface of the beads indicating that ZIF-8 particles are coated and dispersed on the outer surface of the beads. It is evident from the figure that the outer surface of the composite spheres are covered by ZIF-8 particles and the coverage becomes more pronounce as the ZIF-8 loading increases. For the PES spheres the outer surface of the beads are very smooth without any particles on the surface. As the ZIF-8 loading increases, the top surface contains more ZIF-8 particles. As ZIF-8 particles migrate to the surface, large pores are created at the outer surface of the composite bead. Apart from the creation of large pores on the surface, the polymer keeps the ZIF particles together very uniform in the composite texture. This results in more exposure of the ZIF particles to the oil and organic molecules and leads to a higher performance. The creation of the large pores on the surface also facilitates the pollutant absorption and diffusion into the composite bead framework.

For investigation of the inner structure of ZIF polymer composite beads, a single bead was cut into half. From the cross sectional images it can be seen that ZIF-8 particles are fully dispersed within the pores of the polymer framework. Fig. 3-3 shows the coverage at different magnifications. The cross section of the ZIF-8/PES beads shows a very porous structure with large channels of macrometer sizes which are covered by ZIF-8 particles. The ZIF-8 particles are distributed inside the pores and have the diameter of about 250 nm. The macropores inside the beads facilitate ZIF-8 incorporation in the beads matrices. As can be seen from the SEM images, ZIF-8 particles are fairly well distributed among the channels and inside the pores. The porous framework within the polymer matrix consists of large micrometre pores which were created during the phase inversion process. Fig. 3-4 shows the inversion process and how the macrometer pores are created in the polymer sphere during this process.

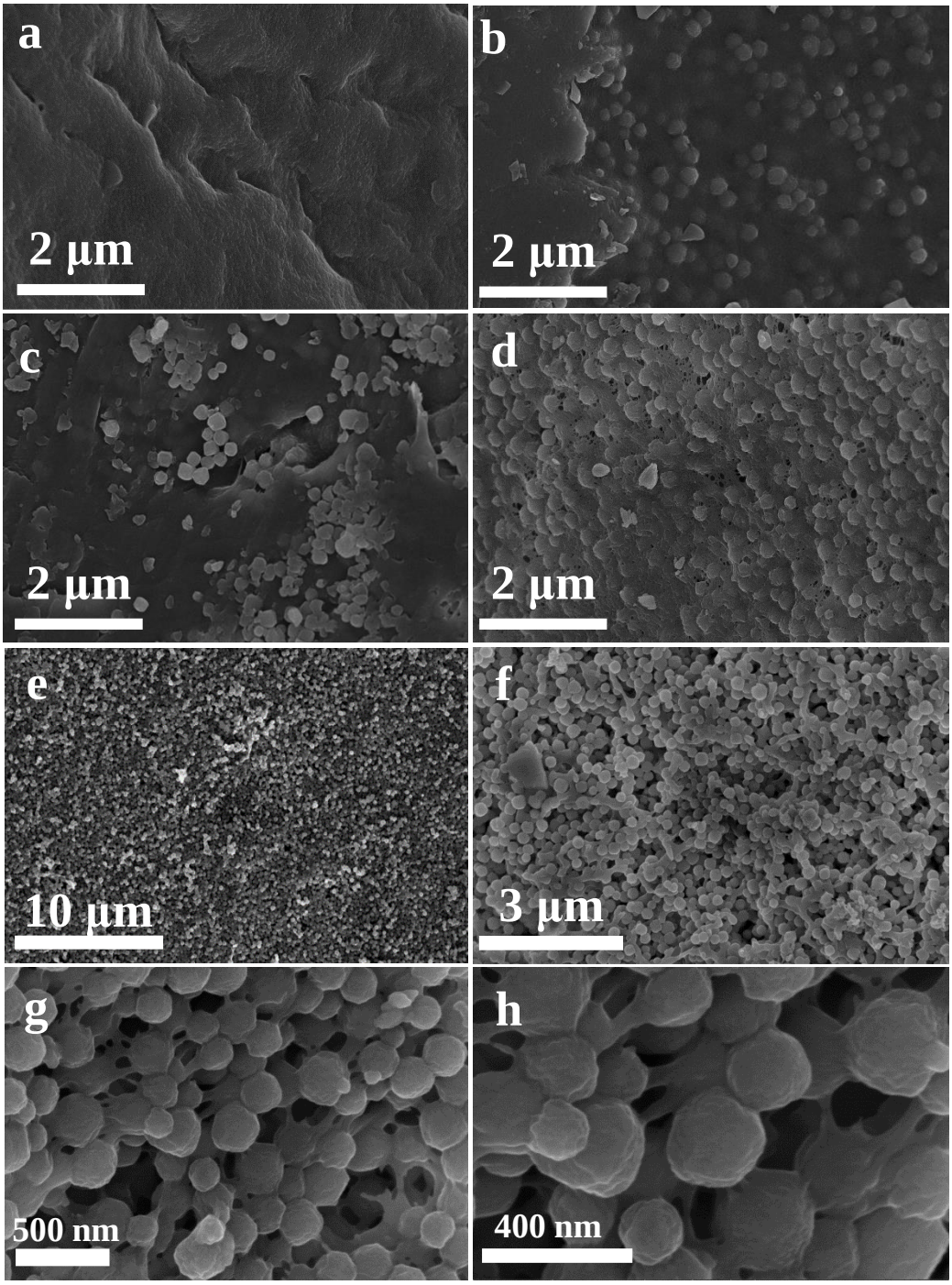

Fig. 3-2 Top-surface SEM images of PES (a), ZIF/PES-0.5 (b), ZIF/PES-1 (c) and ZIF/PES-2 (d). The images (e-h) show the top surface of ZIF/PES-4.

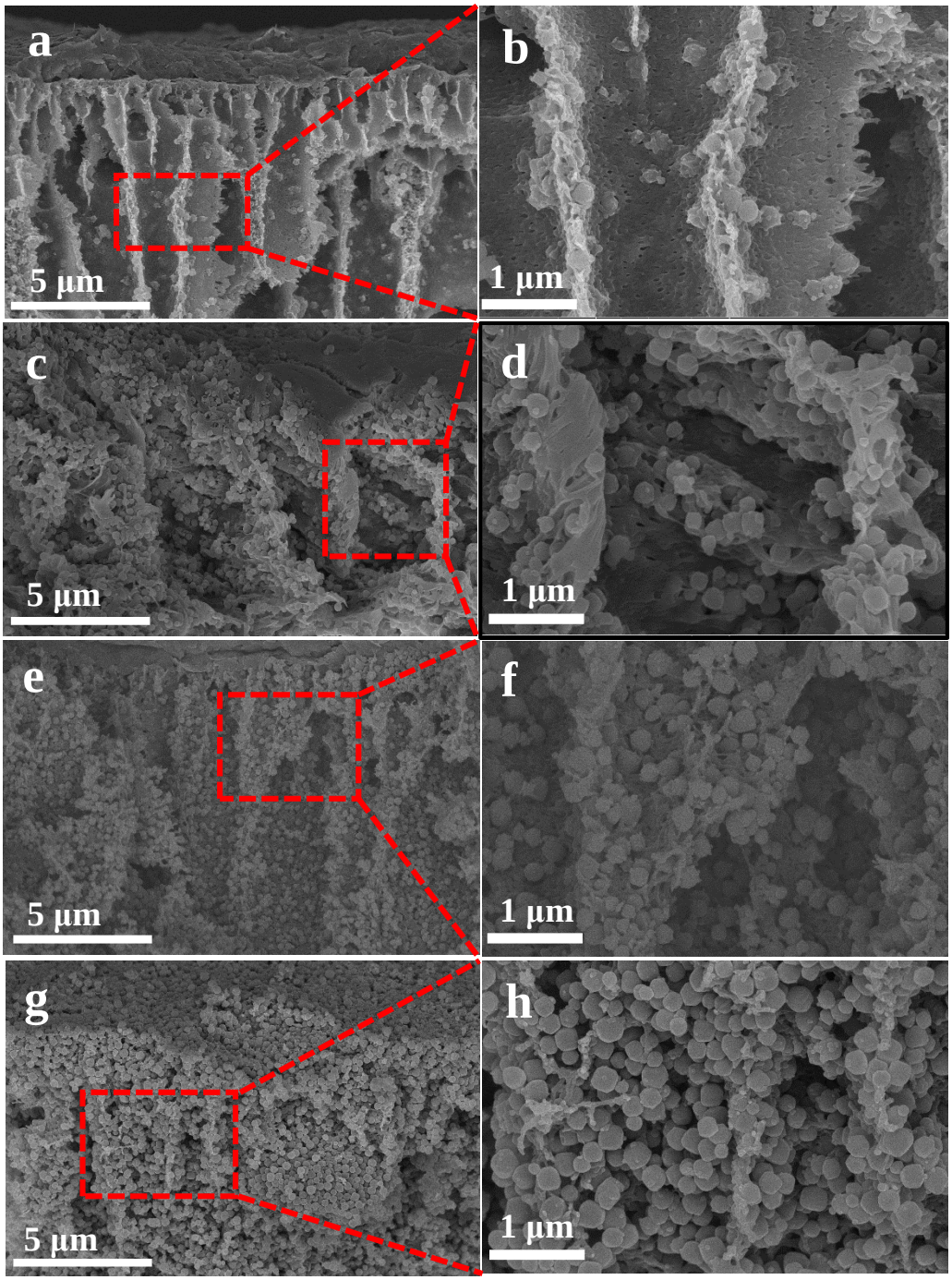

Fig. 3-3 Cross sectional SEM images of ZIF/PES-o.5 (a, b), ZIF/PES-1 (c, d), ZIF/PES-2 (e, f) and ZIF/PES-4 (g, h).

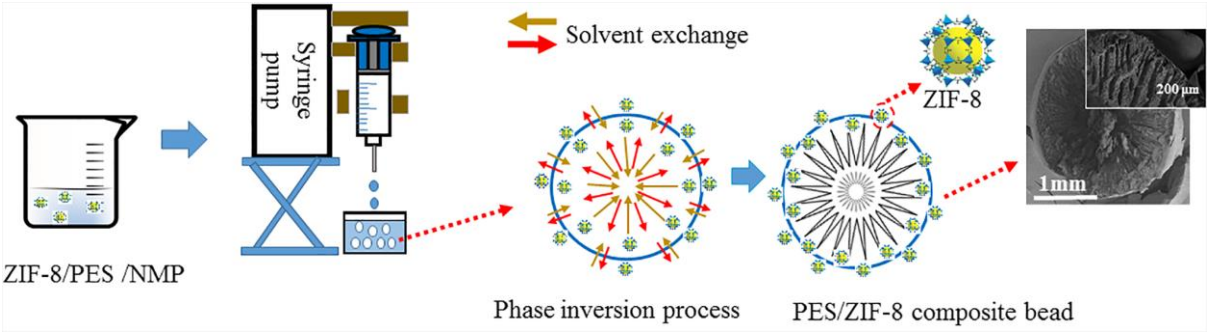

Fig. 3-4 Schematic illustration of formation of ZIF-8/PES composite beads via phase inversion and the creation of porous framework

Nitrogen adsorption-desorption isotherms at 77 K for the composite beads are shown in Fig. 3-5. As can be seen from Fig. 3-5 the surface areas of the composite beads increased with raising the loading of ZIF-8 powder into the polymer matrix. Therefore, the adsorption capacities of the oil and organic compounds increased accordingly. ZIF-8 is well-known for having very high surface area (1384.2 m^2/g BET and 1849 m^2/g Langmuir surface area) as reported in Table 3-1.

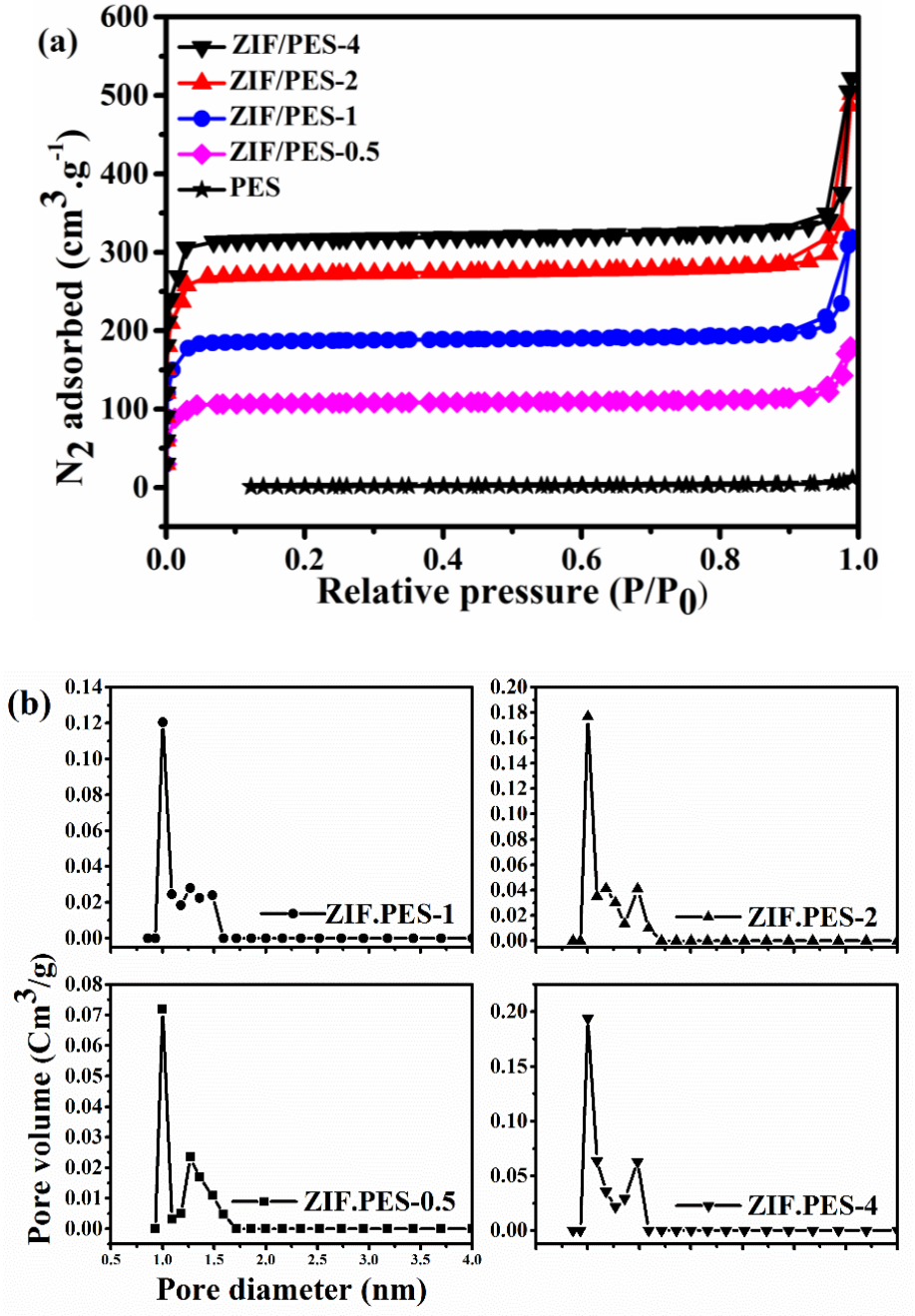

Fig. 3-5 Nitrogen adsorption-desorption isotherm of PES and ZIF-8/PES composite beads (a) and the pore size distributions for ZIF-8/PES composite beads (b).

Table 3-1 Surface area analysis parameters of ZIF-8, PES and ZIF-8/PES composite beads.

Sample	BET surface area ($m^2.g^{-1}$)	Langmuir surface area ($m^2.g^{-1}$)	Total pore volume[a] ($cm^3.g^{-1}$)	Micropore volume ($cm^3.g^{-1}$)
ZIF-8	1384.2±33.5	1849±35.1	1.1±0.18	0.63±0.014
ZIF/PES-4	1030.6±20.9	1382±10.8	0.81	0.47
ZIF/PES-2	882.3±17.9	1185.2±10.1	0.77	0.4
ZIF/PES-1	602±13.7	814.8±5.02	0.49	0.27
ZIF/PES-0.5	343.2±8.5	470.8±5.9	0.27	0.16
PES	0.6	NA	0.01	0.0

[a] At P/P0=0.99

With increasing the loading of ZIF-8 particles in the polymer composite, the BET surface area increases as 343.2, 602, 882.3 and 1030.6 for ZIF/PES-0.5, ZIF/PES-1, ZIF/PES-2 and ZIF/PES-4 respectively. ZIF/PES-4 has the highest surface area among the polymer composite beads and the surface area is very close to the pure ZIF-8 powder's surface area. ZIF/PES-4 exhibits the highest adsorption capacity for all the oil and organic model compounds which can be attributed to the very high surface area as well as its high pore volume. The pore size distributions are demonstrated in Fig. 3-5. The ZIF-8/PES beads exhibit pore size distributions similar to ZIF-8.

The pore size distribution of the PES beads was defined using the mercury intrusion porosimetry to analyse the macroporous structure of the PES beads, since the nitrogen sorption analysis is only applicable for microporous and mesoporous materials. Therefore, the pore size distribution of ZIF-8 was determined by nitrogen adsorption-desorption analysis but for PES spheres, mercury porosimetry was utilized. The macro meter pore size distribution of PES

spheres is shown in Fig. 3-6. The macropore size from the mercury porosimetry is defined in the range of 1-3 μm which is consistent with the SEM results (Fig. 3-3).

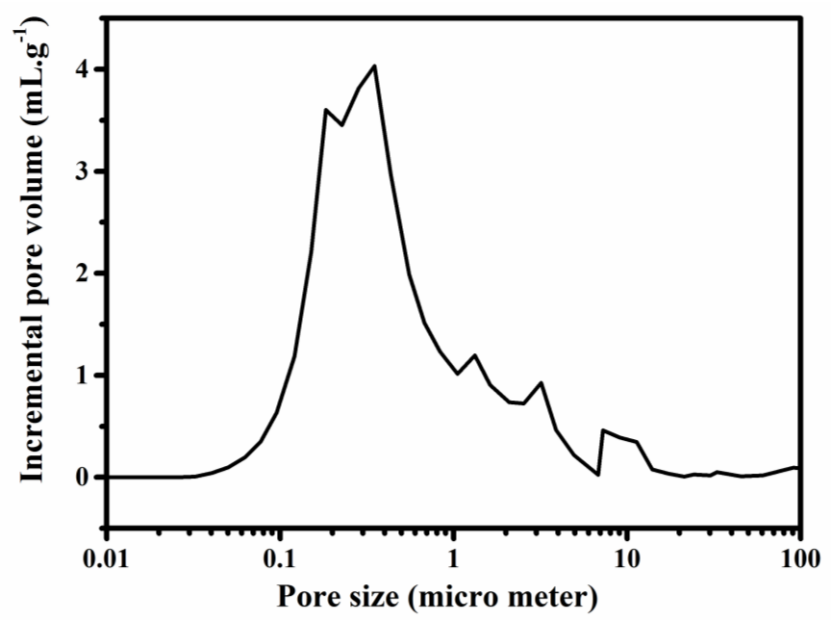

Fig. 3-6 Mercury porosimetry curve of PES.

FTIR spectra of ZIF-8/PES beads were very similar to the pure ZIF-8 (Fig. 3-7). The peaks at 3135 and 2929 are characteristic of aromatic and aliphatic C-H stretch of imidazole while the peaks observed at 1584 and 800-1500 (759, 1145, 1306 and 1444) are assigned to C=N stretch mode and entire imidazole ring vibrations mode, respectively [39].

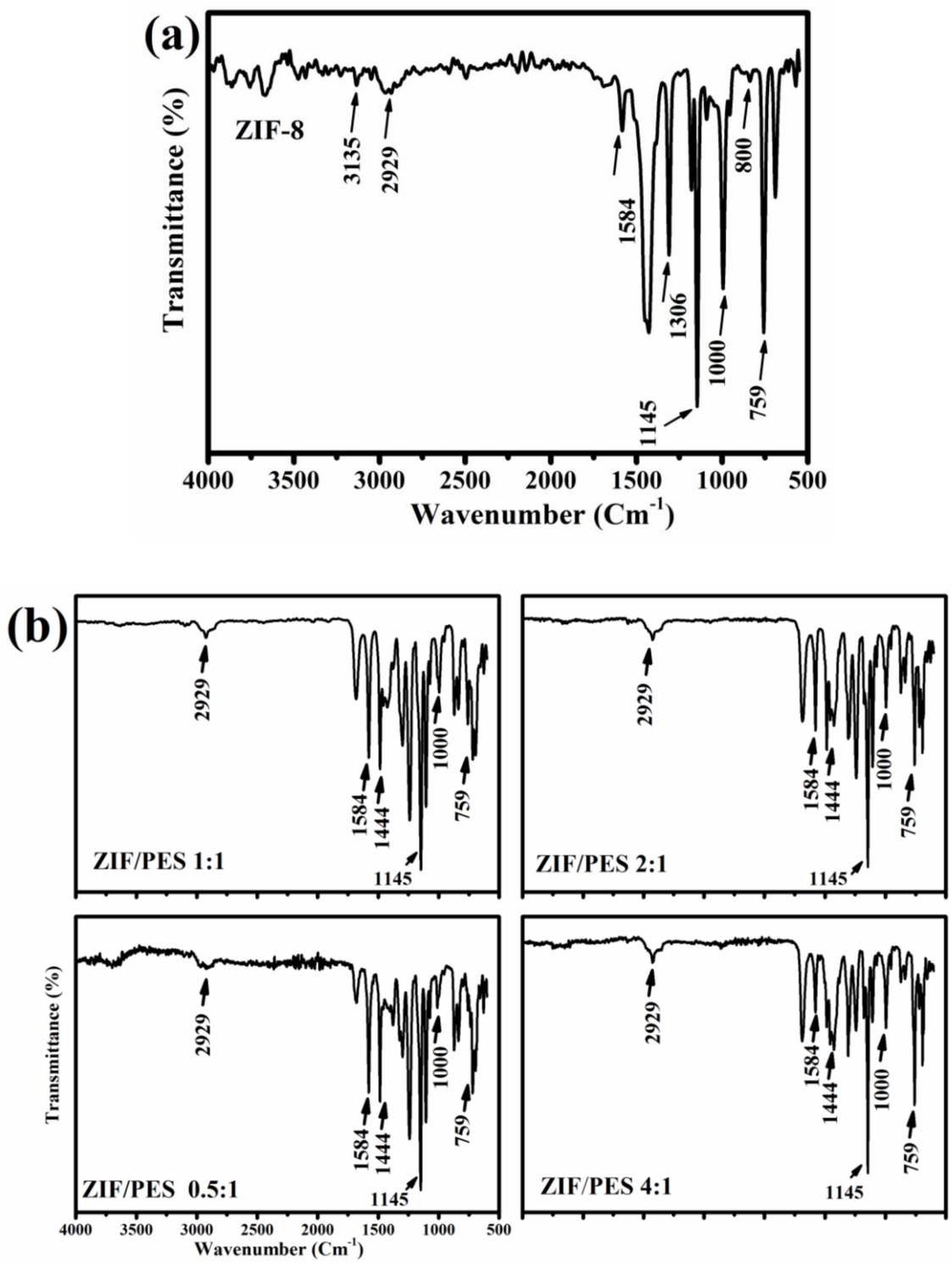

Fig. 3-7 FTIR spectra of ZIF-8 (a) and ZIF/PES beads with different ZIF/PES ratios (b)

3.6.2. Oil sorption of ZIF-8/PES composite beads

The bulk densities of the ZIF-8/PES composite beads were calculated as 0.035, 0.053, 0.173, 0.1875 and 0.2657 g/Cm^3 corresponding to PES, ZIF/PES-0.5, ZIF/PES-1, ZIF/PES-2 and ZIF/PES-4 respectively as shown in Table 3-2.

Table 3-2 Bulk densities of the ZIF-8/PES composite beads in comparison with ZIF-8 and PES

Material	Bulk density (g.cm^{-3})
ZIF-8	0.36±0.017
ZIF/PES-4	0.26±0.012
ZIF/PES-2	0.18±0.008
ZIF/PES-1	0.17±0.006
ZIF/PES-0.5	0.053±0.002
PES	0.035±0.0012

The very low bulk density allows the beads to float easily on the surface of water. Consequently, these ZIF-8/PES composite beads are evaluated as sorbents for oil spillage clean-up.

The ZIF-8/PES composite beads with various loadings are shown in Fig. 3-8. It can be seen that by increasing the ZIF-8 loading, the shape of the beads changes from spheres to ovals. The diameter of the PES beads and ZIF-8 composite beads are 1-2 mm and 2-3 mm respectively. To demonstrate ZIF-8/PES beads adsorb oil efficiently, paraffin oil which was labelled with oil red was poured on the surface of water. Then ZIF-8/PES composite beads were gently placed on the surface of oil-water as illustrated in Fig. 3-9. The figure shows that composite beads absorb oil efficiently from the surface of water.

The oil adsorption capacity depends on the hydrophobic nature of the adsorbent since oil droplets are hydrophobic in nature. Thus hydrophobic interaction between the oil molecules

and the adsorbent surface facilitates the oil sorption process. It is believed that the suitable oil sorbent is required to be hydrophobic. Improving hydrophobicity of the sorbent surface will enhance the van der Waals force and hydrophobic interaction between oil droplets and sorbent materials which leads to high sorption capacity. Sorbent materials are also required to have high surface area and porosity to offer adequate surface sorption sites for catching oil molecules [40].

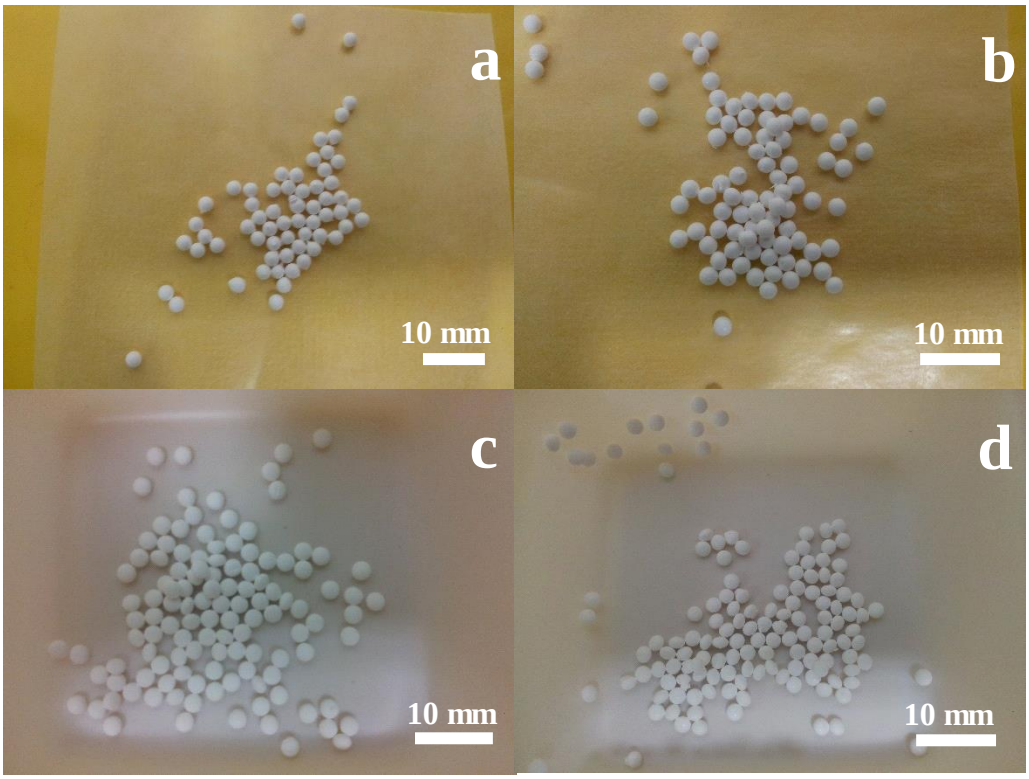

Fig. 3-8 Digital images of ZIF-8 composite beads: ZIF/PES-0.5 (a), ZIF/PES-1 (b), ZIF/PES-2 (c) ZIF/PES-4 (d)

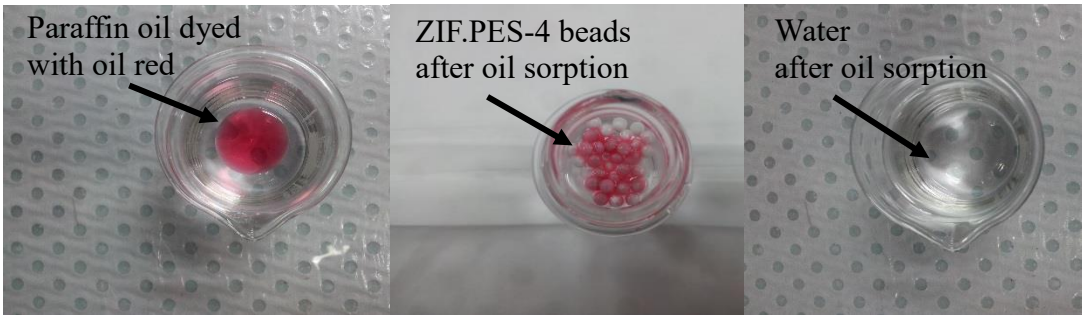

Fig. 3-9 Digital images of ZIF-8 composite beads floating on the surface of water and paraffin oil sorption marked with oil red.

Several oils and organic solvents were used to examine the saturated oil sorption capacities of the ZIF-8/PES composite beads for different kind of pollutants and the results are presented in Fig. 3-10. It can be seen that the composite beads have more tendency to adsorb paraffin and olive oil rather than *n*-Hexane and toluene organic solvents. The ZIF-8/PES beads with ZIF-8: PES ratio of 4, can adsorb up to 37.6% of their volume for paraffin oil while the corresponding uptake for olive oil is 35.6%. The corresponding uptakes for the composite beads with the ZIF-8: PES ratios of 0.5, 1 and 2 were 6.5, 10.2 and 24.9% for paraffin oil and 3.2, 8.5 and 18.9% for olive oil respectively.

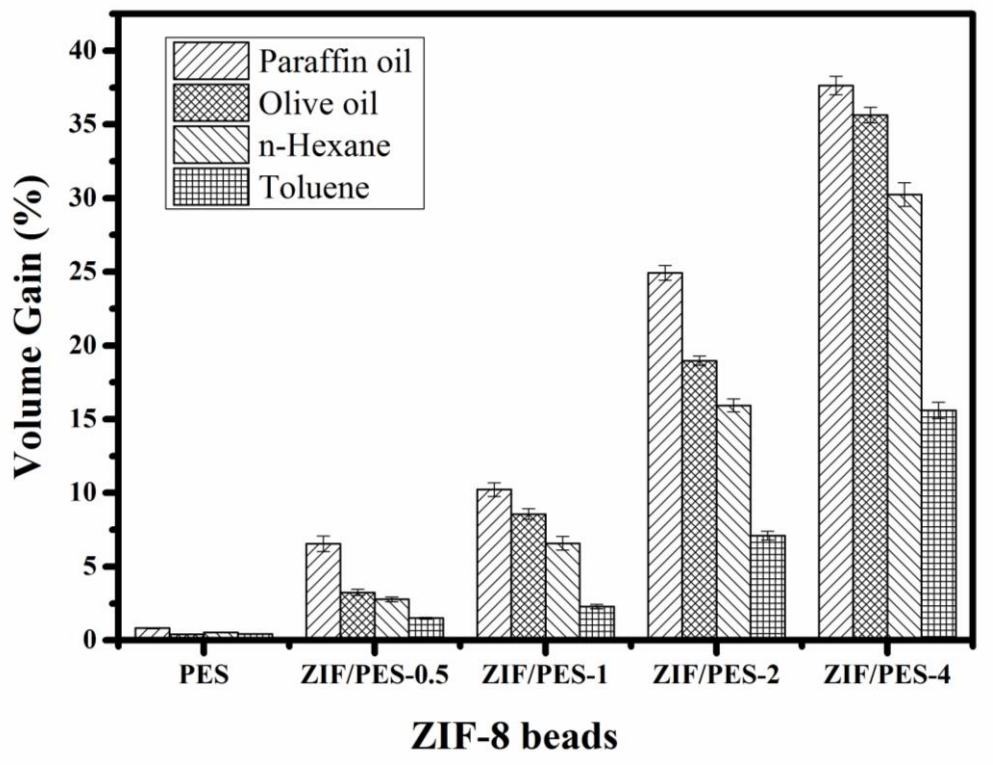

Fig. 3-10 Oil sorption capacities of ZIF-8 composite beads for oils and organic solvents in terms of volume gain.

ZIF-8 has been reported to be a highly hydrophobic microporous material [41-44]. The hydrophobicity of ZIF-8 has been investigated and proved by water adsorption [42]. This hydrophobicity is attributed to its chemical composition i.e. the methyl-functionalized *Im* linkers as well as the coordinative saturation of the metal sites. Typically, ZIF materials can have hydrophobic framework if the *Im* linkers do not consist of hydrophilic functionalities [41]. The increasing of the ZIF-8 loading in the composite beads framework, results in a large amount of ZIF-8 particles to be present on the beads surfaces (refer to the SEM image in Fig. 3-2). This feature is further confirmed by the water contact angle measurement shown in Fig. 3-11. The water contact angle of the samples was measured, and the left and right angles of ZIF-8 powder were (120 ± 2) º and (118 ± 2)˚, respectively as shown in Fig. 3-11 (a). The left and right contact

angles of ZIF/PES-4 composite beads were determined to be (100 ± 2)º and (115 ± 2)˚, respectively as can be seen from Fig. 3-11 (b). Thus, increasing the ZIF-8 loading helps to benefit from both hydrophobicity and high surface area of ZIF-8 particles for oil adsorption. Therefore, we can observe much higher adsorption properties for the highest ZIF-8 loading (ZIF/PES-4) compared to lower ZIF-8 loadings and PES spheres.

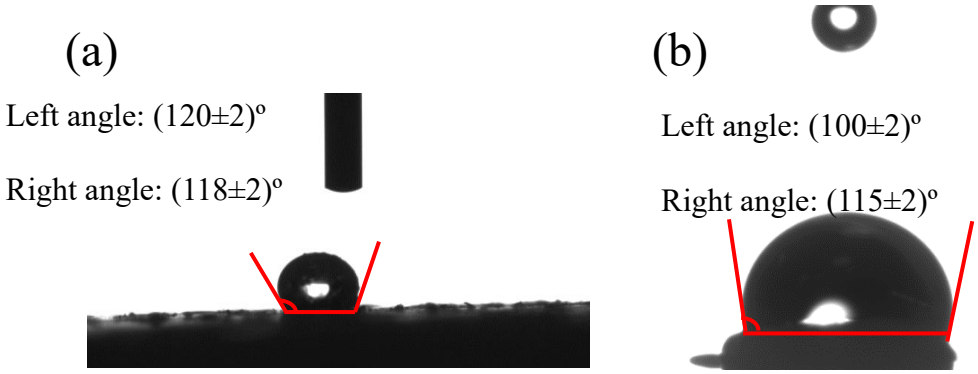

Fig. 3-11 The water contact angle of ZIF-8 powder (left angle: (120±2)º and right angle: (118±2)º) (a) and ZIF/PES-4 (left angle: (100±2)º and right angle: (115±2)º) (b)

The hydrophobic interactions between ZIF-8 and hydrophobic chains of oil molecules result in the adsorption of oil compounds on the surface of ZIF-8/PES composite beads. In order to understand the reason behind the difference in oil adsorption capacity amongst the ZIF-8/PES beads, the morphologies, surface areas and the pore size distributions of the composite beads were investigated.

The performance of ZIF-8 composite beads is shown in Fig. 3-10. As shown in the figure, all the ZIF-8/PES beads show the highest sorption for paraffin oil followed by olive oil, *n*-hexane and toluene. It is observed that increasing the ZIF-8 loading for ZIF/PES-2 and ZIF/PES-4 increases the sorption capacity dramatically. For example, for paraffin oil, the sorption capacity raises from 6.5 and 10 percent (volume gain) for ZIF/PES-0.5 and ZIF/PES-1 to 24.9 and 37.6 percent for ZIF/PES-0.2 and ZIF/PES-4. The equivalent sorption capacity (weight basis) for ZIF/PES-4 is calculated as 1260 mg/g which is quite high in comparison with

most natural sorbents like activated carbon (Table 3-4). The high sorption capacity could be due to the high surface area of the composite beads as well as the created pores on the surface which is the result of large amount of ZIF-8 particles movement toward the outer surface of the polymer composite beads. These pores offer little resistance to diffusion of the oil molecules into the sphere, increasing the adsorption capacity.

From Fig. 3-10 it can be seen that ZIF-8/PES beads have a high tendency to adsorb *n*-Hexane. The critical diameter[2] of *n*-hexane is 0.43 nm [45]. ZIF-8/PES composite beads adsorb *n*-hexane up to 30.2 percent of their volumes for the ZIF/PES-4. The high adsorption capacity of ZIF-8 for *n*-hexane is in accordance with the findings in literature [45]. It is worth noting that the adsorption of *n*-hexane might have been underestimated since it has a low boiling point of 68℃ and evaporates rapidly. To explore the ZIF-8/PES composite beads' capacities for the adsorption of branched organic molecules, toluene was used as an aromatic molecule in this study. In contrast with what has been reported in literature, we found the ZIF-8/PES beads have fairly moderate tendency to adsorb toluene. It has been reported that toluene (kinetic diameter of 0.58 nm) cannot enter and diffuse into the microporous structure of ZIF-8 (with accessible pore size of 0.34 nm) [46, 47]. ZIF-8 was reported to have almost nil adsorption capacity for toluene. In another study it was declared that branched alkanes cannot penetrate the pores of ZIF-8 [48]. However, in our study we report that ZIF-8 composite beads show fairly high adsorption capacity for toluene which might be due to the formation of large pores on the top surface of the composite beads at higher ZIF-8 loadings. There are similar reports in the literature which show ZIF-8 has the potential to adsorb the molecules larger than the ZIF-8 pore opening. Adsorption of benzene [45] and *p*-xylene [49] in liquid phase on ZIF-8 has been

[2] The critical diameter refers to the smallest cross-sectional diameter of the molecule.

reported. The investigations showed that ZIF-8 is capable of adsorbing benzene and *p*-xylene although the kinetic diameters of these molecules are much larger than the pore size of ZIF-8 particles. Benzene, toluene and *p*-xylene have the kinetic diameters of 0.58 nm [50] which is almost twice the ZIF-8 aperture size and ZIF-8 tendency for adsorption of these molecules show the flexibility of ZIF-8 structure. It was also stated that ZIF-8 adsorbs organic molecules in the order of alkane > alkene > aromatic [49] which was confirmed in this study, as *n*-hexane adsorbed at much higher levels than toluene as an aromatic compound.

The difference in the oil and organic sorption can be related to the viscosity and surface tension of the oil and organic compounds as well. Viscosity can affect the sorption in two ways. High viscosity can improve the adherence of oil on to the sorbent surface which increases the sorption capacity. On the other hand, viscous oils are difficult to penetrate into the inner surfaces of the sorbents [51]. Key properties of several oils and organic solvents are listed in Table 3-3.

Table 3-3 Densities and normal boiling points of the organic compounds.

Organic compounds	Density ($g.cm^{-3}$)	Viscosity (cp)	Normal boiling point (˚C)
Paraffin oil	0.89	20	260-450
Olive oil	0.9	69	300
n-hexane	0.65	0.3	69
Toluene	0.86	0.59	110

The sorption capacity of the sorbents shown in Fig. 3-10 agrees with the decreasing tendency of oil viscosities. The composite beads show higher sorption capacities for paraffin and olive oils with higher viscosities compared to *n*-hexane and toluene which have much lower viscosities. The sorption of *n*-hexane is still comparable with the sorption of paraffin and olive

oils despite the low viscosity of *n*-hexane, probably due to the very small kinetic diameter of this solvent which makes its penetration into the ZIF-8 pores much easier. Although the oil diffusion rate is inversely proportional to the viscosity, the hydrophobic nature of ZIF-8 particles and the large pores on the surface of the beads at high ZIF-8 loading overcome the penetration difficulty leading to high sorption capacities.

It is necessary for an adsorbent to be regenerated and reused in the adsorption process. The reusability of the beads for organic solvents was tested by heating the beads up to the normal boiling point of *n*-hexane (68℃) and toluene (110℃) for one hour. The beads showed almost one hundred percent regeneration efficiency. However, the normal boiling point of paraffin oil is in the range of 260-450℃, therefore, the solvent washing method was utilized to regenerate the composite beads for desorbing paraffin oil form the beads. Although heat treatment is a more effective method in recycling adsorbents, due to the low stability of ZIF-8 (300℃) and polymer framework (185℃) at high temperatures, the solvent method was utilized for recycling of the composite beads for paraffin oil.

The regeneration test was done for the composite beads after paraffin oil sorption and the used beads were washed with ethanol. The regeneration results are shown in Fig. 3-12 (a) demonstrating that composite beads are able to retain 88 percent of the original oil sorption after 5 regeneration cycles. This indicates that solvent washing is a simple and effective method for the regeneration of the composite beads and can be considered as an alternative to heat treatment for recycling purposes. The XRD patterns of the ZIF-8 composite beads before oil sorption and after regeneration are illustrated in Fig. 3-12 (b) showing that the XRD pattern of the beads after 5 cycles of regeneration is similar to the beads before oil sorption. This indicates the composite beads have a stable structure and can be reused for oil sorption.

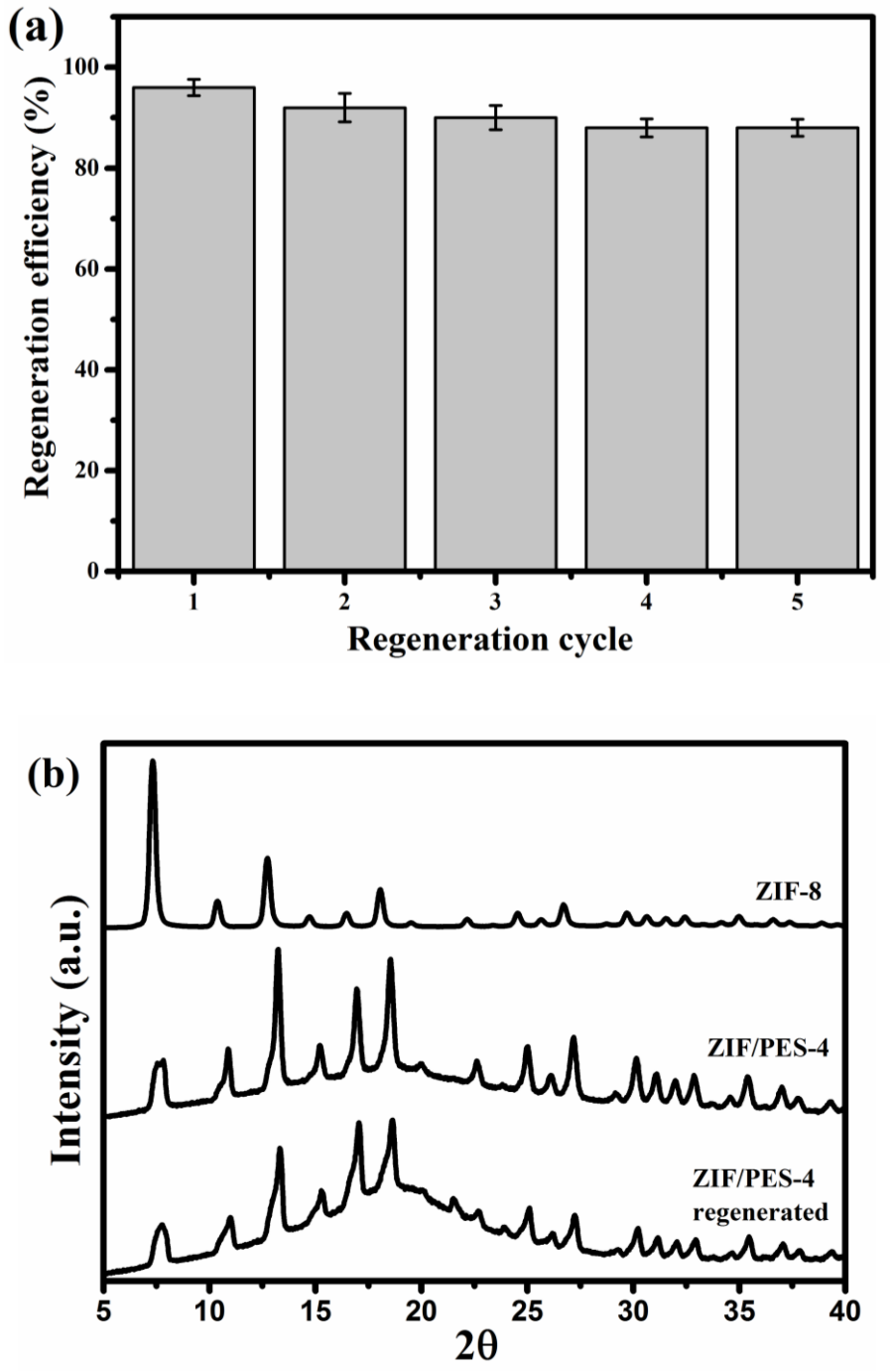

Fig. 3-12 Recyclability of ZIF-8/PES composite beads. Regeneration efficiency of the composite beads (a) and XRD patterns of ZIF-8/PES beads before and after oil sorption (b)

Table 3-4 summarizes the oil sorption capacities of different kind of sorbents for comparison. The capacity of the ZIF-8 composite beads was converted to weight basis from volume basis to be comparable with the sorption capacities from literature. The table shows

that the ZIF composite beads can compete with other sorbents for oil sorption and have very high sorption capacities.

Table 3-4 Comparison of oil/organic sorption capacities of different sorbents.

Sorbent	Long-chain oil ($mg.g^{-1}$)	Sorbent density ($g.cm^{-3}$)	Reference
ZIF/PES-4 composite beads	1260	0.26	This study
Pure ZIF-8 powder	3000	NA[a]	[36]
Pure ZIF-8 powder	2650	0.36	This study
UHMOF-100	2000	NA	[52]
HFGO@ZIF-8	200	NA	[53]
Sponge@HFGO@ZIF-8	2000	NA	[53]
HKUST-1 (MOF)	260	1.22	[54]
hollow carbon beads	1557	0.2	[24]
Carbon/TiO_2 beads	1151.7	0.6	[55]
Activated carbon	50	NA	[54]
Activated carbon	167	NA	[7]
Activated carbon	300	2	[56]
Bentonite	378	1.15	[57]
Zeolite	55-100	1.6-2.4	[8]

The ZIF-8 composite beads have lower sorption capacities compared with the pure ZIF-8 powder, which is due to the fact that the beads include polymer in their matrices and the bead framework is composed of a mixture of ZIF-8 particles as well as polymer. Moreover, the ZIF-8 powder has more accessible surface area to the oils and organic solvents since the particles are nano-sized and have high exposure to the pollutant molecules. The sorption capacity of ZIF-8 powder is based on the weight of pure ZIF-8 powder while the sorption capacity of composite beads is based on the weight of the ZIF/PES composite beads. It is also shown that the ZIF-8/PES composite beads have greater oil sorption capacities compared with HKUST-1 metal

organic framework. The composite beads also exhibit appropriate sorption capacities in comparison with UHMOF-100 and HFGO@ZIF-8 considering the fact that the above-mentioned sorbents are difficult to handle and recycle. Although pure ZIF-8, UHMOF-100 and HFGO@ZIF-8 exhibit higher sorption capacities compared to ZIF-8 composite beads, they are in powder form which is simply not useful for practical oil spillage clean-up purposes. The composite beads in this study have the advantage of keeping ZIF-8 particles in a rigid, robust and stable framework to enable simple handling during oil sorption and recycling processes.

In comparison with hollow carbon beads and carbon/TiO_2 beads, the ZIF-8 composite beads still show good sorption properties. In particular, when compared with natural sorbents like activated carbon, zeolite and bentonite, the ZIF-8/PES beads exhibit much higher sorption capacities. It is worth mentioning that ZIF-8 composite beads present a very low bulk density compared to the other sorbents listed in Table 3-2. HKUST-1 metal organic framework has bulk density of 1.22 $g.cm^{-3}$ which is higher than water density. The bulk density of zeolite is in the range of 1.6-2.4 $g.cm^{-3}$ and that of activated carbon is 2 $g.cm^{-3}$, which are much higher than the bulk density of ZIF/PES-4 beads reported in this study. The bulk density of the ZIF-8 composite beads is even lower than the carbon/TiO_2 beads and close to that of hollow carbon beads. As mentioned previously, the natural sorbents mostly exhibit poor buoyancy which is not suitable for cleaning oil spills from the surfaces of water. These natural sorbents cannot float on the surface of water and therefore have limitation regarding with oil spill removals. These materials do not benefit from simultaneous high oil sorption capacity and good buoyancy. In most cases, either sorption capacity or buoyancy is sacrificed. In contrast, ZIF-8 composite beads benefit from both high sorption uptake and suitable buoyancy which makes them interesting for oil spillage uptake. The ZIF-8/PES beads have bulk densities even lower than ZIF-8 powder (0.36 $g.cm^{-3}$).

It is worth noting that in comparison with other beads which are reported for oil spill removal like hollow carbon beads and carbon/TiO_2 beads, ZIF-8/PES beads have the advantage of being prepared from a simple one step method, while the carbon beads are prepared via a second carbonization step which is time and energy consuming. The HFGO@ZIF-8 and sponge@HFGO@ZIF-8 are also prepared from several complicated steps which restricts practical application. The stability of the beads after oil sorption experiments was also evaluated by XRD analysis. It can be observed from Fig. 3-12 (b) that the prepared beads exhibit stability after oil adsorption since the XRD pattern is quite similar before and after oil adsorption.

Therefore, the high oil sorption capacity along with the rigidity and robustness of the beads frameworks, plus low bulk density and excellent buoyancy make these composite beads suitable candidates for oil spill clean-up in practical purposes. In addition, the simple one step method for fabrication of ZIF-8 is superior to other complicated techniques utilized for preparing the other synthetic sorbent materials.

3.7. Conclusions

The ZIF-8 composite beads were prepared successfully using the phase inversion method. This is a very simple and straight forward technique and the prepared ZIF-8/PES beads are quite rigid and stable. The SEM and XRD analyses confirmed the uniform incorporation of ZIF-8 particles in the polymer matrix. The surface area of the ZIF-8/PES composite beads increased with increasing the ZIF-8 loading up to 1030.6 m^2/g close to the surface area of pure ZIF-8 (1384.2 m^2/g). The oil sorption experiments showed that the composite beads are capable of adsorbing oils and organic solvents efficiently. The oil adsorption capacity of the ZIF-8/PES-4 composite beads was 1260 mg/g which is significantly higher than that of natural adsorbents such as activated carbon, zeolite and bentonite with adsorption capacities of 300, 100 and 378

mg/g, respectively. The ZIF-8/PES-4 composite beads also exhibited a very low bulk density (0.26 g/cm^3) in comparison with ZIF-8 powder with a bulk density of 0.36 g/cm^3 as well as natural adsorbents such as activated carbon, zeolite and bentonite with bulk densities of 2, 1.6 and 1.15 g/cm^3, respectively. This low bulk density of the ZIF-8/PES beads resulted in excellent buoyancy compared with the natural adsorbents.

The high sorption is attributed to the hydrophobicity and high surface area of the ZIF-8 particles. This study showed ZIF-8 composite beads can compete with other sorbent materials and exhibit much higher sorption capacities in comparison with activated carbon. The synthesized composite beads are easy to handle and recycle and can retain up to 88 percent of the oil sorption capacity after five regeneration cycles.

3.8. References

[1] H. Bi, X. Xie, K. Yin, Y. Zhou, S. Wan, L. He, F. Xu, F. Banhart, L. Sun, R.S. Ruoff, Spongy graphene as a highly efficient and recyclable sorbent for oils and organic solvents, Adv. Funct. Mater. 22 (2012) 4421-4425.

[2] Y. Gao, Y.S. Zhou, W. Xiong, M. Wang, L. Fan, H. Rabiee-Golgir, L. Jiang, W. Hou, X. Huang, L. Jiang, J.-F. Silvain, Y.F. Lu, Highly efficient and recyclable carbon soot sponge for oil cleanup, ACS Appl. Mater. Interfaces. 6 (2014) 5924-5929.

[3] S. Kabiri, D.N.H. Tran, T. Altalhi, D. Losic, Outstanding adsorption performance of graphene–carbon nanotube aerogels for continuous oil removal, Carbon, 80 (2014) 523-533.

[4] X. Dong, J. Chen, Y. Ma, J. Wang, M.B. Chan-Park, X. Liu, L. Wang, W. Huang, P. Chen, Superhydrophobic and superoleophilic hybrid foam of graphene and carbon nanotube for selective removal of oils or organic solvents from the surface of water, Chem. Commun. 48 (2012) 10660-10662.

[5] S.B. Ummalyma, R.K. Sukumaran, Cultivation of microalgae in dairy effluent for oil production and removal of organic pollution load, Bioresour. Technol. 165 (2014) 295-301.

[6] J. Zhao, W. Ren, H.-M. Cheng, Graphene sponge for efficient and repeatable adsorption and desorption of water contaminations, J. Mater. Chem. 22 (2012) 20197-20202.

[7] A.L. Ahmad, S. Sumathi, B.H. Hameed, Residual oil and suspended solid removal using natural adsorbents chitosan, bentonite and activated carbon: a comparative study, Chem. Eng. J. 108 (2005) 179-185.

[8] M.A. Shavandi, Z. Haddadian, M.H.S. Ismail, N. Abdullah, Continuous metal and residual oil removal from palm oil mill effluent using natural zeolite-packed column, J. Taiwan Ins. Chem. Eng. 43 (2012) 934-941.

[9] M.O. Adebajo, R.L. Frost, J.T. Kloprogge, O. Carmody, S. Kokot, Porous materials for oil spill cleanup: a review of synthesis and absorbing properties, J. Porous. Mater. 10 (2003) 159-170.

[10] S.-J. Choi, T.-H. Kwon, H. Im, D.-I. Moon, D.J. Baek, M.-L. Seol, J.P. Duarte, Y.-K. Choi, A polydimethylsiloxane (PDMS) sponge for the selective absorption of oil from water, ACS Appl. Mater. Interfaces. 3 (2011) 4552-4556.

[11] A. Li, H.-X. Sun, D.-Z. Tan, W.-J. Fan, S.-H. Wen, X.-J. Qing, G.-X. Li, S.-Y. Li, W.-Q. Deng, Superhydrophobic conjugated microporous polymers for separation and adsorption, Energ. Environ. Sci. 4 (2011) 2062-2065.

[12] Q. Zhu, Y. Chu, Z. Wang, N. Chen, L. Lin, F. Liu, Q. Pan, Robust superhydrophobic polyurethane sponge as a highly reusable oil-absorption material, J. Mater. Chem. A. 1 (2013) 5386-5393.

[13] X. Gui, J. Wei, K. Wang, A. Cao, H. Zhu, Y. Jia, Q. Shu, D. Wu, Carbon nanotube sponges, Adv. Mater. 22 (2010) 617-621.

[14] J. Li, F. Wang, C.-y. Liu, Tri-isocyanate reinforced graphene aerogel and its use for crude oil adsorption, J. Colloid Interface Sci. 382 (2012) 13-16.

[15] H. Liu, C.-Y. Cao, F.-F. Wei, P.-P. Huang, Y.-B. Sun, L. Jiang, W.-G. Song, Flexible macroporous carbon nanofiber film with high oil adsorption capacity, J. Mater. Chem. A. 2 (2014) 3557-3562.

[16] H.-W. Liang, Q.-F. Guan, L.-F. Chen, Z. Zhu, W.-J. Zhang, S.-H. Yu, Macroscopic-scale template synthesis of robust carbonaceous nanofiber hydrogels and aerogels and their applications, Angew. Chem. Int. Ed., 51 (2012) 5101-5105.

[17] Y. Li, S. Cheng, P. Dai, X. Liang, Y. Ke, Large-pore monodispersed mesoporous silica spheres: synthesis and application in HPLC, Chem. Commun. (2009) 1085-1087.

[18] W. Zhao, H. Chen, Y. Li, L. Li, M. Lang, J. Shi, Uniform rattle-type hollow magnetic mesoporous spheres as drug delivery carriers and their sustained-release property, Adv. Funct. Mater. 18 (2008) 2780-2788.

[19] P.M. Arnal, M. Comotti, F. Schüth, High-temperature-stable catalysts by hollow sphere encapsulation, Angew. Chem. 118 (2006) 8404-8407.

[20] M. Najafi, Y. Yousefi, A.A. Rafati, Synthesis, characterization and adsorption studies of several heavy metal ions on amino-functionalized silica nano hollow sphere and silica gel, Sep. Purif. Technol. 85 (2012) 193-205.

[21] H. Zhang, G.C. Hardy, Y.Z. Khimyak, M.J. Rosseinsky, A.I. Cooper, Synthesis of hierarchically porous silica and metal oxide beads using emulsion-templated polymer scaffolds, Chem. Mater. 16 (2004) 4245-4256.

[22] J. Yao, K. Wang, M. Ren, J. Zhe Liu, H. Wang, Phase inversion spinning of ultrafine hollow fiber membranes through a single orifice spinneret, J. Membr. Sci. 421–422 (2012) 8-14.

[23] J. Huang, K. Zhang, K. Wang, Z. Xie, B. Ladewig, H. Wang, Fabrication of polyethersulfone-mesoporous silica nanocomposite ultrafiltration membranes with antifouling properties, J. Membr. Sci. 423–424 (2012) 362-370.

[24] Y. Zeng, K. Wang, J. Yao, H. Wang, Hollow carbon beads fabricated by phase inversion method for efficient oil sorption, Carbon, 69 (2014) 25-31.

[25] L. Li, J. Yao, P. Xiao, J. Shang, Y. Feng, P.A. Webley, H. Wang, One-step fabrication of ZIF-8/polymer composite spheres by a phase inversion method for gas adsorption, Colloid Polym. Sci. 291 (2013) 2711-2717.

[26] N.A. Khan, Z. Hasan, S.H. Jhung, Adsorptive removal of hazardous materials using metal-organic frameworks (MOFs): a review, J. Hazard. Mater. 244–245 (2013) 444-456.

[27] N.A. Khan, B.K. Jung, Z. Hasan, S.H. Jhung, Adsorption and removal of phthalic acid and diethyl phthalate from water with zeolitic imidazolate and metal–organic frameworks, J. Hazard. Mater. 282 (2015) 194-200.

[28] J.A. Gee, J. Chung, S. Nair, D.S. Sholl, Adsorption and diffusion of small alcohols in zeolitic imidazolate frameworks ZIF-8 and ZIF-90, J. Phys. Chem. C, 117 (2013) 3169-3176.

[29] U.P.N. Tran, K.K.A. Le, N.T.S. Phan, Expanding applications of metal−organic frameworks: zeolite imidazolate framework ZIF-8 as an efficient heterogeneous catalyst for the Knoevenagel reaction, ACS Catal. 1 (2011) 120-127.

[30] C.M. Miralda, E.E. Macias, M. Zhu, P. Ratnasamy, M.A. Carreon, Zeolitic imidazole framework-8 catalysts in the conversion of CO2 to chloropropene carbonate, ACS Catal. 2 (2012) 180-183.

[31] B.K. Jung, J.W. Jun, Z. Hasan, S.H. Jhung, Adsorptive removal of p-arsanilic acid from water using mesoporous zeolitic imidazolate framework-8, Chem. Eng. J. 267 (2015) 9-15.

[32] Y.-n. Wu, M. Zhou, B. Zhang, B. Wu, J. Li, J. Qiao, X. Guan, F. Li, Amino acid assisted templating synthesis of hierarchical zeolitic imidazolate framework-8 for efficient arsenate removal, Nanoscale, 6 (2014) 1105-1112.

[33] J.-Q. Jiang, C.-X. Yang, X.-P. Yan, Zeolitic imidazolate framework-8 for fast adsorption and removal of benzotriazoles from aqueous solution, ACS Appl. Mater. Interfaces. 5 (2013) 9837-9842.

[34] J. Li, Y.-n. Wu, Z. Li, B. Zhang, M. Zhu, X. Hu, Y. Zhang, F. Li, Zeolitic imidazolate framework-8 with high efficiency in trace arsenate adsorption and removal from water, J. Phys. Chem. C, 118 (2014) 27382-27387.

[35] Z. Abbasi, E. Shamsaei, S.K. Leong, B. Ladewig, X. Zhang, H. Wang, Effect of carbonization temperature on adsorption property of ZIF-8 derived nanoporous carbon for water treatment, Microporous Mesoporous Mater. 236 (2016) 28-37.

[36] K.-Y.A. Lin, Y.-C. Chen, S. Phattarapattamawong, Efficient demulsification of oil-in-water emulsions using a zeolitic imidazolate framework: adsorptive removal of oil droplets from water, J. Colloid Interface Sci. 478 (2016) 97-106.

[37] L.D. O'Neill, H. Zhang, D. Bradshaw, Macro-/microporous MOF composite beads, J. Mater. Chem. 20 (2010) 5720-5726.

[38] S. Aguado, J. Canivet, D. Farrusseng, Facile shaping of an imidazolate-based MOF on ceramic beads for adsorption and catalytic applications, Chem Commun. 46 (2010) 7999-8001.

[39] T. Zhang, L. Lin, X. Zhang, H. Liu, X. Yan, Z. Liu, K.L. Yeung, Facile preparation of ZIF-8@Pd-CSS sandwich-type microspheres via in situ growth of ZIF-8 shells over Pd-loaded colloidal carbon spheres with aggregation-resistant and leach-proof properties for the Pd nanoparticles, Appl. Surf. Sci. 351 (2015) 1184-1190.

[40] X. Zhou, F. Wang, Y. Ji, W. Chen, J. Wei, Fabrication of hydrophilic and hydrophobic sites on polypropylene nonwoven for oil spill cleanup: two dilemmas affecting oil sorption, Environ. Sci. Technol. 50 (2016) 3860-3865.

[41] K. Zhang, R.P. Lively, M.E. Dose, A.J. Brown, C. Zhang, J. Chung, S. Nair, W.J. Koros, R.R. Chance, Alcohol and water adsorption in zeolitic imidazolate frameworks, Chem. Commun. 49 (2013) 3245-3247.

[42] P. Küsgens, M. Rose, I. Senkovska, H. Fröde, A. Henschel, S. Siegle, S. Kaskel, Characterization of metal-organic frameworks by water adsorption, Microporous Mesoporous Mater. 120 (2009) 325-330.

[43] K. Zhang, R.P. Lively, C. Zhang, R.R. Chance, W.J. Koros, D.S. Sholl, S. Nair, Exploring the framework hydrophobicity and flexibility of ZIF-8: from biofuel recovery to hydrocarbon separations, J. Phys. Chem. Lett. 4 (2013) 3618-3622.

[44] N.C. Burtch, H. Jasuja, K.S. Walton, Water stability and adsorption in metal–organic frameworks, Chem. Rev. 114 (2014) 10575-10612.

[45] L. Diestel, H. Bux, D. Wachsmuth, J. Caro, Pervaporation studies of n-hexane, benzene, mesitylene and their mixtures on zeolitic imidazolate framework-8 membranes, Microporous Mesoporous Mater. 164 (2012) 288-293.

[46] S. Eslava, L. Zhang, S. Esconjauregui, J. Yang, K. Vanstreels, M.R. Baklanov, E. Saiz, Metal-organic framework ZIF-8 films as low-κ dielectrics in microelectronics, Chem. Mater. 25 (2013) 27-33.

[47] B. Liu, M. Tu, R.A. Fischer, Metal–organic framework thin films: crystallite orientation dependent adsorption, Angew. Chem. Int. Ed. 52 (2013) 3402-3405.

[48] A. Henschel, I. Senkovska, S. Kaskel, Liquid-phase adsorption on metal-organic frameworks, Adsorption, 17 (2011) 219-226.

[49] D. Peralta, G. Chaplais, A. Simon-Masseron, K. Barthelet, C. Chizallet, A.-A. Quoineaud, G.D. Pirngruber, Comparison of the behavior of metal–organic frameworks and zeolites for hydrocarbon separations, J. Am. Chem. Soc. 134 (2012) 8115-8126.

[50] C.D. Baertsch, H.H. Funke, J.L. Falconer, R.D. Noble, Permeation of aromatic hydrocarbon vapors through silicalite−zeolite membranes, J. Phys. Chem. 100 (1996) 7676-7679.

[51] J. Wu, N. Wang, L. Wang, H. Dong, Y. Zhao, L. Jiang, Electrospun porous structure fibrous film with high oil adsorption capacity, ACS Appl. Mater. Interfaces. 4 (2012) 3207-3212.

[52] S. Mukherjee, A.M. Kansara, D. Saha, R. Gonnade, D. Mullangi, B. Manna, A.V. Desai, S.H. Thorat, P.S. Singh, A. Mukherjee, S.K. Ghosh, An ultrahydrophobic fluorous metal–organic framework derived recyclable composite as a promising platform to tackle marine oil spills, Chem. Eur. J. 22 (2016) 10937-10943.

[53] K. Jayaramulu, K.K.R. Datta, C. Rösler, M. Petr, M. Otyepka, R. Zboril, R.A. Fischer, Biomimetic superhydrophobic/superoleophilic highly fluorinated graphene oxide and ZIF-8 composites for oil–water separation, Angew. Chem. Int. Ed. 55 (2016) 1178-1182.

[54] K.-Y.A. Lin, H. Yang, C. Petit, F.-K. Hsu, Removing oil droplets from water using a copper-based metal organic frameworks, Chem. Eng. J. 249 (2014) 293-301.

[55] X. Gu, K. Zhou, Y. Li, J. Yao, Millimeter-sized carbon/TiO_2 beads fabricated by phase inversion method for oil and dye adsorption, RSC Adv. 6 (2016) 16314-16318.

[56] M.A. Lillo-Ródenas, D. Cazorla-Amorós, A. Linares-Solano, Behaviour of activated carbons with different pore size distributions and surface oxygen groups for benzene and toluene adsorption at low concentrations, Carbon, 43 (2005) 1758-1767.

[57] K. Okiel, M. El-Sayed, M.Y. El-Kady, Treatment of oil–water emulsions by adsorption onto activated carbon, bentonite and deposited carbon, Egyptian J. Petrol. 20 (2011) 9-15.

Chapter 4. Effect of carbonization temperature on adsorption property of ZIF-8 derived nanoporous carbon for water treatment

4.1. Overview

In previous chapter, ZIF-8 beads were utilized for the adsorption of oil and organic compounds. In this chapter, ZIF-8 and its derived nanoporous carbons were examined for the adsorption of a basic positively charged dye to investigate the capability of these materials for the removal of basic dyes from water. The adsorbents were characterized using a variety of techniques to investigate the textural and morphological change of ZIF-8 and its nanoporous carbons under carbonization conditions. A systematic and mechanistic approach was used to study the adsorption isotherms, kinetics and mechanisms. The ZIF-8 derived carbon nanoparticles were found to be efficient adsorbents for water treatment purposes due to the satisfactory adsorption properties. The outcomes of this study provides helpful information for future applications of MOF derived nanoporous carbons for water treatment.

This chapter has been formatted from the following published manuscript (Copyright reference number: 4071161227024, Elsevier).

Z.Abbasi, E. Shamsaei, S. Leong, B. Ladewig, H. Wang, Effect of carbonization temperature on adsorption property of ZIF-8 derived nanoporous carbon for water treatment. *Microporous Mesoporous Mater*. 2016, 236, 28-37.

4.2. Introduction

Nanoporous carbon (NPC) materials have promising characteristics such as high surface area, good chemical and thermal stabilities, fast kinetics as well as tendency to organic contaminants which makes them attractive for adsorption and separation applications [1, 2]. For example, they have been used as supercapacitor [3-5], catalyst support [6-8] and adsorbent for hydrogen storage [9] as well as CO_2 capture [2, 10-12]. In particular, they are widely used as adsorbents to remove organic and heavy metal contaminants from water in water treatment and purification [13-18].

A wide range of methods have been developed to prepare nanoporous carbons, including chemical vapor deposition (CVD) [19], templating [20, 21] and chemical or physical activation method [22]. Inorganic hard templates like zeolites and mesoporous silica [23, 24] and Soft template method [25, 26] have been utilized to prepare nanoporous carbon particles. In addition, organic spheres are considered as common starting materials for the production of carbon nanoparticles through carbonization [27]. Recently, porous metal organic frameworks (MOFs) with uniform pore sizes, highly crystalline structures, and high surface areas have been studied as adsorbents and for use as precursors of nanoporous carbons [3, 4, 27-33].

Different kinds of metal organic framework materials have been investigated for the adsorption of dye molecules such as methylene blue from water and wastewater. However, their

adsorption capacity is low compared to nanoporous carbons. For example, CU-BTC [BTC=1,3,5-benzenetricarboxylate] also known as HKUST-1 as well as Fe_3O_4@MIL-100(Fe) have been studied for the removal of MB from water and they showed adsorption capacities of 15.28 μmol/g (equivalent to 4.8 mg/g) and 49.4 mg/g respectively [34, 35]. Among MOF materials, zeolitic immidazolate frameworks (ZIFs) are a class of MOFs that show many outstanding features like high thermal and chemical stability. ZIF-8 is one of mostly studied ZIFs, and has a molecular formula of Zn(2-methylimidazolate)$_2$ and sodalite-related zeolitic structure; it is composed of six membered-ring pore windows (0.34 nm) and larger pores (1.14 nm) and has been reported as an adsorbent for the removal of various pollutants from water [31]. It is worth noting that ZIF-8 has fast adsorption rate and high adsorption capacity for the removal of benzotriazols from aqueous solutions [36]; however, this material has very low adsorption capacity for the removal of methylene blue dye from water. The low MB uptake could be due to the net positive charge of ZIF-8 and its small pores which hinder adsorption of large and positively charged molecules such as methylene blue. Therefore, much work has been carried out to convert MOFs (ZIFs) into nanoporous carbons to achieve desirable adsorption properties [27]. MOFs have large carbon contents and play the roles of sacrificial template and carbon precursor during carbonization process [4].

To date, there have been a few reports in the literature about the utilization of MOF derived nanoporous carbon for water treatment. For instance, nanoporous carbons derived from ZIF-67, MIL-100 and MOF-5 were prepared, and they had improved adsorption capacity for the removal of MB from water [1, 37, 38]. The nanoporous carbon was also obtained by carbonizing ZIF-8 at 800℃ [2, 39]. However, the methylene blue adsorption capacity of ZIF-8-derived carbon was low (59 mg/g), which was because the carbonization temperature (800℃)

was lower than the boiling point of Zn (908℃), limiting the surface area and pore volume of the nanoporous carbon [40, 41].

Even after steam treatment was conducted at 800℃ to promote the porous carbon network, the adsorption capacity of the resulting carbon was still low (105.7 mg/g). This indicates the importance of carbonization temperature on the adsorption property of ZIF-8-derived nanoporous carbon.

In this study, we focused on the effect of carbonization temperature on the adsorption capacity of ZIF-8 for water treatment, particularly the removal of methylene blue as a model dye pollutant from water. The changes of the ZIF-8 characteristics due to carbonization such as morphology, surface area and pore size distribution, surface charge, surface functional groups and hydrophobicity were studied. Our studies showed that the ZIF-8 derived nanoporous carbon prepared at 1000℃ had significantly greater adsorption capacity than that at lower temperature.

4.3. Materials and Methods

4.3.1. Materials

Zinc nitrate hexahydrate ($Zn(NO_3)_2.6H_2O$), 2-methylimidazole (Hmim) (99%), Brilliant Green (BG), Rhodamine B (RhB), Methyl Orange (MO), NaOH and HCl were purchased from Sigma Aldrich. Methylene blue was (MB) purchased from Merck. All chemicals were used as received without any purification. ZIF-8 parent was synthesized by environmentally friendly synthesis method in aqueous solution reported by Koji Kida et al. [42] as shown in Fig. 4-1. Typically, 0.744 g (2.5 mmol) of $Zn(NO_3).6H_2O$ and 12.3 g (0.15 mol) of Hmim were dissolved in 10 ml and 90 ml of deionized water respectively. After being stirred for 24 hours, ZIF-8 nanocrystals were collected by washing with deionized water and centrifuging (8000 rpm, 30 min) for three times and then dried at 80℃ overnight. ZIF-8 was directly carbonized at various

temperatures (600, 1000 and 1200℃) under a flow of argon gas. The temperatures rose steadily from room temperature to the target temperatures with a heating rate of 5℃/min. After reaching the target temperatures, the powders were annealed at the target temperatures for 6 hours. These products were denoted as CZIFs (carbonized ZIF-8) and as CZIF600, CZIF1000 and CZIF1200 to indicate the heat treatment temperatures.

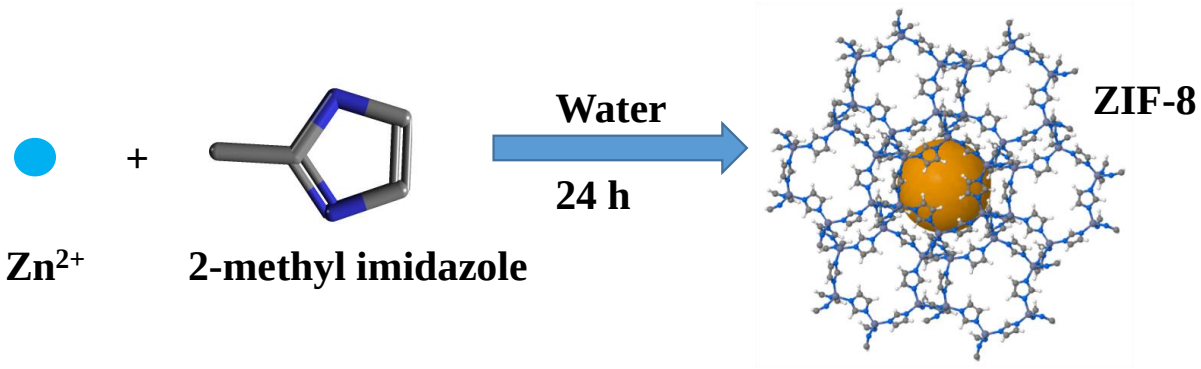

Fig. 4-1 Schematic of ZIF-8 synthesis in water at room temperature.

After the carbonization the nanoporous carbon samples were directly used for characterization and adsorption experiments without any further activation or acid washing to present a simple and environmentally friendly approach.

4.3.2. Characterization

Nitrogen adsorption and desorption isotherms were measured at liquid nitrogen temperature (77 K) using an accelerated surface area and porosimetry system (ASAP 2010, Micromeritics, USA) for surface area measurements. The crystal structures of the samples were identified using an X-ray diffractometer (Miniflex 600, Rigaku) with Cu Kα radiation at 40 kV and 20 mA over the 2θ range of 2-90°. The morphology of the adsorbent materials was observed using a scanning electron microscope (FEI Nova NanoSEM 450 FEG SEM). Transmission electron microscopy of the carbonized ZIFs was done by FEI Tecnai G2 T20 TWIN TEM under the working conditions of 200 kV. Thermogravimetric analyses (TGA) were carried out on a

SETARAM (TGA 92) device from 30 to 1200℃ at a heating rate of 10℃/min under Ar flow. The zeta potentials of the samples were determined using a Zetasizer Nano (Malvern) at the pH ranging from 1 to 11. The powders were dispersed by sonication in water with the concentration of 0.5mg/10ml and the dispersion was used for zeta potential measurement. Since ZIF-8 is not stable in acidic conditions, the pH adjustment for ZIF-8 was done only for basic conditions to measure zeta potentials.

The Raman spectra were recorded on WITEC Alpha 300 confocal micro-Raman system equipped with a 532 nm laser source and 100X objective lens. The concentration of methylene blue was measured using a UV-vis spectrophotometer (UVmini-1240, Shimadzu) at the wavelength of 665 which corresponds to the maximum adsorption of the methylene blue dye.

FTIR spectra of the samples were recorded using an attenuated total reflectance (ATR) Fourier Transform Infrared (FTIR) (Perkin Elmer, USA) in the range of 500-4000 cm^{-1} at an average of 32 scans with a resolution of 4 cm^{-1}. XPS measurements were taken ona Kratos AXIS Nova (Kratos Analytical Ltd, UK), equipped with a monochromated Al Kα X-ray source (hv=1486.6 eV) operating at 150 W. Survey spectra were acquired at 1 eV intervals and a pass energy of 160 eV.

4.3.3. Adsorption experiments

Adsorption on the prepared samples was carried out in batch experiments. The adsorption capacity of these materials was evaluated by adsorption of an organic cationic dye methylene blue (MB) in aqueous solution. Rhodamine B (RhB), Brilliant Green (BG) and Methyl Orange (MO) were also used to examine the capability of the carbonized samples for adsorption of different types of dye molecules. However, the adsorption isotherms and kinetics were conducted for methylene blue only as a model dye compound. An aqueous stock solution of

MB ($C_{16}H_{18}N_3SCl$, MW: 373.9), RhB, BG and MO with 1000 ppm concentration was prepared in milli-Q water. Aqueous solutions with different concentrations of dyes were prepared by successive dilution of the stock solution with water. For isotherm experiments specific amount of adsorbents (10 mg) was put in the aqueous dye solutions (20 ml) having fixed concentrations from 100 ppm to 500 ppm. The solutions containing the adsorbents were mixed for 24 hours at room temperature (22℃).

For kinetic experiments 10 mg of adsorbent was put in 20 ml dye solution with 100 ppm concentration of MB. Then the dye solutions containing the adsorbents were mixed well with magnetic stirring and maintained for a fixed time (5 min to 24 h) at room temperature (22℃).

After adsorption for a pre-determined time, the solutions were separated from the adsorbents with a syringe filter (Nylon, hydrophobic, 0.45 μm). The adsorption isotherm and kinetic experiments were done without any pH adjustment and at the natural pH of the solution i.e. 5.5. The dye solution was prepared to the desired concentrations using Milli-Q water. The pH of the solution was adjusted using 0.1 M HCl and 0.1 M NaOH for defining the effect of pH on adsorption performance.

4.4. Results and Discussions

4.4.1. Characterization of nanoporous carbon particles

To examine the crystal phase transformation of ZIF-8 under the treatment conditions, X-ray diffraction (XRD) analysis was conducted. Fig. 4-2 shows the XRD pattern of as synthesized ZIF-8 and carbonized materials. As the temperature increases to the boiling point of zinc (908℃), carbon-reduced zinc metal evaporates under carbonization conditions and leaves with the Ar flow [32, 40, 41]. Therefore, at 1000℃, no diffraction peaks of Zn impurities can be seen [32] and the two broad peaks at 2θ=23° and 44° represent the characteristics of

amorphous carbon [3, 41]. The reduced Zn probably plays the role of a template for the formation of nanoporous carbon. During the carbonization, zinc is reduced by carbon. Vaporization of Zn at above 908℃ and the release of zinc species is probably in charge of the formation of the porous framework [43].

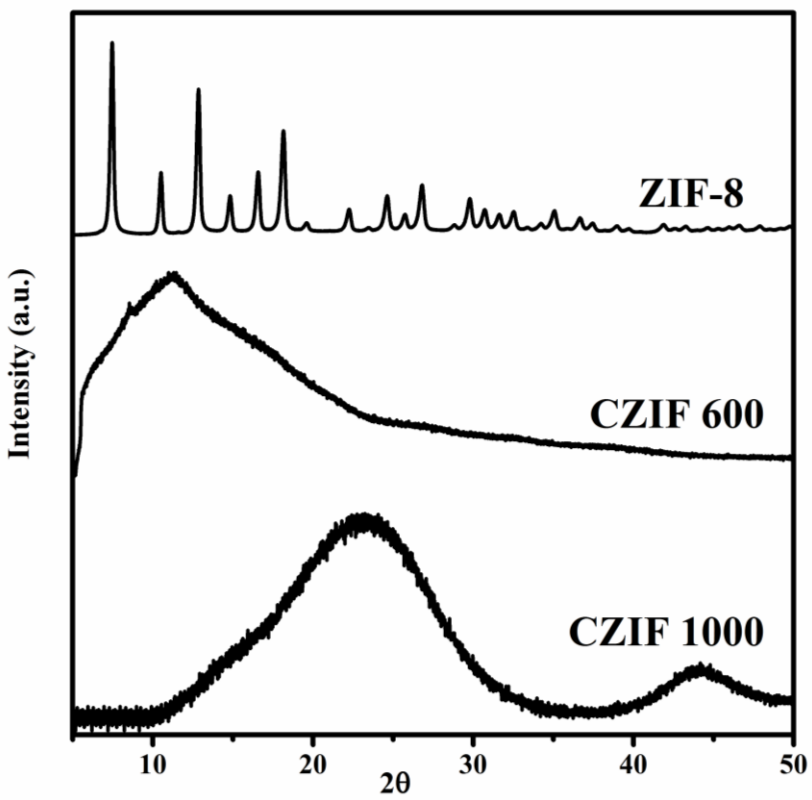

Fig. 4-2 XRD patterns of synthesized ZIF-8 and its derived carbons at 600℃ and 1000℃

In addition, the samples before and after the carbonization were analysed by scanning electron microscopy (SEM) and transmission electron microscopy (TEM) to identify the change in the morphology of the samples. Fig. 4-3 shows the SEM and TEM of the original and carbonized ZIF-8 (at different temperatures); no change in the morphology and structure of the synthesized ZIF-8 was observed, even after carbonization at high temperatures. This observation is in accordance with literature [1, 27].

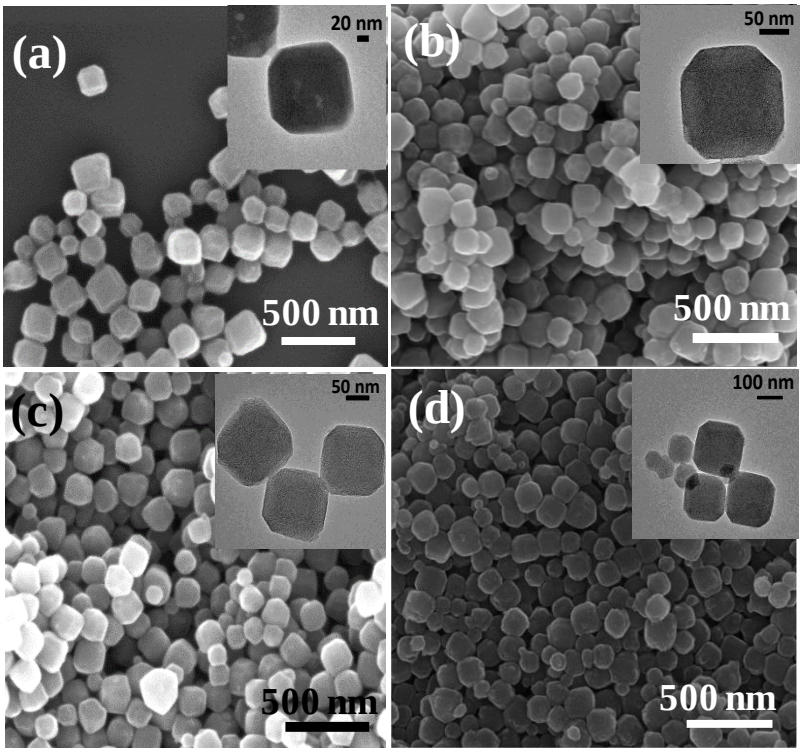

Fig. 4-3 SEM and TEM images of (a) ZIF-8 (b) CZIF600 (c) CZIF1000 and (d) CZIF1200

An adsorbent material must have high internal volume accessible to the components being removed from the solvent. Surface area, in particular the internal surface area, pore size and the nature of the pores strongly affect the adsorption process [44]. The nanoporous structures of prepared carbons were investigated by N_2 adsorption-desorption isotherms (Fig. 4-4).

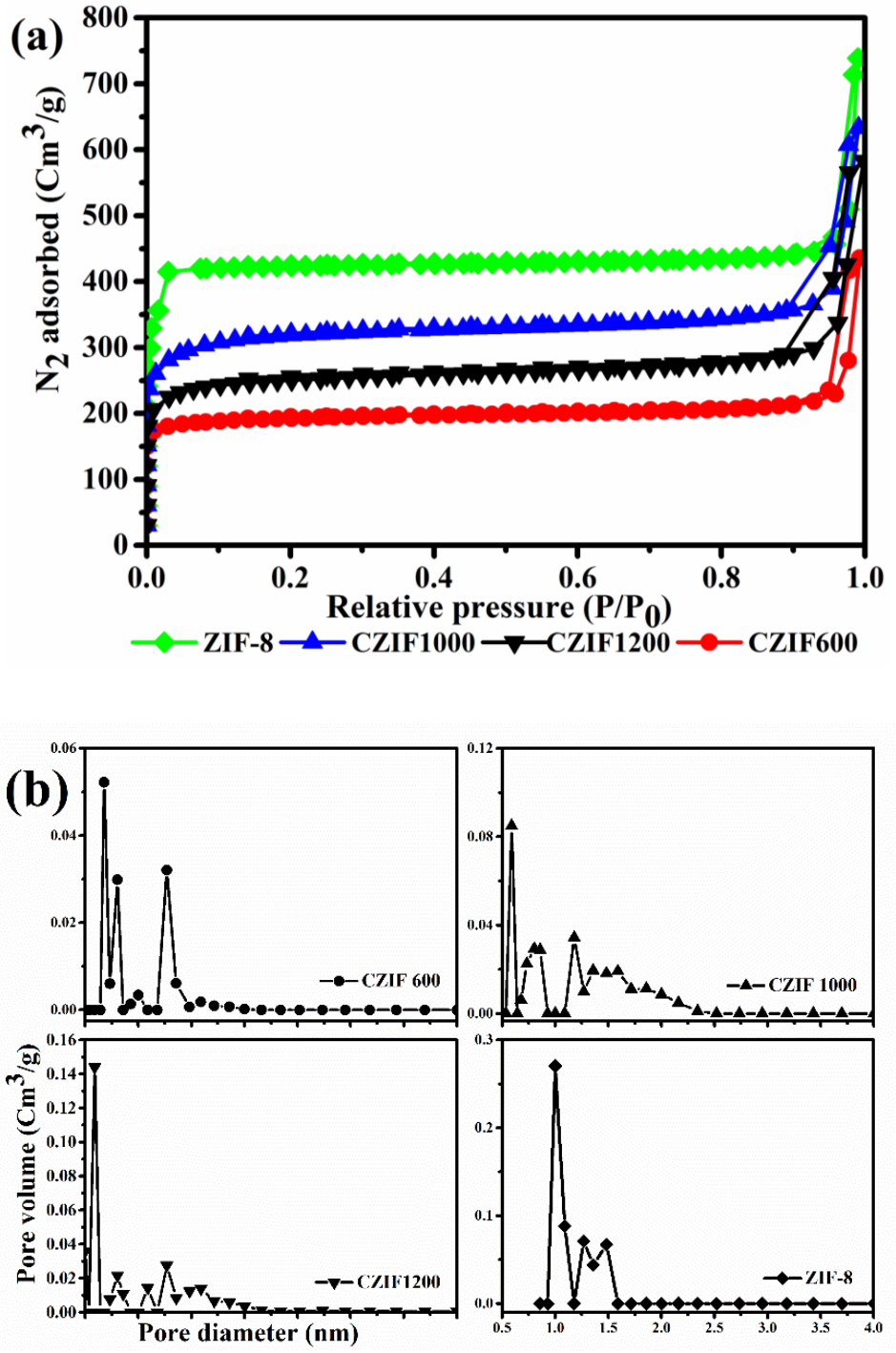

Fig. 4-4 Nitrogen adsorption-desorption isotherm of ZIF-8 and the nanoporous carbons at 600, 1000 and 1200℃ (a) and the corresponding pore size distributions (b). All horizontal axes of pore size distributions have the same scale of ZIF-8 graph i.e. pore diameter is in the range of 0.5-4 nm.

ZIF-8 and carbonized samples exhibited Type I isotherms with sharp nitrogen consumption at low pressure ($P/P_0 < 0.05$) and small uptake and high pressure ($P/P_0 > 0.9$) addressing a microporous framework with some macropores formed between particles (inter particle voids)

[4]. The microporous structure may come from ZIF-8 as well as evaporation of Zn during heat treatment [45]. The Brunauer, Emmet and Teller (BET) surface areas and pore volumes are presented in Table 4-1. It is worth mentioning that after direct carbonization the nano porous carbons still had high surface areas which enhanced their adsorption performances.

Table 4-1 Surface area analysis parameters of ZIF-8 and its derived carbons at 600, 1000 and 1200℃.

Sample	BET surface area (m^2/g)	Langmuir surface area (m^2/g)	Total pore volume[a] (Cm^3/g)	Micropore volume (Cm^3/g)
ZIF-8	1384.2±33.5	1849±35.1	1.1±0.18	0.63±0.014
CZIF600	625.5±12.4	811.9±3.65	0.67	0.26
CZIF1000	1043.1±17.6	1305±12.5	0.98	0.4
CZIF1200	818.7±14.7	1037.8±8.9	0.9	0.32

[a] At P/P0=0.99

As reflected in the table, the surface areas of the carbonized sample at 600℃ decreased after carbonization while the surface area of the sample treated at 1000℃ increased. Interestingly, ZIF-8 carbonized at 1200℃ exhibits surface area lower than CZIF 1000. This could be addressed to the harsh conditions (very high temperature) of carbonization which results in the destruction of carbon structure and consequently reduction of the surface area.

For the carbonized samples, the pore size distribution became to some extent broader as a result of carbonization (as evidenced from Fig. 4-4(b)). Therefore, heat treatment of ZIF-8 resulted in the modification of the pore size distribution and this feature along with the high surface area facilitates the diffusion of MB molecules into the carbon network and helps the increase in adsorption capacity of the materials. The molecular dimension of MB is 1.43 nm × 0.61nm × o.4 nm [1] and is within the broad pore size range of the carbonized ZIF-8 shown in Fig. 4-4. The tails in the isotherms for carbonized samples show N_2 uptake at high relative

nitrogen pressure which could be assigned to condensation effects in externally formed pores between the nanoparticles [11].

The effect of heat treatment on the surface area of ZIF-8 is in consistent with the results reported by Gadipelli et. al. [46]. In their study, it was shown that carbonization of MOF-5 (a metal organic framework containing Zn) at temperatures below 900℃, resulted in a decrease in surface area. On the contrary, heat treatment at temperatures higher than the evaporation temperature of Zn (908℃) caused an increase in the surface area. The reason was attributed to the reduction of ZnO with carbon and the evolution of Zn, CO and CO_2 which results in a more porous network. The increase in the surface area and porosity of the carbon materials could be explained with reference to the thermogravimetric analysis of ZIF-8 material as illustrated in Fig. 4-5.

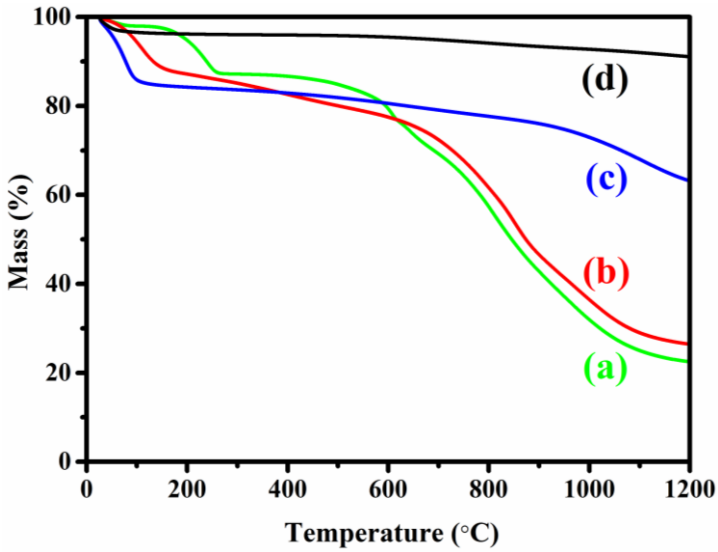

Fig. 4-5 TGA analysis of ZIF-8 (a), CZIF 600 (b), CZIF 1000 (c) and CZIF1200 (d)

As shown in Fig. 4-5, ZIF-8 organic linkers start to decompose at around 500-600℃ and the generated Zn species probably block the pores and this results in a lower surface area [45]. However, by increasing the temperature up to 1000℃, Zn species evaporate at 908℃ and this might lead to the production of porosity within the framework which further expands the surface

area. The sample carbonized at higher temperature had higher surface area and this shows that the carbonization temperature is very important for the structural formation of the resulting carbon materials. Despite the decrease in the surface area of ZIF-8 after carbonization at 600℃, the surface areas of the carbonized samples increased with temperature of carbonization at 1000℃ although it reduced again at carbonization temperature of 1200℃. Similar results have been reported in literature [4]. The pore size of the samples has been defined by density functional theory (DFT) method. As can be seen from Fig. 4-4, the pore size distribution of the samples changed after carbonization and the distribution covered a broader range of pore sizes with a slight shift towards larger pore diameters. This observation is also similar to the reported study for ZIF-8 carbonization [4]. However, the carbonized ZIF-8 at 1200℃ exhibited pore size distribution of smaller pore diameters.

It is worth noting that the reduction in porosity and pore volumes of the nanoporous carbons in comparison with ZIF-8 precursor is associated with the shrinkage of the structure because of Zn nodes migration into the pore cavities [11]. Also the pore broadening of CZIF1000 indicates the evaporation of Zn metal at temperatures above its boiling point. About the pore size distribution, it is interesting that there is a great portion of pore sizes of less than 1 nm which reflects the collapse of the framework as well as graphitization. The second portion of the pores are 1.2 nm which is similar to the size of the cavities of ZIF-8. A small part of the pores are produced due to the defects resulting from thermal decomposition with a 2 nm width. These observations are in good agreement with previous reports [11, 47-49].

The adsorption ability of the surface is determined by an important factor which is called the point of zero charge (pzc). To determine the point of zero charge of a sample, the zeta potential (measured at various pH values) is plotted against pH. The pH at which the zeta potential is zero is called point of zero charge (pzc). As can be seen from Fig. 4-6, the pzc of

ZIF-8 is above 10. This means the adsorption of positively charged MB molecules on ZIF-8 is only possible at pH levels higher than 10, ignoring the very small accessible pore size of ZIF-8 which is too small (0.34 nm) for taking up large MB molecules (1.43 nm × 0.61 nm × 0.4 nm) [50]. In comparison, the points of zero charge for the carbonized ZIF-8 samples are around 4.5-5.5 and as can be seen from Fig.4-6 at pH levels of around 7-8 (the typical pH of industrial wastewaters) the zeta potentials are highly negative which is an indication of potential adsorption capabilities of the synthesized carbon materials for positively charged molecules like methylene blue. It is also observed that the zeta potential for CZIF 1200 is more positive compared with CZIF 600 at pH=5.5 which is the pH at which MB adsorption was conducted. This observation helps to understand the reason behind the low adsorption capacity of CZIF 1200 compared with CZIF 600 and CZIF 1000 despite higher carbonization temperature.

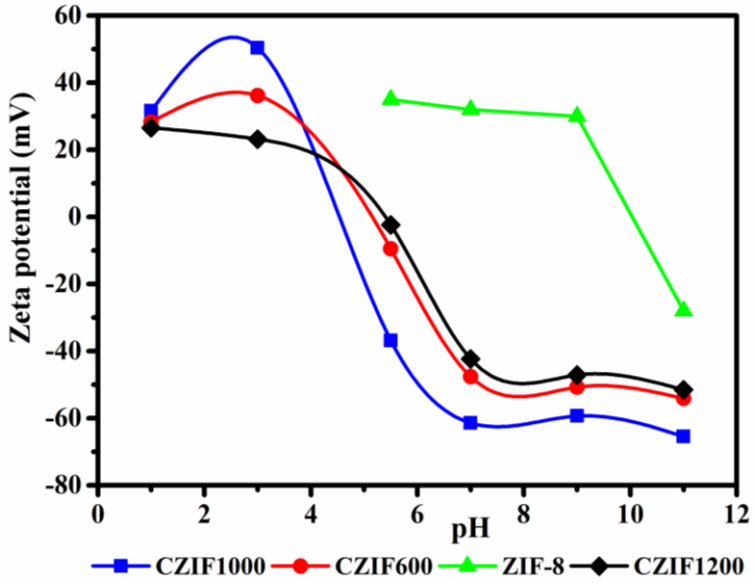

Fig. 4-6 Zeta potential comparison of ZIF-8 and ZIF derived nano porous carbons over the range pH=1-11.

The samples were further analysed by Fourier transform infrared spectroscopy (FTIR) to obtain more information about the local structures and surface functional groups in the carbonized ZIF-8 materials. As it is shown in Fig. 4-7 all of the carbon materials show O-H stretching vibrations in the range of 3600-3200 cm^{-1} indicating the presence of hydroxyl groups

and adsorbed water molecules [41, 51]. The peaks at 1710 and 1620 cm^{-1} are associated with C=O bonds of carboxyl groups and some nitrogen containing species like C=N stretching vibrations in the region 1480-1610 cm^{-1}. The more complicated bands within 1000-1300 cm^{-1} may be addressed to C-O groups [52]. For ZIF-8 material, the peaks observed at 3135 and 2929 are characteristics of aromatic and aliphatic C-H stretch of imidazole and the peaks at 1584, 800-1500 and 421 cm^{-1} are indications of C=N stretch mode, entire imidazole ring vibrations and Zn-N stretch mode respectively [51].

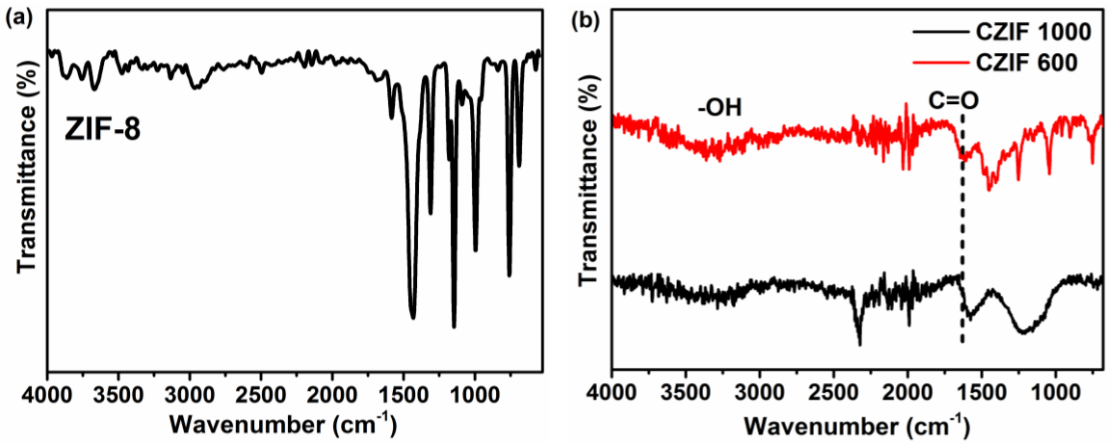

Fig. 4-7 FTIR spectra of ZIF-8 (a) and its nanoporous carbons at 600 and 1000℃ (b)

The thermal behaviour of the samples are also shown in the TGA graphs (Fig. 4-5). At the temperature below 150℃, the mass loss is due to evaporation of adsorbed water molecules in the pores of the materials. Between 400 and 600℃, the mass loss could be due to the framework decomposition which results in carbon. The mass loss from 900℃ onwards, could be attributed to the evolution Zn through the reduction of Zn by carbon and evaporation [46]. This mass loss is more pronounce for ZIF-8 and CZIF 600. In contrast, CZIF 1000 and CZIF 1200 show little mass loss since they already had been treated at 1000 and 1200℃.

The local structures of the resulting nano porous carbons were investigated using Raman spectroscopy and the results are shown in Fig. 4-8.

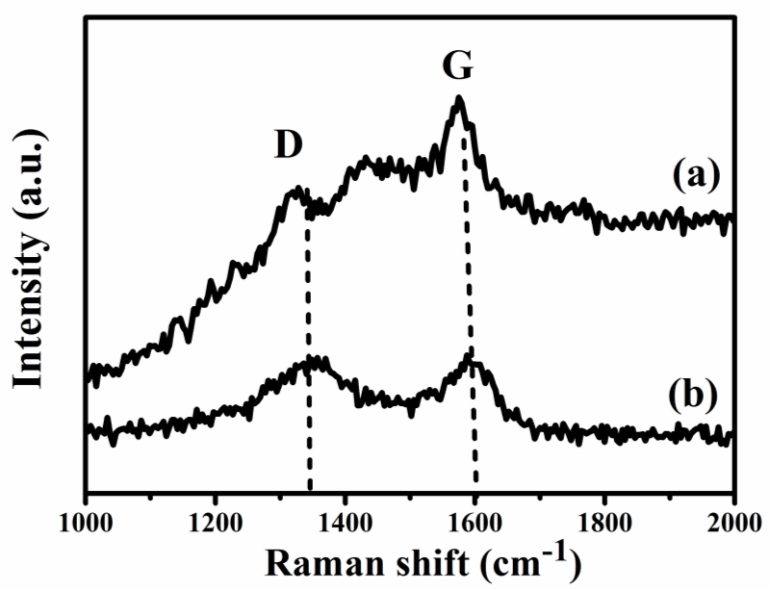

Fig. 4-8 Raman spectra of (a) CZIF-600 and (b) CZIF-1000

The carbonization is also confirmed by the Raman spectra considering the graphitic G and D bands at 1350 and 1600 cm^{-1}, respectively [11]. These broadened peaks at 1350 and 1600 cm^{-1} show a disordered carbon network as evidenced by XRD. Typically, the D band illustrates the presence of disordered carbon structures, while the G band is basically attributed to hexagonal graphitic networks in the porous carbon matrix. The intensity ratio of D peak to G peak (I_D/I_G) is an indication of the amount of defects in the carbon materials [11, 53]. This value also shows as the carbonization temperature increases, more defects are produced in the carbon matrix. These defects produce more accessible surface areas which promote charge accumulation being advantageous for charge transferring in the adsorption process [53]. Therefore, this feature reflects a favourable characteristic for adsorption capacity of the samples carbonized at higher carbonization temperatures.

XPS analysis was performed to identify the surface elements of original ZIF-8 and its derived nanoporous carbons to better understand the adsorption mechanism over these adsorbents and to determine the change in the amount of C, N and Zn after carbonization. As can be seen from Fig. 4-9 the XPS spectra of original ZIF-8 shows that the adsorbent mainly consists of Zn, C and N elements. Two characteristics peaks of Zn were identified at 1021.4 and 1044.5 eV which can be attributed to Zn $2p_{3/2}$ and Zn $2p_{1/2}$, respectively [54]. It is not easy to distinguish the oxidation states of Zn by only using Zn 2p spectra since the binding energy range of Zn^0 and Zn^{2+} overlaps. Therefore, ZnLMM Auger spectra were also considered to define the chemical states of Zn element as shown in the figure.

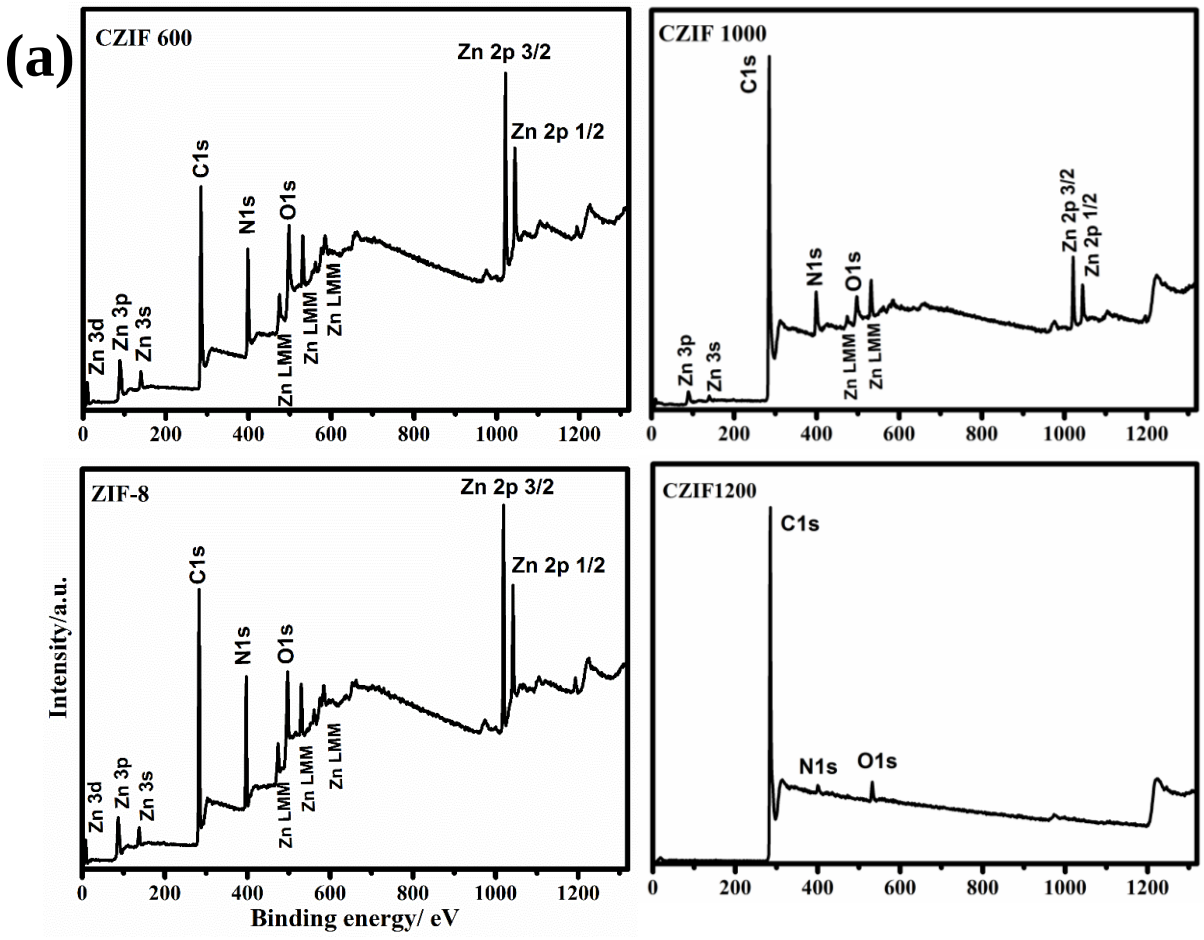

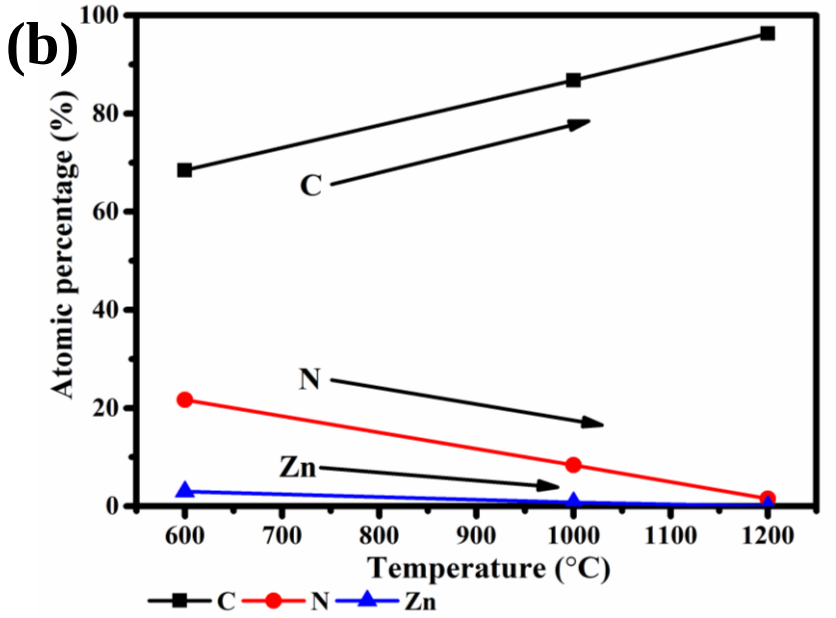

Fig. 4-9 XPS spectra of ZIF-8 and its nanoporous carbons (a) and XPS atomic percentage of C, N and Zn in ZIF-8 and its nanoporous carbons (b). For a more clear comparison, the adsorbed oxygen is eliminated

The spectra with the binding energy at 399.1 eV are assigned to the N in $C = N -$ and $C - NH -$ groups [55]. The predominant peak at 399 eV is assigned to a pyridinic nitrogen which is a nitrogen atom bonded to two carbon atoms in a hexagon ring [56]. It is reported in literature that the incorporation of nitrogen atoms into carbon produces defects in the structure. Therefore, the carbon atoms at the edge locations are highly reactive and react with physically adsorbed oxygen to form oxygen containing groups when the atoms are exposed to air [57].

The peaks with binding energy of 532.5 eV and 284.85 eV are associated with O1s and C1s respectively [58]. Also oxygen is in the forms of $Zn - OH$ and H_2O [59]. The O1s peak is related to physically adsorbed oxygen atoms bound to carbon as $C - OH$ and/or $-C = O$ (carboxylic) group [60, 61]. The surface adsorbed oxygen is present without any chemical interactions. In the ZIF-8 framework, the $Zn - N_4$ coordination and the methyl groups $-CH_3$ on imidazole linker are the weakest bonds before the decomposition of the linker [62].

Therefore, increasing the carbonization temperature leads to the change of the chemical interactions between C, N and Zn atoms as it is observed from the qualitative variations of the peak shift. By increasing the temperature from 600 to 1200 ºC, a gradual shift of C1s to 284.6 eV for pure graphitic carbon (sp^2 $C = C$) is observed and suggests a considerable loss of N atoms [63, 64]. The existence of Zn in ZIF-8 nanoporous carbons at temperatures above 900 ºC can be assigned to the very strong Zn-N interactions (although it is expected that Zn evaporates at temperatures higher than 907 ºC) [11].

The quantitative values of the elements before and after carbonization based on the XPS spectra are given in Table 4-2. Hydrogen is not in the list because it cannot be detected using XPS technique [65]. It is seen that by increasing the temperature from 600 ºC to 1200 ºC, the carbon content increases while the oxygen content decreases. While for increasing the

temperature up to 600 ºC, this trend is opposite since the carbon content decreases slightly and the nitrogen content increases marginally. The nitrogen loss for CZIF 1000 and CZIF 1200 is very severe since nitrogen is unstable at high temperatures. These findings are consistent with other studies [45, 66, 67]. The peak positions corresponding to the elements are as follows: 283, 397, 530 and 1019 eV for C1s, N1s, O1s and Zn 2p, respectively.

Table 4-2 Atomic elemental percentage of C, N, Zn and O from the surface analysis of ZIF-8 and the nanoporous carbons by XPS analysis

Material	C1s (%)	N1s (%)	O1s (%)	Zn 2p (%)
ZIF-8	70.88	20.13	6.06	2.94
CZIF 600	68.43	21.69	6.86	2.99
CZIF 1000	86.77	8.39	4.04	0.8
CZIF 1200	96.28	1.51	2.2	0

4.4.2. Adsorption study for the removal of Methylene Blue (MB) dye

The obtained nanoporous carbons were evaluated for their adsorption capabilities with several dyes including MB, RhB, BG and MO to reflect the capability of carbonized ZIF-8 for adsorption of a variety of dyes. For the evaluation of adsorption capacity of the samples, the aqueous solution of MB, RhB and BG (as positively charged model pollutants) and MO (as negatively charged model pollutant) dye were used. The dimensions of MB molecule are 1.43 nm × 0.61 nm × 0.4 nm as mentioned previously [1]. Rhodamine b has the dimensions of 1.44 nm×1.09 nm×0.64 nm [68] and methyl orange molecular size is reported as 1.31 nm×0.55 nm×0.18 nm [69]. The carbonized ZIF-8 at 1000℃ showed the adsorption capacity of 84.3, 153.5, 200 and 186.3 mg/g for Rhodamine B (RhB), Methyl Orange (MO), Brilliant Green (BG) and Methylene Blue (MB) dyes respectively (Fig. 4-10). These results show that carbonized ZIF-8 at 1000 C has tendency to adsorb positively charged dyes, i.e. Methylene Blue, Rhodamine B and Brilliant Green (BG). However, it has much higher adsorption capacity

for Brilliant Green and Methylene blue probably due to the smaller molecular size of MB and BG compared with RhB molecule (1.44 nm×1.09 nm×0.64 nm) [68].

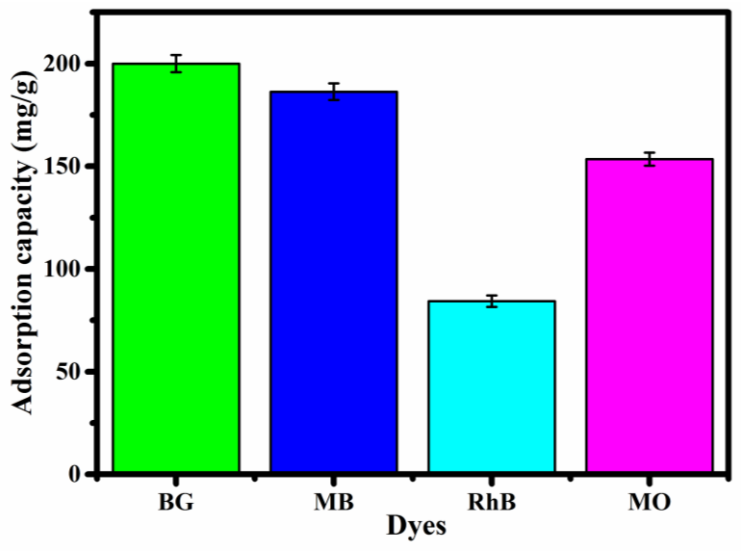

Fig. 4-10 Adsorption capacity of CZIF1000 for various cationic and anionic dyes

It is very interesting that CZIF 1000 has also high adsorption capacity for methyl orange which is a negatively charged dye molecule. This feature could be addressed to the fact that the molecular size of MO (1.31nm×0.55 nm×0.18 nm) [69] is smaller than MB dye (1.43 nm × 0.61nm × o.4 nm) [1]. This feature compensates for the negative charge of MO molecule and facilitates MO adsorption on the carbonized ZIF-8 samples.

The adsorption capacities of nano porous carbons and ZIF-8 for adsorption of MB are shown and compared in Fig. 4-11. Since CZIF1200 had an adsorption capacity lower than CZIF600 and CZIF1000, the adsorption kinetics and isotherms were derived only for the samples carbonized at 600 and 1000℃. The low adsorption capacity of CZIF1200 towards MB dye could be attributed to the more positive surface charge at pH=5.5 reflected as zeta potential (Fig. 4-6) and lower surface area as well as smaller pore size distribution after harsh carbonization condition. It is evidenced from Fig. 4-4 that pore size distribution covers a smaller range of pore diameters compared with CZIF600 and CZIF1000.

It can be seen that the carbonized ZIF-8 materials have significantly higher adsorption capacities in comparison with ZIF-8. It is also observed that the heat treatment temperature had a remarkable effect on the adsorption capacity of the samples. ZIF-8 carbonized at 1000℃ exhibited much higher adsorption capacity compared to the ZIF-8 carbonized at 600 and 1200℃.

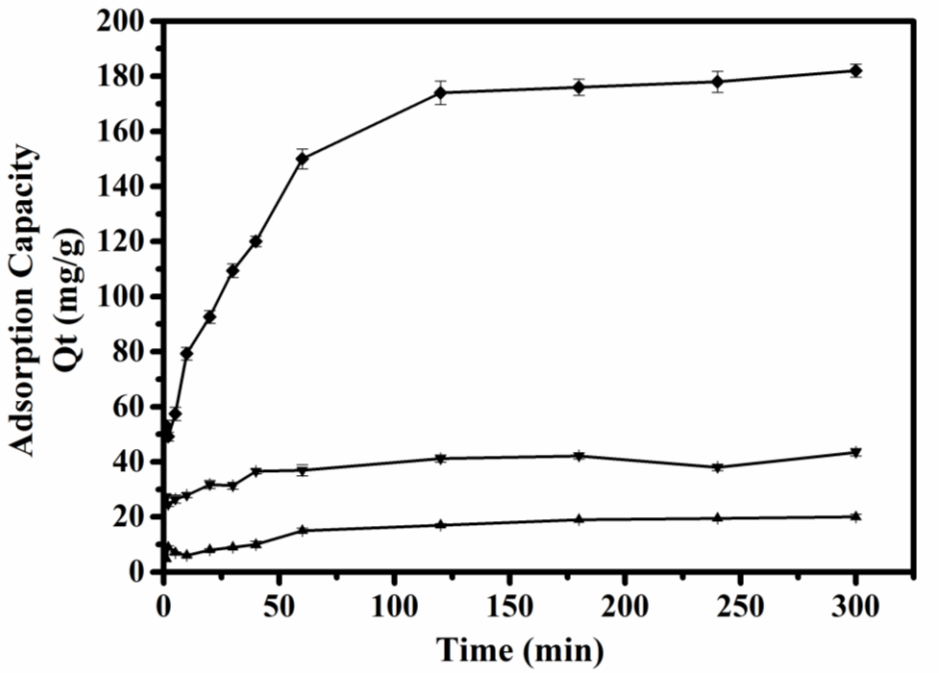

Fig. 4-11 Adsorption capacity of ZIF-8 and nano porous carbons for MB removal (initial dye concentration 100 ppm, adsorbent dosage 10 mg, solution volume 20 ml, initial pH=5.5)

The weak adsorption of ZIF-8 can be attributed to the small pore size (1.3 nm) which has the accessible pore sizes of 0.34 nm [70] as well as the positive surface charge (Fig. 4-6). After conversion to carbon the surface and bulk properties of ZIF-8 are modified; therefore, the resulting carbonized materials possess high negative surface charges, larger surface areas with broader pore size distributions. These features facilitate high adsorption of MB molecules with nanoporous carbons. In addition, MB molecules can interact with the carbon surface because of the π-π interaction between MB molecules and sp^2 graphitic carbon in the carbon matrices. This is confirmed by Raman analysis shown in Fig. 4-8 [1]. The superior removal capacity of

the nanoporous carbons compared to ZIF-8 is evidenced from Fig. 4-11, having adsorption capacity of 186.3 mg/g for CZIF1000, 43.5 mg/g for CZIF600 and 36.7 mg/g for CZIF 1200 compared with 19.5 mg/g adsorption capacity of ZIF-8.

The amount of MB uptake into the adsorbent materials was calculated using the following formula by simply considering the final and initial concentrations of dye solutions.

The percentage of dye removal (%) and the amount of dye adsorbed per unit of adsorbent (q) were calculated by the following equations:

$$\% = (C_i - C_e) \times \frac{100}{C_i} \quad (1)$$

$$Q_{e=} \frac{(C_i - C_e) \times V}{m} \quad (2)$$

where C_i and C_e are the initial and equilibrium concentrations (mg/l) respectively, V is the volume of dye solution (ml) and m is the weight of the adsorbents (g).

Table 4-3 summarises the comparison of adsorption capacities of MB on various MOF derived nanoporous carbons as well as activated carbons prepared from different sources.

Table 4-3 Adsorption capacities of MB on various carbon based adsorbents

	Adsorption		Carbonization		
Adsorbent	isotherm	Adsorption pH	T (℃)	Q_m (mg/g)	Reference
ZIF-67 derived carbon*	Langmuir	NA	600, 800 ℃	300.3, 500	[1]
Mixture of MIL-53 and MIL-58B carbon composite	Langmuir	NA	500, 600 ℃	74	[71]
MOF derived carbon (MIL-100 (Fe))	Langmuir	NA	500, 600 ℃	303.95	[37]
Polystyrene @ ZIF-8 core-shell microspheres	NA	NA	1000 ℃	NA	[72]
ZIF-8 derived carbon*	Langmuir	5.5	600℃	43.5	This study
ZIF-8 derived carbon*	Langmuir	5.5	1000 ℃	186.3	This study
ZIF-8 derived carbon*	NA	NA	800℃	59	[2]
Magnetic carbonized MOF-5*	Langmuir	6	900℃	292.4	[38]
AC[1] from date palm leaflets	Langmuir	7	550℃	270	[73]
AC from walnut shells	Redlich-Peterson	7	350-600℃	315	[74]
AC from cotton stalk	Langmuir	7	NA	193.5	[75]
AC from waste biomass	Langmuir	6	600℃	16.43	[76]
AC from waste tea	Langmuir	7	800℃	554.3	[77]
AC from Posidonia oceanica-dead leaves	Langmuir	6.5	600℃	285.7	[78]

*Prepared by direct carbonization

[1] AC: Activated carbon

Nanoporous carbon derived from ZIF-67 exhibits the highest adsorption capacity in MB removal among the MOF derived carbon materials while activated carbon from waste tea has the highest adsorption capacity for MB dye compared to activated carbons from other sources.

The properties of activated carbon depends on the source material, therefore the adsorption capacities for dye removal differs for different kind of activated carbons. In most cases the activated carbons were treated and functionalized under harsh acidic conditions (or other chemical conditions) to make them suitable for adsorption. However, in this work, no treatment (by any means) was used and the ZIF-8 derived carbons were used directly after carbonization. For example, activated carbon derived from date palm leaflets were prepared using KOH activation followed by nitric acid oxidation to develop oxidized activated carbon. In addition, basic activated carbons were produced using ethylene diamine and propylene diamine to functionalize the surface of the carbons. The treated activated carbons had MB adsorption capacity in the range of 200-300 mg/g. The initial basic activated carbon had 270 mg/g adsorption capacity [73]. It is observed that ZIF-8 derived carbons show promising adsorption capacities in comparison with other materials. Therefore, untreated carbonized ZIF-8 with MB removal capacity of 186.3 mg/g can compete with the other conventional carbon adsorbents for the removal of MB dye from water. Fig. 4-12 Shows the electrostatic interaction between MB and ZIF-8 derived nanoporous carbons.

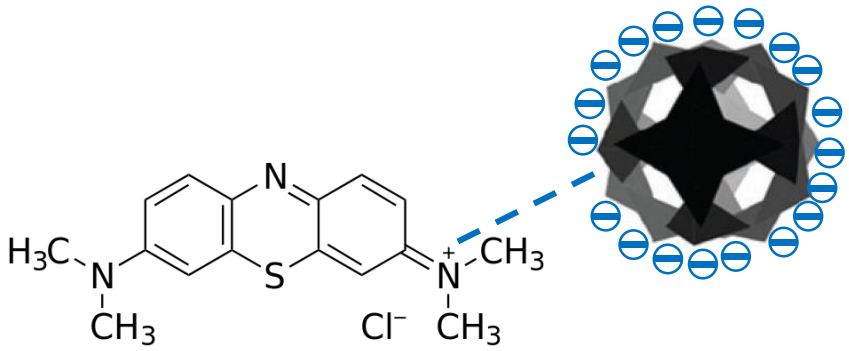

Fig. 4-12 Electrostatic interaction between methylene blue dye and nanoporous carbons

4.4.3. Adsorption isotherms

Analysis of the adsorption isotherm is of a great importance in order to define how adsorbate substances interact with the adsorbent surface. Equilibrium adsorption studies define the capacity of the adsorbent and also illustrate the adsorption isotherms by constants whose values express the surface properties and affinity of the adsorbents. It is required to understand the relationship between equilibrium adsorption data and either theoretical or practical equations in order to interpret and predict the extent of adsorption [79].

Among the adsorption isotherms the Langmuir and Freundlich models are the most common isotherms due to their simplicity and capability to describe experimental results in wide ranges of concentration [80].

The Langmuir adsorption isotherm model assumes that adsorption takes place at specific homogenous sites on the adsorbent. This model has been used successfully for many adsorption processes of monolayer adsorption. This model is expressed with the following equation:

$$Q_e = \frac{Q_m K_L C_e}{1 + K_L C_e} \tag{3}$$

The equation can be linearized to the following forms:

$$\frac{1}{Q_e} = \frac{1}{Q_m} + \frac{1}{K_L Q_m}\frac{1}{C_e} \tag{4}$$

or

$$\frac{C_e}{Q_e} = \frac{C_e}{Q_m} + \frac{1}{K_L Q_m} \tag{5}$$

where Q_m is the maximum amount of adsorption with complete monolayer coverage on the adsorbent surface (mg g^{-1}), and K_L is considered the Langmuir constant related to the energy of adsorption (l mg^{-1}). The Langmuir constants K_L and Q_m can be determined from the linear plot

of $1/C_e$ versus $1/Q_e$. The Langmuir isotherm is explained according to the assumption that the structure of the adsorbent is homogeneous and all sorption sites have equal energy levels. This means the adsorption process should include equal sorption activation energy and represents the formation of monolayer coverage of the adsorbate molecule on the adsorbent surface.

The Freundlich isotherm model considers a heterogeneous adsorption surface that has unequal sites with different adsorption energies. This model is not restricted to the monolayer formation and is presented as follows:

$$Q_e = K_f C_e^{1/n} \tag{6}$$

Eq. (4) can be rearranged to a linear form by taking logarithms as follows:

$$\log Q_e = \log K_F + {}^{1}/_{n} \log C_e \tag{7}$$

where Q_e is the amount of dye uptake per unit mass of adsorbent at equilibrium (mg/g), C_e is the concentration of dye solution at equilibrium (mg/l), K_F ($mg^{1-1/n}\ l^{1/n}\ g^{-1}$) and n are the Freundlich adsorption isotherm constants. K_F and $1/n$ values can be calculated from the intercept and slope of the linear plot between log C_e and log Q_e.

Favourable adsorption by a material can be determined from the Freundlich constants. K_F is indicative of the adsorption capability of the adsorbent, i.e. the greater K_F value shows the greater adsorption capacity. *n* is another Freundlich constant which is a measure of the deviation from linearity of the adsorption and typically illustrates the types of adsorption. If *n* is equal to unity, the adsorption is linear. Furthermore, an *n* value below unity indicates that the adsorption is a chemical process; whereas, an *n* value above unity is attributed to favorable adsorption and a physical process [81]. Adsorption isotherms were derived for CZIF 600 and CZIF 1000 to compare the equilibrium adsorption data for different carbonization temperatures.

Table 4-4 shows the calculated values of Langmuir and Freundlich model's parameters.

Table 4-4 MB adsorption isotherm parameters of carbonized ZIF-8 prepared at 600 and 1000℃.

sample		Langmuir isotherm			Freundlich isotherm		
	Q_e	K_L	Q_m	R^2	K_F	n	R^2
CZIF1000	186.3	0.86	185.2	0.999	126.6	10.52	0.7944
CZIF600	43.5	0.21	49.5	0.9975	35.6	17.1	0.7752

According to the graphs and calculations the equilibrium data showed a better fit to the Langmuir equation with $r^2>0.99$ addressing the homogeneous active sites and monolayer coverage of MB onto nanoporous carbons (Fig. 4-13 a and b). The experimental data is verified by comparing the calculated maximum adsorption capacity (Q_m) and equilibrium adsorption (Q_e) (Table 4-4).

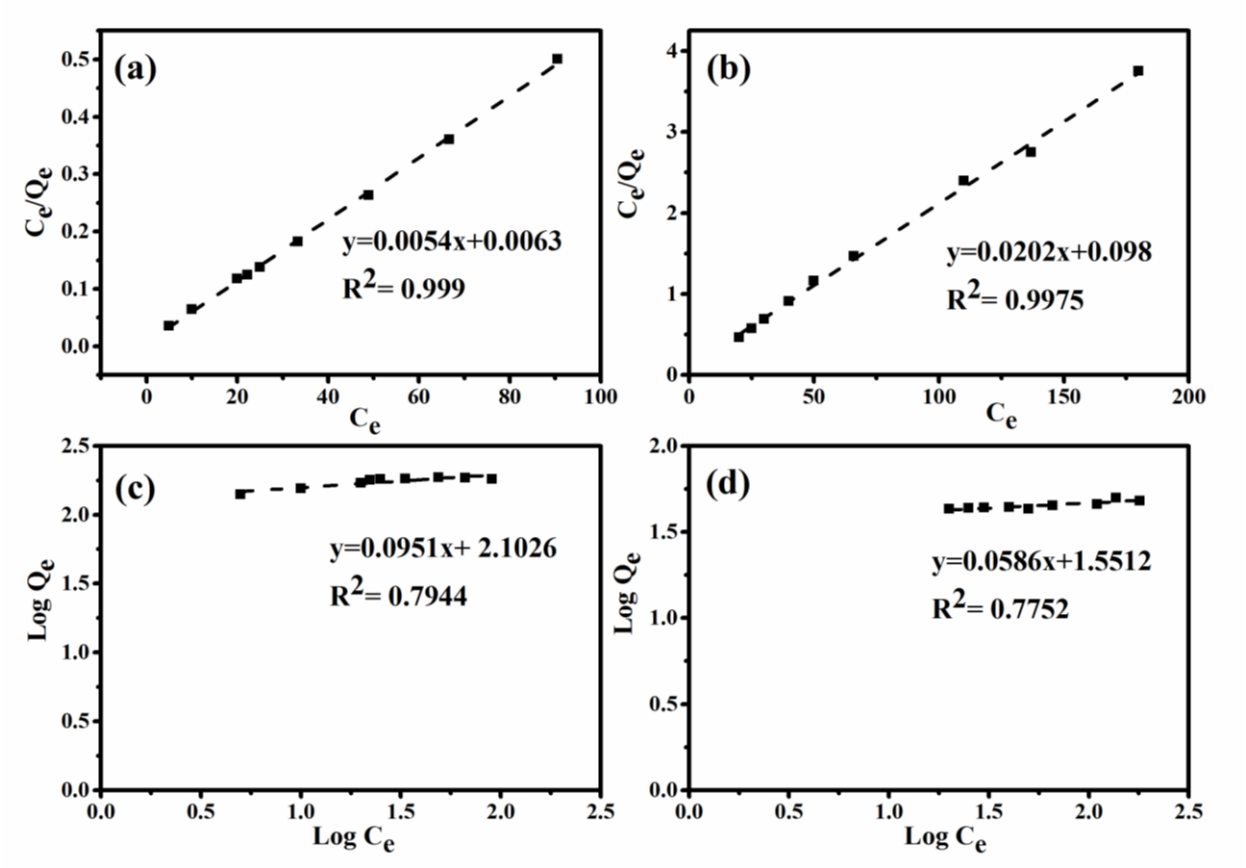

Fig. 4-13 Adsorption isotherms for adsorption of MB on carbonized ZIF-8 at 600 and 1000℃: (a) and (b) Langmuir isotherms, (c) and (d) Freundlich isotherms for CZIF1000 and CZIF600 respectively (adsorbent dosage 10 mg, solution volume 20 ml, initial pH=5.5).

The carbonized ZIF-8 at 1000℃ shows an impressive adsorption capacity for MB dye with 186.3 mg/g which is almost 10 times and four times the amount adsorbed by carbonized ZIF at 600℃ and ZIF-8 respectively.

The separation factor (R_L) was also calculated from Langmuir isotherms and is illustrated in Fig. 4-14. The favourable adsorption of Langmuir isotherm can be explained by means of a dimensionless separation factor R_L [82].

$$R_L = \frac{1}{1 + K_L C_i} \tag{8}$$

R_L values are described based on the categories shown in Table 4-5:

Table 4-5 R_L values according to the adsorption isotherms

R_L	Type of isotherm
$R_L>1$	Unfavorable
$R_L=1$	Linear
$0<R_L<1$	Favourable
$R_L=0$	Irreversible

As illustrated in Fig. 4-14, since the RL values are all between zero and unity, thus it is confirmed the adsorption process over nanoporous carbons is favourable.

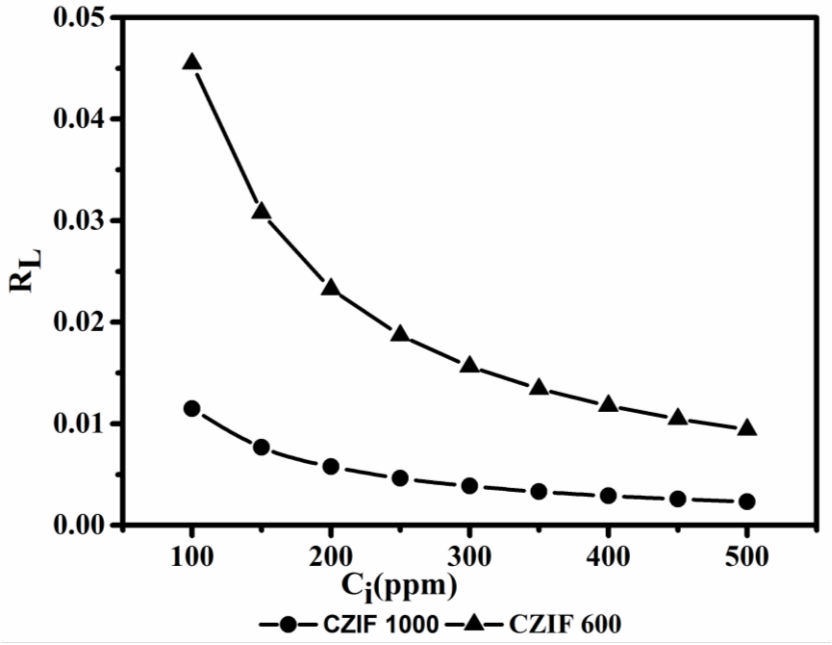

Fig. 4-14 RL values of the ZIF-8 derived nanoporous carbons at different initial concentrations (adsorbent dosage 10 mg, solution volume 20 ml, initial pH=5.5).

4.4.4. Adsorption kinetics

There are several adsorption kinetic models for defining the controlling mechanism of dye adsorption from aqueous solution. It is worth noting that the rate of adsorption of a particular

molecule depends upon its mobility in the solution phase, the adsorbent pore structure, the particle size, and the hydrodynamics of contact between the solution and the particle phase [83]. Pseudo-first order and Pseudo-second order models are widely used for the adsorption processes. The adsorption kinetics were performed for CZIF 600 and CZIF 1000 to compare the kinetic results for two different carbonization temperatures.

Pseudo-first order model is according to the assumption that the rate of solute uptake with time is directly proportional to the difference in equilibrium concentration and the amount of adsorbate uptake with time.

$$\frac{dQ_t}{d_t} = k_1(Q_e - Q_t) \tag{9}$$

when $Q_t = 0$ at $t = 0$, Eq. (6) can be integrated into following equation:

$$\log(Q_e - Q_t) = \log Q_e - \frac{k_1 t}{2.303} \tag{10}$$

where Q_t is the amount of dye uptake per unit mass of adsorbent (mg/g) at time t, k_1 is the pseudo-first order rate constant (min^{-1}), and t is the contact time (min). The adsorption rate constant (k_1) is calculated from the plot of log (Q_e-Q_t) against t.

Ho and McKay [84] presented the pseudo-second-order kinetic as:

$$\frac{dQ_t}{Q_t} = k_2(Q_e - Q_t)^2 \tag{11}$$

Integrating Eq. (8) and noting that $Q_t = 0$ at $t = 0$, the obtained equation can be rearranged into a linear form:

$$\frac{t}{Q_t} = \frac{1}{k_2 Q_e^2} + \frac{t}{Q_t} \tag{12}$$

where k_2 is the pseudo-second order rate constant (g mg^{-1} min^{-1}).

The calculated kinetic parameters of the carbonized samples are given in Table 4-6.

Table 4-6 MB adsorption on carbonized ZIF-8 samples: kinetics parameters

	Pseudo first order			Pseudo second order			Intra particle diffusion		
sample	K_1 ($\times 10^{-3}$) (min^{-1})	Q_e ($mg.g^{-1}$)	R^2	K_2 ($\times 10^{-3}$) ($g.mg^{-1}.min^{-1}$)	Q_e ($mg.g^{-1}$)	R^2	K_i ($mg.g^{-1}.min^{-1}$)	C	R^2
CZIF1000	15.8	125.1	0.9503	0.38	188.67	0.9964	13.41	34.59	0.9808
CZIF600	15.2	16.87	0.9736	4.6	42.19	0.9935	1.66	23.63	0.9318

The experimental data was analysed by comparing the calculated q_t against time from the two kinetic models and thereafter was defined by linear regression. As it is shown in Fig. 4-15 the carbonized samples fitted kinetic models well. Nevertheless, the pseudo-second order model shows a better fit for the experimental data when comparing r^2 as it shows a higher r^2 (>0.99) compared to the pseudo-first order model. The calculated adsorption capacity from the latter is also very close to the experimental value. These results confirm the applicability of the pseudo-second-order equation. They also indicate that the sorption of MB into the nanoporous carbons follows the pseudo-second-order model.

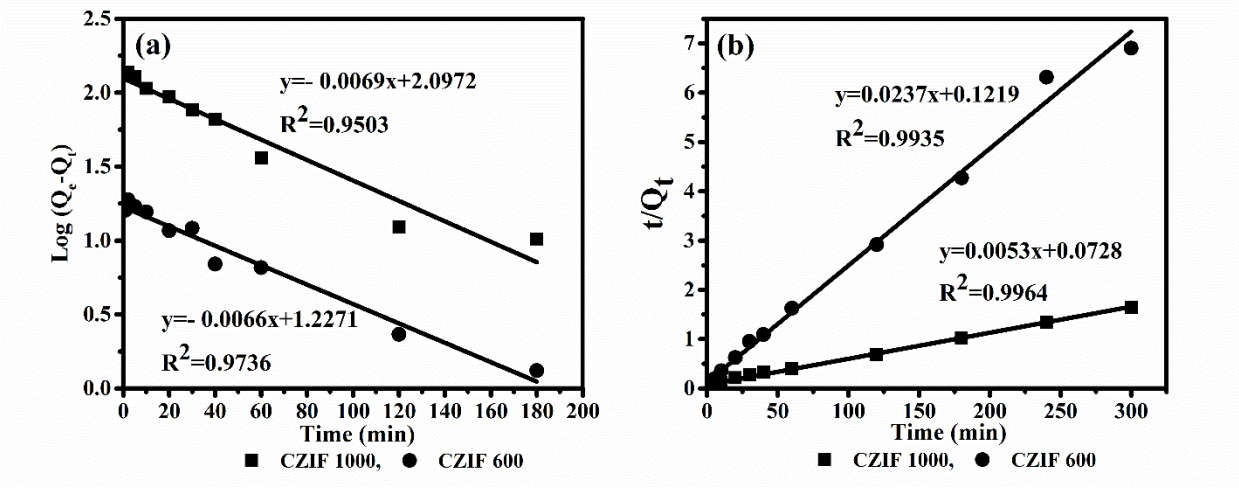

Fig. 4-15 Adsorption kinetics for adsorption of MB on CZIFs (initial dye concentration 100 ppm, adsorbent dosage 10 mg, solution volume 20 ml, initial pH=5.5) (a) Pseudo first order and (b) Pseudo second order kinetics.

4.4.5. Adsorption mechanism

Adsorption is usually controlled by either the liquid phase mass transport rate or the intraparticle mass transport rate. Weber and Morris [85] proposed the use of the intra-particle diffusion model to determine diffusion mechanisms of adsorption processes. The effect of intra-particle diffusion resistance on adsorption process is presented by the following relationship:

$$Q_t = K_{id} t^{1/2} + I \quad (13)$$

where k_{id} is the intra-particle diffusion rate constant (mg g^{-1} $min^{-1/2}$). From Eq. (13), when adsorption mechanism follows the intra-particle diffusion model, a plot of q_t against $t_{1/2}$ gives a linear line with slope k_{id} and intercept I. Values of I provide information about the thickness of the boundary layer, i.e. the larger intercept means a greater boundary layer effect.

There are a series of resistances to mass transfer during the adsorption processes. These resistances can be attributed to either “external resistance” which happens when the molecules diffuse through the solute film toward the adsorbent surface or “internal resistance” which occurs while the molecules penetrate through the liquid inside the adsorbents pores. The

external resistance is described in terms of mass transfer coefficient. While the internal resistance can be evaluated by the internal pores as well as solids diffusive characteristics. The different regions of the plot of q_t versus $t_{1/2}$ reflect the external mass transfer followed by intraparticle diffusion in macro, meso and micropores [86].

The intraparticle diffusion plots of the nanoporous carbons provided linear curves (Fig. 4-16). However, the plots did not pass through the origin which reflects that the intraparticle diffusion was constituted in the adsorption process but was not the only rate limiting step. Fitting the experimental data gives us three-phased graph.

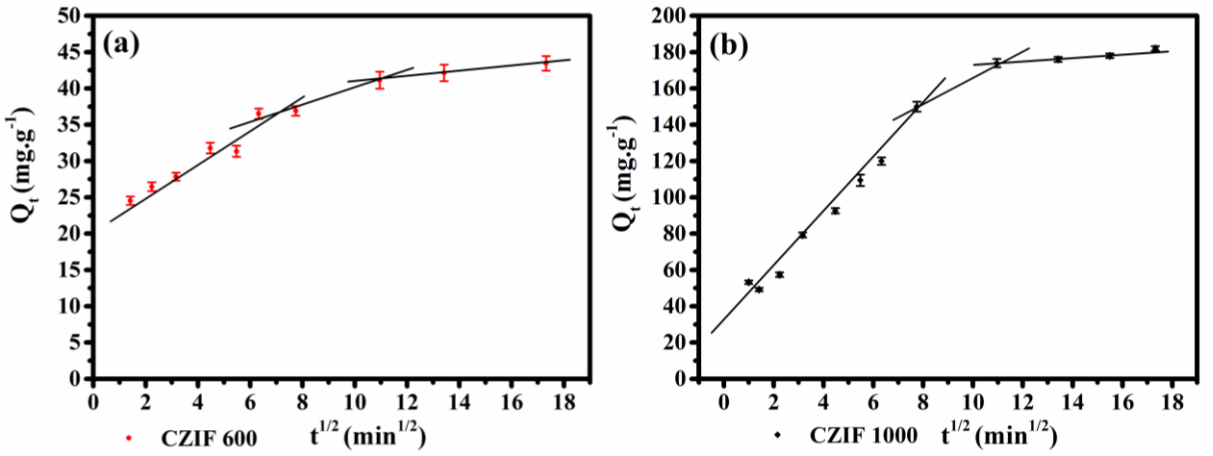

Fig. 4-16 Intra particle diffusion model for adsorption of MB on carbonized ZIF-8 (a) CZIF600 and (b) CZIF1000 (initial dye concentration 100 ppm, adsorbent dosage 10 mg, solution volume 20 ml, initial pH=5.5).

The line in the initial stage does not pass through the origin which indicates that the adsorption at this stage is mainly due to the external surface uptake instead of intra particle diffusion process. In this initial stage the adsorptive molecule diffuses through the solution to the external surface of the adsorbent or to the boundary layer diffusion where the adsorption rate is high. In the second stage, adsorption is faster reflecting the gradual adsorption step where intraparticle diffusion is rate-controlling. In the third section, diffusion remains relatively

constant which means the intra-particle diffusion begins to slow down and then the maximum adsorption is achieved [79].

The intraparticle rate constant (K_{id}) as can be seen from Table 4-6 is much higher for CZIF 1000 compared with CZIF 600 which can be attributed to a combination relationship between parameters such as specific surface areas and pore sizes of the adsorbents. The decrease in the pore size of the nanoporous carbon, would reduce the free path of adsorbate molecules into the adsorbent pores. This results in a decline in the values of intra-particle rate constant.

Intraparticle diffusion model does not define the overall controlling step during the sorption process. Therefore, to further confirm the main rate controlling stage of the whole adsorption process, the kinetic data were also analysed by the kinetic expression reported by Boyd et al. [87]. The following equation was derived to address if the pore diffusion is the limiting step:

$$F = 1 - \left({}^{6}/_{\pi^2}\right)\sum_{n=1}^{\infty}\left({}^{1}/_{n^2}\right)exp(-n^2Bt) \tag{14}$$

where F is the fraction of adsorbate adsorbed at different times and Bt is a mathematical function of F.

$$F = {}^{Q_t}/_{Q_e} \tag{15}$$

where Q_t and Q_e are the amount of dye uptakes (mg/g) at time t and at equilibrium, respectively. Bt is determined as the following equation:

$$B = {}^{(\pi^2 D_i)}\Big/_{r_0^2} \tag{16}$$

From the above equation, the values of B cannot be estimated for each adsorption fraction. Reichenberg [88] derived the following estimation using Fourier transform and integration:

For F values >0.85

$$B_t = -0.4977 - \ln(1 - F) \quad (17)$$

while for F values <0.85

$$B_t = \left(\sqrt{\pi} - \sqrt{\pi - (\pi^2 F/3)}\right)^2 \quad (18)$$

Bt can be plotted against time as it is shown in Fig. 4-17. It can be seen that the plots were linear but did not pass through the origin. This shows that the external transport mainly controls the whole adsorption process of MB over nanoporous carbons as it is the rate limiting step [89].

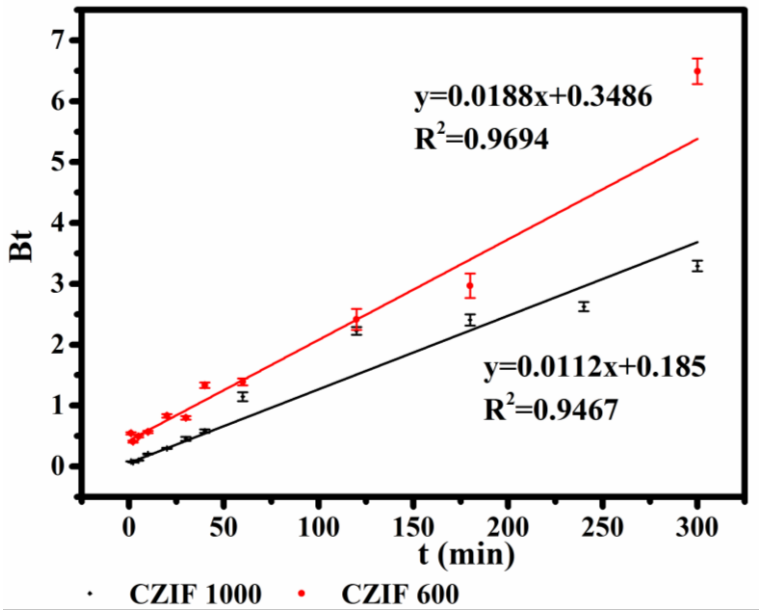

Fig. 4-17 Boyd film diffusion kinetic for adsorption of MB on carbonized ZIF-8 (initial dye concentration 100 ppm, adsorbent dosage 10 mg, solution volume 20 ml, initial pH=5.5).

4.4.6. Effect of pH on adsorption

One of the most important parameters which often affects the adsorption processes is pH of the solution. The adsorption mechanism and the removal efficiency of adsorbents are

influenced by pH since the hydrogen ion concentration impacts the ionization of dyes as well as the surface properties of the adsorbents [90, 91]. The effect of initial pH of the dye solution on the removal efficiency of MB was investigated over the pH range of 1-11 as shown in Fig. 4-18. It is observed that the amount of dye adsorbed on ZIF-8 and nanoporous carbons increased with increasing pH. However, the change in the adsorption performance with pH is not very significant. The change in dye uptake is more pronounce in the pH levels higher than 7. A slight change of the adsorption capacity can be observed at pH around 6 and 7. This behaviour can be explained by point of zero charge (pH_{pzc}).

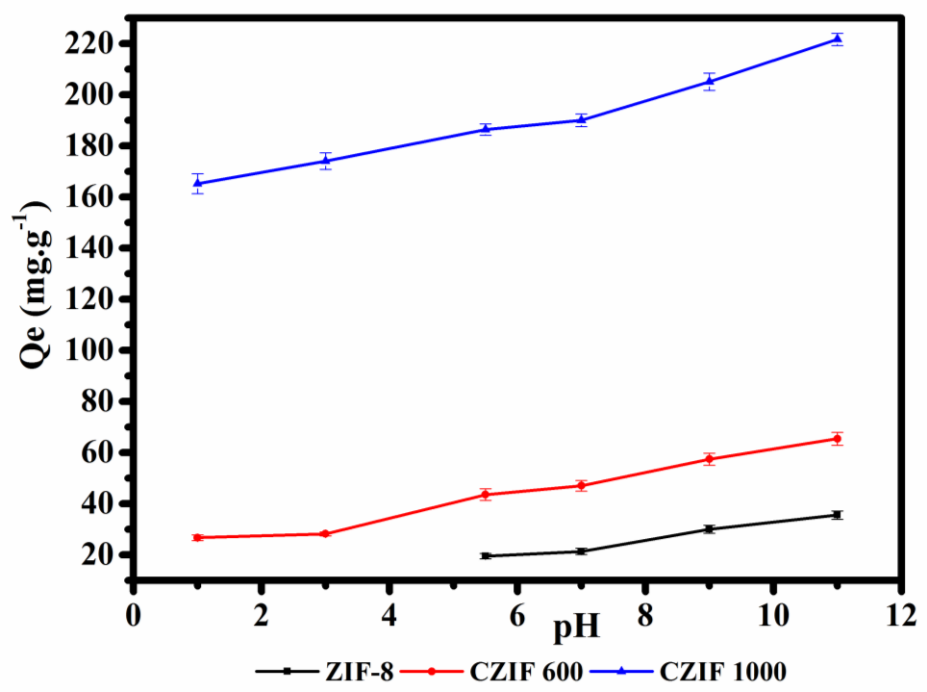

Fig. 4-18 Effect of solution pH on adsorption performance of adsorbents (initial dye concentration 100 ppm, adsorbent dosage 10 mg, solution volume 20 ml)

The point of zero charge (pzc) is the pH at which the surface charge is zero and is generally used to quantify or define the electro kinetic properties of a surface. The value of pH is used to describe pzc only for systems in which H^+/OH^- are the potential determining ions. Due to the presence of functional groups such as OH^-, cationic dye adsorption is favoured at pH > pH_{pzc} where the surface gets negatively charged, while the adsorption of anionic dye is favoured at

$pH < pH_{pzc}$ where the surface becomes positively charged [92]. To define the pzc, the surface charge of a sample is measured as zeta potential using a Zeta sizer. Zeta potential (ζ) is an important pH related parameter that determines the surface properties of solids in aqueous solutions. This parameter is used to explain the adsorption mechanism of an adsorbate at the metal oxide-water interface. Zeta measurement plays an important role in defining the adsorption mechanism of adsorbates at the solid/solution interface as well as determining the colloid stability [93]. From Fig. 4-6 it can be seen that the points of zero charge (the point at which the overall charge of adsorbent is zero) for ZIF-8, CZIF-600 and CZIF-1000 are 10, 5.5 and 4.5, respectively. At $pH < pH_{pzc}$ since H^+ ions compete with the cation group on MB molecules for adsorption sites, the surface of the adsorbent adsorbs more hydrogen ions which results in the reduction of bonding of MB molecules on the sorbent surface. While, at $pH > pH_{pzc}$ the surface of the adsorbents become more negatively charged. Thus, the increase of electrostatic attraction between positive adsorbate molecules and adsorbent surface would cause the increase of the adsorption capacity of methylene blue dye [94]. A similar behaviour has been reported by other studies [76, 95].

4.4.7. Effect of solution temperature

Solution temperature is another important factor which influences the uptake of pollutants form water on the adsorbents. The effect of temperature was investigated using the following relationships:

$$\Delta G° = \Delta H° - \Delta S°T \quad (19)$$

And the van't Hoff equation as:

$$\ln K_C = \frac{\Delta S°}{R} - \frac{\Delta H°}{RT} \quad (20)$$

where K_C is the equilibrium constant and is explained as the ratio of the dye equilibrium concentration on the adsorbent to the dye equilibrium concentration in solution. K_C can be calculated from the following equation:

$$K_c = \left({}^{Q_e W}/_{C_e V}\right) \quad (21)$$

where Q_e is equilibrium adsorption capacity, C_e is equilibrium concentration, W is the weight of adsorbent and V is the volume of dye solution.

R is the ideal gas constant (8.314 $Jmol^{-1}K^{-1}$) and T is the adsorption temperature in Kelvin. By plotting $\ln K_C$ against ${}^{1}/_{T}$ a linear line would be drawn and the values of $\Delta H°(kJ\ mol^{-1})$ and $\Delta S°$ ($J\ mol^{-1}K^{-1}$) can be calculated form the slope and intercept of van't Hoff plot.

The influence of temperature on adsorption of MB is demonstrated in Fig. 4-19 and the thermodynamic parameters are presented in Table 4-7.

Table 4-7 Thermodynamics parameters for the adsorption of MB on nanoporous carbons

Material	ΔGº (Kj/mol)					
	25ºC	40ºC	50ºC	60ºC	ΔHº (Kj/mol)	ΔSº(j/molK)
CZIF1000	-5.39	-7.1	-8.25	-9.39	28.68	114.3
CZIF600	-0.69	-1.36	-1.8	-2.24	12.44	44.1

Increasing the temperature from 25 to 60 ºC gradually increased the adsorption of MB on nanoporous carbons which indicates an endothermic process. This means the adsorption is more favourable at higher temperatures as confirmed by the positive values of ΔHº values. Similar observations have been reported for methylene blue uptake over different carbon materials [78, 96]. The negative values of ΔGº indicate the feasibility of the adsorption process for the

nanoporous carbons for MB removal and it confirms the spontaneous nature of the adsorption. The positive values of ΔS^{o} shows an increase in randomness at the interface of solid and solution [97].

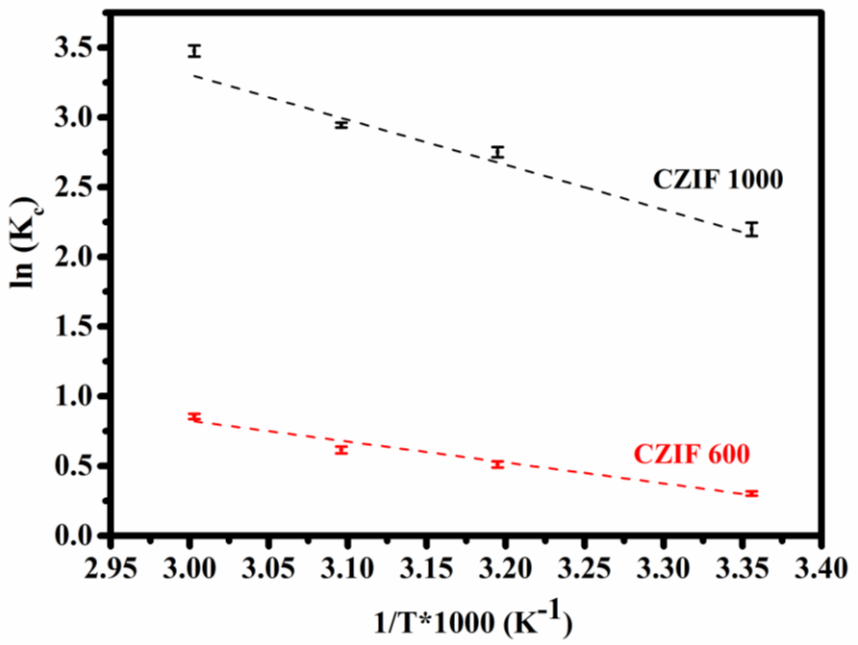

Fig. 4-19 Effect of solution temperature on adsorption performance of adsorbents (initial dye concentration 100 ppm, adsorbent dosage 10 mg, solution volume 20 ml, initial pH=5.5)

4.4.8. Effect of initial dye concentration

The effect of initial concentration of MB on adsorption performance of the nanoporous carbons was tested under equilibrium conditions as shown in Fig. 4-20. The dye removal decreased by increasing the initial dye concentration from 50 to 250 mg/L. This behaviour can be related to the limitation of adsorption sites on nanoporous carbons. The adsorption of CZIF1000 and CZIF 600 reached the saturation at 100 mg/L with capacities of 186 and 43.5 mg/g, respectively.

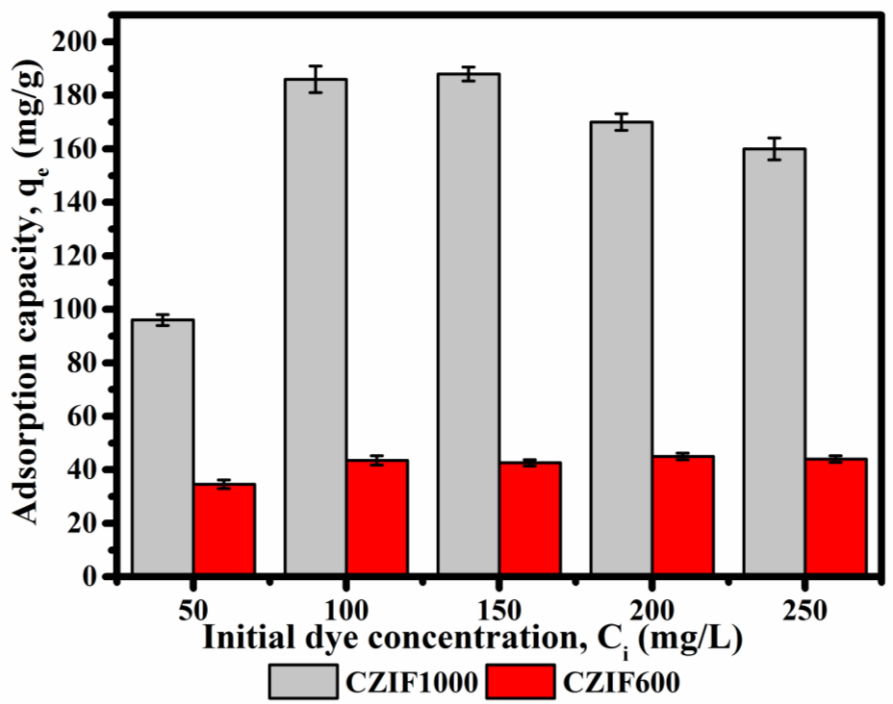

Fig. 4-20 Effect of initial dye concentration on removal capacity by nanoporous carbons (adsorbent dosage 10 mg, solution volume 20 ml, initial pH=5.5)

4.4.9. Regeneration and recyclability of nanoporous carbons

One of the most important characteristics of an efficient adsorbent is recyclability with high adsorption capacity. The adsorbent is required to be reusable and restorable to its original properties after adsorption and reuse. The regeneration of active sites is proportional to the stability of the adsorbents. This aspect is very essential in terms of industrial application. Reusing the adsorbents has two benefits. First, it decreases the operational costs of adsorption process and second, it avoids the secondary pollution to enter the environment.

The nanoporous carbons were regenerated by heat treatment at 200 ºC and reused. After adsorption, the nanoporous carbons were heated at 200 ºC for about half an hour to decompose and release the methylene blue vapour. The adsorption capacities of nanoporous carbons before and after heat treatment are shown in Fig. 4-21. After 5 regeneration cycles, the dye uptakes of

nanoporous carbons only slightly decreased. Therefore, this method is very effective for recycling the carbonized ZIF-8 particles and destroying the dye molecules.

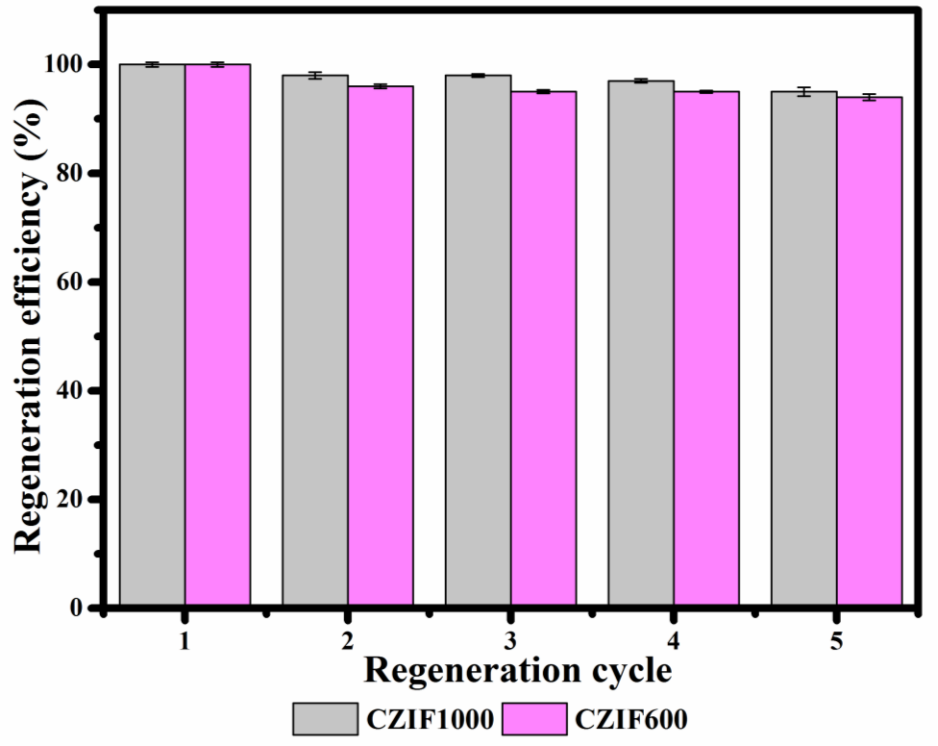

Fig. 4-21 Regeneration efficiency of nanoporous carbons

4.5. Mechanism of thermal decomposition of ZIF-8 during carbonization

The mechanism of ZIF-8 carbonization has been investigated in two temperature regions of up to 300 ºC [98] and 600-1100 ºC [11] in different studies.

James and Lin [98] reported a mechanistic study about the thermal decomposition of ZIF-8 at 300ºC under different atmospheres including air, nitrogen, argon and H_2/CO using the formula of $C_{24}H_{30}N_{12}Zn_3$ representative of ZIF-8 molecular formula. They suggested the following carbonization equation for ZIF-8 at 300 ºC under inert environment:

$$C_{24}H_{30}N_{12}Zn_3 + heat \rightarrow C_{17}H_{21}N_5Zn_3 + gaseous\ products \quad (21)$$

The mechanism of decomposition was suggested by comparison of the FTIR spectra of ZIF-8 and the carbons derived at 300 ºC as shown in Fig. 4-22. The weakening/broadening of the bands between 1350 and 1500 cm^{-1} as well as 900-1350 cm^{-1} and below 800 cm^{-1} which were assigned to the entire stretching and bending of imidazole ring, respectively, showed the disordering and carbonization of imidazole substituents of ZIF-8 framework in the porous carbons derived. The breaking of Zn-N, C=N, and aliphatic/aromatic C-H bonds of imidazole ring was recognized with the loss or broadening of the intensity at the bands located at 421, 1584 and 2929 or 3135 cm^{-1}, respectively. The dissociation of methyl groups of imidazole ring can be realized from the weakening of the IR intensity at 1384 cm^{-1}. The introduction of IR modes at 904, 1041, 1251 and 2200 cm^{-1} was related to disordering bonds produced between C and N. Also the specific IR mode at 1041 cm^{-1} was related to the formation of an aliphatic amine which is linked to zinc after the decomposition of ring. It was reported that the molecules containing nitrogen and carbon are only released from the framework when the temperature reaches at least 600 or 700ºC.

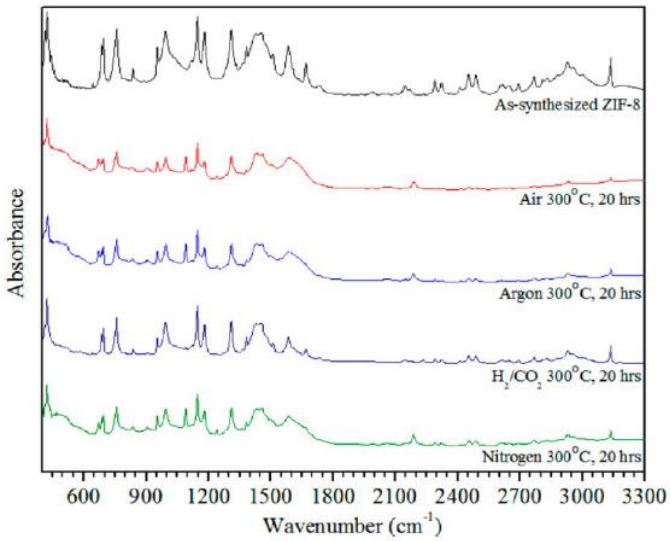

Fig. 4-22 FTIR analysis of ZIF-8 and carbonized ZIF-8 after heat treatment at 300 º C under different atmospheres [98]

According to TGA analysis in literature, the decomposition temperatures for unsubstituted and substituted imidazole and triazole molecules are around 200-300 ºC [99, 100]. During the carbonization of ZIF-8, an olefin gaseous product and a solid residual amine structure are produced without the existence of a strong base. Aniyappan and Maroulis [100, 101] have studied the thermal decomposition of imidazole and triazole ligands and they suggested that the thermolytic bond cleavage is the main mechanism for imidazole thermal decomposition. They suggested that after thermal decomposition of imidazole, azirine molecules were produced. According to these findings from literature, James and Lin [98] proposed the decomposition reactions as the following equation:

$$Zn(C_4H_5N_2)_2 + heat \rightarrow C_4H_5N_2 - Zn - C_2H_2N + gaseous\ products \quad (22)$$

where the chemical composition of ZIF-8 is representative of a single building block of ZIF-8 which includes a zinc cation which is coordinated with two imidazole rings. They proposed that the carbonized ZIF-8 framework after decomposition in inert atmosphere at 300ºC includes a zinc cation in coordination with a nitrogen atom of a 2-methylimidazole linker and the nitrogen atom of an azirine substituent from decomposition of imidazole ligand. This structural formation is illustrated in Fig. 4-23:

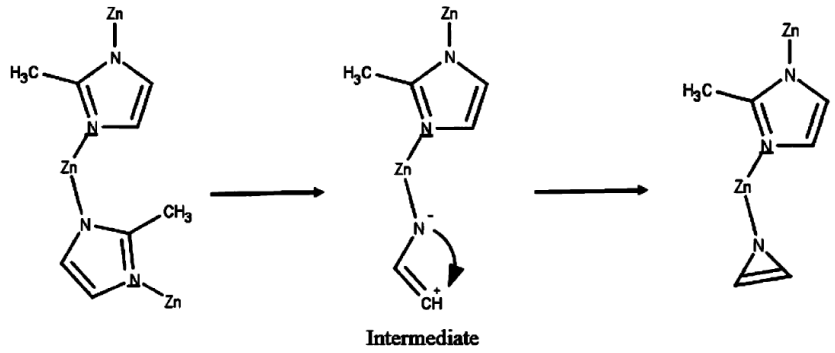

Fig. 4-23 Decomposition mechanism and carbonized ZIF-8 building block after heat treatment at 300 ºC for 20 hours in environments of nitrogen, argon and H_2/CO [98]

It is reported that in the ZIF-8 structure, the Zn-N coordination bond and the C-C bond connecting the imidazole linker to the methyl substituent are the weak bonds in the framework [62]. The methyl group dissociates through homolytic cleavage at the C-CH_3 bond of the imidazole linker. The methyl radical decomposition would lead to the production of hydrogen radicals. These hydrogen radicals further interact at the decomposing imidazole ring or reconnect with other methyl radicals to make C_2H_6. During the decomposition process, the nitrogen which underwent heterolytic cleavage with zinc, would undergo heterolytic cleavage at C-N bond of the decomposing ring. This results in the formation of a positively charged carbon atom in the framework. Moreover, heterolytic cleavage should also occur at the opposite nitrogen atom, which is still bonded to zinc atom, in which the N-C bond is broken and the nitrogen atom retains both electrons and forms a highly negative charged nitrogen atom at the decomposed structure. It is suggested that an azirine ring is produced after the negatively charged nitrogen atom donates the electrons to the positively charged carbocation. Therefore, it is proposed that a heterogeneous carbon is derived from ZIF-8 framework which contains both 2-methylimidazole and azirine rings after heat treatment at 300 ºC in an inert environment [98].

Gadipelli and Guo [11] also systemically investigated the carbonization process of ZIF-8 in the temperature range of 600-1100 ºC and they mentioned that ZIF-8 carbonization involves ligand decomposition and metal evaporation. It was reported that during carbonization of ZIF-8 at temperatures above 600 ºC, the volatile methyl groups dissociate from the main framework and then the nitrogen and vaporized zinc metal are further released. The study reveals that at the temperature below 500 ºC, the first components which dissociate are the methyl groups ($-CH_3$) of the imidazole ligands. The ligand nitrogen atoms are observed at the temperatures between 600 and 800 ºC. At this range of temperature, ligand is decomposed and the $-C-N-H$ mixtures are released from the framework. Above 900 ºC Zn evaporates and leaves the framework.

For defining the detail structural formation during ZIF-8 carbonization, a TG-MS analysis was performed by Gadipelli and Guo [11] to investigate the decomposition of ligand at 600-700, 800-900 and 1000 ºC. Fig. 4-24 shows a schematic of ZIF-8 structural change during carbonization.

ZIF-8 mass loss during the carbonization as reported in TGA graph in this work in Fig. 4-5 (Section 4.4.1) is similar to the weight loss reported in Fig. 4-24. The results from the TGA and XPS data in this study are consistent with the structural evolution of ZIF-8 during carbonization in Fig. 4-24. This is particularly interesting regarding to the nitrogen and carbon content and their ratios in ZIF-8 and the derived carbons at 600, 1000 and 1200 ºC. As it is noted from XPS results in Table 4-2, for CZIF 600 the amount of carbon decreased while the nitrogen content increased. This could be explained according to the dissociation and evolution of methyl groups in temperature range of up to 600 ºC as shown in Fig. 4-24. Carbonization up to 600 ºC results in the reduction of carbon content in comparison with nitrogen which is still within the matrix of material. In the temperature range of 600 to 1000 ºC, the carbon content of CZIF1000

compared with the nitrogen content, increases while the nitrogen decreases severely at high temperatures as seen in Fig. 4-9. Nitrogen and zinc are released from the framework around 900-1000 ºC. Then for CZIF1200 the zinc content approaches zero and the nitrogen content decreases significantly which results in the increase of the portion of carbon in the material matrix.

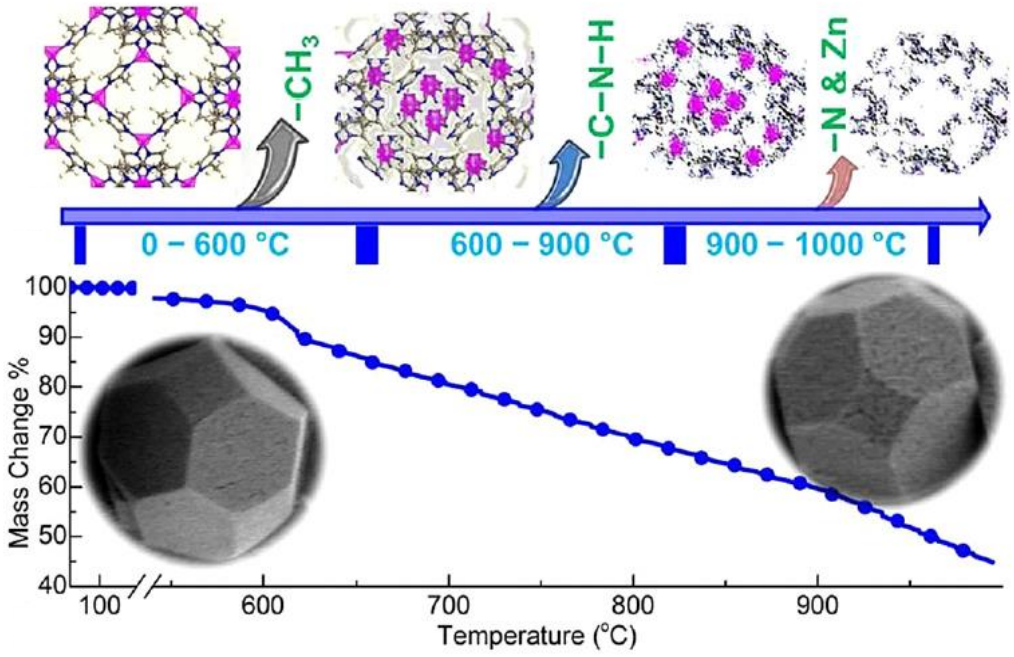

Fig. 4-24 Structural transition of ZIF-8 during carbonization. The atoms in the framework are determined as C gray, H white, N blue and Zn purple [11]

As can be seen from the schematic (Fig. 4-24) and the SEM and TEM images (Fig. 4-3) the resulting carbons have crystallite shapes and surface structures similar to the structure of ZIF-8 precursor. The reason for this similarity is attributed to the slow carbonization of ZIF-8 compared with the rapid carbonization of MOFs such as MOF-5 or MOF-74. During the carbonization of MOF-5 and MOF-74, there is a rapid release of decomposition products like CO_2, while this behaviour is not observed for ZIF-8 carbonization [11]. Therefore, there are no microcracks on the ZIF-8 crystals after carbonization and the morphology is preserved.

4.6. Conclusions

In this study, the effect of carbonization temperature on adsorption capacity of ZIF-8 for water treatment was investigated. Nano porous carbons were prepared by direct carbonization of ZIF-8 at 600℃, 1000℃ and 1200℃. The SEM and TEM images proved that the nanoporous carbon particles retained the original morphology and structure after heat treatment. Zeta potentials provided information about the change in the surface charge of the samples addressing the negatively charged carbon nanoparticles compared with the positively charged ZIF-8 particles. The surface area of ZIF-8 decreased with increasing heat treatment temperature to 600℃ and increased by raising the temperature to 1000℃. However, it declined at carbonization temperature of 1200℃. The pore size distribution became broader after carbonization which facilitated adsorption of MB. The adsorption studies revealed that nano porous carbon derived from ZIF-8 at 1000℃ had outstanding adsorption capacity compared with ZIF-8. The isotherm and kinetics studies showed that the adsorption process followed the Langmuir model and agreed with pseudo-second order kinetic model. It was shown the adsorption process was endothermic and the effect of pH was insignificant. This study illustrates that the heat treatment has significant effect on adsorption properties of ZIF-8 for the removal of organic pollutants from water.

4.7. References

1. Torad, N.L., M. Hu, S. Ishihara, H. Sukegawa, A.A. Belik, M. Imura, K. Ariga, Y. Sakka, and Y. Yamauchi, *Direct Synthesis of MOF-Derived Nanoporous Carbon with Magnetic Co Nanoparticles toward Efficient Water Treatment.* Small, 2014. **10**(10): p. 2096-2107.
2. Chen, B., G. Ma, D. Kong, Y. Zhu, and Y. Xia, *Atomically homogeneous dispersed ZnO/N-doped nanoporous carbon composites with enhanced CO2 uptake capacities and high efficient organic pollutants removal from water*. Carbon, 2015. **95**: p. 113-124.
3. Liu, B., H. Shioyama, H. Jiang, X. Zhang, and Q. Xu, *Metal–organic framework (MOF) as a template for syntheses of nanoporous carbons as electrode materials for supercapacitor.* Carbon, 2010. **48**(2): p. 456-463.
4. Chaikittisilp, W., M. Hu, H. Wang, H.-S. Huang, T. Fujita, K.C.W. Wu, L.-C. Chen, Y. Yamauchi, and K. Ariga, *Metal–organic framework (MOF) as a template for syntheses of nanoporous carbons as electrode materials for supercapacitor* Chemical Communications, 2012. **48**(58): p. 7259-7261.
5. Salunkhe, R.R., Y. Kamachi, N.L. Torad, S.M. Hwang, Z. Sun, S.X. Dou, J.H. Kim, and Y. Yamauchi, *Fabrication of symmetric supercapacitors based on MOF-derived nanoporous carbons.* Journal of Materials Chemistry A, 2014. **2**(46): p. 19848-19854.
6. Peer, M., A. Qajar, R. Rajagopalan, and H.C. Foley, *On the effects of confinement within a catalyst consisting of platinum embedded within nanoporous carbon for the hydrogenation of alkenes.* Carbon, 2014. **66**: p. 459-466.
7. Vasiliev, A.N., L.V. Golovko, V.A. Povazhny, E. Zlotnikov, J. Chen, and J.G. Khinast, *Functionalized nanoporous carbon as a catalyst for Suzuki coupling reactions.* Microporous and Mesoporous Materials, 2007. **101**(3): p. 342-347.
8. Lee, J.J., S. Han, H. Kim, J.H. Koh, T. Hyeon, and S.H. Moon, *Performance of CoMoS catalysts supported on nanoporous carbon in the hydrodesulfurization of dibenzothiophene and 4,6-dimethyldibenzothiophene.* Catalysis Today, 2003. **86**(1–4): p. 141-149.
9. Yang, Z., Y. Xia, and R. Mokaya, *Enhanced Hydrogen Storage Capacity of High Surface Area Zeolite-like Carbon Materials.* Journal of the American Chemical Society, 2007. **129**(6): p. 1673-1679.
10. Ma, X., L. Li, S. Wang, M. Lu, H. Li, W. Ma, and T.C. Keener, *Ammonia-treated porous carbon derived from ZIF-8 for enhanced CO2 adsorption.* Applied Surface Science, 2016. **369**: p. 390-397.
11. Gadipelli, S. and Z.X. Guo, *Tuning of ZIF-Derived Carbon with High Activity, Nitrogen Functionality, and Yield – A Case for Superior CO2 Capture.* ChemSusChem, 2015. **8**(12): p. 2123-2132.
12. Hao, G.-P., W.-C. Li, D. Qian, and A.-H. Lu, *Rapid Synthesis of Nitrogen-Doped Porous Carbon Monolith for CO2 Capture.* Advanced Materials, 2010. **22**(7): p. 853-857.
13. Han, S., S. Kim, H. Lim, W. Choi, H. Park, J. Yoon, and T. Hyeon, *New nanoporous carbon materials with high adsorption capacity and rapid adsorption kinetics for removing humic acids.* Microporous and Mesoporous Materials, 2003. **58**(2): p. 131-135.

14. Ruparelia, J.P., S.P. Duttagupta, A.K. Chatterjee, and S. Mukherji, *Potential of carbon nanomaterials for removal of heavy metals from water.* Desalination, 2008. **232**(1–3): p. 145-156.
15. László, K., E. Tombácz, and P. Kerepesi, *Surface chemistry of nanoporous carbon and the effect of pH on adsorption from aqueous phenol and 2,3,4-trichlorophenol solutions.* Colloids and Surfaces A: Physicochemical and Engineering Aspects, 2003. **230**(1–3): p. 13-22.
16. Xiao, B. and K.M. Thomas, *Competitive Adsorption of Aqueous Metal Ions on an Oxidized Nanoporous Activated Carbon.* Langmuir, 2004. **20**(11): p. 4566-4578.
17. Yazdankhah, A., S.E. Moradi, S. Amirmahmoodi, M. Abbasian, and S.E. Shoja, *Enhanced sorption of cadmium ion on highly ordered nanoporous carbon by using different surfactant modification.* Microporous and Mesoporous Materials, 2010. **133**(1–3): p. 45-53.
18. Güzel, F., H. Sayğılı, G.A. Sayğılı, and F. Koyuncu, *Elimination of anionic dye by using nanoporous carbon prepared from an industrial biowaste.* Journal of Molecular Liquids, 2014. **194**: p. 130-140.
19. Zheng, B., C. Lu, G. Gu, A. Makarovski, G. Finkelstein, and J. Liu, *Efficient CVD Growth of Single-Walled Carbon Nanotubes on Surfaces Using Carbon Monoxide Precursor.* Nano Letters, 2002. **2**(8): p. 895-898.
20. Yang, Xu, A. Tomita, and T. Kyotani, *The Template Synthesis of Double Coaxial Carbon Nanotubes with Nitrogen-Doped and Boron-Doped Multiwalls.* Journal of the American Chemical Society, 2005. **127**(25): p. 8956-8957.
21. Jensen, M.P., M.P. Mehn, and L. Que, *Intramolecular Aromatic Amination through Iron-Mediated Nitrene Transfer.* Angewandte Chemie, 2003. **115**(36): p. 4493-4496.
22. Ahmadpour, A. and D.D. Do, *The preparation of active carbons from coal by chemical and physical activation.* Carbon, 1996. **34**(4): p. 471-479.
23. Ryoo, R., S.H. Joo, and S. Jun, *Synthesis of Highly Ordered Carbon Molecular Sieves via Template-Mediated Structural Transformation.* The Journal of Physical Chemistry B, 1999. **103**(37): p. 7743-7746.
24. Kim, T.-W., P.-W. Chung, I.I. Slowing, M. Tsunoda, E.S. Yeung, and V.S.Y. Lin, *Structurally Ordered Mesoporous Carbon Nanoparticles as Transmembrane Delivery Vehicle in Human Cancer Cells.* Nano Letters, 2008. **8**(11): p. 3724-3727.
25. Liu, J., T. Yang, D.-W. Wang, G.Q. Lu, D. Zhao, and S.Z. Qiao, *A facile soft-template synthesis of mesoporous polymeric and carbonaceous nanospheres.* Nat Commun, 2013. **4**.
26. Wang, Y., X. Wang, M. Antonietti, and Y. Zhang, *Facile One-Pot Synthesis of Nanoporous Carbon Nitride Solids by Using Soft Templates.* ChemSusChem, 2010. **3**(4): p. 435-439.
27. Torad, N.L., M. Hu, Y. Kamachi, K. Takai, M. Imura, M. Naito, and Y. Yamauchi, *Facile synthesis of nanoporous carbons with controlled particle sizes by direct carbonization of monodispersed ZIF-8 crystals.* Chemical Communications, 2013. **49**(25): p. 2521-2523.
28. Khan, N.A., Z. Hasan, and S.H. Jhung, *Adsorptive removal of hazardous materials using metal-organic frameworks (MOFs): A review.* Journal of Hazardous Materials, 2013. **244–245**(0): p. 444-456.
29. Jhung, S.H., N.A. Khan, and Z. Hasan, *Analogous porous metal-organic frameworks: synthesis, stability and application in adsorption.* CrystEngComm, 2012. **14**(21): p. 7099-7109.

30. Khan, N.A. and S.H. Jhung, *Effect of central metal ions of analogous metal-organic frameworks on the adsorptive removal of benzothiophene from a model fuel*. Journal of Hazardous Materials, 2013. **260**(0): p. 1050-1056.
31. Khan, N.A., B.K. Jung, Z. Hasan, and S.H. Jhung, *Adsorption and removal of phthalic acid and diethyl phthalate from water with zeolitic imidazolate and metal–organic frameworks.* Journal of Hazardous Materials, 2015. **282**: p. 194-200.
32. Jiang, H.-L., B. Liu, Y.-Q. Lan, K. Kuratani, T. Akita, H. Shioyama, F. Zong, and Q. Xu, *From Metal–Organic Framework to Nanoporous Carbon: Toward a Very High Surface Area and Hydrogen Uptake.* Journal of the American Chemical Society, 2011. **133**(31): p. 11854-11857.
33. Chaikittisilp, W., K. Ariga, and Y. Yamauchi, *A new family of carbon materials: synthesis of MOF-derived nanoporous carbons and their promising applications.* Journal of Materials Chemistry A, 2013. **1**(1): p. 14-19.
34. Lin, S., Z. Song, G. Che, A. Ren, P. Li, C. Liu, and J. Zhang, *Adsorption behavior of metal–organic frameworks for methylene blue from aqueous solution.* Microporous and Mesoporous Materials, 2014. **193**: p. 27-34.
35. Shao, Y., L. Zhou, C. Bao, J. Ma, M. Liu, and F. Wang, *Magnetic responsive metal–organic frameworks nanosphere with core–shell structure for highly efficient removal of methylene blue.* Chemical Engineering Journal, 2016. **283**: p. 1127-1136.
36. Jiang, J.-Q., C.-X. Yang, and X.-P. Yan, *Zeolitic Imidazolate Framework-8 for Fast Adsorption and Removal of Benzotriazoles from Aqueous Solution.* ACS Applied Materials & Interfaces, 2013. **5**(19): p. 9837-9842.
37. Xiao, J.-D., L.-G. Qiu, X. Jiang, Y.-J. Zhu, S. Ye, and X. Jiang, *Magnetic porous carbons with high adsorption capacity synthesized by a microwave-enhanced high temperature ionothermal method from a Fe-based metal-organic framework.* Carbon, 2013. **59**: p. 372-382.
38. Jiao, C., Y. Wang, M. Li, Q. Wu, C. Wang, and Z. Wang, *Synthesis of magnetic nanoporous carbon from metal-organic framework for the fast removal of organic dye from aqueous solution.* Journal of Magnetism and Magnetic Materials, 2016. **407**: p. 24-30.
39. Bakhtiari, N., S. Azizian, S.M. Alshehri, N.L. Torad, V. Malgras, and Y. Yamauchi, *Study on adsorption of copper ion from aqueous solution by MOF-derived nanoporous carbon.* Microporous and Mesoporous Materials, 2015. **217**: p. 173-177.
40. Liu, B., H. Shioyama, T. Akita, and Q. Xu, *Metal-Organic Framework as a Template for Porous Carbon Synthesis.* Journal of the American Chemical Society, 2008. **130**(16): p. 5390-5391.
41. Zhang, P., F. Sun, Z. Xiang, Z. Shen, J. Yun, and D. Cao, *ZIF-derived in situ nitrogen-doped porous carbons as efficient metal-free electrocatalysts for oxygen reduction reaction.* Energy & Environmental Science, 2014. **7**(1): p. 442-450.
42. Kida, K., M. Okita, K. Fujita, S. Tanaka, and Y. Miyake, *Formation of high crystalline ZIF-8 in an aqueous solution.* CrystEngComm, 2013. **15**(9): p. 1794-1801.
43. Shi, Y., X. Zhang, L. Wang, and G. Liu, *MOF-derived porous carbon for adsorptive desulfurization.* AIChE Journal, 2014. **60**(8): p. 2747-2751.
44. Sen Gupta, S. and K.G. Bhattacharyya, *Kinetics of adsorption of metal ions on inorganic materials: A review.* Advances in Colloid and Interface Science, 2011. **162**(1–2): p. 39-58.
45. Zhong, H.-x., J. Wang, Y.-w. Zhang, W.-l. Xu, W. Xing, D. Xu, Y.-f. Zhang, and X.-b. Zhang, *ZIF-8 Derived Graphene-Based Nitrogen-Doped Porous Carbon Sheets as*

Highly Efficient and Durable Oxygen Reduction Electrocatalysts. Angewandte Chemie International Edition, 2014. **53**(51): p. 14235-14239.
46. Srinivas, G., V. Krungleviciute, Z.-X. Guo, and T. Yildirim, *Exceptional CO2 capture in a hierarchically porous carbon with simultaneous high surface area and pore volume.* Energy & Environmental Science, 2014. **7**(1): p. 335-342.
47. Wu, H.B., S. Wei, L. Zhang, R. Xu, H.H. Hng, and X.W. Lou, *Embedding Sulfur in MOF-Derived Microporous Carbon Polyhedrons for Lithium–Sulfur Batteries.* Chemistry – A European Journal, 2013. **19**(33): p. 10804-10808.
48. Almasoudi, A. and R. Mokaya, *Preparation and hydrogen storage capacity of templated and activated carbons nanocast from commercially available zeolitic imidazolate framework.* Journal of Materials Chemistry, 2012. **22**(1): p. 146-152.
49. Han, Y., P. Qi, S. Li, X. Feng, J. Zhou, H. Li, S. Su, X. Li, and B. Wang, *A novel anode material derived from organic-coated ZIF-8 nanocomposites with high performance in lithium ion batteries.* Chemical Communications, 2014. **50**(59): p. 8057-8060.
50. Tabrizi, N.S. and M. Yavari, *Methylene blue removal by carbon nanotube-based aerogels.* Chemical Engineering Research and Design, 2015. **94**: p. 516-523.
51. Zhang, T., L. Lin, X. Zhang, H. Liu, X. Yan, Z. Liu, and K.L. Yeung, *Facile preparation of ZIF-8@Pd-CSS sandwich-type microspheres via in situ growth of ZIF-8 shells over Pd-loaded colloidal carbon spheres with aggregation-resistant and leach-proof properties for the Pd nanoparticles.* Applied Surface Science, 2015. **351**: p. 1184-1190.
52. Biniak, S., G. Szymański, J. Siedlewski, and A. Świtkowski, *The characterization of activated carbons with oxygen and nitrogen surface groups.* Carbon, 1997. **35**(12): p. 1799-1810.
53. Liu, Y., X. Xu, M. Wang, T. Lu, Z. Sun, and L. Pan, *Metal-organic framework-derived porous carbon polyhedra for highly efficient capacitive deionization.* Chemical Communications, 2015. **51**(60): p. 12020-12023.
54. Dom, R., R. Subasri, N.Y. Hebalkar, A.S. Chary, and P.H. Borse, *Synthesis of a hydrogen producing nanocrystalline ZnFe2O4 visible light photocatalyst using a rapid microwave irradiation method.* RSC Advances, 2012. **2**(33): p. 12782-12791.
55. Deng, S., G. Yu, S. Xie, Q. Yu, J. Huang, Y. Kuwaki, and M. Iseki, *Enhanced Adsorption of Arsenate on the Aminated Fibers: Sorption Behavior and Uptake Mechanism.* Langmuir, 2008. **24**(19): p. 10961-10967.
56. Pels, J.R., F. Kapteijn, J.A. Moulijn, Q. Zhu, and K.M. Thomas, *Evolution of nitrogen functionalities in carbonaceous materials during pyrolysis.* Carbon, 1995. **33**(11): p. 1641-1653.
57. Okpalugo, T.I.T., P. Papakonstantinou, H. Murphy, J. McLaughlin, and N.M.D. Brown, *High resolution XPS characterization of chemical functionalised MWCNTs and SWCNTs.* Carbon, 2005. **43**(1): p. 153-161.
58. Titirici, M.M., A. Thomas, and M. Antonietti, *Replication and Coating of Silica Templates by Hydrothermal Carbonization.* Advanced Functional Materials, 2007. **17**(6): p. 1010-1018.
59. Wahab, R., S.G. Ansari, Y.S. Kim, H.K. Seo, G.S. Kim, G. Khang, and H.-S. Shin, *Low temperature solution synthesis and characterization of ZnO nano-flowers.* Materials Research Bulletin, 2007. **42**(9): p. 1640-1648.
60. Huang, H., J.-J. Lv, D.-L. Zhou, N. Bao, Y. Xu, A.-J. Wang, and J.-J. Feng, *One-pot green synthesis of nitrogen-doped carbon nanoparticles as fluorescent probes for mercury ions.* RSC Advances, 2013. **3**(44): p. 21691-21696.

61. Datsyuk, V., M. Kalyva, K. Papagelis, J. Parthenios, D. Tasis, A. Siokou, I. Kallitsis, and C. Galiotis, *Chemical oxidation of multiwalled carbon nanotubes.* Carbon, 2008. **46**(6): p. 833-840.
62. Gadipelli, S., W. Travis, W. Zhou, and Z. Guo, *A thermally derived and optimized structure from ZIF-8 with giant enhancement in CO2 uptake.* Energy & Environmental Science, 2014. **7**(7): p. 2232-2238.
63. Zhang, C., L. Fu, N. Liu, M. Liu, Y. Wang, and Z. Liu, *Synthesis of Nitrogen-Doped Graphene Using Embedded Carbon and Nitrogen Sources.* Advanced Materials, 2011. **23**(8): p. 1020-1024.
64. Burress, J.W., S. Gadipelli, J. Ford, J.M. Simmons, W. Zhou, and T. Yildirim, *Graphene Oxide Framework Materials: Theoretical Predictions and Experimental Results.* Angewandte Chemie International Edition, 2010. **49**(47): p. 8902-8904.
65. Tian, F., A.M. Cerro, A.M. Mosier, H.K. Wayment-Steele, R.S. Shine, A. Park, E.R. Webster, L.E. Johnson, M.S. Johal, and L. Benz, *Surface and Stability Characterization of a Nanoporous ZIF-8 Thin Film.* The Journal of Physical Chemistry C, 2014. **118**(26): p. 14449-14456.
66. Geng, D., Y. Chen, Y. Chen, Y. Li, R. Li, X. Sun, S. Ye, and S. Knights, *High oxygen-reduction activity and durability of nitrogen-doped graphene.* Energy & Environmental Science, 2011. **4**(3): p. 760-764.
67. Wang, Y., Y. Shao, D.W. Matson, J. Li, and Y. Lin, *Nitrogen-Doped Graphene and Its Application in Electrochemical Biosensing.* ACS Nano, 2010. **4**(4): p. 1790-1798.
68. Huang, J.-H., K.-L. Huang, S.-Q. Liu, A.T. Wang, and C. Yan, *Adsorption of Rhodamine B and methyl orange on a hypercrosslinked polymeric adsorbent in aqueous solution.* Colloids and Surfaces A: Physicochemical and Engineering Aspects, 2008. **330**(1): p. 55-61.
69. Goscianska, J., M. Marciniak, and R. Pietrzak, *Mesoporous carbons modified with lanthanum(III) chloride for methyl orange adsorption.* Chemical Engineering Journal, 2014. **247**: p. 258-264.
70. Lu, G., S. Li, Z. Guo, O.K. Farha, B.G. Hauser, X. Qi, Y. Wang, X. Wang, S. Han, X. Liu, J.S. DuChene, H. Zhang, Q. Zhang, X. Chen, J. Ma, S.C.J. Loo, W.D. Wei, Y. Yang, J.T. Hupp, and F. Huo, *Imparting functionality to a metal–organic framework material by controlled nanoparticle encapsulation.* Nat Chem, 2012. **4**(4): p. 310-316.
71. Banerjee, A., R. Gokhale, S. Bhatnagar, J. Jog, M. Bhardwaj, B. Lefez, B. Hannoyer, and S. Ogale, *MOF derived porous carbon-Fe3O4 nanocomposite as a high performance, recyclable environmental superadsorbent.* Journal of Materials Chemistry, 2012. **22**(37): p. 19694-19699.
72. Lee, H.J., S. Choi, and M. Oh, *Well-dispersed hollow porous carbon spheres synthesized by direct pyrolysis of core-shell type metal-organic frameworks and their sorption properties.* Chemical Communications, 2014. **50**(34): p. 4492-4495.
73. El-Shafey, E.I., S.N.F. Ali, S. Al-Busafi, and H.A.J. Al-Lawati, *Preparation and characterization of surface functionalized activated carbons from date palm leaflets and application for methylene blue removal.* Journal of Environmental Chemical Engineering, 2016. **4**(3): p. 2713-2724.
74. Yang, J. and K. Qiu, *Preparation of activated carbons from walnut shells via vacuum chemical activation and their application for methylene blue removal.* Chemical Engineering Journal, 2010. **165**(1): p. 209-217.
75. Deng, H., L. Yang, G. Tao, and J. Dai, *Preparation and characterization of activated carbon from cotton stalk by microwave assisted chemical activation—Application in*

methylene blue adsorption from aqueous solution. Journal of Hazardous Materials, 2009. **166**(2–3): p. 1514-1521.
76. Karagöz, S., T. Tay, S. Ucar, and M. Erdem, *Activated carbons from waste biomass by sulfuric acid activation and their use on methylene blue adsorption.* Bioresource Technology, 2008. **99**(14): p. 6214-6222.
77. Auta, M. and B.H. Hameed, *Optimized waste tea activated carbon for adsorption of Methylene Blue and Acid Blue 29 dyes using response surface methodology.* Chemical Engineering Journal, 2011. **175**: p. 233-243.
78. Dural, M.U., L. Cavas, S.K. Papageorgiou, and F.K. Katsaros, *Methylene blue adsorption on activated carbon prepared from Posidonia oceanica (L.) dead leaves: Kinetics and equilibrium studies.* Chemical Engineering Journal, 2011. **168**(1): p. 77-85.
79. Lorenc-Grabowska, E. and G. Gryglewicz, *Adsorption characteristics of Congo Red on coal-based mesoporous activated carbon.* Dyes and Pigments, 2007. **74**(1): p. 34-40.
80. Sun, D., X. Zhang, Y. Wu, and X. Liu, *Adsorption of anionic dyes from aqueous solution on fly ash.* Journal of Hazardous Materials, 2010. **181**(1–3): p. 335-342.
81. Özcan, A.S., B. Erdem, and A. Özcan, *Adsorption of Acid Blue 193 from aqueous solutions onto BTMA-bentonite.* Colloids and Surfaces A: Physicochemical and Engineering Aspects, 2005. **266**(1–3): p. 73-81.
82. Hall, K.R., L.C. Eagleton, A. Acrivos, and T. Vermeulen, *Pore- and Solid-Diffusion Kinetics in Fixed-Bed Adsorption under Constant-Pattern Conditions.* Industrial & Engineering Chemistry Fundamentals, 1966. **5**(2): p. 212-223.
83. Okolo, B., C. Park, and M.A. Keane, *Interaction of Phenol and Chlorophenols with Activated Carbon and Synthetic Zeolites in Aqueous Media.* Journal of Colloid and Interface Science, 2000. **226**(2): p. 308-317.
84. Ho, Y.S. and G. McKay, *Pseudo-second order model for sorption processes.* Process Biochemistry, 1999. **34**(5): p. 451-465.
85. Jalil, A.A., S. Triwahyono, S.H. Adam, N.D. Rahim, M.A.A. Aziz, N.H.H. Hairom, N.A.M. Razali, M.A.Z. Abidin, and M.K.A. Mohamadiah, *Adsorption of methyl orange from aqueous solution onto calcined Lapindo volcanic mud.* Journal of Hazardous Materials, 2010. **181**(1–3): p. 755-762.
86. Ho, Y.S. and G. McKay, *The kinetics of sorption of basic dyes from aqueous solution by sphagnum moss peat.* The Canadian Journal of Chemical Engineering, 1998. **76**(4): p. 822-827.
87. Boyd, G.E., A.W. Adamson, and L.S. Myers, *The Exchange Adsorption of Ions from Aqueous Solutions by Organic Zeolites. II. Kinetics1*. Journal of the American Chemical Society, 1947. **69**(11): p. 2836-2848.
88. Reichenberg, D., *Properties of Ion-Exchange Resins in Relation to their Structure. III. Kinetics of Exchange.* Journal of the American Chemical Society, 1953. **75**(3): p. 589-597.
89. Vadivelan, V. and K.V. Kumar, *Equilibrium, kinetics, mechanism, and process design for the sorption of methylene blue onto rice husk.* Journal of Colloid and Interface Science, 2005. **286**(1): p. 90-100.
90. Iqbal, M.J. and M.N. Ashiq, *Adsorption of dyes from aqueous solutions on activated charcoal.* Journal of Hazardous Materials, 2007. **139**(1): p. 57-66.
91. Ramakrishna, K.R. and T. Viraraghavan, *Use of slag for dye removal.* Waste Management, 1998. **17**(8): p. 483-488.

92. Yagub, M.T., T.K. Sen, S. Afroze, and H.M. Ang, *Dye and its removal from aqueous solution by adsorption: A review.* Advances in Colloid and Interface Science, 2014. **209**: p. 172-184.
93. Zadaka, D., A. Radian, and Y.G. Mishael, *Applying zeta potential measurements to characterize the adsorption on montmorillonite of organic cations as monomers, micelles, or polymers.* Journal of Colloid and Interface Science, 2010. **352**(1): p. 171-177.
94. Senthilkumaar, S., P.R. Varadarajan, K. Porkodi, and C.V. Subbhuraam, *Adsorption of methylene blue onto jute fiber carbon: kinetics and equilibrium studies.* Journal of Colloid and Interface Science, 2005. **284**(1): p. 78-82.
95. Hameed, B.H. and M.I. El-Khaiary, *Equilibrium, kinetics and mechanism of malachite green adsorption on activated carbon prepared from bamboo by K2CO3 activation and subsequent gasification with CO2.* Journal of Hazardous Materials, 2008. **157**(2–3): p. 344-351.
96. Wang, P., M. Cao, C. Wang, Y. Ao, J. Hou, and J. Qian, *Kinetics and thermodynamics of adsorption of methylene blue by a magnetic graphene-carbon nanotube composite.* Applied Surface Science, 2014. **290**: p. 116-124.
97. Alkan, M., Ö. Demirbaş, and M. Doğan, *Adsorption kinetics and thermodynamics of an anionic dye onto sepiolite.* Microporous and Mesoporous Materials, 2007. **101**(3): p. 388-396.
98. James, J.B. and Y.S. Lin, *Kinetics of ZIF-8 Thermal Decomposition in Inert, Oxidizing, and Reducing Environments.* The Journal of Physical Chemistry C, 2016. **120**(26): p. 14015-14026.
99. Fox, D.M., J.W. Gilman, H.C. De Long, and P.C. Trulove, *TGA decomposition kinetics of 1-butyl-2,3-dimethylimidazolium tetrafluoroborate and the thermal effects of contaminants.* The Journal of Chemical Thermodynamics, 2005. **37**(9): p. 900-905.
100. Hadjiantoniou-Maroulis, C.P., A.P. Charalambopoulos, and A.J. Maroulis, *Pyrolysis and photolysis of 1-aroylamino-4,5-diaryl-1,2,3-triazoles: Generation and thermal transformations of 4,5-diaryl-1,2,3-triazolyl radicals.* Journal of Heterocyclic Chemistry, 1998. **35**(4): p. 891-894.
101. Anniyappan, M., S.H. Sonawane, S.J. Pawar, and A.K. Sikder, *Thermal decomposition and kinetics of 2,4-dinitroimidazole: An insensitive high explosive.* Thermochimica Acta, 2015. **614**: p. 93-99.

Chapter 5. Investigation of adsorption properties of iron loaded ZIF-8 derived nanoporous carbons modified by re-carbonization for water treatment

5.1. Overview

In previous chapter, a systematic and comprehensive investigation on the adsorption property of carbonized ZIF-8 materials was done. In this chapter the effect of carbonization temperature on the characteristics and the performances of ZIF-8 derived nanoporous carbons impregnated by iron nanoparticles is reported. For incorporating iron particles, the wet impregnation method was employed and the nominal iron loading was 14%. The magnetic samples were further carbonized at 600 and 1000 ºC. Interestingly, the results showed the magnetic nanoporous carbons carbonized at 1000 ºC exhibited similar adsorption capacity to the original ZIF-8 derived nanoporous carbons. Although the surface area reduced after loading iron on the samples but the reduction of iron species to zero valent iron at high temperature, resulted in better adsorption capability of the magnetic adsorbent. The mechanism of the interaction between iron species with dye molecules was explained. Different characterization

techniques were utilized to address adsorption characteristics and performance for the magnetic nanoporous carbons. The results from XRD confirmed the presence of iron oxides and reduced metallic iron at 600 and 1000 ˚C, respectively. SEM results showed that iron nanoparticles were well distributed in the matrices of the magnetic carbons with nanosized particles in the range of 10 to 100 nm. The Fe/CZIF1000 showed high adsorption capacity and excellent magnetic performance which confirms the suitability of this material for adsorption of pollutants form water.

This chapter has been formatted from the following submitted manuscript:

Z.Abbasi, B. Ladewig, H. Wang, Investigation of adsorption properties of iron loaded ZIF-8 derived nanoporous carbons modified by re-carbonization for water treatment. *Asia Pac. J. Chem. Eng.* 2017 (Submitted).

5.2. Introduction

The dyes discharged from industry have become a source of environmental pollution as they severely affect human life, aquatic animals and life cycle [1]. Adsorption is a very efficient and simple approach for the elimination of dyes from water. Therefore, a variety of adsorbents have been investigated regarding dye removal including the carbon materials. Among the carbon materials, nanoporous carbons are greatly interesting because of the robust porous networks as well as the advantageous features in terms of being environmental friendly and chemically stable against acidic and basic conditions [2, 3]. Metal organic frameworks (MOFs) are interesting porous crystalline materials made from metal ions and organic ligands. MOFs are specifically attractive due to their unique and special features such as high surface area, high porosity, controlled pore size and potential applications in gas storage, catalysis and adsorption [4, 5]. Zeolitic immidazolate frameworks (ZIFs) are a branch of MOFs that exhibit many

interesting properties like porous frameworks and high surface areas. ZIF-8 is one of the most popular ZIFs, with a molecular formula of Zn(2-methylimidazolate)$_2$ which has the large pores of 1.14 nm size and the accessible aperture size of 0.34 nm [6].

Regarding the special characteristics of MOFs such as large carbon content and highly porous framework, these materials have been considered for the production of nanoporous carbons. The carbons derived from MOF materials have also more interesting properties like porosity and chemical stability which made them on the focus of the researchers for a wide range of applications similar to MOFs' applications in particular adsorption of pollutants from water [7, 8].

However, although nanoporous carbons derived from MOF materials show good adsorption properties and performances, it is difficult to separate them from water. Thus, this issue limits their applications in water treatment. Incorporation of magnetic particles into these nanaoporous frameworks, can broaden the areas of their application especially in adsorption since magnetic property makes the separation of the nanoporous carbon particles from aqueous solution much easier [9]. Different methods have been utilized for generating magnetic nanoporous carbons including template carbonization [8, 10], hydrothermal methods [9] and heat treatment of organometallic materials [11]. Wet impregnation is a simple, inexpensive and effective method for introducing different functionalities into materials for the applications such as catalysis and adsorption [12]. Utilization of this technique along with the usage of low-cost adsorbents and catalysts has been in the focus of many studies to produce more efficient composite materials with magnetic properties for easy separations from water [13, 14]. Activated carbon [15, 16] and other kinds of porous carbons [17-20] have been impregnated by iron particles for adsorption of organic pollutants form water and have shown high performance as well as high magnetic response. However, the magnetic nanoporous carbons derived from

metal organic framework and their adsorption properties have not been investigated using a simple technique such as wet impregnation. Other methods for introducing magnetic functionality into the porous frameworks and carbons usually include several steps, requires dangerous chemicals and high temperatures or are very time consuming and complicated [21-26]. For example, magnetic nanoparticles were synthesized using a very complex procedure [27] using sodium hydroxide and diethylene glycol solution by heating at 120 ºC under nitrogen atmosphere along with preparing a mixture of PAA, $FeCl_3$ and DEG heated to 220 ºC under nitrogen flow. The mixture of the chemicals including sodium hydroxide in a high temperature environment is very dangerous and it requires special equipment which resists harsh basic and hot conditions. The usage of nitrogen flow in all of the synthesis steps (mixing, heating, etc.) also makes this procedure very difficult and complicated. This method was utilized to produce nano particles in the range of 30-180 nm. In another method, carbon encapsulated iron nanoparticles with core-shell structure was synthesized with detonation decomposition of explosive compound consisting iron components [28, 29]. This method also requires a complicated facility and it is not a preferred method especially in terms of safety considerations while it does not have any advantage in controlling the resulting magnetic carbon structure [30].

The wet impregnation method is an efficient, safe, environmentally friendly and uncomplicated technique which can be utilized for introducing functionalities such as magnetic iron particles into the framework of the materials. In this study, we report enhanced loading of ZIF-8 derived nanoporous carbons by iron nanoparticles using wet impregnation approach. The obtained impregnated carbons had good adsorption capacity and excellent magnetic property because of the presence of iron nanoparticles well distributed in the carbon framework. The iron nanoparticles were produced in the range of 10 nm to 100 nm similar to what was reported

in literature using a complicated technique and harsh conditions. However, the approach we introduced is very straightforward and environmentally friendly.

5.3. Materials and Methods

5.3.1. Materials

Iron nitrate nonahydrate (Fe $(NO_3)_3.9H_2O$), Zinc nitrate hexahydrate ($Zn(NO_3)_2.6H_2O$) and 2-methylimidazole (Hmim) (99%) were purchased from Sigma Aldrich. Methylene blue (MB), NaOH and HCl were purchased from Merck. All chemicals were used as received without any purification.

ZIF-8 was synthesized by the method reported by Koji Kida et al. [31] in aqueous solution. Briefly, 0.744 g (2.5 mmol) of $Zn(NO_3).6H_2O$ and 12.3 g (0.15 mol) of Hmim were dissolved in 10 ml and 90 ml of deionized water respectively. After mixing for 24 hours, ZIF-8 nanocrystals were collected by washing with deionized water and centrifuging (8000 rpm, 30 min) for three times and then dried at 70℃ overnight. The synthesized ZIF-8 powder was directly carbonized at 600 and 1000℃ under argon atmosphere. The temperatures increased from room temperature to the target temperatures with a heating rate of 5℃/min. The powders were carbonized at the target temperatures for 6 hours. The obtained nanoporous carbons were denoted as CZIFs and as CZIF600 and CZIF1000.

The magnetic carbons were produced by a wet impregnation method [32] by combining nanoporous carbons CZIF600 and CZIF1000 and a solution of iron nitrate nonahydrate with nominal iron loading of 14% (weight percent). The mixtures were stirred for 2 hours and the resulting materials were collected by centrifugation, washed by water several times and dried at 70 ºC overnight. The dried samples were further re-carbonized at 600 and 1000 ºC in argon atmosphere in a tube furnace for 6 h. The products were denoted as Fe/CZIF600 and

Fe/CZIF1000. The obtained magnetic samples were directly used for characterization and adsorption experiments.

5.3.2. Characterization

Nitrogen adsorption and desorption isotherms were measured at liquid nitrogen temperature (77 K) using an accelerated surface area and porosimetry system (ASAP 2020, Micromeritics, USA) for surface area measurements. The crystal structures of the samples were identified using an X-ray diffractometer (Miniflex 600, Rigaku) with Cu Kα radiation at 40 kV and 20 mA over the 2θ range of 2-100°. The morphology of the magnetic samples was observed using a scanning electron microscope (JEOL 7001F FEG SEM). Thermogravimetric analysis (TGA) was performed on a SETARAM (TGA 92) device from 30 to 1000℃ at a heating rate of 10℃/min under Ar flow. The zeta potentials of the samples were determined using a Zetasizer Nano (Malvern) at the pH ranging from 1 to 11. The powders were dispersed by sonication in water with the concentration of 0.5mg/10ml and the dispersion was used for zeta potential measurement. The concentration of methylene blue was measured using a UV-vis spectrophotometer (UVmini-1240, Shimadzu) at the wavelength of 665 which corresponds to the maximum adsorption of the methylene blue dye.

5.3.3. Adsorption experiments

Adsorption for the samples was carried out in batch experiments. The adsorption capacity was evaluated by adsorption of an organic cationic dye methylene blue (MB) in aqueous solution. An aqueous stock solution of MB ($C_{16}H_{18}N_3SCl$, MW: 319.85), with 1000 ppm concentration was prepared and the desired concentration of dye was made by successive dilution of the stock solution. The mixture of dye solutions and the adsorbents were stirred for 24 hours at room temperature (22℃).

After adsorption for a specific time, the solutions were separated from the adsorbents with a syringe filter (Nylon, hydrophobic, 0.45 μm). The adsorption experiments were done at the natural pH of the solution i.e. 5.5 without any pH adjustment. The pH of the solution was adjusted using 0.1 M HCl and 0.1 M NaOH to determine the pH effect on the adsorption performance.

5.4. Results and Discussions

5.4.1. Characterization of magnetic nanoporous carbon particles

The crystal phase of the synthesized magnetic carbons was defined by X-ray diffraction (XRD) analysis and the XRD patterns are shown in Fig. 5-1. The XRD analysis shows the presence of iron oxide and metallic iron phase for Fe/CZIF600 and Fe/CZIF1000, respectively.

In the XRD patterns of Fe/CZIF 600, the peaks related to ZnO can be observed while there is no diffraction peaks of zinc in Fe/CZIF 1000 sample which is due to the reduction of ZnO by carbon and evaporation of zinc particles at 908 ºC (boiling point of zinc).

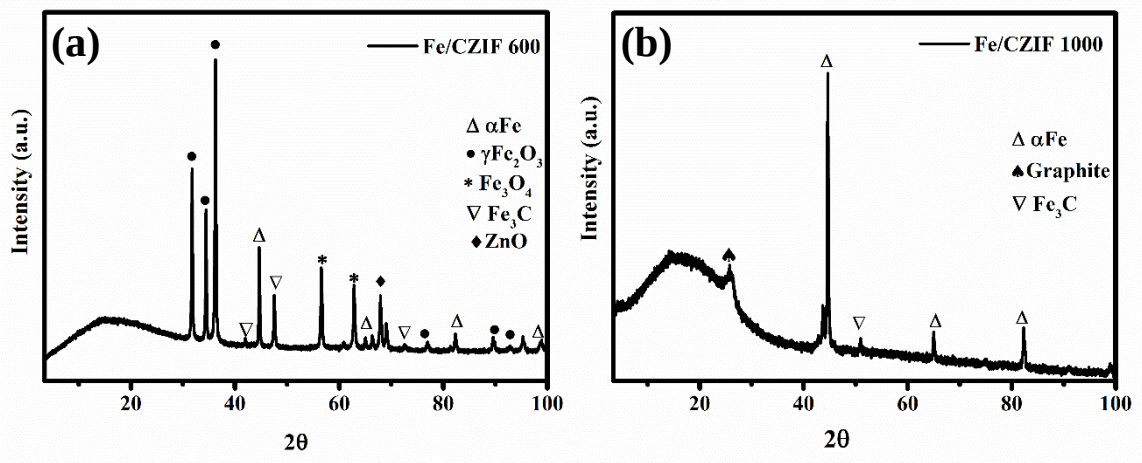

Fig. 5-1 XRD patterns of magnetic ZIF-8 nanoporous carbons: (a) Fe/CZIF 600 and (b) Fe/CZIF 1000

The crystallinity and phase composition of iron loaded nanoporous carbons changes with increasing the carbonization temperature. Xu et al. [33] reported magnetic and oxidization state of iron loaded on carbon nanofibers for electrochemical performance. It was reported that at carbonization temperature of 400 ºC, the XRD peaks are related to standard card of Fe_2O_3 while at higher temperatures Fe_3O_4 was formed. At temperatures of above 800 ºC, Fe_3O_4 is reduced to FeO and at 1000 ºC, the carbothermal reduction is more severe and iron oxide is reduced to Fe along with the formation of Fe_3C. Hu et al. [34] also indicated that during carbothermal reduction at temperatures above 500 ºC, the product has pure Fe_3O_4 phase while at temperatures lower than 500 ºC, Fe_2O_3 impurity phase can be observed. However, in this study, in the XRD patterns of magnetic carbon particles at 600 ºC, we observed more Fe_2O_3 phase at 600 ºC than Fe_3O_4 phase, which agrees with some other results published in literature [35]. The XRD pattern of Fe/CZIF600 revealed that γ-Fe_2O_3, α-Fe and Fe_3O_4 were the main products and the remaining contained the small portions of iron carbide (Fe_3C) and ZnO. As temperature increased to above 600 ˚C, the γ-Fe_2O_3 is transformed to Fe_3C and once the temperature raised to 1000 ˚C, the magnetic products (γ-Fe_2O_3 and Fe_3C) were converted to α-Fe as shown in Fig. 5-1. The diffraction peaks for the magnetic products matched with the reported values as for γ-Fe_2O_3 (JCPDS No. 39-1346) [36], Fe_3C (JCPDS No. 35-0772) [37] and α-Fe (JCPDS No. 06-0696) [37]. The peaks related to reduced zero valent iron (Fe^0) at 1000 ºC, can be observed mainly at 2Θ=45, 65 and 82º along with three small peaks at 50, 76 and 92 [38]. The XRD patterns are consistent with results from literature [32]. The XRD results confirm the formation of iron phases in the composite material and supports their magnetic behaviour. To understand the morphology of the samples and to investigate the dispersion of the iron particles within the nanoporous carbons matrices, the samples were further analysed by scanning electron microscopy (SEM).

Fig. 5-2 shows the SEM and elemental mapping of the iron loaded carbon samples.

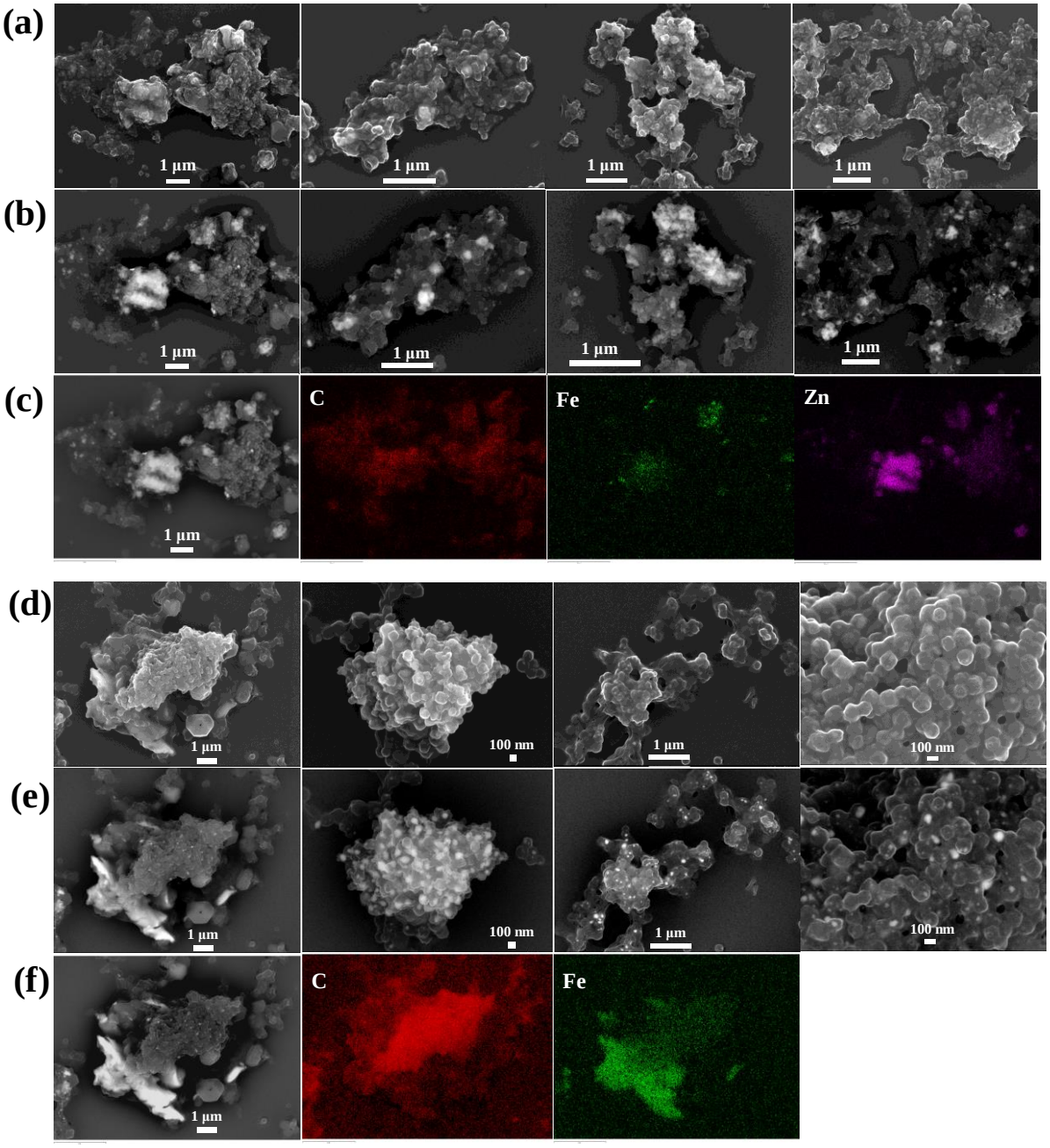

Fig. 5-2 SEM images in original and high contrast modes and C, Fe, Zn elemental maps of (a, b, c) Fe/CZIF 600 and (d, e, f) Fe/CZIF 1000

The SEM images are presented in two sets of original images and their corresponding high contrast mode images in order to clearly see the distribution of iron nanoparticles. The shiny dots in the high contrast SEM images are representative of iron nanoparticles. The images

reveal that the iron nanoparticles are well distributed in the nanoporous carbons but the particles have different sizes from roughly 10 nm to 100 nm. The iron particles can be seen shiny in the whole SEM image due to the higher atomic number of iron particles compared with carbon. For the sample Fe/CZIF 600 because of the presence of zinc particles, the shiny dots might be related to zinc as well. However, for Fe/CZIF 1000 the shiny dots are only assigned to the iron particles and zinc particles were not observed in elemental mapping because of evaporation of zinc particles at 1000 ºC as mentioned previously. These observations are in accordance with XRD results. The iron nanoparticles in sample treated at higher temperature (Fe/CZIF1000) are smaller than the nanoparticles on Fe/CZIF600 which could be due to effect of high temperature on the reduction of iron oxides (formed at 600 ˚C) to metallic iron Fe^0 (formed at 1000 ˚C).

The surface areas of the magnetic and nanoporous carbons were determined by N_2 adsorption-desorption isotherms as shown in Fig. 5-3 and Fig. 5-4 (a). The surface areas of Fe/CZIF1000 and Fe/CZIF600 are compared with those of the original nanoporous carbons. The figures show that samples exhibited Type I isotherms with sharp nitrogen consumption at low pressure ($P/P_0 < 0.05$) and small uptake and high pressure ($P/P_0 > 0.9$) addressing microporous frameworks with some macropores formed between particles (inter particle voids) [39]. Therefore, the iron loaded nanoporous carbons still show microporous frameworks with rather high surface areas. The Brunauer, Emmet and Teller (BET) surface areas and pore volumes are presented in Table 5-1 as it is shown in the table, after loading iron nanoparticles the surface area and the micro pore volume of the magnetic samples decreased which shows the iron particles are mostly coated inside the micro pores which is desirable in terms of adsorption applications.

Table 5-1 Surface area analysis parameters of magnetic and original nanoporous carbons

Sample	BET surface area (m^2/g)	Langmuir surface area (m^2/g)	Total pore volume[a] (Cm^3/g)	Micropore volume (Cm^3/g)
CZIF1000	1043.1±17.6	1305±12.5	0.98	0.4
Fe/CZIF 1000	571.9±7.9	673.4±11.4	0.87	0.15
CZIF 600	625.5±12.4	811.9±3.65	0.67	0.26
Fe/CZIF 600	356.6±5.6	437.5±4.4	0.67	0.11

[a] At P/P0=0.99

The reduction in micropore volume can be observed from the pore size distributions (Fig. 5-3 and Fig. 5-4 (b)). The pore size distributions show an increase in the intensity and number of pores with 1.2 nm for the magnetic samples. In addition, the pore size curves became broader after loading iron particles and heat treatment. It is shown that Fe/CZIF1000 has a broader range of pores from 2.5 to 10 nm in comparison with CZIF1000. Furthermore, the pore size distribution of Fe/CZIF600 has developed and broadened in the range of 1.5 to 4 nm. Therefore, it seems that after iron loading and carbothermal reduction some pores are developed to the meso pore range. Zhu et al. [40] reported the synthesis of magnetic carbon composites using hydrochar as the carbon content for the removal of organic pollutants from water. Their study showed that the reduction reactions (Eq. (1) and (2)) of iron oxide could improve the development of pores in magnetic carbon composites. It was reported that the formation of reduced Fe helped for further pore development.

$$2Fe_2O_3 + 3C \rightarrow 4Fe + 3CO_2 \qquad T \geq 500℃ \qquad (1)$$

$$Fe_3O_4 + 4C \rightarrow 3Fe + 4CO \qquad T \geq 500℃ \qquad (2)$$

The slight increase of the pore size and pore development in the magnetic sample could be a reason for high adsorption capacity of Fe/CZIF1000 even after loading magnetic particles and a decrease in the surface area and micropore volume.

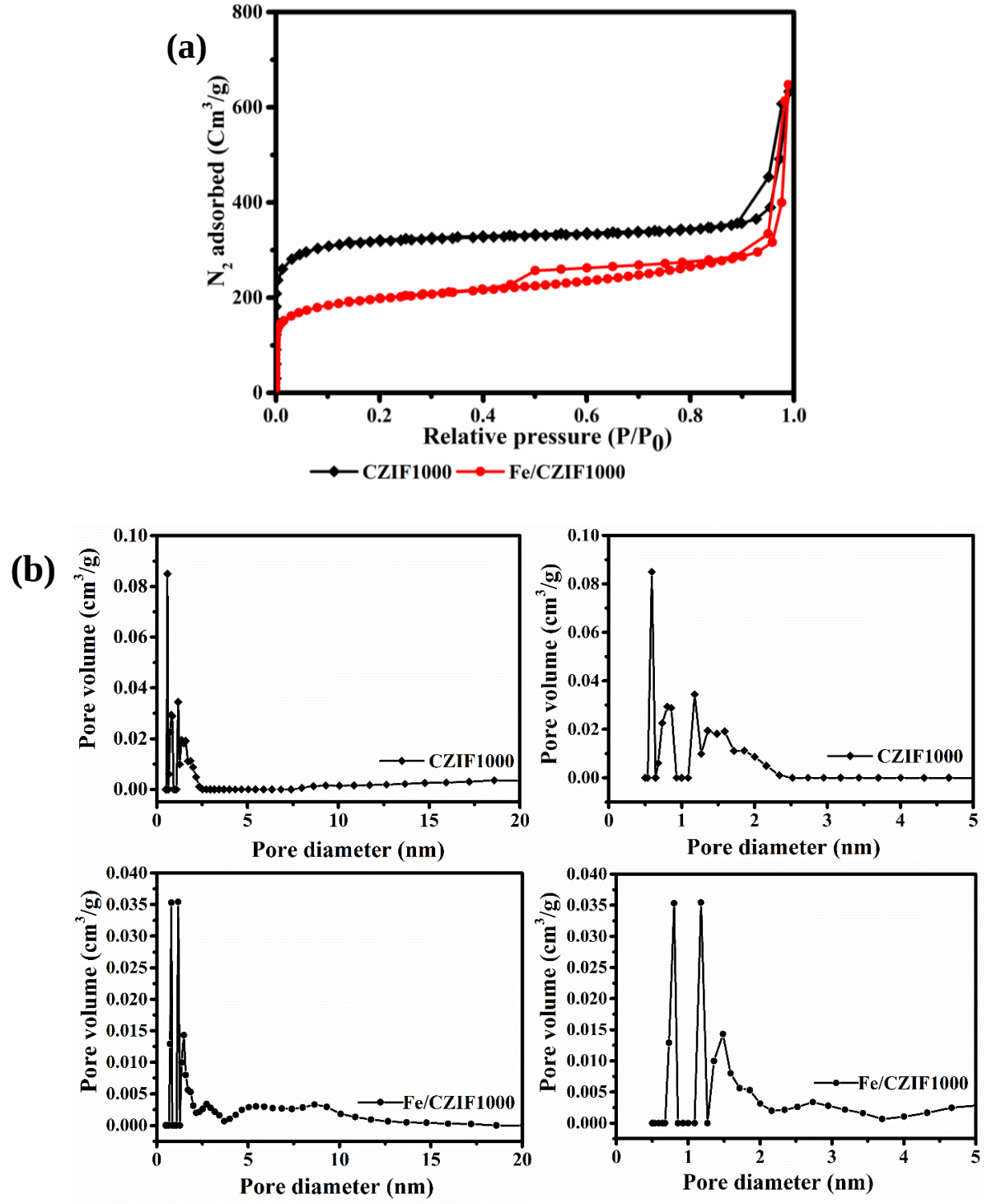

Fig. 5-3 Nitrogen adsorption-desorption isotherms of Fe/CZIF1000 compared with CZIF1000 (a) and the corresponding pore size distributions (b)

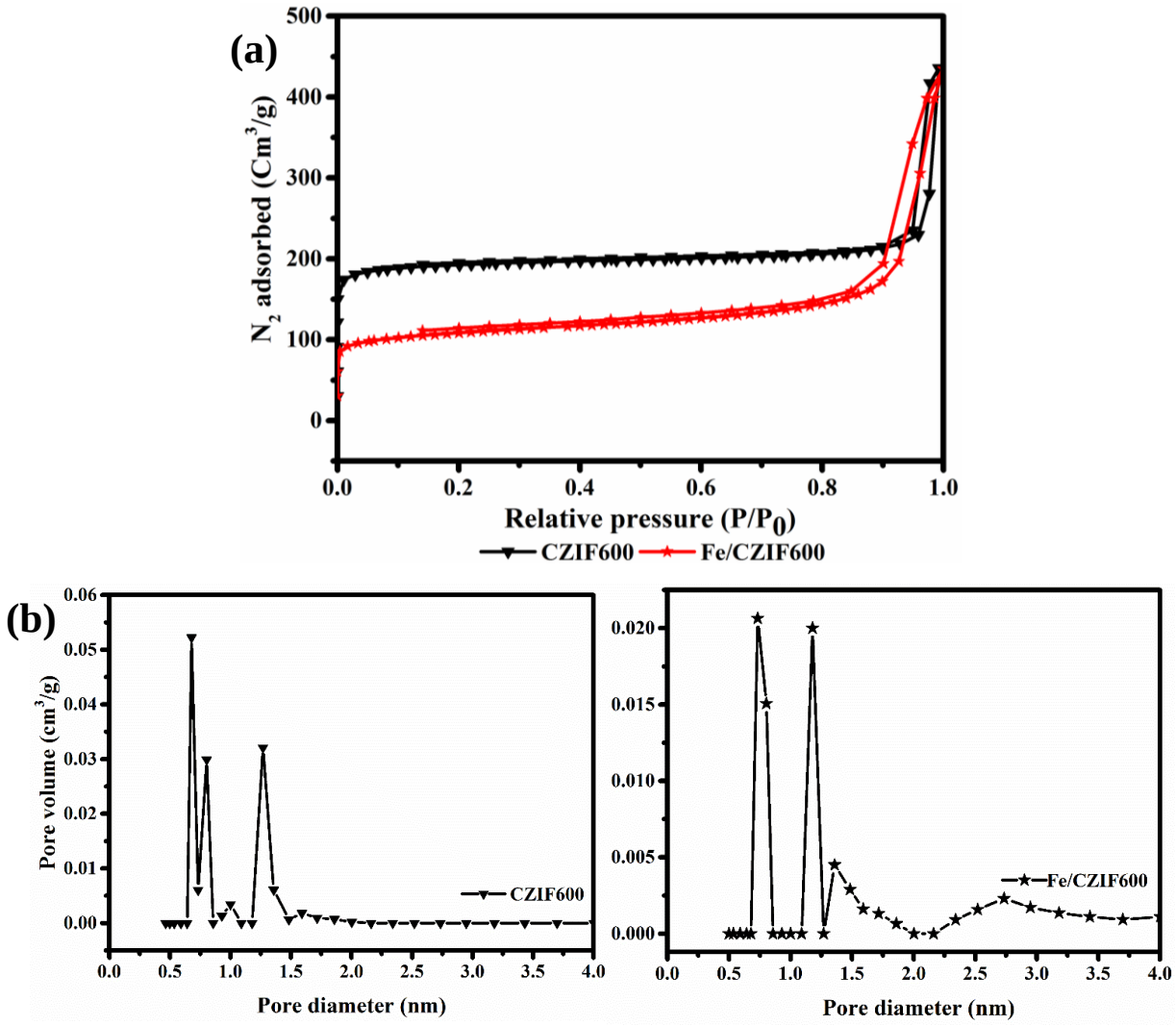

Fig. 5-4 Nitrogen adsorption-desorption isotherms of Fe/CZIF600 compared with CZIF600 (a) and the corresponding pore size distributions (b)

TGA analysis of the magnetic and non-magnetic samples are shown in TGA graphs in Fig. 5-5 (a) and (b). For the magnetic samples the mass loss behaviour is different from non-magnetic nanoporous carbons. It can be seen that for Fe/CZIF1000 there is very little mass loss from 25 to around 400 ˚C. Then from 450 to 650 ˚C there is a sharp decrease and the mass loss continues until 1000 ˚C. The mass losses can be attributed to the carbothermal reduction between carbon particles and Fe_3O_4 and production of reduced Fe_3C and Fe^0 [41]. The mass loss between 450 and 650 ˚C is related to the reduction of Fe_2O_3 to Fe_3O_4 and FeO and the maximum decomposition occurs at 650 ˚C and continues to 1000 ˚C which is assigned to the

reduction of FeO to Fe [42-44]. While for the TGA curve of CZIF1000, at the temperature below 150℃, the mass loss is due to evaporation of adsorbed water molecules in the pores of the materials. Between 400 and 600℃, the mass loss could be due to the framework decomposition which results in carbon formation. The mass loss from 900℃ onwards, could be attributed to the reduction of Zn by carbon and evaporation [45]. For Fe/CZIF600, the reduction in mass loss follows the similar trend of CZIF 600, except slightly different behaviour at temperature range of 100 to 650 ºC which could be due to the conversion of iron hydroxides to Fe_2O_3 at temperatures below 400 ºC and small reduction of iron at temperatures between 500 and 650 ºC. The rest of the mass loss in the whole range of temperature is attributed to the framework decomposition and zinc evaporation as mentioned before.

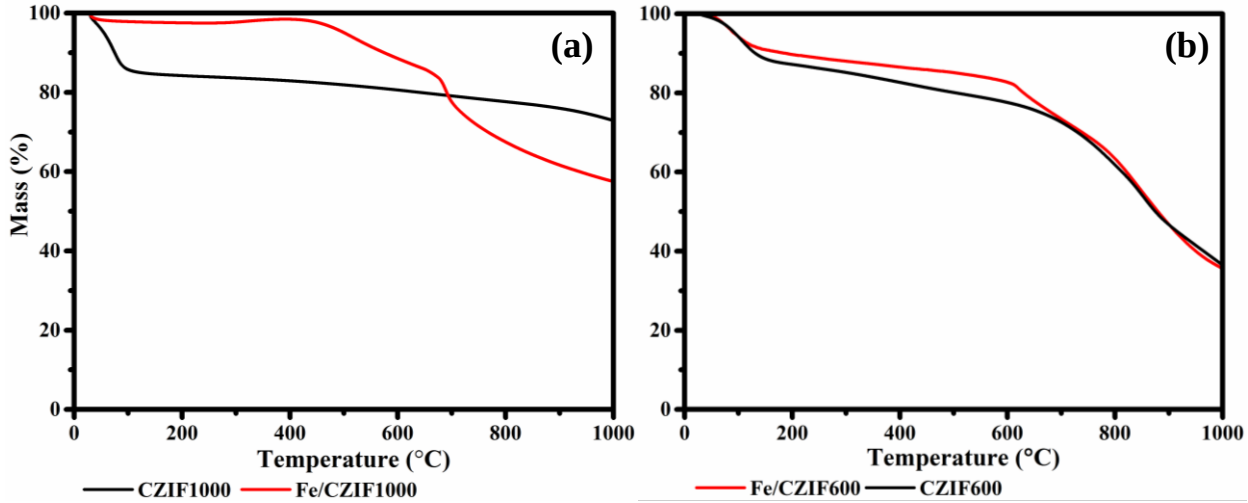

Fig. 5-5 TGA analysis of CZIF1000 and Fe/CZIF1000 (a), CZIF600 and Fe/CZIF600 (b)

For producing magnetic Fe/CZIF1000, the CZIF1000 was used as the precursor and it was already underwent the heat treatment. Therefore, in the TGA graph of the Fe/CZIF1000, the mass loss cannot be due to the framework decomposition or the evaporation of zinc particles and it could be only due to the carbothermal reduction of iron species in the inert environment.

5.4.2. Adsorption study for the removal of Methylene Blue (MB) dye

The magnetic nanoporous carbons were tested for the removal of MB dye from water to compare their adsorption capabilities with those of original nanoporous carbons. Fig. 5-6 exhibits the magnetic property of Fe/CZIF 1000 after adsorption of methylene blue dye form water. Fe/CZIF 600 did not show good adsorption performance (not shown in the graphs) which indicates even the slight pore development as shown in N_2 adsorption-desorption graphs, could not improve the low adsorption capacity of CZIF600. Considering the fact that pore development as a result of iron loading and carbonization occurred in both Fe/CZIF600 and Fe/CZIF1000, the reason for exhibiting low adsorption capacity for Fe/CZIF600 might be due to the lack of reduced iron particles on this sample as a result of low carbonization temperature (600 ºC).

Fe/CZIF 1000 showed excellent magnetic performance as well as high adsorption capacity which indicates that iron loaded nanoporous carbon CZIF 1000 is a suitable adsorbent for the removal of pollutants from water. These observations also confirm that loading magnetic nanoparticles do not have any adverse effect on the adsorption property of Fe/CZIF 1000 for the removal of MB dye form water, although the iron nanoparticles reduced the surface area and pore volume of the nanoporous carbons. Interestingly, the adsorption capacity of magnetic nanoporous carbons is equal to the original nanoporous carbon CZIF1000 (as compared in Fig. 5-6). This behaviour can be explained based on the presence of reduced iron in magnetic nanoporous carbon.

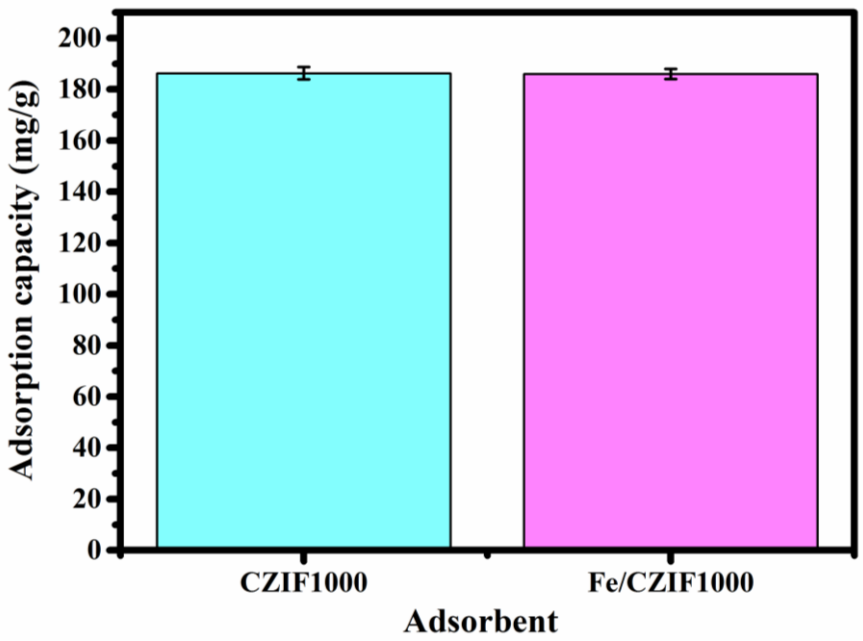

Fig. 5-6 Adsorption capacity of CZIF1000 and Fe/CZIF1000 for MB removal (initial dye concentration 100 ppm, adsorbent dosage 10 mg, solution volume 20 ml, initial pH=5.5)

The methylene blue removal by magnetic nanoporous carbon could be due to electrostatic interaction of MB dye molecules and magnetic nanoporous carbon particles in addition to the interaction between reduced iron nanoparticles and MB dye. Fan et al. [46] and Sohn et al. [47] proposed that decolorization of dyes proceeds through the reaction between Fe and H_2O or H^+. Atomic hydrogen is generated via this reaction which can destroy the chromophore group of dyes [46]. Moreover, in this reaction the intermediate products such as Fe^{2+}, Fe^{3+} and iron hydroxide complexes are produced which are thermodynamically unstable and active [47]. Additionally, the passive iron oxide shells which include Fe_2O_3, Fe_3O_4 and FeOOH on the surface on iron nanoparticles could adsorb dye molecules from water [48].

In our case, although the surface area and micropore volume decreased after iron loading, the reason for high adsorption capacity could be attributed to the presence of reduced iron nanoparticles at 1000 ºC.

It is worth mentioning that during the heat treatment, the transformation of iron species is controlled by the following equations. First Fe^{3+} ions are hydrolysed to iron hydroxides ($Fe(OH)_3$ and $FeO(OH)$ below 350 ºC. The iron hydroxides are converted to Fe_2O_3 below 400 ºC. As temperature increases to above 500 ºC, Fe_2O_3 could be reduced to Fe_3O_4 by the reducing agent (amorphous carbon). Finally, Fe_2O_3 and Fe_3O_4 could be further reduced by carbon which leads to the production of metallic iron [32, 49].

$$Fe^{3+} + 3H_2O \rightarrow Fe(OH)3 \quad + 3H^+ \qquad T \leq 350\ ℃ \qquad (3)$$

$$Fe(OH)_3 \rightarrow FeO(OH) \rightarrow Fe_2O_3 \qquad T \leq 400\ ℃ \qquad (4)$$

$$3Fe_2O_3 + C \rightarrow \ 2Fe_3O_4 \ + CO(CO_2) \qquad T \geq 500\ ℃ \qquad (5)$$

$$2Fe_2O_3 + 3C \rightarrow 4Fe + 3CO_2 \qquad T \geq 500℃ \qquad (6)$$

$$Fe_3O_4 + 4C \rightarrow 3Fe + 4CO \qquad T \geq 500℃ \qquad (7)$$

Iron nanoparticles have adsorption capacities for the removal of pollutants from water. Carbonization of carbon supported iron oxides is an inexpensive technique to introduce magnetic property into nanoporous carbons and at the same time produce reduced iron nanoparticles which have adsorption capabilities toward different pollutants.

Methylene blue is a cationic thiazine dye and has the chemical name of tetramethylthionine chloride. When methylene blue is in the oxidized form, it has a deep blue colour while in the reduced state (leukomethylene blue (LMB)) it is colorless [50]. This dye molecule has been extensively employed in environmental studies to determine whether adsorbent materials are suitable for dye removal from water and waste water [51-53]. Noubactep [50] indicated that the removal of MB by iron species occurs via the Eq. (8-12):

$$Fe^{2+} + 2e^- \leftrightarrow Fe^0 \quad (8)$$

$$Fe^{3+}_{(s)} + e^- \leftrightarrow Fe^{2+}_{(s)} \quad (9)$$

$$MB^+ + 2e^- + H^+ \leftrightarrow LMB \quad (10)$$

$$Fe^{3+}_{(aq)} + e^- \leftrightarrow Fe^{2+}_{(aq)} \quad (11)$$

$$O_{2(aq)} + 2H_2O + 4e^- \leftrightarrow 4OH^- \quad (12)$$

During the Fe^0 (zero valent iron) oxidation, the dissolved iron species are released as Fe^{II} and Fe^{III} which undergo hydrolysis with the increase in pH and precipitate as hydrous oxides or corrosion products [54]. Thus, a Fe^0/H_2O treatment system consists of Fe^0, iron oxides and water [55]. The reduction of adsorbed or co-precipitated pollutants can proceed through direct or indirect reduction. In direct reduction, electrons are transferred from Fe^0 while in indirect reduction the electron come from Fe^{II} and H/H_2. The co-precipitation occurs when iron oxides precipitate in the presence of pollutant molecules such as organic compounds [50].

It was reported that the removal efficiency of the adsorbents was: "Fe^0 + activated carbon (physically mixed)" > Fe^0 > activated carbon > Fe_3O_4. Since both Fe^0 and activated carbon act as adsorbents, the combination of these two materials would result in higher removal efficiency. Although the removal of MB on the combination of these two materials will go through different mechanisms which is adsorption for activated carbon and reduction/co-precipitation for reduced iron nanoparticles [50]. It was proposed that the removal mechanism of MB could be due to the reduction of MB (dark blue) to LMB (colourless) by Fe^0 and $Fe^{II}_{(s)}$ species as well as adsorption and co-precipitation of MB on in situ generated products during the corrosion process [50].

There are similar reports in literature which confirm the effectiveness of zero valent iron in the composite materials for the removal of different pollutants in particular methylene blue dye [56-58]. For example, the removal of arsenic form water by zero valent iron supported on activated carbon was studied by Zhu et al. [59]. It was shown that after loading of 8.2 wt% nano zero-valent iron on activated carbon, the surface area decreased from 821.7 to 69.4 m^2/g (roughly 90% reduction) and the total pore volume was reduced from 0.45 to 0.078 cm^3/g (roughly 80% reduction). However, in our study, after loading the 14 wt% of iron and heat treatment at 1000 ° C, the surface area decreased from 1043.1 to 571.9 m^2/g (only 45 % reduction), the total pore volume reduced from 0.98 to 0.87 cm^3/g (around 11% reduction) and the micropore volume decreased from 0.4 to 0.15 cm^3/g (62% reduction). This shows nanoporous carbon derived from metal organic framework ZIF-8 is a more suitable support for loading the active species specifically magnetic particles.

In our study, the effective role of iron nanopraticles on dye removal can compensate for the reduction of adsorbent's surface area due to the coverage of iron particles. Furthermore, the good dispersion and nano sized iron particles help for the better removal of dye from water. Therefore, we can observe the magnetic Fe/CZIF1000 still show great adsorption capacity while exhibiting high magnetic performance.

In case of Fe/CZIF600, the low adsorption capacity could be due to several reasons. First, the CZIF600 support material itself does not have high adsorption capacity for adsorption of dyes as mentioned in our previous study [60]. Second, after coating the iron nanoparticles, definitely the surface area and micropore volume decreases. Also the iron species on this material are in oxide forms. There are evidences in literature which shows removal efficiency of iron oxides is lower than activated carbon and zero valent iron for the removal of methylene

blue form water [50]. Therefore, Fe/CZIF600 shows poor adsorption performance for MB adsorption from water.

Fig. 5-7 shows the magnetic property of the iron loaded nanoporous carbon CZIF1000 after MB adsorption.

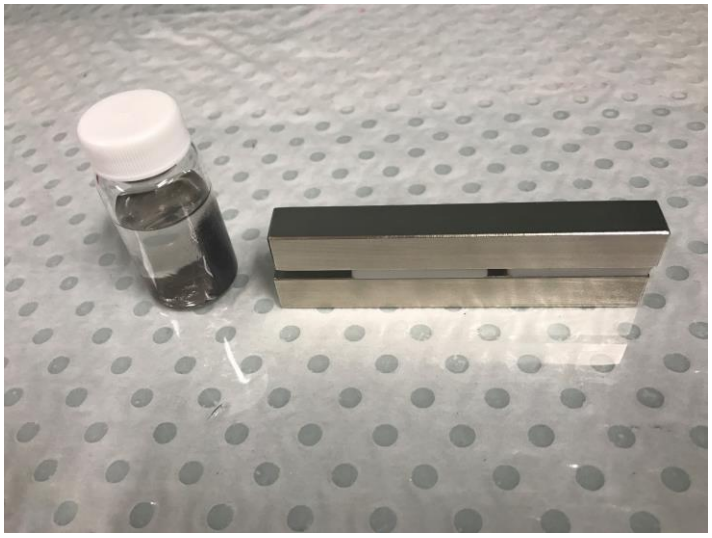

Fig. 5-7 Magnetic property of Fe/CZIF 1000 after adsorption of MB from water.

5.4.3. Effect of pH on adsorption

Effect of pH on the adsorptive removal of methylene blue by magnetic and original nanoporous carbons was investigated and shown in Fig. 5-8 for comparison. The adsorption capacity of magnetic sample at low pH=1-5.5 is lower than the original nanoporous carbon. At pH of 5.5, the magnetic sample shows adsorption performance similar to CZIF1000 and the capacity increases with increase in the pH of solution for both adsorbents with slightly higher adsorption capacity for the CZIF1000 sample. The slightly lower adsorption capacity of the magnetic sample could be due to the more positive zeta potential (Fig. 5-8 (a)) at higher pH levels which could be attributed to the presence of iron particles in the adsorbent. However, the difference in the adsorption performance is negligible. It is seen that at low pH the magnetic sample has a lower adsorption capacity. At acidic pH both adsorbents are positively charged,

therefore, the lower adsorption capacity of the magnetic sample while both adsorbents are positively charged, could be due to the lower surface area. At pH values higher than 4, iron solubility is low [61] and one possible dye removal mechanism apart from electrostatic interaction could be related to iron oxide precipitation and MB removal through co-precipitation. Also redox reaction with Fe^{II} species through the oxide-film around the zero valent iron were reported [62]. Thus, MB dye molecules can be reduced to LMB after co-precipitation [50]. It is worth noting that the point of zero charge for zero valent iron is around 7.7 [56, 63] and the point of zero charge for the magnetic sample was shifted from 4.5 for CZIF1000 to 4.7 for Fe/CZIF1000.

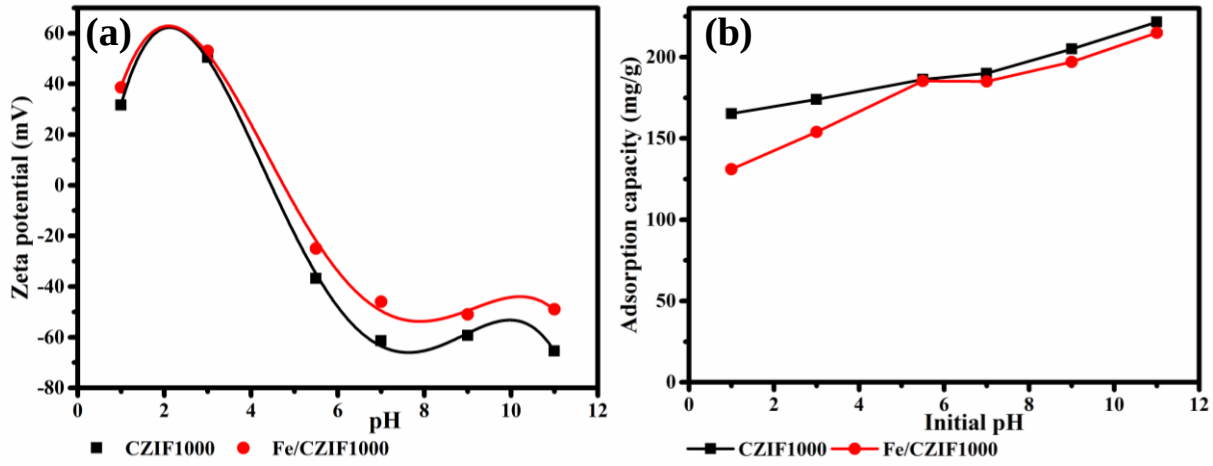

Fig. 5-8 Comparison of CZIF1000 and Fe/CZIF1000: (a) Zeta potential and (b) effect of initial pH on adsorption capacity.

5.4.4. Regeneration and recyclability of nanoporous carbons

The spent magnetic adsorbent was regenerated by heat treatment at 200 ºC. The comparison of the regeneration efficiency for the magnetic and non-magnetic samples is shown in Fig. 5-9.

The figure shows that the performance of Fe/CZIF1000 decreased slightly after repeated use and regeneration for five cycles but the regeneration efficiency is still higher than 80 %

which indicates the magnetic nanoporous carbons can be recycled and reused while having high adsorption performance.

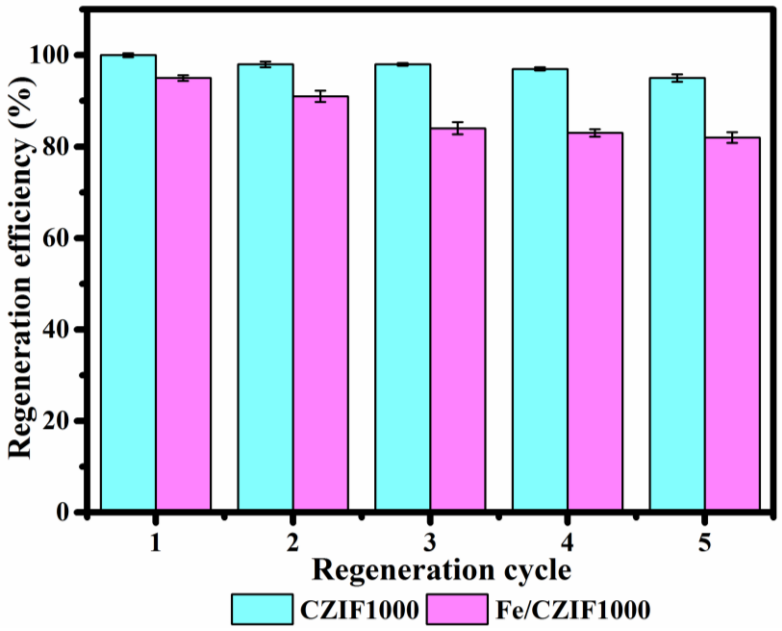

Fig. 5-9 Regeneration efficiency of Fe/CZIF1000 compared with CZIF1000.

5.5. Conclusions

The effect of carbonization temperature on adsorption properties of iron loaded nanoporous carbon ZIF-8 was investigated. The iron loading was 14% (nominal) for the samples and the nanoporous carbons were further heat treated at 600 and 1000 ˚C to investigate the effect of further heat treatment on adsorption property of the magnetic samples. The Fe/CZIF1000 exhibited high adsorption capacity similar to CZIF1000 which could be attributed to the presence of zero valent iron produced during annealing at high temperature. XRD patterns confirmed the presence of iron oxides on Fe/CZIF600 and reduced metallic iron on Fe/CZIF1000. The SEM images showed the nano sized iron particles were well distributed within the magnetic adsorbents with sizes from 10-100 nm using the combination of a simple wet impregnation and carbonization. This study demonstrated that nanoporous carbons can be

loaded by magnetic nano particles through a simple and efficient impregnation method without losing their high adsorption capacity.

5.6. References

1. Cestari, A.R., E.F.S. Vieira, A.A. Pinto, and E.C.N. Lopes, *Multistep adsorption of anionic dyes on silica/chitosan hybrid: 1. Comparative kinetic data from liquid- and solid-phase models.* Journal of Colloid and Interface Science, 2005. **292**(2): p. 363-372.
2. Ryoo, R., S.H. Joo, M. Kruk, and M. Jaroniec, *Ordered mesoporous carbons.* Advanced Materials, 2001. **13**(9): p. 677-681.
3. Xia, Y., Z. Yang, and R. Mokaya, *Templated nanoscale porous carbons.* Nanoscale, 2010. **2**(5): p. 639-659.
4. O'Keeffe, M., *Design of MOFs and intellectual content in reticular chemistry: a personal view.* Chemical Society Reviews, 2009. **38**(5): p. 1215-1217.
5. Kurmoo, M., *Magnetic metal–organic frameworks.* Chemical Society Reviews, 2009. **38**(5): p. 1353-1379.
6. Khan, N.A., B.K. Jung, Z. Hasan, and S.H. Jhung, *Adsorption and removal of phthalic acid and diethyl phthalate from water with zeolitic imidazolate and metal–organic frameworks.* Journal of Hazardous Materials, 2015. **282**: p. 194-200.
7. Liu, X., C. Wang, Q. Wu, and Z. Wang, *Metal-organic framework-templated synthesis of magnetic nanoporous carbon as an efficient absorbent for enrichment of phenylurea herbicides.* Analytica Chimica Acta, 2015. **870**: p. 67-74.
8. Torad, N.L., M. Hu, S. Ishihara, H. Sukegawa, A.A. Belik, M. Imura, K. Ariga, Y. Sakka, and Y. Yamauchi, *Direct Synthesis of MOF-Derived Nanoporous Carbon with Magnetic Co Nanoparticles toward Efficient Water Treatment.* Small, 2014. **10**(10): p. 2096-2107.
9. Baikousi, M., A.B. Bourlinos, A. Douvalis, T. Bakas, D.F. Anagnostopoulos, J.i. Tuček, K.r. Šafářová, R. Zboril, and M.A. Karakassides, *Synthesis and characterization of γ-Fe2O3/carbon hybrids and their application in removal of hexavalent chromium ions from aqueous solutions.* Langmuir, 2012. **28**(8): p. 3918-3930.
10. Banerjee, A., R. Gokhale, S. Bhatnagar, J. Jog, M. Bhardwaj, B. Lefez, B. Hannoyer, and S. Ogale, *MOF derived porous carbon–Fe3O4 nanocomposite as a high performance, recyclable environmental superadsorbent.* Journal of Materials Chemistry, 2012. **22**(37): p. 19694-19699.
11. Wang, C.F., J.N. Wang, and Z.M. Sheng, *Solid-Phase Synthesis of Carbon-Encapsulated Magnetic Nanoparticles.* The Journal of Physical Chemistry C, 2007. **111**(17): p. 6303-6307.
12. Zhang, C., S.N. Oliaee, S.Y. Hwang, X. Kong, and Z. Peng, *A Generic Wet Impregnation Method for Preparing Substrate-Supported Platinum Group Metal and Alloy Nanoparticles with Controlled Particle Morphology.* Nano Letters, 2016. **16**(1): p. 164-169.
13. Mohan, D., A. Sarswat, V.K. Singh, M. Alexandre-Franco, and C.U. Pittman Jr, *Development of magnetic activated carbon from almond shells for trinitrophenol removal from water.* Chemical Engineering Journal, 2011. **172**(2–3): p. 1111-1125.
14. Ribeiro, R.S., A.M.T. Silva, J.L. Figueiredo, J.L. Faria, and H.T. Gomes, *Catalytic wet peroxide oxidation: a route towards the application of hybrid magnetic carbon nanocomposites for the degradation of organic pollutants. A review.* Applied Catalysis B: Environmental, 2016. **187**: p. 428-460.
15. Han, Z., B. Sani, J. Akkanen, S. Abel, I. Nybom, H.K. Karapanagioti, and D. Werner, *A critical evaluation of magnetic activated carbon's potential for the remediation of*

sediment impacted by polycyclic aromatic hydrocarbons. Journal of Hazardous Materials, 2015. **286**: p. 41-47.

16. Yang, C., D. Wang, and Q. Tang, *The synthesis of NdFeB magnetic activated carbon and its application in degradation of azo dye methyl orange by Fenton-like process.* Journal of the Taiwan Institute of Chemical Engineers, 2014. **45**(5): p. 2584-2589.
17. Kitajima, M., M. Sato, and H. Nishide, *Preparation of flat porous carbon films from paper-thin wood shavings and control of their mechanical, electrical and magnetic properties.* Carbon, 2013. **61**: p. 260-269.
18. Imshennik, V.K., I.P. Suzdalev, O.N. Stavinskaya, N.I. Shklovskaya, V. Schünemann, A.X. Trautwein, and H. Winkler, *Preparation and characterization of porous carbon loaded with iron particles: a possible magnetic carrier of medical drugs.* Microporous Materials, 1997. **10**(4): p. 225-230.
19. Qu, S., F. Huang, S. Yu, G. Chen, and J. Kong, *Magnetic removal of dyes from aqueous solution using multi-walled carbon nanotubes filled with Fe2O3 particles.* Journal of Hazardous Materials, 2008. **160**(2–3): p. 643-647.
20. Keller, N., C. Pham-Huu, C. Estournès, J.-M. Grenèche, G. Ehret, and M.J. Ledoux, *Carbon nanotubes as a template for mild synthesis of magnetic CoFe2O4 nanowires.* Carbon, 2004. **42**(7): p. 1395-1399.
21. Lu, G., S. Li, Z. Guo, O.K. Farha, B.G. Hauser, X. Qi, Y. Wang, X. Wang, S. Han, X. Liu, J.S. DuChene, H. Zhang, Q. Zhang, X. Chen, J. Ma, S.C.J. Loo, W.D. Wei, Y. Yang, J.T. Hupp, and F. Huo, *Imparting functionality to a metal–organic framework material by controlled nanoparticle encapsulation.* Nat Chem, 2012. **4**(4): p. 310-316.
22. Fuertes, A.B. and P. Tartaj, *Monodisperse Carbon–Polymer Mesoporous Spheres with Magnetic Functionality and Adjustable Pore-Size Distribution.* Small, 2007. **3**(2): p. 275-279.
23. Lou, X.W. and L.A. Archer, *A General Route to Nonspherical Anatase TiO2 Hollow Colloids and Magnetic Multifunctional Particles.* Advanced Materials, 2008. **20**(10): p. 1853-1858.
24. Ni, S., X. Wang, G. Zhou, F. Yang, J. Wang, and D. He, *Designed synthesis of wide range microwave absorption Fe3O4–carbon sphere composite.* Journal of Alloys and Compounds, 2010. **489**(1): p. 252-256.
25. Yang, Y., Z. Guo, H. Zhang, D. Huang, J. Gu, Z. Huang, F. Kang, T.A. Hatton, and G.C. Rutledge, *Electrospun magnetic carbon composite fibers: Synthesis and electromagnetic wave absorption characteristics.* Journal of Applied Polymer Science, 2013. **127**(6): p. 4288-4295.
26. Pang, F., M. He, and J. Ge, *Controlled Synthesis of Fe3O4/ZIF-8 Nanoparticles for Magnetically Separable Nanocatalysts.* Chemistry - A European Journal, 2015. **21**(18): p. 6879-6887.
27. Ge, J., Y. Hu, M. Biasini, W.P. Beyermann, and Y. Yin, *Superparamagnetic Magnetite Colloidal Nanocrystal Clusters.* Angewandte Chemie International Edition, 2007. **46**(23): p. 4342-4345.
28. Luo, N., X. Li, X. Wang, H. Yan, C. Zhang, and H. Wang, *Synthesis and characterization of carbon-encapsulated iron/iron carbide nanoparticles by a detonation method.* Carbon, 2010. **48**(13): p. 3858-3863.
29. Luo, N., X. Li, Y. Sun, and X. Wang, *Synthesis and characteristic of carbon-encapsulated ferronickel nanoparticles by detonation decomposition of doping with nitrate explosive precursors.* Journal of Alloys and Compounds, 2010. **505**(1): p. 352-356.

30. Zhu, M. and G. Diao, *Review on the progress in synthesis and application of magnetic carbon nanocomposites.* Nanoscale, 2011. **3**(7): p. 2748-2767.
31. Kida, K., M. Okita, K. Fujita, S. Tanaka, and Y. Miyake, *Formation of high crystalline ZIF-8 in an aqueous solution.* CrystEngComm, 2013. **15**(9): p. 1794-1801.
32. Hoch, L.B., E.J. Mack, B.W. Hydutsky, J.M. Hershman, J.M. Skluzacek, and T.E. Mallouk, *Carbothermal Synthesis of Carbon-supported Nanoscale Zero-valent Iron Particles for the Remediation of Hexavalent Chromium.* Environmental Science & Technology, 2008. **42**(7): p. 2600-2605.
33. Xu, Z., L. Wang, W. Wang, N. Li, C. Chen, C. Li, C. Yang, H. Fu, and L. Kuang, *Migration behavior, oxidation state of iron and graphitization of carbon nanofibers for enhanced electrochemical performance of composite anodes.* Electrochimica Acta, 2016. **222**: p. 385-392.
34. Hu, P., S. Zhang, H. Wang, D.a. Pan, J. Tian, Z. Tang, and A.A. Volinsky, *Heat treatment effects on Fe3O4 nanoparticles structure and magnetic properties prepared by carbothermal reduction.* Journal of Alloys and Compounds, 2011. **509**(5): p. 2316-2319.
35. Lee, H.J., W. Cho, E. Lim, and M. Oh, *One-pot synthesis of magnetic particle-embedded porous carbon composites from metal-organic frameworks and their sorption properties.* Chemical Communications, 2014. **50**(41): p. 5476-5479.
36. Kim, B.H., N. Lee, H. Kim, K. An, Y.I. Park, Y. Choi, K. Shin, Y. Lee, S.G. Kwon, H.B. Na, J.-G. Park, T.-Y. Ahn, Y.-W. Kim, W.K. Moon, S.H. Choi, and T. Hyeon, *Large-Scale Synthesis of Uniform and Extremely Small-Sized Iron Oxide Nanoparticles for High-Resolution T1 Magnetic Resonance Imaging Contrast Agents.* Journal of the American Chemical Society, 2011. **133**(32): p. 12624-12631.
37. Liu, D.H., Y. Guo, L.H. Zhang, W.C. Li, T. Sun, and A.H. Lu, *Switchable Transport Strategy to Deposit Active Fe/Fe3C Cores into Hollow Microporous Carbons for Efficient Chromium Removal.* Small, 2013. **9**(22): p. 3852-3857.
38. Xi, Y., M. Megharaj, and R. Naidu, *Dispersion of zerovalent iron nanoparticles onto bentonites and use of these catalysts for orange II decolourisation.* Applied Clay Science, 2011. **53**(4): p. 716-722.
39. Chaikittisilp, W., M. Hu, H. Wang, H.-S. Huang, T. Fujita, K.C.W. Wu, L.-C. Chen, Y. Yamauchi, and K. Ariga, *Metal–organic framework (MOF) as a template for syntheses of nanoporous carbons as electrode materials for supercapacitor* Chemical Communications, 2012. **48**(58): p. 7259-7261.
40. Zhu, X., F. Qian, Y. Liu, D. Matera, G. Wu, S. Zhang, and J. Chen, *Controllable synthesis of magnetic carbon composites with high porosity and strong acid resistance from hydrochar for efficient removal of organic pollutants: An overlooked influence.* Carbon, 2016. **99**: p. 338-347.
41. Shi, W.P., W.F. Liu, L. Chen, L. Qin, Y.Z. Yang, and X.G. Liu, *Effect of annealing temperature on the structure of carbon encapsulated Fe3O4 nanospheres.* RSC Advances, 2015. **5**(129): p. 106787-106794.
42. Sun, R., H.-B. Zhang, J. Yao, D. Yang, Y.-W. Mai, and Z.-Z. Yu, *In situ reduction of iron oxide with graphene for convenient synthesis of various graphene hybrids.* Carbon, 2016. **107**: p. 138-145.
43. Schnepp, Z., S.C. Wimbush, M. Antonietti, and C. Giordano, *Synthesis of Highly Magnetic Iron Carbide Nanoparticles via a Biopolymer Route.* Chemistry of Materials, 2010. **22**(18): p. 5340-5344.

44. Petnikota, S., S.K. Marka, A. Banerjee, M.V. Reddy, V.V.S.S. Srikanth, and B.V.R. Chowdari, *Graphenothermal reduction synthesis of 'exfoliated graphene oxide/iron (II) oxide' composite for anode application in lithium ion batteries.* Journal of Power Sources, 2015. **293**: p. 253-263.
45. Srinivas, G., V. Krungleviciute, Z.-X. Guo, and T. Yildirim, *Exceptional CO2 capture in a hierarchically porous carbon with simultaneous high surface area and pore volume.* Energy & Environmental Science, 2014. **7**(1): p. 335-342.
46. Fan, J., Y. Guo, J. Wang, and M. Fan, *Rapid decolorization of azo dye methyl orange in aqueous solution by nanoscale zerovalent iron particles.* Journal of Hazardous Materials, 2009. **166**(2): p. 904-910.
47. Sohn, K., S.W. Kang, S. Ahn, M. Woo, and S.-K. Yang, *Fe (0) nanoparticles for nitrate reduction: stability, reactivity, and transformation.* Environmental Science & Technology, 2006. **40**(17): p. 5514-5519.
48. Bandara, J., J.A. Mielczarski, and J. Kiwi, *1. Molecular Mechanism of Surface Recognition. Azo Dyes Degradation on Fe, Ti, and Al Oxides through Metal Sulfonate Complexes.* Langmuir, 1999. **15**(22): p. 7670-7679.
49. Liu, W.-J., K. Tian, Y.-R. He, H. Jiang, and H.-Q. Yu, *High-Yield Harvest of Nanofibers/Mesoporous Carbon Composite by Pyrolysis of Waste Biomass and Its Application for High Durability Electrochemical Energy Storage.* Environmental Science & Technology, 2014. **48**(23): p. 13951-13959.
50. Noubactep, C., *Characterizing the discoloration of methylene blue in Fe 0/H 2 O systems.* Journal of hazardous materials, 2009. **166**(1): p. 79-87.
51. Dutta, K., S. Mukhopadhyay, S. Bhattacharjee, and B. Chaudhuri, *Chemical oxidation of methylene blue using a Fenton-like reaction.* Journal of Hazardous Materials, 2001. **84**(1): p. 57-71.
52. Ma, L., Z. Ding, T. Gao, R. Zhou, W. Xu, and J. Liu, *Discoloration of methylene blue and wastewater from a plant by a Fe/Cu bimetallic system.* Chemosphere, 2004. **55**(9): p. 1207-1212.
53. Pande, S., S.K. Ghosh, S. Nath, S. Praharaj, S. Jana, S. Panigrahi, S. Basu, and T. Pal, *Reduction of methylene blue by thiocyanate: Kinetic and thermodynamic aspects.* Journal of colloid and interface science, 2006. **299**(1): p. 421-427.
54. Vetter, K., *General kinetics of passive layers on metals.* Electrochimica Acta, 1971. **16**(11): p. 1923-1937.
55. Noubactep, C., *A critical review on the process of contaminant removal in Fe0–H2O systems.* Environmental technology, 2008. **29**(8): p. 909-920.
56. Zhou, Y., B. Gao, A.R. Zimmerman, H. Chen, M. Zhang, and X. Cao, *Biochar-supported zerovalent iron for removal of various contaminants from aqueous solutions.* Bioresource technology, 2014. **152**: p. 538-542.
57. Miyajima, K. and C. Noubactep, *Effects of mixing granular iron with sand on the efficiency of methylene blue discoloration.* Chemical Engineering Journal, 2012. **200–202**: p. 433-438.
58. Jia, H. and C. Wang, *Adsorption and dechlorination of 2,4-dichlorophenol (2,4-DCP) on a multi-functional organo-smectite templated zero-valent iron composite.* Chemical Engineering Journal, 2012. **191**: p. 202-209.
59. Zhu, H., Y. Jia, X. Wu, and H. Wang, *Removal of arsenic from water by supported nano zero-valent iron on activated carbon.* Journal of Hazardous Materials, 2009. **172**(2–3): p. 1591-1596.

60. Abbasi, Z., E. Shamsaei, S.K. Leong, B. Ladewig, X. Zhang, and H. Wang, *Effect of carbonization temperature on adsorption property of ZIF-8 derived nanoporous carbon for water treatment.* Microporous and Mesoporous Materials, 2016. **236**: p. 28-37.
61. Rickard, D., *The solubility of FeS.* Geochimica et Cosmochimica Acta, 2006. **70**(23): p. 5779-5789.
62. Stratmann, M. and J. Müller, *The mechanism of the oxygen reduction on rust-covered metal substrates.* Corrosion Science, 1994. **36**(2): p. 327-359.
63. Almeelbi, T. and A. Bezbaruah, *Aqueous phosphate removal using nanoscale zero-valent iron.* Journal of Nanoparticle Research, 2012. **14**(7): p. 900.

Chapter 6. Enhanced removal of a basic dye and heavy metals from wastewater using magnetic Victorian brown coal fly ash modified by weathering

6.1. Overview

In previous chapters the adsorption properties of ZIF-8 and its nanoporous carbons were extensively investigated. These materials displayed interesting features and remarkable adsorption capabilities. The utilized methods for preparing them were also considered among the most straightforward and the least expensive strategies. However, compared with available natural adsorbents, the high cost of these synthetic materials is still arguable. In this chapter, the adsorption properties of Victorian brown coal fly ashes as local free wastes were thoroughly studied to provide a detailed survey about their possible future application. The fly ash materials were investigated for the adsorption of a basic dye and heavy metals and effect of weathering modification on the adsorption properties was evaluated. It was revealed that the fly ash adsorbents had greater or comparable capacity for the removal of methylene blue dye and heavy metals and could be considered as promising adsorbents for neutralizing acidic mining wastewaters. The outcomes of this study would help for future applications of these wastes and to resolve the environmental issues resulting from their disposal.

This chapter has been formatted from the following submitted manuscript:

Z.Abbasi, E. Shamsaei, B. Ladewig, H. Wang, Enhanced Removal of a Basic Dye and Heavy Metals from Wastewater Using Magnetic Victorian Brown Coal Fly Ash Modified by Weathering. 2017, *Chem. Eng. J.* 2017 (Submitted).

6.2. Introduction

Synthetic dyes are extensively used in industrial applications and as a result a large amount of waste water is produced. Many of these dyes are hazardous and are required to be removed from wastewater before discharge to the environment. Dyes and pigments inhibit the sunlight penetration into the water bodies and reduce the photosynthetic reaction. In addition, some dyes are even carcinogenic and it is very vital to remove them from the water bodies [1, 2]. Methylene blue is the most common dye which is used for dying cotton and fabric. It can cause eye burns and inhalation problems as well as nausea, vomiting and mental confusion in humans [3, 4]. Therefore, the treatment of dyed wastewaters is highly important regarding the harmful impacts on the environment and ecosystem.

The presence of heavy metals in wastewaters also threatens the human life and ecosystem due to their toxicity. Contrary to organic contaminants which are mostly biodegradable, heavy metals cannot degrade to non-hazardous materials. Therefore, the treatment of wastewaters polluted by heavy metal is crucial. This requires the concentration of heavy metals into smaller volumes followed by a safe and secure disposal [5].

Adsorption is widely used for the removal of different pollutants from water especially those that are difficult to be destroyed using the conventional and biological water treatment systems. The synthetic dyes usually contain aromatic structures which lead to the physicochemical and thermal stability of dye molecules as well as resistance to conventional

waste water treatment. Heavy metals are also toxic to microorganisms in traditional biological treatment systems.

Adsorption is an attractive option for the treatment of polluted waters containing dyes and heavy metals. This method can be an economical option specifically if a low cost adsorbent is selected and employed [1]. Therefore, the recent research in literature has focused on inexpensive and locally available materials to replace the activated carbon which is costly and complicated to be recycled [6].

Fly ash is a waste and by-product of coal combustion processes which is generated in large volumes in the power plants. This industrial waste is considered as a low-cost adsorbent due to its low cost and local availability [7]. The application of these waste materials has been limited to cement production [8]. Therefore, there is a strong need to develop new applications for the utilization of fly ash waste material such as using as adsorbents in water treatment purposes. A variety of fly ash wastes have been utilized as zero cost adsorbents for adsorption of organics, dyes and heavy metals from water [9-13]. Most of the studies have focused on the adsorption property of fly ash wastes while the usage of these materials strongly depends on the original source, mineralogy and physicochemical properties. The effect of mineralogy and physicochemical characteristics on adsorptive properties of fly ash waste in water treatment has not been reported yet.

Fly ash from sources such as incinerators is not suitable for water treatment since heavy metals are leached and released from these materials [14]. Bagasse fly ash from sugar industry does not contain toxic materials but is also not available in many places [15]. However, there are many thermal power plants which operate with coal as their fuel in many countries around the world. The coal fly ash is obtained as the waste product from coal-firing power stations in large quantities. The fly ash waste is collected in precipitators and disposed of in landfills. Thus,

there is a high demand about developing new ways of re-using this inexpensive by-product to avoid further environmental issues.

Victorian brown coal is the largest source for providing 85% of the electricity demands of Victoria State, Australia. 50×10^9 kg of brown coal is mined annually for electricity generation in main electricity generating complexes of Hazelwood (1600 MWe), Yallourn (1450 MWe), Loy Yang Power (2000 MWe) and Edison Mission Energy facilities (1000 MWe, a section of the Loy Yang Power) [16]. As a result, around 1.3 million tons of fly ash per year is produced in Latrobe Valley. The fly ash is transferred to an ash disposal pond after mixing with water, resulting in a slurry with high water to ash ratio. Nevertheless, the capacity of the ash ponds is limited [16] and the disposal of ash in ash pond is not a sustainable solution since currently the quality of ground water is an environmental concern [17].

There are differences in physical and chemical characteristics of the fly ash at Loy Yang, Hazelwood and Yallourn due to the difference in coal quality as well as in operation between these power plants. The main mineral compounds in coal which are considered as the source of ash formation in Latrobe Valley include thenardite (Na_2SO_4), halite (NaCl), periclase (MgO), haematite (Fe_2O_3), magnetite (Fe_3O_4), lime (CaO), anhydrite ($CaSO_4$), alpha-quartz (α-SiO_2) and alumina (Al_2O_3) [16]. Table 6-1 shows the comparison of fly ash materials obtained from different power plants in Latrobe Valley.

Table 6-1. Comparison of Latrobe Valley brown coal ashes in 2000 (wt%) [16]

Species	Loy Yang	Yallourn	Hazelwood
SiO_2	60.4[a]	1.4	6.6
Al_2O_3	13.3[a]	2.1	1.8
Fe_2O_3	8.5	24.5	8.7
TiO_2	1.7	0.1	0.2
K_2O	1.2	0.4	0.4
MgO	2.2	18	18.8
Na_2O	2.1	11	4.5
CaO	1.0	12.3	28.4
SO_3	3.4	21.7	15.6
Cl	<0.1	<0.1	3.4

[a] highly variable

Fly ash materials are composed of inorganic-organic mixtures. They have heterogeneous and variable compositions [18]. An empirical formula was proposed by Iyer and Scott [19] for fly ash materials according to the presence of major elements: $Si_{1.0}\,Al_{0.45}\,Ca_{0.51}\,Na_{0.047}\,Fe_{0.039}\,Mg_{0.02}\,K_{0.013}\,Ti_{0.011}$. The percentage and composition of these elements differ for fly ashes based on the source of the coal and the combustion process conditions and parameters. Fly ash wastes are identified as type F and type C products. Type F fly ash is produced from anthracite, bituminous or sub-bituminous coals and it has low amount of lime (< 7%). This type of fly ash has more silica, alumina as well as iron oxide. On the other hand, type C fly ash is produced from burning of lignite coal and has more lime (15-30%) [19]. In this study, Yallourn fly ash is a low lime and Hazelwood fly ash is a high lime fly ash (class C).

Fly ash is known to have a hydrophilic surface and high surface area. These two characteristics are important in terms of physical properties which reflect its reactivity [20]. During the weathering process in ash ponds, the ash is in contact with water and air for a long period of time and the precipitation processes dominate the solubility of the solids. Natural weathering occurs in the ash ponds through the carbonation, dissolution, co-precipitation and fluid transport mechanisms which cause chemical, physical and geochemical changes in fly ash materials. For example, from mineralogical point of view, fresh fly ash is composed of quartz, mullite, hematite, magnetite and lime while weathered ash is composed of additional phases such as calcite and aragonite[3] [21].

New techniques for reusing this waste material are strongly required to address the environmental concerns and simultaneously take the advantage of using a low-cost and locally available product. In this study, the adsorption properties of Victorian brown coal fly ashes including Yallourn, Hazelwood and Weathered fly ashes (resulting from weathering of Hazelwood fly ash) are investigated and compared for the first time for the adsorption of methylene blue dye and heavy metals from water. The effect of weathering process on characteristics and adsorption properties of Hazelwood fly ash is also investigated. The effect of adsorption process parameters such as pH and temperature on adsorption capacity of Victorian brown coal fly ash adsorbents was explored and the adsorption mechanisms were comprehensively investigated.

[3] calcite and aragonite are two crystal forms of calcium carbonate ($CaCO_3$)

6.3. Materials and Methods

6.3.1. Materials

Methylene blue (MB) was purchased from Merck. Zinc nitrate hexahydrate ($Zn(NO_3)_2.6H_2O$), nickel nitrate hexahydrate ($Ni(NO_3)_2.6H_2O$), copper nitrate hexahydrate ($Cu(NO_3)_2.\ 6H_2O$), cobalt nitrate hexahydrate ($Co(NO_3)_2.\ 6H_2O$), NaOH and HCl were purchased from Sigma Aldrich. All chemicals were used as received without any purification. Hazelwood and Yallourn fly ash samples were collected from the electrostatic precipitator in Hazelwood and Energy Australia power plants, which are based in Latrobe Valley located in Victoria, Australia. Weathered fly ash was obtained after mixing the same Hazelwood fly ash with water and exposure to the atmosphere in the ash pond for one year. Fly ash materials were sieved to 37- 63 μm and dried in oven at 110 °C before use. The fly ash materials are sometimes denoted as YFA (Yallourn fly ash), HZW or HFA (Hazelwood fly ash) and WFA (Weathered fly ash) in this report.

6.3.2. Characterization

The crystal structures of the fly ash samples were determined using an X-ray diffractometer (Miniflex 600, Rigaku) with Cu Kα radiation at 40 kV and 20 mA over the 2θ range of 2-90°. Nitrogen adsorption and desorption isotherms were analysed at liquid nitrogen temperature (77 K) using an accelerated surface area and porosimetry system (ASAP 2010, Micromeritics, USA) for measuring surface areas of the samples. The morphology of the fly ash samples was observed using a scanning electron microscope (JEOL 7001F FEG SEM). FTIR spectra of the fly ash samples were analysed using an attenuated total reflectance (ATR) Fourier Transform Infrared (FTIR) (Perkin Elmer, USA) in the range of 500-4000 cm^{-1} at an average of 32 scans with a resolution of 4 cm^{-1}. UV-vis spectrophotometer (UVmini-1240, Shimadzu) was

employed to measure the concentration of methylene blue at the wavelength of 665 (maximum absorption of the methylene blue). The zeta potentials were determined using a Zetasizer Nano (Malvern) at the natural pH of the solution after fly ash dispersion. The powders were dispersed by sonication in water with the concentration of 0.5mg/10ml and the dispersion was used for zeta potential measurement. The concentration of heavy metals (Zn, Ni, Co and Cu) was analysed by a Perkin-Elmer Optima 7000 DV ICP-OES spectrometer with a dual-view (axial-radial) optical system.

6.3.3. Adsorption experiments

Adsorption on the fly ash adsorbents was conducted in batch experiments. The adsorption capacity was investigated by adsorption of a cationic dye (methylene blue) and heavy metals (Cu, Zn, Ni and Co) in aqueous solution. An aqueous stock solution of MB ($C_{16}H_{18}N_3SCl$, MW: 319.85), with 1000 ppm concentration was prepared in milli-Q water. Aqueous solutions with different dye concentrations were prepared by successive dilution of the stock solution with water. The same procedure was used for preparing heavy metal stock solutions and adsorption experiments.

Specific amount of adsorbents (0.2 g) was put in 50 ml of aqueous dye or metal solution having fixed concentrations. The dye or metal solutions containing the adsorbents were mixed well with magnetic stirring and maintained for a fixed time (5 min to 24 h) at room temperature (25°C). After adsorption for a pre-determined time, the solutions were separated from the adsorbents with centrifugation (8000 rpm, 20 min for dye solutions) and with a syringe filter (Nylon, hydrophobic, 0.45 µm for heavy metal solutions). The dye or heavy metal concentration was calculated after dilution (if necessary).

The adsorption isotherm and kinetic experiments for methylene blue were done without any pH adjustment and at the natural pH of the solution i.e. 8.3 for Yallourn, 9.5 for Weathered and 10.5 for Hazelwood fly ash samples. The dye solution was prepared to the desired concentrations using Milli-Q water. The pH of the solution was adjusted using 0.1 M HCl and 0.1 M NaOH for defining the effect of pH on adsorption performance. The adsorption experiments for heavy metals were performed without any pH adjustment. The initial heavy metal solution pH after dispersion of fly ash adsorbents was in the range of 7.5 to 8.4 for Yallourn fly ash, 8.9 to 9.6 for Hazelwood fly ash and 8.1 to 9.1 for Weathered fly ash.

6.4. Results and Discussions

6.4.1. Characterization and textural properties of fly ash materials textural properties of fly ash materials

The XRD patterns of fly ash samples are shown in Fig. 6-1. The mineralogical composition and peak identification for the Victorian brown coal fly ashes have been done by Hosseini et al. [22, 23] in different studies. The XRD patterns of the Yallourn fly ash indicates that iron exists as magnesioferrite ($MgFe_2O_4$) which confirms the presence of magnetic phase in this fly ash which leads to a magnetic behaviour. The other major crystalline phase includes quartz (SiO_2) and there are minor peaks related to titanium as well. Calcium (8.1% in the oxide form) and calcium alumina-silicate contents existed as amorphous phases and were not detectable by XRD analysis [23].

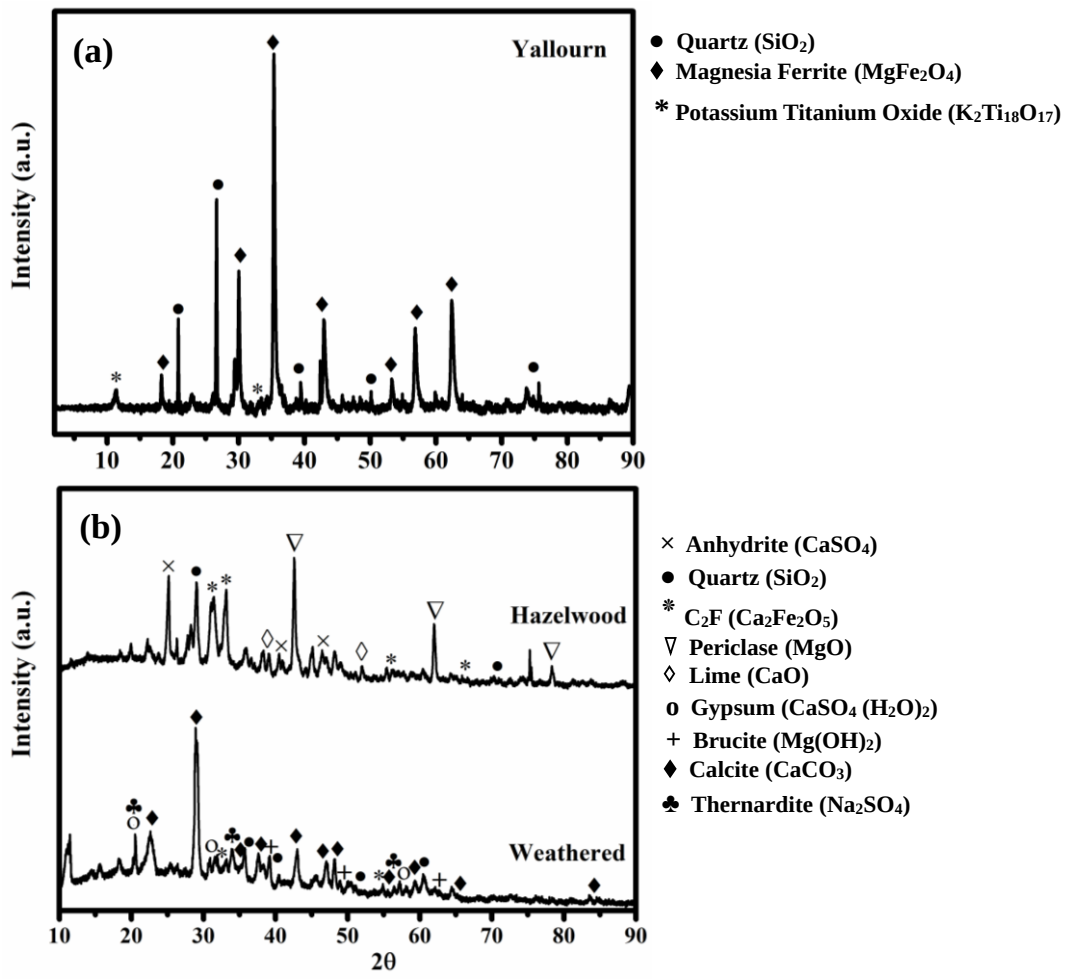

Fig. 6-1 XRD patterns of Yallourn fly ash (a) and Hazelwood and Weathered fly ash (b)

Mg in Hazelwood fly ash exists as periclase (MgO) while iron is in the form of C_2F ($Ca_2Fe_2O_5$) which is called calcium ferrite. However, this fly ash exhibits minor magnetic properties because of the lower amount of iron compared to Yallourn fly ash. Calcium is the major component of Hazelwood fly ash which is present in the crystalline forms of C_2F ($Ca_2Fe_2O_5$), anhydrite ($CaSO_4$) and lime (CaO). Iron, aluminium and calcium may form C_4AF ($Ca_2Fe_{0.28}Al_{1.72}O_5$) which exists in Hazelwood fly ash in very small amount not detectable by XRD analysis.

The XRD pattern of Weathered fly ash illustrates the presence of calcite ($CaCO_3$) as the main phase and major source of calcium content. After weathering process in which the

Hazelwood fly ash is in contact with water and atmosphere, lime (CaO) is hydrated to form $Ca(OH)_2$ which reacts with CO_2 to produce $CaCO_3$ (calcite). Anhydrite ($CaSO_4$), the other calcium containing compound, results in some other phases like gypsum ($CaSO_4$ $(H_2O)_2$) under weathering conditions. Periclase (MgO) of Hazelwood fly ash also converts to brucite ($Mg(OH)_2$) in Weathered fly ash as a result of weathering process as can be observed in the XRD spectra. In addition, it can be seen that the amount of quartz (SiO_2) is significantly reduced which could be due to the dissolution and reaction of this phase under alkaline conditions of ash-water system in weathering process. The quantities of anhydrite ($CaSO_4$), quartz (SiO_2) and C_4AF ($Ca_2Fe_{0.28}Al_{1.72}O_5$) were reduced after weathering process in weathered fly ash sample. This indicates that these species interacted in aqueous environment to transfer into some species with low crystallinity which cannot be detected by XRD analysis [22].

To define the composition of these ashes, XRF analysis was utilized. The XRF of Yallourn fly ash was done by Bureau Veritas Australia and those of Hazelwood and Weathered fly ashes were reported from the study published by Hosseini et. al. [22]. Table 6-2 indicates the XRF analysis of different elements (in form of oxides) in Yallourn, Hazelwood as well as Weathered fly ash.

Table 6-2 XRF analysis of Victorian brown coal fly ash in this study

	Yallourn[1]	Hazelwood [22, 23]	Weathered [22]
SiO_2	10.4	5.82	3.86
Al_2O_3	3.87	3.01	3.65
Fe_2O_3	47.3	14.00	16.8
CaO	8.1	32.4	30.97
MgO	18.6	29.3	32.51
TiO_2	0.23	0.68	na
Na_2O	1.82	0.2	0.22
K_2O	0.19	0.17	0.15
P_2O_5	0.03	0.41	na
SO_3	6.1	12.8	9.44
MnO	0.61	0.67	na
ZnO	na	0.04	na

[1] Based on certificate analysis of Bureau Veritas

The major elements existing in these samples are Fe, Ca and Mg. Yallourn fly ash is rich in iron supporting its magnetic behaviour and contains little calcium but Hazelwood fly ash mainly contains calcium and magnesium indicating its basic properties in solution. The results from XRF are in good agreement with XRD spectra which defines the major elements and phases in these waste materials.

To have a better understanding about the morphology of the samples, SEM analysis was conducted. This technique helped identifying the different textures of these materials resulting in different properties. The SEM images of fly ash samples and the corresponding EDS elemental mapping are shown in Fig. 6-2 and Fig. 6-3. It can be seen that Yallourn fly ash contains spheres and interesting rod-shaped particles with some pores on the surface even with 50 nm or 100 nm size. As can be observed from images this material contains a combination of a variety of textures and different shapes like spheres, needles and flakes. The morphology of

Hazelwood fly ash is shown in Fig. 6-2 (b). It is observed that its surface is rigid with no regular shape and there are not any pores on the surface.

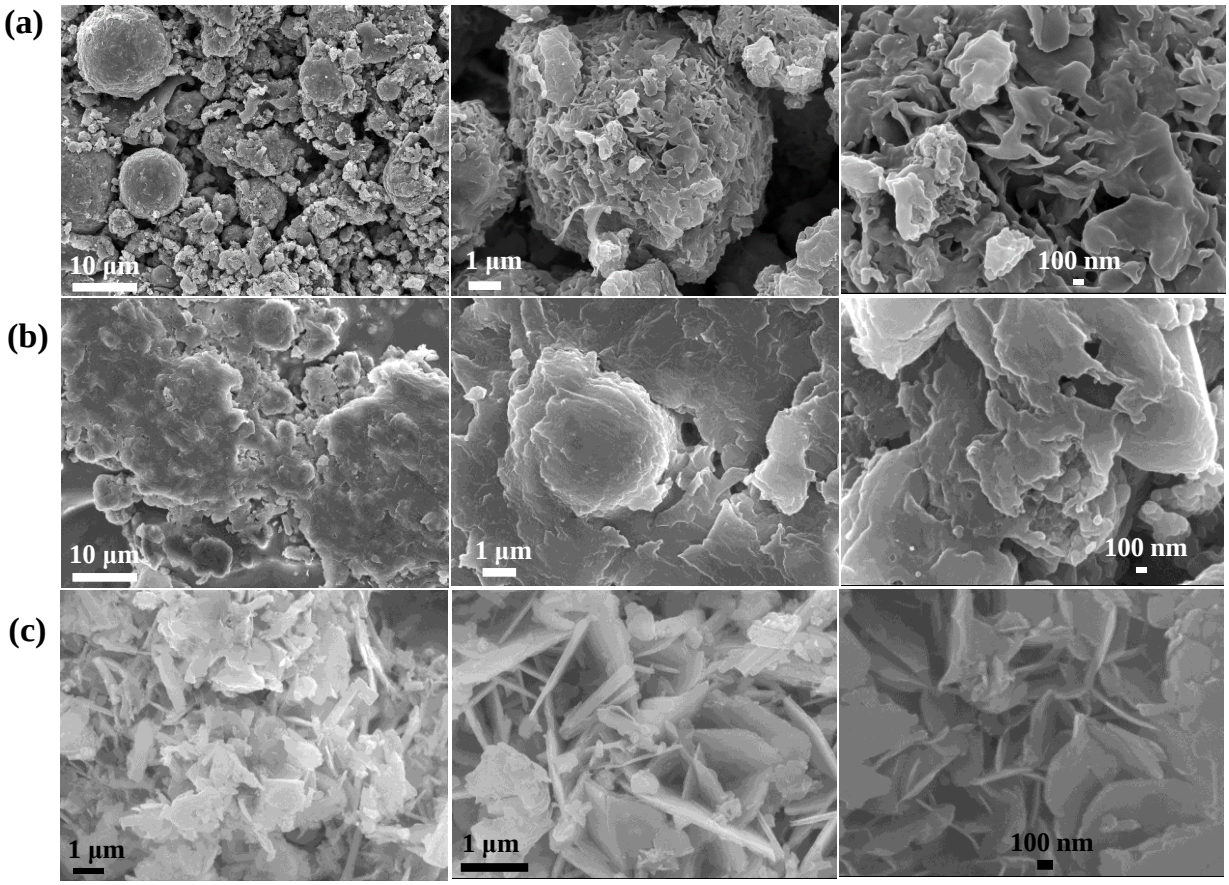

Fig. 6-2 SEM images of Victorian brown coal fly ash: (a) Yallourn fly ash, (b) Hazelwood fly ash and (c) Weathered fly ash.

The SEM images of the Weathered fly ash (the Hazelwood exposed to water and air) can be seen in Fig. 6-2 (c). It is observed the rigid shape of the Hazelwood disappeared and some regular and irregular flakes with interesting orientation are created after undergoing natural weathering. This shows that the morphology of Hazelwood fly ash has changed as a result of atmospheric conditions to a more flexible porous structure. The elemental mapping of the fly ash samples as observed in Fig. 6-2 (a) and (b) shows the elemental composition of Yallourn and Hazelwood fly ash which are rich in Fe, Mg and Ca and these results agree with the XRF data. The reason for creation of some porous structures in Hazelwood fly ash after weathering

process could be related to the formation of calcium silicates through the pozzolanic reaction [24, 25].

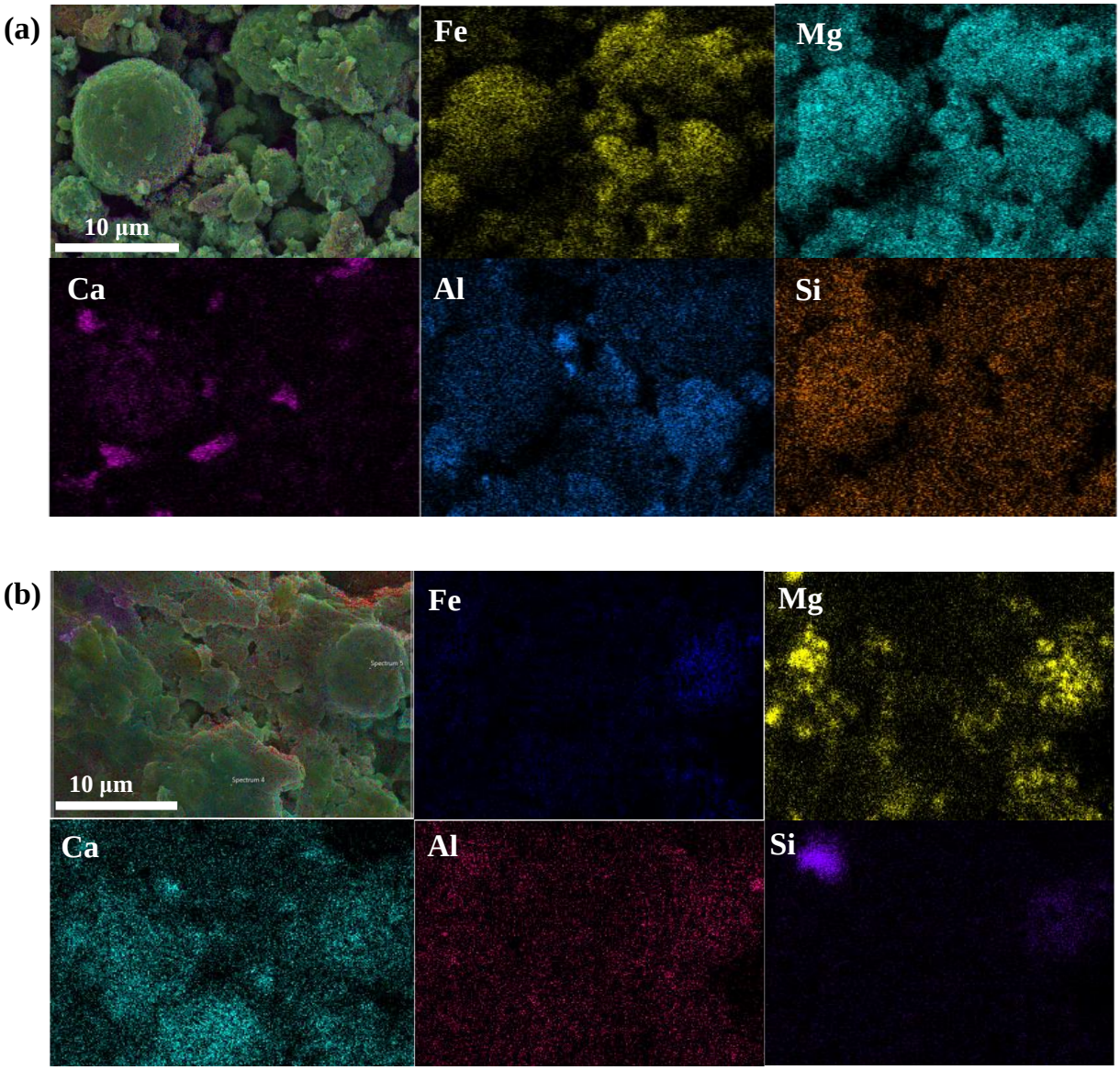

Fig. 6-3 EDS elemental mapping of Yallourn fly ash (a) and Hazelwood fly ash (b)

In this reaction calcium is chemically adsorbed on the surface of silanol groups [26]. In a very basic environment, SiO_2 in the fly ash structure is dissolved and reacts with Ca^{2+} according to the following equation to produce calcium silicate.

$$SiO_2(s) + xCa^{2+}(aq) + 2xOH^-(aq) + (y-x)H_2O \rightarrow xCaO.SiO_2.yH_2O \quad (1)$$

where x is in the range of 0.8-1.5 and y is between 0.5-2.5 [27, 28]. The resulting calcium silicate has large surface area and a porous framework. Therefore, the porous structure observed in the SEM image of the Weathered fly ash could be due to the formation of calcium silicate formed at the very basic condition during the weathering process of Hazelwood fly ash in ash pond. The surface areas of the fly ashes have been analysed and are shown in Fig. 6-4.

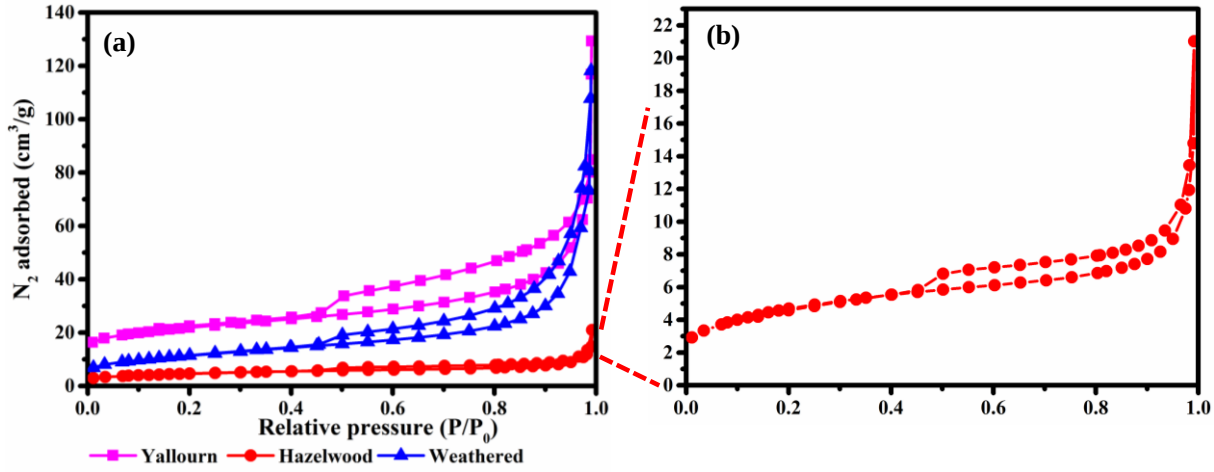

Fig. 6-4 N_2 adsorption-desorption isotherms of Victorian fly ashes (a) and (b)

The nitrogen adsorption desorption isotherms show that the isotherm of all fly ash samples are typical of type V, characteristic of nonporous materials. This isotherm features a hysteresis loop generated by inter-particles voids. The surface areas and the pore volumes of the samples are given in Table 6-3. The results show that Yalourn fly ash has the highest surface area followed by Weathered and Hazelwood fly ashes. The greater pore volume of Yallourn fly ash indicates larger porosity in the framework of this fly ash sample as reflected in the SEM images. The micropore volume of Yallourn sample also reveals that there is some microporosity in this sample although the portion is small.

Table 6-3 Surface area analysis parameters of fly ash samples

Sample	BET surface area (m^2/g)	Total pore volume[a] (Cm^3/g)	Micropore volume (Cm^3/g)
Yallourn fly ash	70.55±1.4	0.096	0.015
Hazelwood fly ash	15.65±0.27	0.017	0.0
Weathered fly ash	39.63±0.35	0.092	0.001

[a] At P/P0=0.97

It can be noticed that the surface area of the Weathered fly ash increased after undergoing weathering conditions. This shows that the physical properties of Hazelwood fly ash changes after exposure to weathering conditions. Both samples exhibit zero micropore volumes. Although the Hazelwood fly ash has much less pore volume compared to Yallourn fly ash, the pore volume of the weathered sample increases after weathering process. The increase in the surface area and porosity of Hazelwood fly ash after weathering could be due to the formation of porous calcium silicate via pozzolanic reaction as mentioned previously. The significant change in fly ash samples as a result of weathering is quite interesting regarding the applicability of these waste materials in different applications particularly adsorption.

The FTIR spectra of the samples are shown in Fig. 6-5. The presence of strong bands at around 556 cm^{-1} for all of fly ash samples is indicative of the presence of Fe-O stretching vibration. The peaks at 889 cm^{-1} are characteristics of Si-O-Al vibration bands. In addition, there is an intense absorption band at 1100 cm^{-1} for the fly ash samples which is an indication of the presence of SiO_2 [29]. In general, the peaks in the region 981-1466 cm^{-1} are assigned to asymmetric stretching vibrations of Al-O/Si-O bonds [30] and could be attributed to the presence of mullite ($2Al_2O_3.2SiO_2$) [31], while the bands between 618 and 747 cm^{-1} are characteristics of Si-O-Si/Si-O-Al bending bands [30]. Moreover, the band at 875 cm^{-1} could

be related to the Al atoms in the tetrahedral forms of silica framework [32]. The peak at around 3466 cm^{-1} is characteristics of vibration of OH and H-O-H groups from the adsorbed water molecules [33].

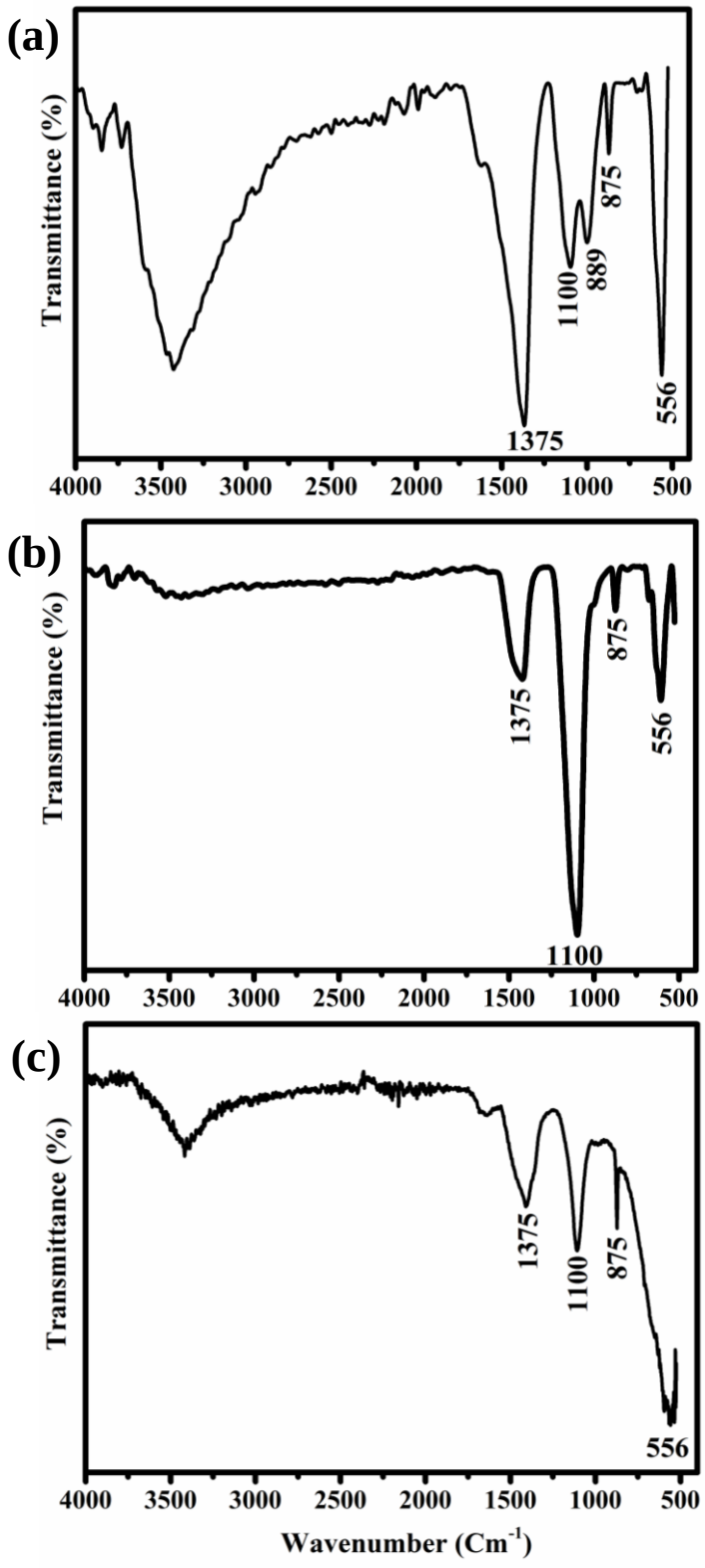

Fig. 6-5 FTIR spectra of the fly ash samples: (a) Yallourn, (b) Hazelwood and (c) Weathered fly ash.

6.4.2. Adsorption study for the removal of Methylene Blue (MB) dye by fly ash adsorbents

The adsorption capacity of the fly ash samples for the removal of MB dye was defined through the batch experiments and methylene blue dye with the dimensions of 1.43 nm × 0.61 nm × 0.4 nm [34] was used to explore the adsorption behaviour of fly ash samples. Methylene blue is a basic cationic and positively charged dye which is used as a model dye compound in this study to investigate the sorption capabilities of fly ash materials for basic dye molecules. The structure of methylene blue is illustrated in Fig. 6-6.

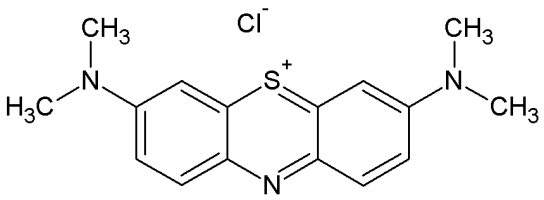

Fig. 6-6 Chemical structure of MB dye.

The adsorption capacity of fly ash samples is compared in Fig. 6-7.

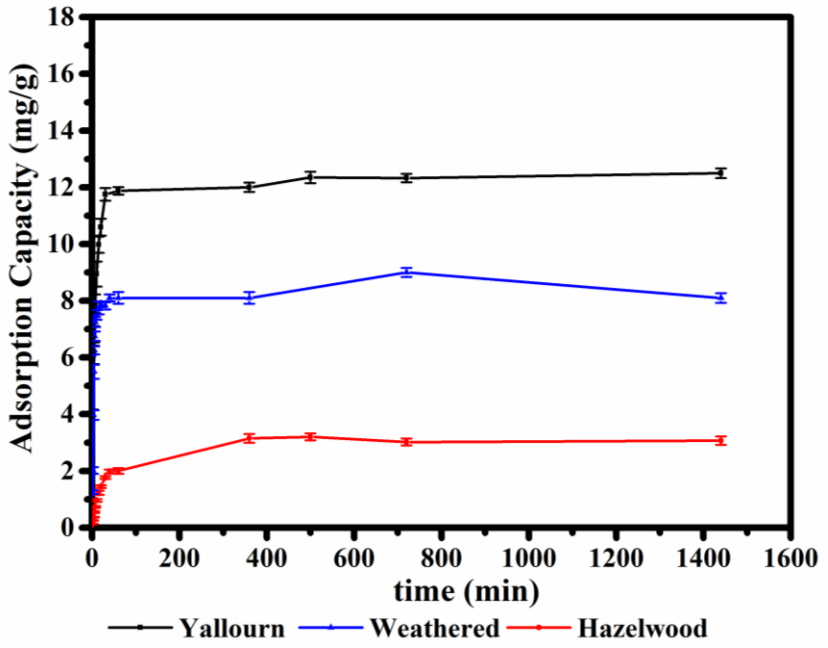

Fig. 6-7 Adsorption capacity of fly ash adsorbents for MB removal (initial dye concentration 50 ppm, adsorbent dosage 0.2 g, solution volume 50 ml, initial pH=8.3 for Yallourn, 9.5 for Weathered and 10.5 for Hazelwood fly ash.)

The figure shows that Yallourn fly ash has the highest adsorption capacity of 12.5 mg/g in comparison with Hazelwood fly ash which has the lowest capacity of 3.2 mg/g. The adsorption capacity of weathered fly ash reaches 8.1 mg/g which shows the superior capacity of this material compared with Hazelwood fly ash after weathering process. The higher capacity of Weathered fly ash can be addressed to the increased surface area as well as more porous structure due to the formation of calcium silicates as confirmed by the SEM images and N_2 adsorption-desorption results. In addition, as can be seen from Table 6-4, the zeta potential of the Weathered fly ash has become more negative after weathering process.

Table 6-4 Zeta potentials of fly ash samples

	Yallourn FA	pH=8.3	Hazelwood FA	pH=10.5	Weathered FA	pH=9.5
Zeta potential	-32.7 ± 0.61		-15.8 ± 0.28		-25 ± 0.52	

This indicates that after weathering process, more negative charges are produced on the surface of fly ash which results in a better electrostatic interaction with positively charged MB dye molecules. The adsorption uptakes by the adsorbent materials were calculated by the following relationship using the initial and final concentration:

$$Q = (C_i - C_e) \times \frac{V}{m} \quad (2)$$

where Q is the adsorption capacity (mg/g), V is the volume of the MB solution (ml), m is the weight of the fly ash adsorbents (g) and C_i and C_e are the initial and equilibrium concentrations (mg/l). The capacity of fly ash samples for methylene blue removal in the current study and the various fly ash samples are compared and summarized in Table 6-5. It can be seen that Victorian brown coal fly ash samples in this study have higher or comparable adsorption capacities with those of fly ashes reported in literature. This reflects that the fly ash derived from Victorian brown coal could be promising for potential application in removal of dyes from polluted waters.

Table 6-5 Comparison of adsorption capacities of MB on various fly ash adsorbents

Adsorbent	Adsorption isotherm	Adsorption pH	Capacity (mg/g)	Reference
Coal fly ash	Langmuir	8	5.7	[35]
Coal fly ash	Langmuir	7.5	3.07	[36]
Coal fly ash	Langmuir	7	1.47	[2]
Coal fly ash[1]	Freundlich	4.4	4.47	[1]
Coal fly ash	Freundlich	10.96	0.672	[37]
Coal fly ash	Langmuir	5.4	1.9	[38]
Coal fly ash[2]	Langmuir & Freundlich	5.4	3.8	[38]
Coal fly ash	Langmuir	6.37	12.7	[39]
Coal fly ash	Langmuir	5	1.1	[40]
Yallourn fly ash	Langmuir	8.3	12.5	This study
Weathered ash	Langmuir	9.5	8.1	This study
Hazelwood ash	Langmuir	10.5	3.2	This study
AC[3] from date palm leaflets	Langmuir	7	270	[41]

[1] treated by HCl [2] NaOH and sonochemical treatment [3] AC: Activated carbon

It is worth noting some fly ash materials reported in literature have been modified by different methods such as acid or base treatment. However, the capacity of fly ash samples even after treatment is still low or comparable with the results reported in this sturdy. Australian brown coal fly ashes exhibit promising dye adsorption potential in comparison with the common fly ashes reported in literature.

6.4.3. Adsorption isotherms

To investigate the interaction of methylene blue molecules with the fly ash samples, Freundlich and Langmuir models [42] were employed and the results were compared.

The Langmuir model was according to the assumption that the adsorption sites have equal energy and at each adsorption site one molecule can be adsorbed. Therefore, the adsorbent having an energetically homogeneous surface would consist of a monolayer of adsorbate molecules. This concept introduces a monomolecular adsorption on a homogeneous surface of adsorbents where one adsorption site only can be occupied by one molecule [42]. The equation is given by the linear relationship below:

$$\frac{1}{Q_e} = \frac{1}{Q_m} + \frac{1}{K_L Q_m}\frac{1}{C_e} \quad (3)$$

where Q_m is the maximum adsorption capacity when there is a complete monolayer coverage on the adsorbent surface (mg g^{-1}), and K_L is the Langmuir constant related to the energy of adsorption (l mg^{-1}). The Langmuir constants K_L and Q_m can be determined from the linear plot of $1/C_e$ versus $1/Q_e$.

In contrast, Freundlich isotherm explains the non-ideal adsorption of an adsorbent having an energetically heterogeneous surface [43]. This model is expressed as the following linear form:

$$\log Q_e = \log K_F + {}^{1}/_{n} \log C_e \quad (4)$$

where Q_e is the amount of dye uptake per unit of adsorbent at equilibrium (mg/g), C_e is the dye concentration at equilibrium (mg/l), K_F ($mg^{1-1/n}\, l^{1/n}\, g^{-1}$) and n are the Freundlich adsorption isotherm constants. K_F and $1/n$ values can be calculated from the intercept and slope of the linear plot between log C_e and log Q_e.

The adsorption isotherms are beneficial in terms of defining the feasibility of the adsorbent materials for the removal of pollutants from water. In this case, the isotherms express the

relationship between methylene blue concentration and the amount of its accumulation on the surface of adsorbent at constant temperature.

As mentioned Langmuir and Freundlich isotherms are used commonly in solid/liquid systems and they provide a general idea of how effective the adsorbents are in removing the contaminant from water. To further determine the feasibility of a particular adsorption process, the parameters of Langmuir isotherm can be introduced as R_L [44] with the following formula:

$$R_L = \frac{1}{1 + K_L C_i} \quad (5)$$

where Ci is the initial concentration of MB (mg/l) and K_L is the Langmuir constant. The R_L values describe that the adsorption process is either unfavourable if $R_L>1$, linear if $R_L=1$, favourable if $0<R_L<1$ or irreversible if $R_L=0$. Methylene blue adsorption on all fly ash adsorbents was favourable since R_L values were below unity. The R_L values for Yallourn and Weathered fly ash samples were much lower than those of Hazelwood fly ash and approached zero as initial concentration increased (Fig. 6-9). This indicates that MB adsorption on Yallourn and Weathered fly ashes was much more favourable in comparison with Hazelwood fly ash.

The Langmuir and Freundlich model's parameters were calculated and shown in Table 6-6. The calculations show that the equilibrium data for all fly ash samples did not fit to Freundlich equation. This was addressed by the low value of correlation coefficient of $R^2< 0.95$. In contrast, the equilibrium results reflected a bitter fit to the Langmuir relationship with $R^2>0.99$. This addresses homogenous adsorption sites with a monolayer coverage of methylene blue molecules on the surface of the fly ash samples as shown in Fig. 6-8. Also the comparison of calculated maximum monolayer adsorption (Q_m) with equilibrium adsorption uptake (Q_e) from the experiments further supports the validity of Langmuir isotherm.

Table 6-6 MB adsorption isotherm parameters on fly ash samples

sample		Langmuir isotherm			Freundlich isotherm		
	Q_e	K_L	Q_m	R^2	K_F	n	R^2
Yallourn	12.5	0.67	12.7	0.9984	4.8	3.8	0.7790
Hazelwood	3.2	0.038	4.3	0.9844	0.5	2.3	0.8793
Weathered	8.1	0.39	8.6	0.9906	3.1	3.6	0.7137

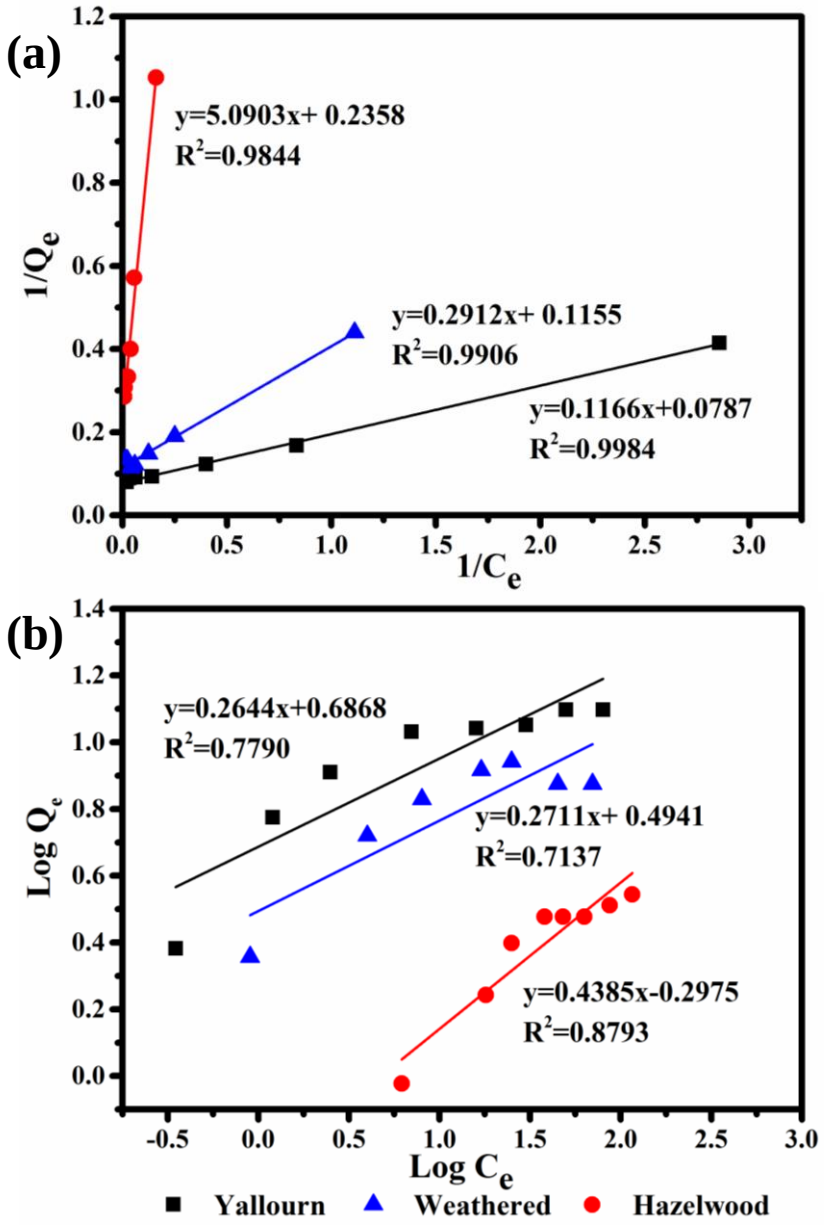

Fig. 6-8 Adsorption isotherms for adsorption of MB on fly ash samples: (a) Langmuir isotherms and (b) Freundlich isotherms (adsorbent dosage 0.2 g, solution volume 50 ml, initial pH=8.3 for Yallourn, 9.5 for Weathered and 10.5 for Hazelwood fly ash).

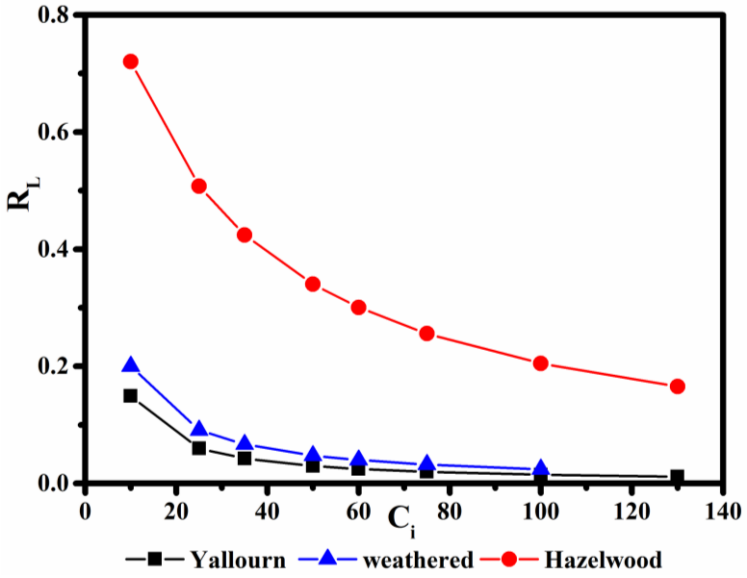

Fig. 6-9 RL values of the fly ash adsorbents at different initial concentrations (adsorbent dosage 0.2 g, solution volume 50 ml, initial pH=8.3 for Yallourn, 9.5 for Weathered and 10.5 for Hazelwood fly ash).

6.4.4. Kinetics study

Different models were obtained to define the dye adsorption kinetics in aqueous environment. The pseudo first order, pseudo second order, intra particle diffusion and Boyd models were used in this study to evaluate the dye removal kinetics and mechanisms on fly ash adsorbents.

6.4.4.1 Pseudo first order model

Pseudo first order model is explained based on Lagergren's kinetic equation [45] which is based on the assumption that the change in the molecule uptake with time is directly correlated to the difference in equilibrium concentration and the solute adsorption uptake with time as the following equation:

$$dQ_t/_{dt} = k_1(Q_e - Q_t) \quad (6)$$

where $Q_t = 0$ at t=0 and the equation can be integrated to give the following relationship:

$$\log(Q_e - Q_t) = logQ_e - \frac{k_1 t}{2.303} \quad (7)$$

where Q_t is the adsorption capacity per unit mass of adsorbent (mgg^{-1}) at time t, k_1 is the pseudo first order rate constant (min^{-1}) and t is the contact time (min). The first order rate constant (k_1) was calculated by plotting of $\log(Q_e - Q_t)$ against t.

6.4.4.2 Pseudo second order model

The pseudo second order model was explained by HO and McKay [46] as the following equation:

$$dQ_t/_{dt} = k_2(Q_e - Q_t)^2 \quad (8)$$

where $Q_t = 0$ at t = 0 and once this equation is integrated, the derived equation can be rearranged to reach the following linear form:

$$\frac{t}{Q_t} = \frac{1}{k_2 Q_e^2} + \frac{t}{Q_e} \quad (9)$$

where k_2 is the pseudo second order rate constant ($gmg^{-1}min^{-1}$). Q_e and k_2 can be calculated by plotting t/Q_t against t.

The kinetic parameters of adsorption of MB onto fly ash samples were calculated and given in Table 6-7.

Table 6-7 The kinetic parameters of MB adsorption on fly ash samples

	Pseudo first order			Pseudo second order			Intra particle diffusion		
sample	K_1 ($\times 10^{-3}$) (min^{-1})	Q_e ($mg.g^{-1}$)	R^2	K_2 ($\times 10^{-3}$) ($g.mg^{-1}.min^{-1}$)	Q_e ($mg.g^{-1}$)	R^2	K_i ($mg.g^{-1}.min^{-1}$)	C	R^2
YFA[1]	0.046	6.1	0.8155	0.016	12.5	0.9999	1.1	5.67	0.9991
HFA[2]	0.017	2.7	0.8803	0.014	3.1	0.999	0.28	0.17	0.9951
WFA[3]	0.18	5.6	0.8851	0.58	8.2	0.998	0.34	6.38	0.9744

1Yallourn fly ash

2 Hazelwood fly ash

3 Weathered fly ash

The kinetic data were analysed by comparison of calculated Q_t versus time from the two kinetic models (as shown in Fig. 6-10) and the kinetic parameters were defined by linear regression. The results showed an excellent fit to the pseudo-second order model ($R^2 > 0.99$) while the first-order kinetic model did not agree well with the data ($R^2<0.95$). The good agreement with the second order model can be verified in terms of similarity of the calculated Q_e values and corresponding experimental values. Similar kinetic data was reported for the adsorption of MB over fly ashes [35, 47].

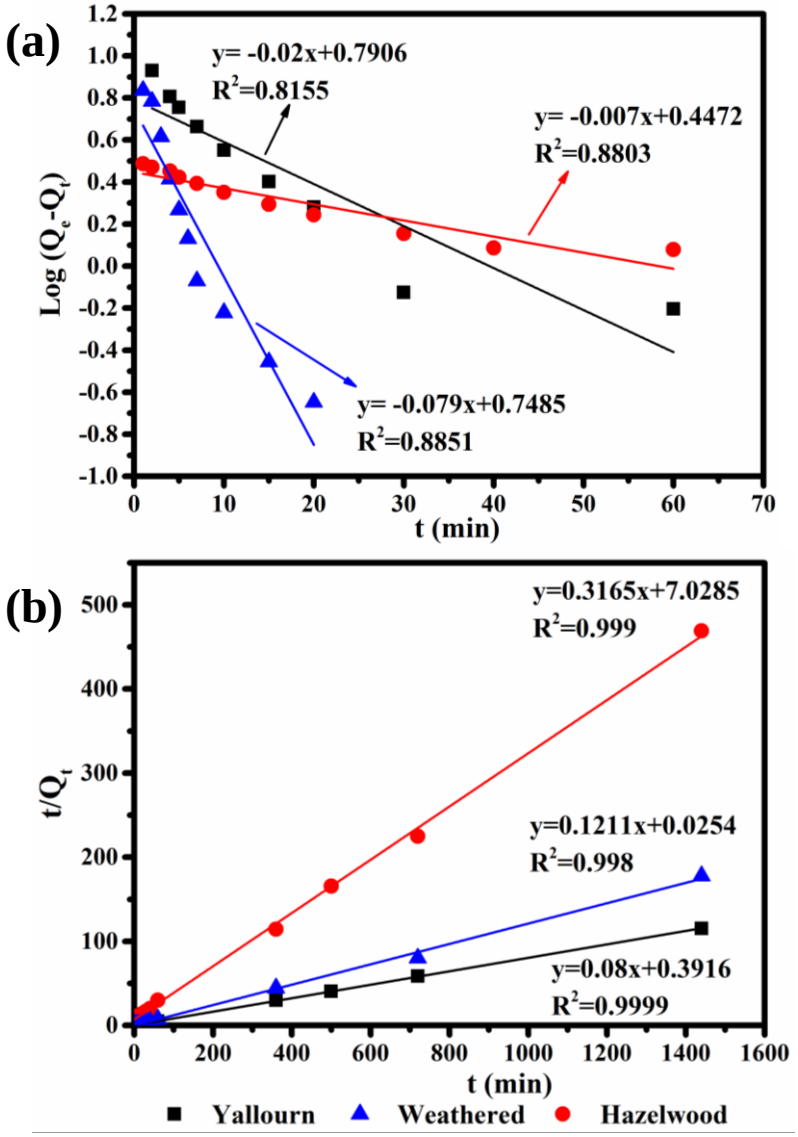

Fig. 6-10 Adsorption kinetics for adsorption of MB on fly ash wastes (initial dye concentration 50 ppm, adsorbent dosage 0.2 g, solution volume 50 ml, initial pH=8.3 for Yallourn, 9.5 for Weathered and 10.5 for Hazelwood fly ash. (a) Pseudo first order and (b) Pseudo second order kinetics).

6.4.4.3 Intra-particle diffusion and Boyd models

The intra-particle diffusion and Boyd models were utilized to determine the dye adsorption mechanism on fly ash samples. The adsorption of dyes includes the transport through both the liquid phase and within the particles. The intra-particle diffusion model was introduced by Weber and Morris [48] to investigate the mechanism of molecule diffusion in an adsorption process. This model is explained by the following equation:

$$Q_t = k_{id} t^{1/2} + C \quad (10)$$

where k_{id} is referred as intra particle diffusion rate constant ($mgg^{-1}min^{-1/2}$). If the adsorption process obeys the intra particle diffusion model, Q_t versus $t^{1/2}$ would be linear with k_{id} as slope and parameter C as the intercept. The C values provide information about the boundary layer thickness which means a larger intercept reflects a larger boundary layer effect.

The intra-particle diffusion model was employed to identify the mechanism of methylene blue adsorption onto fly ash waste materials as shown in Fig. 6-11 (a). It can be seen that the plot range is divided into three linear regions which indicates the adsorption occurs through three steps. The model has been explained by Dogan et al. [49] that the initial stage is related to the external surface adsorption. At this stage, the adsorbate diffuses through the liquid film to the external surface of the adsorbent and this is where the adsorption rate is high. The second stage illustrates the region where the gradual adsorption occurs and the adsorbate molecules diffuse through the particles. At this stage, intra-particle diffusion is involved in the adsorption rate which includes diffusion of the solutes in macro, meso and micropores. The final stage reflects the final equilibrium in which the diffusion of molecules into the particles declines since the maximum adsorption is reached. The intra-particle diffusion graphs of the fly ash samples provided linear plots but none of the plots passed through the origin as the intercepts are not zero. This shows that the intra-particle diffusion is involved in governing the adsorption rate but is not the only rate controlling stage. This addresses some other mechanisms like complexation or ion exchange are probably involved in controlling the adsorption process [50, 51].

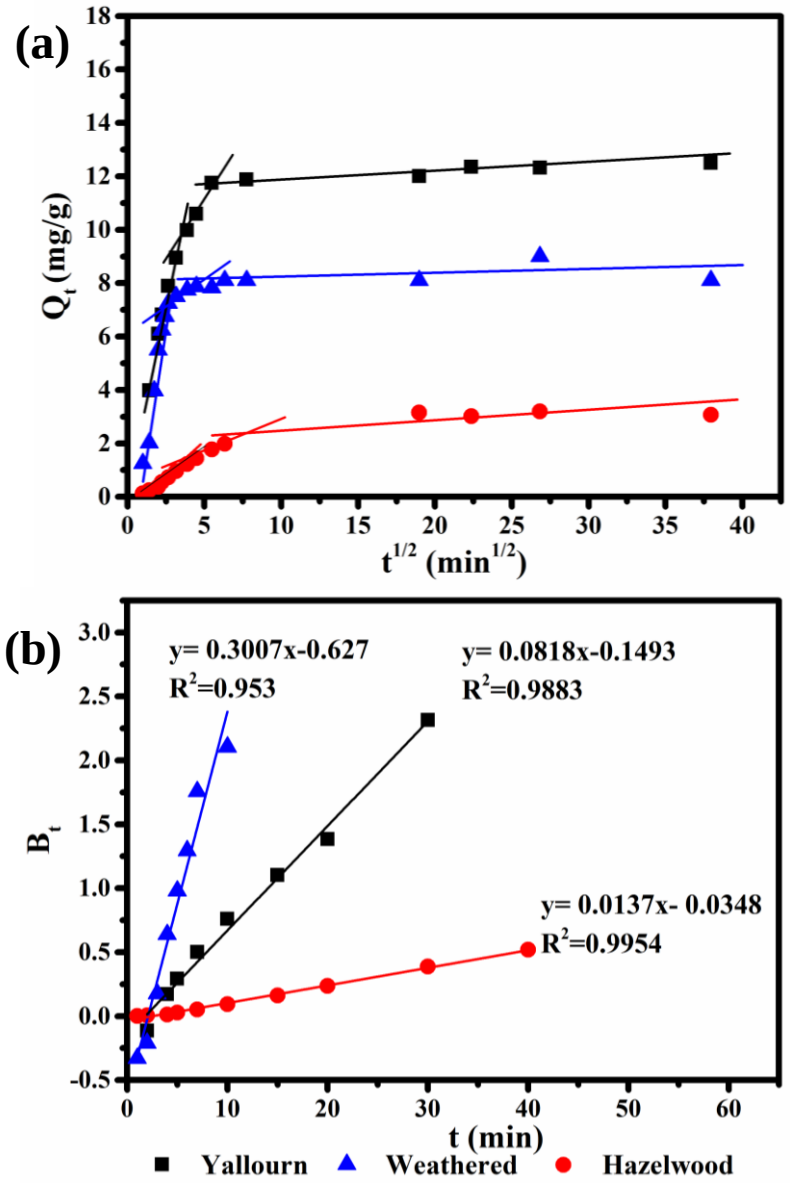

Fig. 6-11 Intra-particle diffusion (a) and Boyd film diffusion kinetic (b) for adsorption of MB onto fly ashes (initial dye concentration 50 ppm, adsorbent dosage 0.2 g, solution volume 50 ml, initial pH=8.3 for Yallourn, 9.5 for Weathered and 10.5 for Hazelwood fly ash).

The slope of the second linear part of the plots determines the parameters related to the intra-particle diffusion model while the intercept of this second linear part represents the boundary layer thickness. The calculated values of intraparticle diffusion kinetic including rate constant (K_{id}) and the intercepts (C) are given in Table 6-7. The greater the intercept, the greater is the effect of boundary layer diffusion on the adsorption which in this case is larger for the Yallourn and Weathered fly ash samples. It can be seen that the Yallourn and Weathred fly ash

plots (second linear part) show a larger deviation from the origin which indicates the diffusion within the boundary layer affects the adsorption when compared with Hazelwood fly ash where the intercept is smaller and close to zero. Similar intra-particle diffusion model data have been reported for the adsorption of MB over fly ash materials [35] and other adsorbents like carbon nanotubes [52] and activated carbons [53].

The adsorption of dyes includes the mass transfer of dye molecules and there are several resistances to mass transfer during the process. The resistances could be either external or interal resistance. The external resistance is faced by solute molecules while they penetrate into the solute film to reach the surface of the particles, while the internal resistance occurs when the adsorbate molecules diffuse into the pores to reach the adsorption sites. The external resistance can be interpreted using the external mass transfer coefficient and the internal resistance can be characterized by the pores of the adsorbents as well as the diffusivity of the adsorbent material [54]. The K_{id} value is not an actual reaction rate constant but it can be used to interpret the influence of intrapraticle diffusion [55]. From the Table 6-7 it is realized that K_{id} values increase in the order of Yallourn> Weathered> Hazelwood which can be attributed to the effect of physical parameters such as surface area and pore size of the adsorbent materials. As the surface area increases the rate parameter increases which is due to the increase of the active sites available for mass transfer resulting in an increase in adsorption and consequently an increase in the rate parameter [56]. Moreover, as the pore size decreases, the free path through which the adsorbate molecules reach the active sites decreases and the intraparticle parameter decreases as a result.

The main limitation about the intraparticle diffusion model is that the rate governing stage cannot be defined using this model. Therefore, to determine the limiting stage of the adsorption process, the Boyd model was employed which is expressed by the following equation:

$$F = 1 - \left({}^{6}/_{\pi^2}\right) \sum_{n=1}^{\infty} \left({}^{1}/_{n^2}\right) exp(-n^2 Bt) \quad (11)$$

F is the fraction regarding the amount of dye adsorbed at different time t and Bt is a function of F which is described as the following relationship:

$$F = {}^{Q_t}/_{Q_e} \quad (12)$$

q_t and q_e are the amount of dye uptake (mg/g) at time t and at equilibrium. Bt is defined using the following relationship:

$$B = {}^{(\pi^2 D_i)}\Big/_{r_0^2} \quad (13)$$

However, the Bt values cannot be calculated using this formula. The following equations were derived by Reichenberg [57] to calculate the Bt values:

for F values >0.85

$$B_t = -0.4977 - \ln(1 - F) \quad (14)$$

while for F values <0.85

$$B_t = \left(\sqrt{\pi} - \sqrt{\pi - (\pi^2 F/3)}\right)^2 \quad (15)$$

The calculated values of B_t versus time were plotted and reported in Fig. 6-11 (b). It can be observed from figure that the plots did not pass through origin which addresses that film diffusion or in other words the external mas transport is the main controlling step in the adsorption process and can be regarded as the rate limiting.

In addition, using the slope of the Boyd model plot, the average B_t value can be defined to determine the effective diffusion coefficient, D_i (cm^2/s) using the equation (8) [58].

The r represents the particle radius. In this study the particle size is in the range of 0.037-0.063 mm (mesh 230-400). It is assumed the particle is spherical and the average particle size was used for calculation. The average diffusion coefficient was calculated as 1.54×10^{-7} cm^2/s for Weathered, 4.31×10^{-8} for Yallourn and 8.68×10^{-9} for Hazelwood fly ash. Michelsen et al. [59] have reported that if the values of D_i is in the order of 10^{-11} cm^2/s, the intraparticle diffusion is a rate limiting stage. In this study, the D_i values are in the order of 10^{-7}, 10^{-8} and 10^{-9} which are four, three and two orders of magnitude higher, indicating that intraparticle diffusion is not the only rate limiting step. Therefore, it can be concluded that both boundary layer (external mass transfer) and intra-particle penetration might be involved in the adsorption process of methylene blue [60]. From the intraparticle diffusion model it is concluded that internal resistance against the diffusion through the pores is included in the mechanism and could contribute to the controlling of the rate of adsorbent but is not the main limiting step. Employing the Boyd plots helped to realize that the external mass transfer and the resistance in the boundary layer mainly control the rate of adsorption.

6.4.5. Effect of solution pH on dye removal mechanism

The solution pH affects the surface charge of the adsorbents and this results in a change in adsorption behaviour of the materials. The change in the solution pH results in the release of hydrogen or hydroxyl ions which might interact with surface functional groups on the active adsorption sites on the adsorbents [58]. The effect of initial solution pH on the adsorptive removal of MB over fly ash adsorbents was studied over the pH range between 2 and 11 at room temperature. The results are shown in Fig. 6-12 (a). The adsorption capacity of all fly ash samples increased as the pH increased but the increase is more pronounce for the Yallourn fly ash and reached the maximum at basic pH around pH=6.5-8.5 while for Hazelwood and Weathered samples the sorption capacity reached the maximum at pH=8.5-10.5. For all fly

ashes the adsorption capacity increased with an increase in pH and then it remained almost constant. The effect of pH on adsorption capacity can be explained based on the electrostatic forces of interaction between the ash samples and the methylene blue molecules.

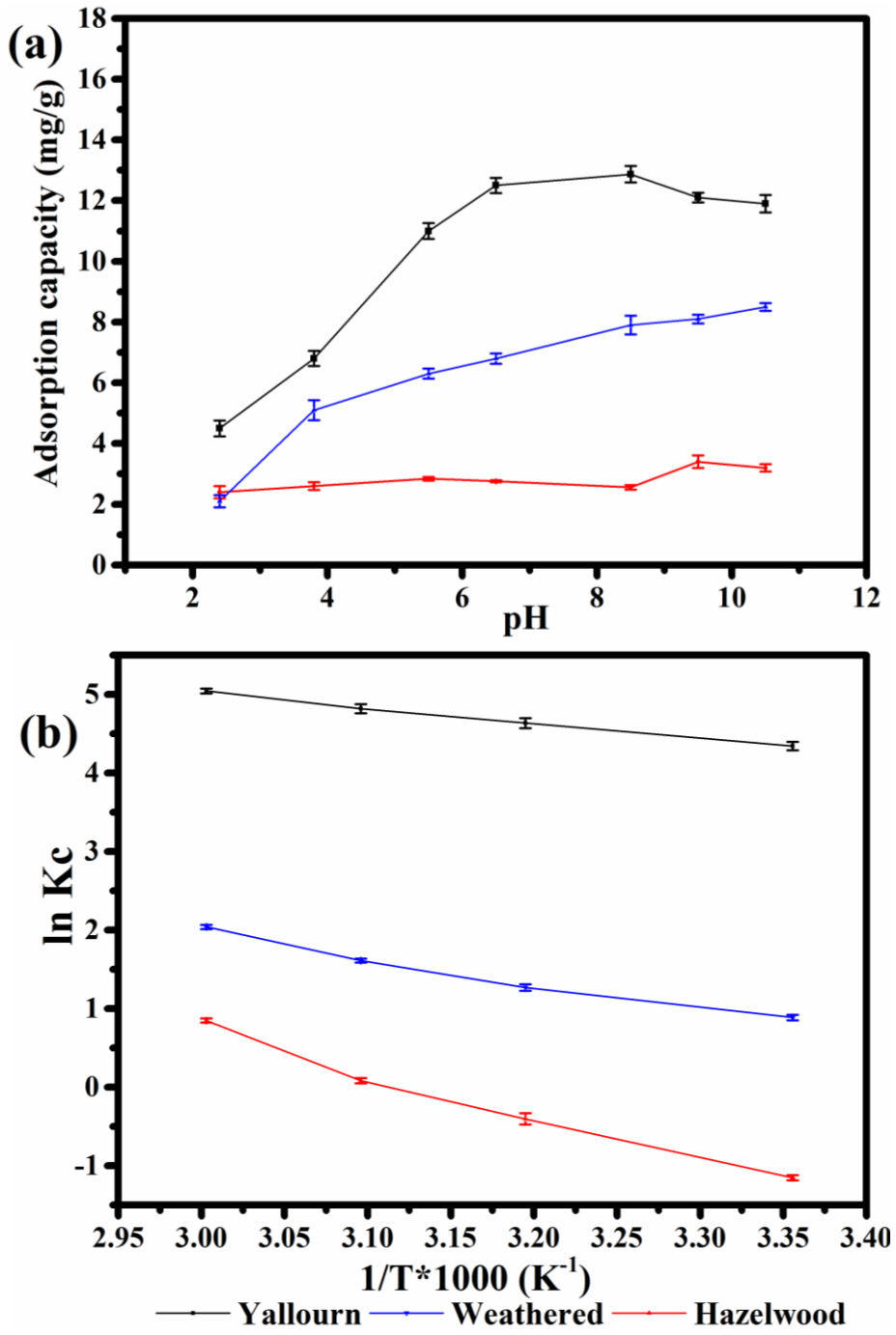

Fig. 6-12 Effect of (a) pH and (b) temperature on adsorption performance of fly ash wastes for the removal of MB from water (initial dye concentration 50 ppm, adsorbent dosage 0.2 g, solution volume 50 ml).

The point of zero charge of the adsorbents gives better understanding about the adsorption behaviour of fly ash samples with the change in solution pH. Generally, when pH > pH_{zpc} the adsorbent surface becomes negatively charged which provides a more suitable environment for the adsorption of a positively charge dye like MB. If the pH < pH_{zpc}, the adsorbent surface becomes positively charged and as a result the positively charged molecules are repelled from the surface of the adsorbent. This leads to the lower removal of MB at lower pH as shown in the figure. It was reported that the point of zero charge for fly ash is typically between 2.4 and 7 [61]. The point of zero charge for low lime fly ash was reported to be 5 and this value shifted to the acidic pH as the lime content of fly ash increased [62]. In this study the resulting pH after dispersion of fly ash in water is in the basic range and above the point of zero charge. Therefore, the adsorbent surface is negatively charged and favours the adsorption of positively charged MB molecules.

The change of the solution pH affects the adsorption capacity of Yallourn fly ash more than Hazelwood and Weathered fly ash which might be due to the alkaline nature of the Hazelwood and Weathered fly ash which neutralizes the acidic pH and results in the stability of ash-water system during the dye adsorption. Similar pH insensitive adsorption was reported by Vimonses et al. for Australian clays- $Ca(OH)_2$ mixtures [63].

When fly ash contacts with water, the calcium undergo dissolution and hydrolysis which results in an increase in the solution pH:

$$CaO + H_2O \leftrightarrow Ca(OH)_2 \leftrightarrow Ca^{2+} + 2OH^- \quad (16)$$

The zeta potentials of the fly ash samples are reported in Table 6-4. According to the XRF analysis of fly ash materials in Table 6-2, we expect Hazelwood and Weathered fly ash, with higher lime content, to have more negative zeta potentials compared with Yallourn fly ash

which has lower calcium content. However, we can see that the negative zeta potential of fly ash samples follows the sequence: Yallourn (-32.7, pH=8.3) > Weathered (-25, pH=9.5) > Hazelwood (-15.8, pH=10.5). Kaya and Yukselen [64] have reported that as pH increases the zeta potential of the kaolinite and montmorinolite in the presence of calcium becomes more negative. However, in very basic solutions (i.e. around pH=11) such behaviour is not observed since near this pH the calcium ion (Ca^{2+}) precipitates as hydroxide from the bulk solution according to the following relation:

$$Ca^{2+} + 2OH^{-} \rightarrow Ca(OH)_2 \downarrow \quad (17)$$

The precipitation of $Ca(OH)_2$ does not allow the accurate measurements of zeta potential of the samples [64]. Therefore, we can observe although the dispersion of Hazelwood and Weathered fly ash results in higher pH values, the zeta potentials are more positive compared with that of Yallourn fly ash. The larger negative zeta potential of Yallourn fly ash in addition to its higher surface area suggest a higher adsorption capacity for the removal of positively charged methylene blue dye from water.

Furthermore, the insoluble MgO and Fe_2O_3 in the fly ash samples will undergo hydration at pH around 12. Kim et al. [65] reported that among the variety of elements which exist in fly ash materials, Fe, Ba, Cd are insoluble, Al, Ca, Mg, Na, K, Mn, are slightly to moderately acid soluble and only Ca and Na are soluble in water. It was found that Fe in fly ash (hematite or magnetite) is an insoluble oxide. Therefore, since in this study the adsorption experiments were performed in deionized water without pH adjustment, it is expected that only Ca is dissolved in water and the raise in the pH and change in the zeta potential of the adsorbents results from the dissolution and hydration of calcium content of fly ash materials. In addition, although the fly ash samples contain aluminium and silica, the solubility of these elements at pH < 9 is very low

[65]. Goyne et al. [66] reported that at high pH values of pH=9.5 the following dissolution occurs:

$$SiO_2(s) + OH^- \leftrightarrow SiO(OH)_3^- + H_2O \quad (18)$$

Moreover, at basic conditions, Al_2O_3 undergoes mineral dissolution:

$$0.5Al_2O_3(s) + 1.5H_2O + OH^- \leftrightarrow Al(OH)_4^- \quad (19)$$

Therefore, in this study after dispersion of Hazelwood and Weathered fly ash samples in water and increase of the solution pH, the occurrence of these two reactions might also lead to the more positive zeta potentials of the samples compared to Yallourn fly ash because of the consumption of hydroxyl groups in solution.

The solution pH seems to be an important parameter which affects the adsorption properties of the fly ash samples. This is due to the fact that the surface charge of the fly ash adsorbents is greatly affected by solution pH. This might be due to the increase in the surface potential of the adsorbents as a result of increasing solution pH. Apart from the electrostatic interactions between positively charged MB and negative charges on the surface of fly ash, the degree of adsorption could be related to the acid-base interactions of surface groups as explained below:

$$SiOH + OH^- \rightarrow SiO^- + H_2O \quad \text{pH} > 1.7 \quad (20)$$

$$AlOH + OH^- \rightarrow AlO^- + H_2O \quad \text{pH} > 7.9 \quad (21)$$

$$SiO^- + MB^+ \rightarrow SiO - MB \quad \text{basic solution} \quad (22)$$

$$AlO^- + MB^+ \rightarrow AlO - MB \quad \text{basic solution} \quad (23)$$

Silanol ($Si - O^-$) and aluminol ($Al - O^-$) are the active surface functional groups. $Si - OH$ and $Si - O^-$ represent the neutral and ionized surface hydroxyl functional groups [58, 67].

At pH values < 4 most silanol and aluminol groups are protonated [68] and thus the adsorption capacity in acidic pH is low. By increasing the pH, these functional groups attain negative charge and result in an increase in the adsorption capacity. The positive charge of methylene blue molecule is located on the sulfur atom and when MB is in contact with the adsorbent surface, it is attracted to the negative sites located on fly ash surface.

6.4.6. Thermodynamic behaviour of fly ash adsorbents

The effect of temperature on adsorption properties of fly ash samples was investigated to further understand the behaviour of these adsorbents during the adsorption process of methylene blue.

Effect of temperature on adsorption can be determined with the thermodynamic parameters like enthalpy (ΔH^o), entropy (ΔS^o) and Gibbs free energy (ΔG^o) using the following equation:

$$\Delta G° = \Delta H° - \Delta S°T \quad (24)$$

$$\Delta G° = -RT\ln K_C \quad (25)$$

Using the above relations, the van't Hoff equation can be derived as:

$$\ln K_C = \frac{\Delta S°}{R} - \frac{\Delta H°}{RT} \quad (26)$$

where Kc is the equilibrium constant and is expressed based on the relation of the dye concentration at equilibrium on the adsorbent surface to the dye concentration at equilibrium in solution which can be calculated using the following relationship:

$$K_c = \left({}^{Q_e W}/_{C_e V}\right) \quad (27)$$

where Q_e is the equilibrium adsorption capacity, C_e is equilibrium concentration, W is the weight of adsorbent and V is the volume of dye solution.

R and T represent the ideal gas constant (8.314 $Jmol^{-1}K^{-1}$) and the adsorption temperature (K). The plot of $\ln K_C$ against $1/T$ gives a linear line as shown in Fig. 6-12 (b) and the values of $\Delta H°(kJ\ mol^{-1})$ and $\Delta S°$ ($J\ mol^{-1}K^{-1}$) can be determined from the slope and intercept of van't Hoff plot as given in Table 6-8. The adsorption of MB over fly ash samples increased with increasing the temperature from 25 to 60 ºC which suggests the adsorption of MB occurs favourably at high temperatures. The positive values of $\Delta H°$ confirm that the adsorption is endothermic and it is a physical process [69].

Table 6-8. Thermodynamic parameters for adsorption of MB on fly ashes at different temperatures

	ΔGº ($KJmol^{-1}$)					
Fly ash	25 ºC	40 ºC	50 ºC	60 ºC	ΔHº ($KJmol^{-1}$)	ΔSº ($Jmol^{-1}$)
Yallourn	-10.73	-12.08	-12.99	-13.9	16.31	90.7
Weathered	-2.06	-3.5	-4.47	-5.43	26.7	96.5
Hazelwood	-0.29	-2.45	-3.88	-5.32	42.53	143.7

The change of Gibbs free energy is in the range of -20 to 0 $kJmol^{-1}$ for physisorption while it is -80 to -400 $kJmol^{-1}$ for chemisorption [70]. The $\Delta G°$of the fly ash adsorbents is negative and between -13.9 (for Yallourn) to -0.3 $kJmol^{-1}$ (for Hazelwood) over the temperature range of 25-60 ºC. The negative value of $\Delta G°$ reflects that adsorption process is spontaneous and physical [69]. The positive values of entropy of fly ashes (90, 96 and 143.6 $J\ mol^{-1}K^{-1}$) suggests an increase in disorder and randomness at the solid-solution interface [71].

6.4.7. Effect of weathering on adsorption property of Hazelwood fly ash

The reason for different adsorption behaviour and characteristics of fly ash after weathering process could be explained according to the weathering reactions and conditions

which affect the textural and mineralogical properties of fly ash materials. As mentioned in other sections, the formation of porous calcium silicates through pozzolanic reaction in the fly ash structure during weathering process contributes to the change in the physical properties of Hazelwood fly ash. There are some other reactions which occur during weathering process and lead to the change in the mineralogy of Hazelwood fly ash.

During the contact between fly ash and water, some secondary hydrated minerals including portlandite and calcite are produced. The portlandite $Ca(OH)_2$ is made by hydration of CaO and subsequently reacts with CO_2 in air based on the following equation to give calcite ($CaCO_3$):

$$Ca(OH)_{2(cr)} \rightarrow Ca(OH)_{2(aq)} + CO_2 \rightarrow CaCO_{3(cr)} + H_2O \quad (28)$$

The process of transformation of portlandite to calcite decreases the high pH. Therefore, we can notice that for the Weathered fly ash the calcium content decreases in comparison with the Hazelwood fly ash and as a result after dispersion of the Weathered fly ash in water, the pH of the mixture (pH=9.5) is lower than the pH of the Hazelwood-water system (pH=10.5).

The change in the morphology of the Hazelwood fly ash after weathering process is very obvious from the SEM images. Such changes in the morphologies which results in more porous structures and changes to chemical compositions are reported by other studies as well [72]. The changes in the morphology of weathered ash samples could be as a result of the formation of porous calcium silicate as well as secondary mineral phases including calcite which is produced through carbonation process. The carbonation process occurs via the reaction of CO_2 with alkaline contents of the fly ash materials [73].

Therefore, there are differences in the properties of the fly ash which is taken from the precipitator and the fly ash which undergoes weathering process in the ash ponds. Natural weathering in ash ponds occurs through carbonation, dissolution and co-precipitation which are

considered the main causes for the physical, chemical and mineralogical changes in fly ash. As mentioned previously, fresh fly ash obtained from precipitators is composed of quartz, mullite, hematite, magnetite and lime while the weathered ash includes additional phases like calcite and aragonite [21].

From the XRF analysis, it is observed that the concentration of Si in the fresh fly ash (5.82%) is higher than that of the weathered sample (3.86%). The decline of the concentration of SiO_2 could be due to the weathering process which results in the dissolution of fly ash and release of some major elements like SiO_2 from the sample over a period of time. This trend has been observed in other works as well [74].

6.4.8. Regeneration of fly ash materials

Regeneration of adsorbents is of great importance in wastewater treatment systems. The used fly ash adsorbents can be recycled and reused for the adsorption applications through different techniques such as heat treatment and utilizing suitable solvents. Regeneration is particularly important in terms of process expenses and reducing waste disposal to the environment. The fly ash samples were recycled using heat treatment at 200 ºC for half an hour and the regeneration was performed for five cycles. Fig. 6-13 shows the adsorption capacities of fly ash samples before and after regeneration. It is observed that after regeneration, the adsorption capacity of Yallourn fly ash only slightly decreased while the adsorption capacities of Hazelwood and Weathered fly ash decreased significantly.

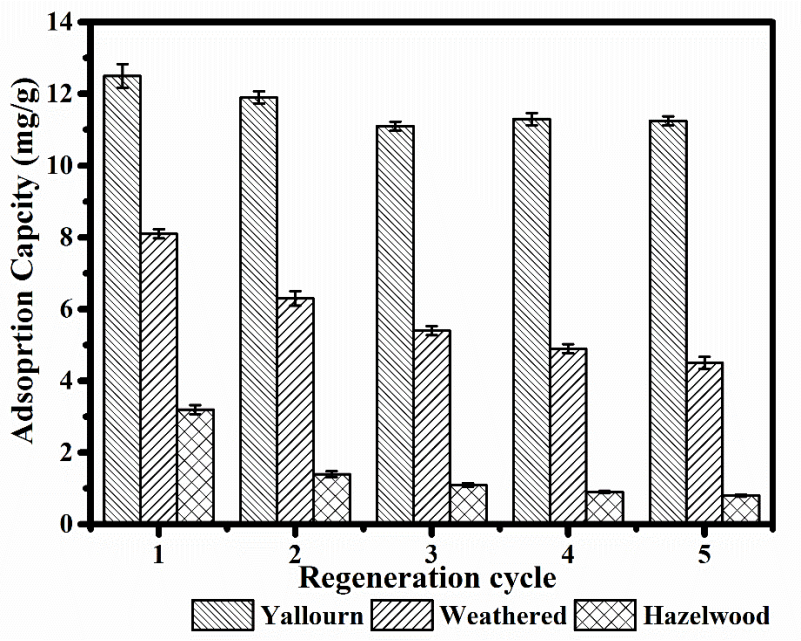

Fig. 6-13 Recyclability of the fly ash adsorbents.

This behaviour could be explained based on the chemical composition and physical characteristics of the fly ash samples. Yallourn fly ash has lower calcium content and higher surface area as well as porous spheres within its structure. However, the nonporous Hazelwood fly ash and slightly porous Weathered fly ash contain higher calcium content and lower surface areas. Therefore, after heat treatment, the adsorption sites of Yallourn fly ash are restored and it gains most of the active sites back for the adsorption. After five regeneration cycles, the adsorption capacity of Yallourn fly ash decreased by around 10%. The corresponding reduction percentages for Weathered and Hazelwood fly ashes were 44% and 75% respectively.

During the adsorption experiments the calcium content of Hazelwood and Weathered fly ashes undergoes dissolution and hydrolysis and enters the liquid phase as it is noticed from the increase of the solution pH once these ashes are brought into contact with water. Therefore, after each adsorption equilibrium some amount of calcium leaves the material matrix and this results in a significant decline in the adsorption capacity for the next adsorption runs. In this case, since Hazelwood is not porous and has low surface area, the alkalinity and the presence

of the negative surface charges resulting from the dissolution of calcium content, plays the major role for the adsorption of methylene blue dye. Therefore, since the major active adsorption components of this fly ash are lost after each experiment, the heat treatment is not effective for restoring the adsorption sites. The reduction in the adsorption capacity after heat treatment for Weathered fly ash is less compared to that of Hazelwood fly ash probably due to more porous structure which helps for the adsorption of MB molecules apart from the high calcium content.

6.4.9. Heavy metal adsorption on fly ash adsorbents

Fly ash has also potential application in heavy metal removal from water due to the physical properties such as surface area and porosity and its chemical constituents including alumina, silica, iron oxides, calcium oxide and magnesium oxide. In addition, the alkalinity of fly ash makes this material a suitable neutralizing agent especially for acidic wastewaters [5]. For example, wastewater from mining industry has high acidity which results in the dissociation of unwanted metals into the solution [75]. Thus, the usage of lime and sodium hydroxide is necessary for adjusting the pH of wastewater to maximize the removal of heavy metals by hydrous oxides [76]. Therefore, class C fly ash could be a suitable source for neutralizing the acidic wastewaters and simultaneously adsorption of toxic metals or organics. Fly ash has been investigated for the removal of several heavy metals such as Ni, Cr, Cu, Cd, As and Hg [8]. For example, fly ash was utilized for the adsorption of chromium ions [77] and cadmium [78] and it was found the removal of these ions was dependent on the solution pH, contact time, metal concentration and solution temperature.

Victorian brown coal fly ashes in this study were used for the removal of Cu, Ni, Zn and Co from water to evaluate their adsorption capabilities for toxic heavy metals. The adsorption capacities for the removal of heavy metals are shown in Fig. 6-14. The dispersion of Yallourn,

Weathered and Hazelwood fly ash materials in heavy metal (Cu, Zn, Ni and Co) solutions resulted in a range of pH from 7.5 to 8.4 for Yallourn fly ash, 8.9 to 9.6 for Hazelwood fly ash and 8.1 to 9.1 for Weathered fly ash. It can be seen that fly ash adsorbents exhibit high adsorption capacities for all of the heavy metals in particular for Cu, Zn and Ni. The extent of removal was obtained in the order of Cu (II) > Zn (II) > Ni (II) > Co (II).

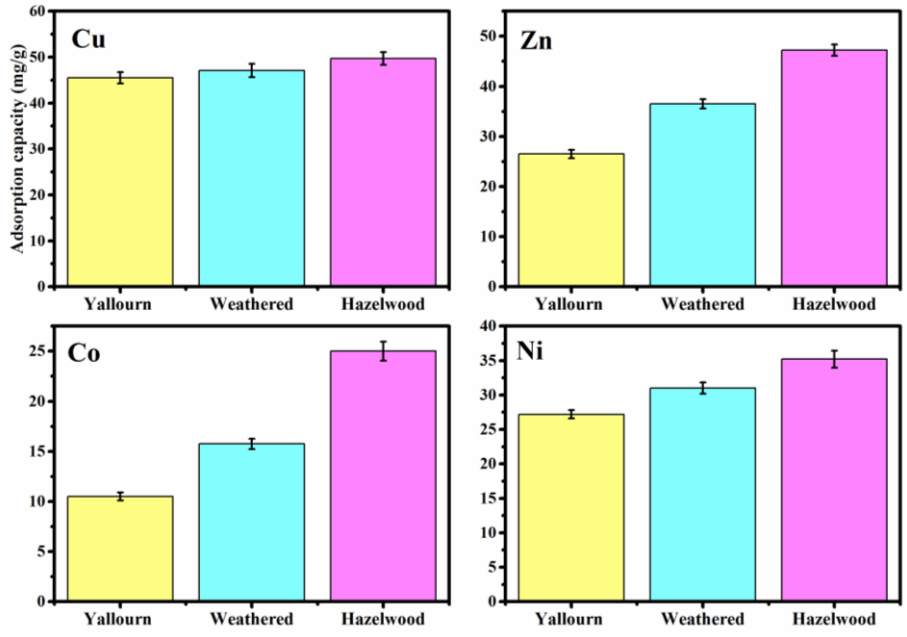

Fig. 6-14 Adsorption capacity of fly ashes for heavy metal removal (initial dye concentration 100 ppm, adsorbent dosage 0.2 g, solution volume 50 ml, pH YFA/Cu= 7.9, pH YFA/Ni= 7.8, pH YFA/Zn= 7.5, pH YFA/Co= 8.4, pH HZ/Cu=9.4, pH HZ/Ni=9.3, pH HZ/Zn= 8.9, pH HZ/Co=9.6, pH WFA/Cu=8.9, pH WFA/Ni=8.8, pH WFA/Zn=8.1 and pH WFA/Co=9.1).

It seems copper adsorbs more easily on the adsorbents compared with other metals which might be due to the better interaction of the resulting complexes with the surface of the adsorbents. This is consistent with literature data which state copper ions are adsorbed more easily compared with other metal ions which is attributed to the differences in the affinities of functional groups for metal ions [79]. Furthermore, although other studies report different orders for the affinity of the adsorbents towards Zn, Ni and Co, they frequently report the highest adsorption of Cu on different adsorbents [79-82]. Yavuz et al. reported that the order of

metal adsorption in their study was Cu (II) > Ni (II) > Co (II) and that this order might be due to the difference in hydrolysis constants as well as ionic radius, electrode potential and solubility of the metal hydroxides as shown in Table 6-9 [83, 84]. Coper ion has the smallest ionic radius which indicates copper can be adsorbed better compared with other ions. Moreover, it has the most positive electron potential which means it has more affinity for electrons on the negatively charged surfaces of the fly ash samples. The solubility product constant (K_{sp}) of copper hydroxide is the lowest which addresses that in high alkaline conditions in which the metal hydroxides are produced, the copper hydroxide has the lowest solubility and can be precipitated and adsorbed much better compared with other metal ions.

Table 6-9. Hydrolysis constants (pK_h), ionic radius, solubility constant (K_{sp}) and electrode potential of metal ions [83, 84].

Metal ion	Co (II)	Ni (II)	Zn (II)	Cu (II)
pK_h	9.6	9.4	8.96	7.34
Ionic radius (A^o)	0.74	0.72	0.74	0.70
Electrode potential (V)	-0.28	-0.25	-0.76	0.34
K_{sp} of $M(OH)_2$	5.92×10^{-15}	5.48×10^{-16}	3×10^{-17}	2.2×10^{-20}

The highest adsorption capacities were achieved for the removal of Cu, Zn, Ni and Co using Hazelwood fly ash with the capacities of 49.7, 47.2, 35.2 and 25 mg/g respectively. The adsorption performance and efficiency decreased in the order of Hazelwood > Weathered > Yallourn fly ash. The better performance of Hazelwood fly ash could be attributed to its higher alkalinity and calcium content. Yallourn fly ash shows the lowest adsorption uptake despite having the highest surface area. This observation reveals that adsorption of heavy metals might mostly depend on the surface charge of the adsorbent and solution pH rather than the surface area. There are similar evidence in literature that suggest the adsorption of heavy metals is very related to the soluble lime (CaO) content of fly ashes [76]. Therefore, the high adsorption

capacity is associated with the electrostatic interaction of the positively charged heavy metals by the negatively charged surface of the adsorbents.

Different mechanisms have been reported to explain the adsorption of heavy metals in aqueous solutions. Ricou-Hoeffer et al. [85] reported that alumina silicate components in fly ash probably contribute to the adsorption process via a SiO_2 bond with metal ions. Bayat [76] also reported that the fly ashes having low content of SiO_2, Al_2O_3 and Fe_2O_3 and high CaO content are more efficient for the removal of metal ions because of the formation of calcium and silica complexes like calcium silicates ($2CaO.SiO_2$). It was suggested that adsorption occurs mostly on the calcium silicates interface through the interaction of hydrolysis forms of metals with surface as follows:

In acidic conditions

$$Si - OH \cdots H - O - H[Me(OH_2)_3]^{2+} \leftrightarrow Si - OMe + H_3O^+ \quad (29)$$

In neutral conditions

$$mCaSiO_3HSiO_3^- + MeOH^+ \leftrightarrow mCaSiO_3MeSiO_3 + H_2O \quad (30)$$

In alkaline conditions

$$mCaSiO_3HSiO_3^- + Me(OH)_2 \leftrightarrow mCaSiO_3MeSiO_3 + H_2O + OH^- \quad (31)$$

where Me is a bivalent metal ion.

Since the dispersion of Yallourn fly ash in heavy metal solutions results in an almost neutral condition (pH=7.5-8.4), the second proposed mechanism can be related to the adsorptive removal of metals onto this material. The third mechanism also can be considered for the adsorption of metals onto Hazelwood (pH=8.9-9.6) and Weathered fly ashes (pH=8.1-9.1) since they provide a basic environment once dispersed in heavy metal solutions.

The other adsorption mechanisms which could be considered in fly ash systems are the interaction of metal ions by silica and alumina content of fly ash by the formation of complexes in the solution system. The metal ion cations can be adsorbed by chemical bonding with the active site (≡SiO^-) and (≡AlO^-) and can form complexes on the surface as illustrated by the following equations [86]:

$$2(\equiv SiO^-) + M^{2+} \rightarrow (\equiv Si - O)_2 M \quad (32)$$

$$2(\equiv AlO^-) + M^{2+} \rightarrow (\equiv Al - O)_2 M \quad (33)$$

It is also suggested that the metal compounds are the hydrated cations which can be adsorbed with partial or total de-hydration:

$$Substrate + Me(H_2O)_n^{z+} \leftrightarrow substrate - Me(H_2O)_{n-x}^{z+} + xH_2O \quad (34)$$

where $0 \leq x \leq n$.

Functional oxides including SiO_2, Al_2O_3, Fe_2O_3 and CaO on the surface of fly ash have a significant role in removing the metal ions from water. Depending on the pH of solution and the acid-base conditions, SiO_2 in fly ash could uptake positive and negative pollutants [76]. The central ion of silicate components has affinity towards electrons resulting in the bounding between the oxygen atoms and its low basicity. Therefore, the surface of silica acts as a weak acid and is able to react with water to produce silanol groups (SiOH). Consequently, the surface of silica becomes positively charged at low pH while it becomes negatively charged in high pH conditions. The point of zero charge for silica is about 2 [87] and that of Fe_2O_3 and Al_2O_3 is 6.7 and 8.5 respectively [88]. Therefore, the high adsorptive removal of metals over the fly ash samples specifically Hazelwood fly ash could be due to the electrostatic interaction of metals with surface iron and alumina sites as well as calcium sites which introduce negative charges on the surface.

Dissolved calcium increases the pH of the solution above the solubility point and leads to the precipitation of metals as metal hydroxides or metal oxides [89]. The precipitation of heavy metals depends on the hydration and dissolution of fly ash materials and their components. The major component of Hazelwood and Weathered fly ash is calcium oxide which undergoes hydration and hydrolysis based on the following reaction:

$$CaO + H_2O \rightarrow Ca^{2+} + 2OH^- \quad (35)$$

When fly ash is dispersed in water, the solid components in fly ash such as $Ca_2Al_2SiO_7$ can release hydroxyl ions gradually according to the following equation:

$$Ca_2Al_2SiO_7 + 7H_2O \rightarrow H_4SiO_4 + 2Al(OH)_3 + 2Ca^{2+} + 4OH^- \quad (36)$$

When the fly ash in solution is brought up in contact with heavy metal ions, sorption and precipitation take place. The hydroxyl ions contribute to the production and precipitation of metal hydroxides. The precipitation of metals by lime is affected by the chemistry of solution and the pH at equilibrium. Cu^{2+} species are formed in solutions up to pH of around 6. The copper hydroxyl species such as $CuOH^+$, $[Cu_2(OH)_2]^{2+}$, $Cu(OH)_2$ and $[Cu(OH)_3]^-$ increases at pH > 5. When the solution pH increases up to 6-8 and 8-12, $Cu_2(OH)_2^{2+}$ and $Cu(OH)_2$ species of copper are formed respectively [90]. Therefore, at high pH conditions, these metal species could precipitate as copper hydroxide compounds ($2Ca(OH)_2^{4-}Cu(OH)_2.H_2O$) [91].

Zinc exists as Zn^{2+}ions at pH < 7.5 and it forms the zinc hydroxides at pH 8-10. The prevalent species of zinc at pH 7.5-11.5 and pH > 11.5 are $Zn(OH)_2$ and $Zn(OH)_3^-$ respectively [90]. Moreover, at pH 7-12 a calcium-zinc hydrated complex $CaZn_2(OH)_6.2H_2O$ might be formed [91].

These investigations indicate that apart from electrostatic attractions between metal ions and the adsorbent's surface, heavy metals adsorption onto fly ash materials mostly occurs

through precipitation of the metal hydroxides at high pH. This can be addressed to the higher metal removal efficiency of Hazelwood fly ash despite having the lowest surface area and nonporosity. Since Hazelwood and Weathered fly ashes have higher calcium content, they introduce more hydroxyl ions in water which leads to the precipitation of metal hydroxides.

Experimental results from literature indicate that heavy metals leaching from the coal fly ash is fairly low [61] and the amount of leaching depends on the conditions of aqueous environment. The amount of trace metals in the leachate depends on a variety of factors including the weight of fly ash, solution pH, percentage of elements, temperature, pressure and the contact time. The fast leaching of most of the trace metals from fly ash particles occurs in low pH values and the trace elements level does not exceed the standard limits [61]. Therefore, since the alkaline Victorian brown coal fly ashes provide a neutral to basic environment it seems they can be used for the removal of dyes and heavy metals without any trace metal leaching to the environment.

Adsorption capacity of Victorian brown coal fly ash samples for heavy metals is compared with other fly ash and adsorbents from literature in Table 6-10. This comparison reveals that, the fly ash samples in our study have greater and comparable adsorption capabilities in comparison with the other fly ash adsorbents investigated so far.

Table 6-10. Comparison of adsorption capacities of heavy metals on different adsorbents

Metal	Adsorbent	Adsorption pH	Capacity (mg/g)	Reference
Zn^{2+}	Fly ash	6.5	6.5-13.3	[92]
	Fly ash	7.5	0.25-2.8	[93]
	Bagasse fly ash	4	13.21	[94]
	Fly ash	4	7.84	[95]
	Activated carbon	7	19.9	[96]
	Yallourn fly ash	7.5	26.5	This study
	Weathered fly ash	8.1	36.5	This study
	Hazelwood fly ash	8.9	47.2	This study
Cu^{2+}	Fly ash	9	20.92	[97]
	Fly ash	5	7.5	[98]
	Fly ash	5	1.7-8.1	[99]
	Bagasse fly ash	4	2.26-2.36	[100]
	Activated carbon	NA	38	[101]
	Yallourn fly ash	7.9	45.5	This study
	Weathered fly ash	8.9	47.1	This study
	Hazelwood fly ash	9.4	49.7	This study
Ni^{2+}	Fly ash	6	9-14	[92]
	Bagasse fly ash	6.5	1.12-1.7	[102]
	Fly ash	7-8	0.4-0.98	[5]
	Activated carbon	5	30.7	[103]
	Yallourn fly ash	7.8	27.2	This study
	Weathered fly ash	8.8	31	This study
	Hazelwood fly ash	9.3	35.2	This study

Table 6-10. (Continued)

Metal	Adsorbent	Adsorption pH	Capacity (mg/g)	Reference
Co^{2+}	African coal fly ash	4	0.4	[104]
	Battery waste	NA	35	[105]
	Activated carbon from rice hills	6.5	10.95	[106]
	Activated carbon from hazelnut	6	13.88	[107]
	Resin	5.3	5.3	[108]
	Yallourn fly ash	8.4	10.5	This study
	Weathered fly ash	9.1	15.75	This study
	Hazelwood fly ash	9.6	25	This study

6.4.10. Magnetic property

Magnetic behaviour of iron rich fly ash materials are due to the presence and formation of magnetite (Fe_3O_4) from iron containing minerals in coal during the combustion process. the amount of iron in the magnetic fraction might be more than 40% which shows that fly ash particles are very heterogeneous from chemical and mineralogical point of view [109]. In this study, Yallourn fly ash exhibited magnetic property as shown in Fig. 6-15. Therefore, after adsorption of methylene blue dye and heavy metals, the fly ash particles can be easily separated from water. The iron concentration is about 47% for Yallourn fly ash whereas those of Hazelwood and Weathered fly ash are 14 and 16% respectively as reflected in the XRF data. Hazelwood and Weathered fly ash did not show any magnetic behaviour due to the low iron content.

Fig. 6-15 Magnetic property of Yallourn fly ash

6.5. Conclusions

Victorian brown coal fly ash samples, namely Yallourn, Hazelwood and Weathered fly ash have been studied for the adsorption of a basic dye and heavy metals from aqueous solution. Yallourn fly ash exhibited the highest adsorption performance (12.5 mg/g) for dye removal followed by Weathered (8.1 mg/g) and Hazelwood (3.2 mg/g) fly ashes. The adsorption process for MB removal was characterized by Langmuir isotherm and followed pseudo second order kinetic model. It was shown that both intraparticle diffusion and external mass transfer involved in governing the adsorption rate while external mass transfer was probably the main rate controlling step. Adsorption of methylene blue was favoured in basic conditions and high temperatures indicating the adsorption process is endothermic. Hazelwood fly ash had the highest capacity for the removal of heavy metals due to its highly alkaline nature followed by Weathered and Yallourn fly ash samples. Magnetic property of Yallourn fly ash makes it an even more interesting adsorbent for adsorptive removal of pollutants from water. Victorian brown coal fly ashes exhibited high removal efficiency particularly for heavy metals. Since once dispersed in water, fly ash provides an alkaline conditions, it can be a good candidate for neutralizing acidic wastewaters such as mining wastewater and simultaneously for the removal

of toxic heavy metals from water. The results of heavy metal adsorption revealed that Yallourn fly ash is more suitable for heavy metal removal from neutral wastewaters since it provides almost neutral conditions once dispersed in water while Hazelwood and Weathered fly ash are mostly suitable for the adsorption of heavy metals from acidic wastewaters since they produce high alkalinity in water.

6.6. References

1. Wang, S., Y. Boyjoo, and A. Choueib, *A comparative study of dye removal using fly ash treated by different methods.* Chemosphere, 2005. **60**(10): p. 1401-1407.
2. Janoš, P., H. Buchtová, and M. Rýznarová, *Sorption of dyes from aqueous solutions onto fly ash.* Water research, 2003. **37**(20): p. 4938-4944.
3. Tan, I., A. Ahmad, and B. Hameed, *Adsorption of basic dye using activated carbon prepared from oil palm shell: batch and fixed bed studies.* Desalination, 2008. **225**(1): p. 13-28.
4. Ghosh, D. and K.G. Bhattacharyya, *Adsorption of methylene blue on kaolinite.* Applied Clay Science, 2002. **20**(6): p. 295-300.
5. Bayat, B., *Comparative study of adsorption properties of Turkish fly ashes: I. The case of nickel(II), copper(II) and zinc(II).* Journal of Hazardous Materials, 2002. **95**(3): p. 251-273.
6. Crini, G., *Non-conventional low-cost adsorbents for dye removal: A review.* Bioresource Technology, 2006. **97**(9): p. 1061-1085.
7. Rafatullah, M., O. Sulaiman, R. Hashim, and A. Ahmad, *Adsorption of methylene blue on low-cost adsorbents: A review.* Journal of Hazardous Materials, 2010. **177**(1–3): p. 70-80.
8. Ahmaruzzaman, M., *A review on the utilization of fly ash.* Progress in Energy and Combustion Science, 2010. **36**(3): p. 327-363.
9. Singh, N., *Adsorption of herbicides on coal fly ash from aqueous solutions.* Journal of Hazardous Materials, 2009. **168**(1): p. 233-237.
10. Sun, D., X. Zhang, Y. Wu, and X. Liu, *Adsorption of anionic dyes from aqueous solution on fly ash.* Journal of Hazardous Materials, 2010. **181**(1–3): p. 335-342.
11. Dizge, N., C. Aydiner, E. Demirbas, M. Kobya, and S. Kara, *Adsorption of reactive dyes from aqueous solutions by fly ash: Kinetic and equilibrium studies.* Journal of Hazardous Materials, 2008. **150**(3): p. 737-746.
12. Wang, S., Y. Boyjoo, A. Choueib, and Z.H. Zhu, *Removal of dyes from aqueous solution using fly ash and red mud.* Water Research, 2005. **39**(1): p. 129-138.
13. Hsu, T.-C., C.-C. Yu, and C.-M. Yeh, *Adsorption of Cu^{2+} from water using raw and modified coal fly ashes.* Fuel, 2008. **87**(7): p. 1355-1359.
14. Brunori, C., S. Balzamo, and R. Morabito, *Comparison between different leaching tests for the evaluation of metal release from fly ash.* Fresenius' Journal of Analytical Chemistry, 2001. **371**(6): p. 843-848.
15. Gupta, V.K., D. Mohan, S. Sharma, and M. Sharma, *Removal of basic dyes (rhodamine B and methylene blue) from aqueous solutions using bagasse fly ash.* Separation Science and Technology, 2000. **35**(13): p. 2097-2113.
16. Mudd, G.M. and J. Kodikara, *Field studies of the leachability of aged brown coal ash.* Journal of Hazardous Materials, 2000. **76**(2–3): p. 159-192.
17. Mudd, G.M., T.R. Weaver, J. Kodikara, and T. McKinley. *Groundwater chemistry of the Latrobe Valley influenced by coal ash disposal-1: Dissimilatory sulphate reduction and acid buffering*. in *International Association of Hydrogeologists Conference: Groundwater: Sustainable Solutions, Melbourne, VIC*. 1998.
18. Vassilev, S.V. and C.G. Vassileva, *A new approach for the classification of coal fly ashes based on their origin, composition, properties, and behaviour.* Fuel, 2007. **86**(10): p. 1490-1512.

19. Iyer, R. and J. Scott, *Power station fly ash—a review of value-added utilization outside of the construction industry.* Resources, Conservation and Recycling, 2001. **31**(3): p. 217-228.
20. Fernández-Jiménez, A. and A. Palomo, *Characterisation of fly ashes. Potential reactivity as alkaline cements☆.* Fuel, 2003. **82**(18): p. 2259-2265.
21. Muriithi, G.N., L.F. Petrik, O. Fatoba, W.M. Gitari, F.J. Doucet, J. Nel, S.M. Nyale, and P.E. Chuks, *Comparison of CO2 capture by ex-situ accelerated carbonation and in in-situ naturally weathered coal fly ash.* Journal of Environmental Management, 2013. **127**(0): p. 212-220.
22. Hosseini, T., B. Han, C. Selomulya, N. Haque, and L. Zhang, *Chemical and morphological changes of weathered Victorian brown coal fly ash and its leaching characteristic upon the leaching in ammonia chloride and hydrochloric acid.* Hydrometallurgy, 2015. **157**: p. 22-32.
23. Hosseini, T., C. Selomulya, N. Haque, and L. Zhang, *Indirect Carbonation of Victorian Brown Coal Fly Ash for CO2 Sequestration: Multiple-Cycle Leaching-Carbonation and Magnesium Leaching Kinetic Modeling.* Energy & Fuels, 2014. **28**(10): p. 6481-6493.
24. Gong, G., S. Ye, Y. Tian, Q. Wang, J. Ni, and Y. Chen, *Preparation of a new sorbent with hydrated lime and blast furnace slag for phosphorus removal from aqueous solution.* Journal of Hazardous Materials, 2009. **166**(2–3): p. 714-719.
25. Lin, R.-B., S.-M. Shih, and C.-F. Liu, *Structural Properties and Reactivities of Ca(OH)2/Fly Ash Sorbents for Flue Gas Desulfurization.* Industrial & Engineering Chemistry Research, 2003. **42**(7): p. 1350-1356.
26. Fernández, J., M.J. Renedo, A. Pesquera, and J.A. Irabien, *Effect of CaSO4 on the structure and use of Ca(OH)2/fly ash sorbents for SO2 removal.* Powder Technology, 2001. **119**(2–3): p. 201-205.
27. Taylor, H.F.W., *Cement Chemistry*. 1997: Thomas Telford.
28. Vimonses, V., B. Jin, and C.W.K. Chow, *Insight into removal kinetic and mechanisms of anionic dye by calcined clay materials and lime.* Journal of Hazardous Materials, 2010. **177**(1–3): p. 420-427.
29. Paper, I., *FT-IR analysis of Neyveli lignite and fly ash samples.* Indian Journal of Pure & Applied Physics, 2001. **40**: p. 207-212.
30. Guo, X., H. Shi, L. Chen, and W.A. Dick, *Alkali-activated complex binders from class C fly ash and Ca-containing admixtures.* Journal of Hazardous Materials, 2010. **173**(1–3): p. 480-486.
31. Akinyemi, S.A., A. Akinlua, W.M. Gitari, and L.F. Petrik, *Mineralogy and Mobility Patterns of Chemical Species in Weathered Coal Fly Ash.* Energy Sources, Part A: Recovery, Utilization, and Environmental Effects, 2011. **33**(8): p. 768-784.
32. Mohan, S. and R. Gandhimathi, *Removal of heavy metal ions from municipal solid waste leachate using coal fly ash as an adsorbent.* Journal of Hazardous Materials, 2009. **169**(1–3): p. 351-359.
33. Guo, X., H. Shi, and W.A. Dick, *Compressive strength and microstructural characteristics of class C fly ash geopolymer.* Cement and Concrete Composites, 2010. **32**(2): p. 142-147.
34. Torad, N.L., M. Hu, S. Ishihara, H. Sukegawa, A.A. Belik, M. Imura, K. Ariga, Y. Sakka, and Y. Yamauchi, *Direct Synthesis of MOF-Derived Nanoporous Carbon with Magnetic Co Nanoparticles toward Efficient Water Treatment.* Small, 2014. **10**(10): p. 2096-2107.

35. Kumar, K.V., V. Ramamurthi, and S. Sivanesan, *Modeling the mechanism involved during the sorption of methylene blue onto fly ash.* Journal of Colloid and Interface Science, 2005. **284**(1): p. 14-21.
36. Basava Rao, V.V. and S. Ram Mohan Rao, *Adsorption studies on treatment of textile dyeing industrial effluent by flyash.* Chemical Engineering Journal, 2006. **116**(1): p. 77-84.
37. Lin, J.X., S.L. Zhan, M.H. Fang, X.Q. Qian, and H. Yang, *Adsorption of basic dye from aqueous solution onto fly ash.* Journal of Environmental Management, 2008. **87**(1): p. 193-200.
38. Wang, S. and Z.H. Zhu, *Sonochemical treatment of fly ash for dye removal from wastewater.* Journal of Hazardous Materials, 2005. **126**(1–3): p. 91-95.
39. Wang, S., Q. Ma, and Z.H. Zhu, *Characteristics of coal fly ash and adsorption application.* Fuel, 2008. **87**(15–16): p. 3469-3473.
40. Woolard, C.D., J. Strong, and C.R. Erasmus, *Evaluation of the use of modified coal ash as a potential sorbent for organic waste streams.* Applied Geochemistry, 2002. **17**(8): p. 1159-1164.
41. El-Shafey, E.I., S.N.F. Ali, S. Al-Busafi, and H.A.J. Al-Lawati, *Preparation and characterization of surface functionalized activated carbons from date palm leaflets and application for methylene blue removal.* Journal of Environmental Chemical Engineering, 2016. **4**(3): p. 2713-2724.
42. Dąbrowski, A., *Adsorption — from theory to practice.* Advances in Colloid and Interface Science, 2001. **93**(1–3): p. 135-224.
43. Wang, S. and Z. Zhu, *Characterisation and environmental application of an Australian natural zeolite for basic dye removal from aqueous solution.* Journal of Hazardous materials, 2006. **136**(3): p. 946-952.
44. Weber, T.W. and R.K. Chakravorti, *Pore and solid diffusion models for fixed-bed adsorbers.* AIChE Journal, 1974. **20**(2): p. 228-238.
45. Bulut, Y. and H. Aydın, *A kinetics and thermodynamics study of methylene blue adsorption on wheat shells.* Desalination, 2006. **194**(1–3): p. 259-267.
46. Ho, Y.S. and G. McKay, *Pseudo-second order model for sorption processes.* Process Biochemistry, 1999. **34**(5): p. 451-465.
47. Keleşoğlu, S., M. Kes, L. Sütçü, and H. Polat, *Adsorption of Methylene Blue from Aqueous Solution on High Lime Fly Ash: Kinetic, Equilibrium, and Thermodynamic Studies.* Journal of Dispersion Science and Technology, 2012. **33**(1): p. 15-23.
48. Weber, W.J. and J.C. Morris, *Kinetics of adsorption on carbon from solution.* Journal of the Sanitary Engineering Division, 1963. **89**(2): p. 31-60.
49. Doğan, M., M. Alkan, A. Türkyilmaz, and Y. Özdemir, *Kinetics and mechanism of removal of methylene blue by adsorption onto perlite.* Journal of Hazardous Materials, 2004. **109**(1–3): p. 141-148.
50. Özcan, A.S., B. Erdem, and A. Özcan, *Adsorption of Acid Blue 193 from aqueous solutions onto BTMA-bentonite.* Colloids and Surfaces A: Physicochemical and Engineering Aspects, 2005. **266**(1): p. 73-81.
51. Poots, V., G. McKay, and J. Healy, *Removal of basic dye from effluent using wood as an adsorbent.* Journal (Water Pollution Control Federation), 1978: p. 926-935.
52. Yao, Y., F. Xu, M. Chen, Z. Xu, and Z. Zhu, *Adsorption behavior of methylene blue on carbon nanotubes.* Bioresource Technology, 2010. **101**(9): p. 3040-3046.

53. Kannan, N. and M.M. Sundaram, *Kinetics and mechanism of removal of methylene blue by adsorption on various carbons—a comparative study.* Dyes and Pigments, 2001. **51**(1): p. 25-40.
54. Ho, Y.S. and G. McKay, *The kinetics of sorption of basic dyes from aqueous solution by sphagnum moss peat.* The Canadian Journal of Chemical Engineering, 1998. **76**(4): p. 822-827.
55. McKay, G., M.S. Otterburn, and J.A. Aga, *Intraparticle diffusion process occurring during adsorption of dyestuffs.* Water, Air, and Soil Pollution, 1987. **36**(3): p. 381-390.
56. Allen, S.J., G. McKay, and K.Y.H. Khader, *Intraparticle diffusion of a basic dye during adsorption onto sphagnum peat.* Environmental Pollution, 1989. **56**(1): p. 39-50.
57. Reichenberg, D., *Properties of Ion-Exchange Resins in Relation to their Structure. III. Kinetics of Exchange.* Journal of the American Chemical Society, 1953. **75**(3): p. 589-597.
58. Banerjee, S., G.C. Sharma, M.C. Chattopadhyaya, and Y.C. Sharma, *Kinetic and equilibrium modeling for the adsorptive removal of methylene blue from aqueous solutions on of activated fly ash (AFSH).* Journal of Environmental Chemical Engineering, 2014. **2**(3): p. 1870-1880.
59. Michelson, L., P. Gideon, E. Pace, and L. Kutal, *US department industry, office of water research and technology.* Bulletin, 1975. **74**.
60. Singh, K.K., R. Rastogi, and S.H. Hasan, *Removal of Cr(VI) from wastewater using rice bran.* Journal of Colloid and Interface Science, 2005. **290**(1): p. 61-68.
61. Ahmaruzzaman, M., *Role of Fly Ash in the Removal of Organic Pollutants from Wastewater.* Energy & Fuels, 2009. **23**(3): p. 1494-1511.
62. Malek, R.I.A. and D.M. Roy, *Electrokinetic Phenomena and Surface Characteristics of Fly Ash Particles.* MRS Proceedings, 1984. **43**.
63. Vimonses, V., B. Jin, C.W.K. Chow, and C. Saint, *Enhancing removal efficiency of anionic dye by combination and calcination of clay materials and calcium hydroxide.* Journal of Hazardous Materials, 2009. **171**(1–3): p. 941-947.
64. Kaya, A. and Y. Yukselen, *Zeta potential of clay minerals and quartz contaminated by heavy metals.* Canadian Geotechnical Journal, 2005. **42**(5): p. 1280-1289.
65. Kim, A.G., G. Kazonich, and M. Dahlberg, *Relative Solubility of Cations in Class F Fly Ash.* Environmental Science & Technology, 2003. **37**(19): p. 4507-4511.
66. Goyne, K.W., A.R. Zimmerman, B.L. Newalkar, S. Komarneni, S.L. Brantley, and J. Chorover, *Surface Charge of Variable Porosity Al2O3(s) and SiO2(s) Adsorbents.* Journal of Porous Materials, 2002. **9**(4): p. 243-256.
67. Weng, C.-H. and Y.-F. Pan, *Adsorption of a cationic dye (methylene blue) onto spent activated clay.* Journal of Hazardous Materials, 2007. **144**(1): p. 355-362.
68. Ai, L., Y. Zhou, and J. Jiang, *Removal of methylene blue from aqueous solution by montmorillonite/CoFe2O4 composite with magnetic separation performance.* Desalination, 2011. **266**(1–3): p. 72-77.
69. Fu, J., Z. Chen, M. Wang, S. Liu, J. Zhang, J. Zhang, R. Han, and Q. Xu, *Adsorption of methylene blue by a high-efficiency adsorbent (polydopamine microspheres): Kinetics, isotherm, thermodynamics and mechanism analysis.* Chemical Engineering Journal, 2015. **259**: p. 53-61.
70. Chu, B.S., B.S. Baharin, Y.B. Che Man, and S.Y. Quek, *Separation of vitamin E from palm fatty acid distillate using silica: I Equilibrium of batch adsorption.* Journal of Food Engineering, 2004. **62**(1): p. 97-103.

71. Liu, R.-L., Y. Liu, X.-Y. Zhou, Z.-Q. Zhang, J. Zhang, and F.-Q. Dang, *Biomass-derived highly porous functional carbon fabricated by using a free-standing template for efficient removal of methylene blue.* Bioresource Technology, 2014. **154**: p. 138-147.
72. Cheerarot, R. and C. Jaturapitakkul, *A study of disposed fly ash from landfill to replace Portland cement.* Waste Management, 2004. **24**(7): p. 701-709.
73. Yeheyis, M.B., J.Q. Shang, and E.K. Yanful. *Chemical and mineralogical transformations of coal fly ash after landfilling*. in *Proceedings of*. 2009.
74. Eze, C.P., S.M. Nyale, R.O. Akinyeye, W.M. Gitari, S.A. Akinyemi, O.O. Fatoba, and L.F. Petrik, *Chemical, mineralogical and morphological changes in weathered coal fly ash: A case study of a brine impacted wet ash dump.* Journal of Environmental Management, 2013. **129**(0): p. 479-492.
75. Dharmappa, H., M. Sivakumar, and R. Singh, *Wastewater characteristics, management and reuse in mining and minerals processing industries*. 2002, Vol. I ed. sl: Oxford, UK.
76. Bayat, B., *Comparative study of adsorption properties of Turkish fly ashes: II. The case of chromium (VI) and cadmium (II).* Journal of Hazardous Materials, 2002. **95**(3): p. 275-290.
77. Dasmahapatra, G., T. Pal, A. Bhadra, and B. Bhattacharya, *Studies on separation characteristics of hexavalent chromium from aqueous solution by fly ash.* Separation science and technology, 1996. **31**(14): p. 2001-2009.
78. Yadava, K., B. Tyagi, K. Panday, and V. Singh, *Fly ash for the treatment of Cd (II) rich effluents.* Environmental Technology, 1987. **8**(1-12): p. 225-234.
79. Chen, J.P. and X. Wang, *Removing copper, zinc, and lead ion by granular activated carbon in pretreated fixed-bed columns.* Separation and Purification Technology, 2000. **19**(3): p. 157-167.
80. Liu, C. and R. Bai, *Extended study of DETA-functionalized PGMA adsorbent in the selective adsorption behaviors and mechanisms for heavy metal ions of Cu, Co, Ni, Zn, and Cd.* Journal of Colloid and Interface Science, 2010. **350**(1): p. 282-289.
81. Kalmykova, Y., A.-M. Strömvall, and B.-M. Steenari, *Adsorption of Cd, Cu, Ni, Pb and Zn on Sphagnum peat from solutions with low metal concentrations.* Journal of Hazardous Materials, 2008. **152**(2): p. 885-891.
82. Jong, T. and D.L. Parry, *Adsorption of Pb(II), Cu(II), Cd(II), Zn(II), Ni(II), Fe(II), and As(V) on bacterially produced metal sulfides.* Journal of Colloid and Interface Science, 2004. **275**(1): p. 61-71.
83. Yavuz, Ö., Y. Altunkaynak, and F. Güzel, *Removal of copper, nickel, cobalt and manganese from aqueous solution by kaolinite.* Water Research, 2003. **37**(4): p. 948-952.
84. Dean, J.A. and N.A. Lange, *Lange's handbook of chemistry*. 1973.
85. Ricou-Hoeffer, P., I. Lecuyer, and P. Le Cloirec, *Experimental design methodology applied to adsorption of metallic ions onto fly ash.* Water Research, 2001. **35**(4): p. 965-976.
86. Visa, M., L. Isac, and A. Duta, *Fly ash adsorbents for multi-cation wastewater treatment.* Applied Surface Science, 2012. **258**(17): p. 6345-6352.
87. Panday, K.K., G. Prasad, and V.N. Singh, *Copper(II) removal from aqueous solutions by fly ash.* Water Research, 1985. **19**(7): p. 869-873.
88. Förstner, U. and G.T. Wittmann, *Metal pollution in the aquatic environment*. 2012: Springer Science & Business Media.

89. Aziz, H.A., M.N. Adlan, and K.S. Ariffin, *Heavy metals (Cd, Pb, Zn, Ni, Cu and Cr(III)) removal from water in Malaysia: Post treatment by high quality limestone.* Bioresource Technology, 2008. **99**(6): p. 1578-1583.
90. Xue, Y., H. Hou, and S. Zhu, *Competitive adsorption of copper(II), cadmium(II), lead(II) and zinc(II) onto basic oxygen furnace slag.* Journal of Hazardous Materials, 2009. **162**(1): p. 391-401.
91. Chen, Q., Z. Luo, C. Hills, G. Xue, and M. Tyrer, *Precipitation of heavy metals from wastewater using simulated flue gas: Sequent additions of fly ash, lime and carbon dioxide.* Water Research, 2009. **43**(10): p. 2605-2614.
92. Banerjee, S., R. Jayaram, and M. Joshi, *Removal of nickel (II) and zinc (II) from wastewater using fly ash and impregnated fly ash.* Separation science and technology, 2003. **38**(5): p. 1015-1032.
93. Bayat, B., *Combined removal of zinc (II) and cadmium (II) from aqueous solutions by adsorption onto high-calcium Turkish fly ash.* Water, Air, and Soil Pollution, 2002. **136**(1-4): p. 69-92.
94. Gupta, V.K. and S. Sharma, *Removal of zinc from aqueous solutions using bagasse fly ash− a low cost adsorbent.* Industrial & engineering chemistry research, 2003. **42**(25): p. 6619-6624.
95. Pehlivan, E., S. Cetin, and B. Yanık, *Equilibrium studies for the sorption of zinc and copper from aqueous solutions using sugar beet pulp and fly ash.* Journal of hazardous materials, 2006. **135**(1): p. 193-199.
96. Leyva Ramos, R., L.A. Bernal Jacome, J. Mendoza Barron, L. Fuentes Rubio, and R.M. Guerrero Coronado, *Adsorption of zinc(II) from an aqueous solution onto activated carbon.* Journal of Hazardous Materials, 2002. **90**(1): p. 27-38.
97. Papandreou, A., C. Stournaras, and D. Panias, *Copper and cadmium adsorption on pellets made from fired coal fly ash.* Journal of Hazardous Materials, 2007. **148**(3): p. 538-547.
98. Ricou, P., I. Lecuyer, and P. Le Cloirec, *Removal of Cu2+, Zn2+ and Pb2+ by adsorption onto fly ash and fly ash/lime mixing.* Water Science and Technology, 1999. **39**(10-11): p. 239-247.
99. Ayala, J., F. Blanco, P. García, P. Rodriguez, and J. Sancho, *Asturian fly ash as a heavy metals removal material.* Fuel, 1998. **77**(11): p. 1147-1154.
100. Gupta, V.K. and I. Ali, *Utilisation of bagasse fly ash (a sugar industry waste) for the removal of copper and zinc from wastewater.* Separation and purification technology, 2000. **18**(2): p. 131-140.
101. Monser, L. and N. Adhoum, *Modified activated carbon for the removal of copper, zinc, chromium and cyanide from wastewater.* Separation and Purification Technology, 2002. **26**(2–3): p. 137-146.
102. Gupta, V.K., C. Jain, I. Ali, M. Sharma, and V. Saini, *Removal of cadmium and nickel from wastewater using bagasse fly ash—a sugar industry waste.* Water Research, 2003. **37**(16): p. 4038-4044.
103. Hasar, H., *Adsorption of nickel(II) from aqueous solution onto activated carbon prepared from almond husk.* Journal of Hazardous Materials, 2003. **97**(1–3): p. 49-57.
104. Musapatika, E.T., M.S. Onyango, and O. Aoyi, *Cobalt(II) removal from synthetic wastewater by adsorption on South African coal fly ash.* South African Journal of Science, 2010. **106**: p. 1-7.

105. Bhatnagar, A., A.K. Minocha, B.H. Jeon, and J.M. Park, *Adsorptive Removal of Cobalt from Aqueous Solutions by Utilizing Industrial Waste and its Cement Fixation.* Separation Science and Technology, 2007. **42**(6): p. 1255-1266.
106. Teker, M., Ö. Saltabaş, and M. İmamoğlu, *Adsorption of cobalt by activated carbon from the rice hulls.* Journal of Environmental Science and Health . Part A: Environmental Science and Engineering and Toxicology, 1997. **32**(8): p. 2077-2086.
107. Demirbaş, E., *Adsorption of Cobalt(II) Ions from Aqueous Solution onto Activated Carbon Prepared from Hazelnut Shells.* Adsorption Science & Technology, 2003. **21**(10): p. 951-963.
108. Rengaraj, S. and S.-H. Moon, *Kinetics of adsorption of Co(II) removal from water and wastewater by ion exchange resins.* Water Research, 2002. **36**(7): p. 1783-1793.
109. Hansen, L.D., D. Silberman, and G.L. Fisher, *Crystalline components of stack-collected, size-fractionated coal fly ash.* Environmental Science & Technology, 1981. **15**(9): p. 1057-1062.

Chapter 7. Conclusions and recommendations for future work

7.1. Conclusions

This thesis focused on addressing some challenges related to the usage of potential adsorbents including metal organic frameworks (in particular ZIF-8) and available local wastes (fly ash) in water treatment and to provide technical knowledge about their characteristics, performance and interactions in adsorption systems. In summary, novel approaches were developed for desirable application of ZIF-8 particles in water treatment and a new perspective was identified to make use of fly ash wastes and modify them to superior adsorbents. The main findings of this research work are summarized as follows.

In chapter 3, an efficient straightforward and environmentally friendly phase inversion technique was utilized to develop ZIF-8/polymer spheres for oil spill clean-up. The polymer performed as binder and ZIF-8 functioned as adsorbent. The fabricated composite spheres demonstrated high surface area, high crystallinity and strong hydrophobicity. These magnificent features resulted in outstanding oil sorption capacity of ZIF-8/PES spheres in comparison with natural adsorbents. The composite spheres displayed 1260 mg/g uptake for oils which is around 4.8, 6.3, 12.6, 3.3 and 4.2-7.5 times higher than the capacity of HKUST-1, HFGO@ZIF-8, zeolite, bentonite and activated carbons respectively. ZIF-8/PES beads showed very low bulk density of 0.26 g/cm^3 compared with that of ZIF-8 powder with a bulk density of 0.36 g/cm^3 and those of natural adsorbents such as activated carbon, zeolite and

bentonite with bulk densities of 2, 1.6 and 1.15 g/cm^3, respectively. Having excellent buoyancy, they floated on the surface of water easily while their robustness was preserved confirming the beads were rigid and stable. The synthesized composite beads were easy to handle and recycle and retained up to 88 percent of the oil sorption capacity after five regeneration cycles. The phase inversion could be utilized as a universal approach for preparing a variety of composite spheres for different applications.

In chapter 4, we reported the adsorption properties of ZIF-8 and its derived nanoprous carbons for the removal of a basic model dye compound. Effect of heat treatment and carbonization temperature on physicochemical, textural and adsorptive performance of ZIF-8 and its nanoporous carbons was evaluated and the results were presented with critical discussions regarding the adsorption kinetics, mechanisms, process parameters and carbonization mechanisms. Nanoporous carbons were prepared by direct carbonization of ZIF-8 at 600℃, 1000℃ and 1200℃ and they retained the original morphology and structure after heat treatment as proved by SEM and TEM images. Effect of temperature on surface area was investigated and it was revealed that the surface area of ZIF-8 (1384.2 m^2/g) decreased with increasing heat treatment temperature to 600℃ (652.5 m^2/g) and increased by raising the temperature to 1000℃ (1043.1 m^2/g); however, it decreased when the carbonization temperature was further increased to 1200℃ (818.7 m^2/g). The total and micropore volumes followed the same trend as the surface areas. The study showed that the pore size distribution became broader after carbonization at 1000℃ and nanoporous carbon at 1000℃ exhibited the highest adsorption capacity indicating that 1000℃ was the optimum carbonization temperature. Zeta potential measurements also illustrated that carbonization temperature had remarkable effect on modifying the surface charge of the porous adsorbents. Nanoporous carbon at 1000℃ exhibited outstanding adsorption capacity (186.3 mg/g) which is 3.76 times of nanoparticles

carbonized at 600℃ (49.5 mg/g), 5 times of carbon particles at 1200℃ (36.7 mg/g) and finally about 10 times of ZIF-8 (19.5 mg/g). Investigation of effect of process parameters on adsorption revealed that adsorption was endothermic and the effect of pH was insignificant. The ZIF-8 derived carbon nanoparticles prepared by straightforward and environmentally friendly direct carbonization strategy were found to be efficient adsorbents for water treatment. This study provides helpful information for future applications of MOF derived nanoporous carbons for water treatment.

In chapter 5, the nanoporous carbons derived from ZIF-8 were magnetized for easy handling and recycling. The iron nanoparticles (14%, nominal weight percent) were introduced into materials framework using wet impregnation method. The resulting magnetic adsorbents were re-carbonized to examine the effect of heat treatment temperature on characteristics and adsorption properties of the iron loaded nanoporous carbons. The results showed the magnetic nanoporous carbons re-carbonized at 1000 ˚C exhibited similar high adsorption capacity to the original ZIF-8 carbon nanoparticles despite the fact that the surface area and micro pore volume reduced significantly after loading iron nanoparticles. XRD results confirmed the presence of iron oxides and reduced metallic iron at 600 and 1000 ˚C, respectively. SEM images showed that iron nanoparticles were well distributed in the matrices of the magnetic carbons and had different sizes from roughly 10 nm to 100 nm. The mechanism of the interaction between iron species with dye molecules was explained. The significant adsorption capacity of the iron loaded carbon nanoparticles was addressed to the role of the zero valent iron (reduced iron) produced at 1000 ˚C and the development and broadening of pore size distribution as a result of the formation of reduced iron particles. This study demonstrated that nanoporous carbons can be loaded by magnetic nano particles through a simple and efficient impregnation method without losing their adsorption capacities. This study demonstrated that MOF derived

nanoporous carbons can be magnetized by magnetic particles through a simple and efficient impregnation method without losing its high adsorption capacity.

In chapter 6, Victorian brown coal fly ashes as local free wastes were used to investigate their textural, mineralogical and physicochemical properties for potential adsorption applications. The adsorption performance of these waste materials was investigated for the adsorption of a basic dye and heavy metals. The adsorption study showed Yallourn fly ash exhibited the highest adsorption performance (12.5 mg/g) for dye removal followed by Weathered (8.1 mg/g) and Hazelwood (3.2 mg/g) fly ashes. It was revealed that natural weathering could be used as an effective method for modifying fly ash textural, mineralogical, physicochemical and adsorption properties. Weathering modification converted the non-porous Hazelwood fly ash to a more porous framework Weathered fly ash with much higher surface area; i.e., 2.5 times higher than the surface area of Hazelwood fly ash and more negative surface charge. Hazelwood fly ash had the highest capacity for the removal of heavy metals due to its highly alkaline nature followed by Weathered and Yallourn fly ash. Yallourn fly ash exhibited strong magnetic property which shows it is a promising material for adsorptive removal of contaminants from water. These remarkable features make these materials suitable candidates for neutralizing and treatment of acidic mining wastewaters containing heavy metals. We anticipate the outcomes of this study would help for future applications of these wastes and would resolve the environmental issues resulting from their disposal.

7.2. Recommendations for Future Work

According to this study, there are several aspects which are required to be explored and developed for future works. The areas of further research are as follows.

1. The phase inversion method explianed in chapter 3 could be used as a universal method for fabrication of other MOF powders into different kinds of polymer binders to investigate their properties for adsorption applications. A variety of materials such as catalyst powders, activated carbon and zeolites could be utilized in composite beads with the usage of different polymers for the applications such as adsoprtion, gas separation, catalysis and water treatment. These composite beads have very low bulk densities and could be studied and utilized in fluidized beds as catalysts for industrial applications. Therefore, although they are rigid and stable, their mechnical resitantce under stress and presssure need to be quantitatively defined. The composite beads could also be carbonized and used for the same applications such as adsorption and catalysis. In the trial tests, we obsereved the ZIF-8/PES beads maintain the spherical shape after carbonization in Ar atmosphere. However, when PES spheres were used, the spherical shape and the structure of the beads collapsed as a result of high temperature heat treatment. It seems that ZIF-8 acts as a binder and helps to retain the original sphere shape even after heat treatment at high temperatures (1000 ^{o}C). Therefore, this is a useful method for preparing carbon beads which could be used for different applications. Since the performance and adsorption capabilities of the prepared carbon beads were not examined, the investigation of characteristics and adsopriton capacity of these MOF derived carbon beads could be considered as a future exploration. Moreover, the magnetic particles could be introduced into the composite beads for even easier collection and recycling. The trial tests revealed that the magnetic

ZIF-8/PES beads after carbonization at high temperature collapsed and the carbon beads could not be prepared in the presence of iron particles. Further investigation is required to overcome this issue and prepare magnetic carbon beads with high sorption performance and strong bodies which preserve the spherical shapes. Effect of temperature on the properties of the prepared carbon spheres such as hydrophobicity could also be investigated.

2. The direct carboniztaion method utilized in chapter 4 could be used for carbonization of other MOF and ZIF materials and effect of carbonization on their physicochemical and adsorption properrties could be investigated for any applications dealing with adsorption including gas separation, catalysis, water treatment and drug delivery. Since MOFs and ZIFs have different elements and components, their behaviour against heat treatment at high temperatures could be quite different. Therefore, it is worth to identify how carboniztaion temperature affects their characteristics and performance in different applications. ZIF-8 and its nanoporous carbons in this study were investigated for the adsorption of dyes. Further research is required to explore the capabilities of MOFs and MOF derived carbon nanoparticles for the adsorption of other pollutants such as aromatic compounds and antibiotics to address the suitability of these adsorbents for various water contaminants. Effect of heating rate on properties of the nanoporous carbons derived from different MOF materials is another aspect which is worth investigating. Considering that MOFs and ZIFs contain a variety of elements and different structures, the rate of carbonization could result in different properties which needs to be studied in next step. The stability of ZIF-8 in water is a serious concern which restrict its practical application. This challenge could be addressed by researching about the possible composite development using ZIF-8 and clay materials.

During the ongoing literature review, we noticed that clay and carbon materials could be used to produce a composite tolerant to aquoues environment. This area was not covered during the timeline of this thesis project since it needs an extensive research focused on the stability of metal organic frameworks in water. Moreover, it was realized from literature that there might be synergistic effect between MOFs and carbon material which may enhance their performance in different applications especially adsorption. These are imposrant reseach areas which could be considered as future works.

3. The magnetic ZIF-8 derived nanoporous carbon in chapter 5 had similar adsorption capacity to those of non-magnetic nanoporous carbons. However, the kinetics, isotherms and mechnaisms were not determined in this study. It is required to identify how fast these magnetic nanoparticles could reach equilibrium in terms of practical applications. The amount of iron loading in this study was 14%, but is needed to examine different loadings and optimize the amount of iron required for introducing the magnetic property and the highest adsoprtion capacity. Obviously, the magnetic MOF derived nanoporous carbons could be investigated in detail for the removal of other categories of pollutions from water. For the magnetic samples at 1000 ºC, since the produced zero valent iron is very reactive, these iron loaded carbon nano particles could be explored for catalytic applications as well.
4. In chapter 6, the local brown coal fly ash materials were investigated for adsorptive removal of heavy metals and a basic dye to not only make use of these abundant free adsorbents but also address the environmental concerns related to their disposal. It was determined that these fly ashes contain interesting features and components such as active metal oxides and magnetic properties. Therefore, it can be suggested that these

materials could be investigated for different catalytic applications. In addition, in this study, for the adsorption of heavy metals, the isotherms and kinetics were not investigated and are required to be addressed in future. The effect of weathring modification was only studied for non-magnetic Hazelwood fly ash. However, effect of weathring for magnetic Yallourn fly ash was not explored in this research project. It is required to identify how the physicochemical properties and mineral phases of this iron containing fly ash changes when it is exposed to weathring conditions and weather it enhances its adsorption performance. Moreover, these waste fly ashes could be loaded with other active metals or could be made compsite with other materials for adsorption and catalytic applications. Hazelwood fly ash showed the highest adsorption capacity for heavy metals removal but it did not demonstrate any magnetic property. In order to convert it to an efficient recyclablae adsorbent, it could be loaded by iron particles. Another future direction could be to combine the non-magnetic Hazelwood fly ash with magnetic Yallourn fly ash and perform calcination to obtain a magnetic mixture for the adsorption of pollutants from water. Additionally, the usage of these materials in different practical applications depends on the life cycle assessments studies. A detailed and precise life cycle analysis is essential to assess the environmental impacts associated with the utilization of Victorian brown coal fly ash in any particular application.